

FINISH-MACHINING STRATEGIES FOR BLADED DISKS

By

Iraitz Arrospide Garro

Submitted in fulfilment of the degree of Engineering Doctorate

October 2022



The
University
Of
Sheffield.

**Department of Mechanical Engineering
Industrial Doctorate Centre in Machining Science
Sheffield, UK**

Supervisors: Prof. N.D. Sims (academic)

Dr D. Curtis (industrial)

ABSTRACT

Integrally Bladed Rotors (IBRs) or Bladed Disks (Blisks) are strategic components of compressor or turbine stages of aircraft engines. Development of manufacturing techniques and materials have aided the integration of two components, blades and the disk, which were originally manufactured separately and then assembled. A single component brings great benefits such as weight reduction, which is key in the aerospace sector.

IBR components bring new challenges to the manufacturing industry due to the difficult to cut materials used, paired with complex geometries which limit the access of tooling and limits various efficient cutting strategies for the finish milling operations. Instead, a point milling strategy is commonly used to achieve drawing specifications but at a cost of machining time.

Therefore, finish milling is by far the most time-consuming machining operation of IBR blades. However, many efforts from industry are directed to optimize machining times through roughing operations, which are faster to implement internally within the manufacturing engineering department, and often are not affected by fixed process approvals that are in place for the last few millimetres of material removal. This includes approval from the materials department on surface integrity modifications of the final surface, and complex approval processes with the final clients.

An EngD project is an ideal scenario for the development of finish machining strategies for the reasons explained above. This thesis takes a real IBR case study as a starting point and navigates through a logical path for the development of its blade finish milling operation to provide a novel industrial optimization strategy.

The research question evolves as each chapter explores different aspects of this challenging industrial problem. Initially, in chapter 2, surface integrity is explored within the typical working window (range or map of parameters selected for a given experiment), due to the relevancy of the surface integrity in the finished component. This is explored through an experimental approach which concludes surface integrity is not affected in the analysed

ABSTRACT

range. Instead, chatter is identified and research efforts are then directed to improve finish machining of IBR blades through the understanding and mitigation of chatter.

Chapter 3 seeks to analyse tool and component dynamics and includes a brief search into literature about process damping to understand how it might play a role in chatter mitigation.

A new research line is then investigated to improve finish milling of IBR blades. A very simple concept of modifying finish milling stock is developed, using a scientific method based on Finite Element Analysis (FEA) and parametrizing the blade in order to maximize natural frequencies of interest.

Once an optimized blade stock geometry has been obtained, a further literature review is carried out on chatter mitigation techniques. A knowledge gap is found in the current literature regarding time domain model for Sinusoidal Variable Spindle Speed (SVSS) model for ball end mill tools. This is observed as an opportunity to do a theoretical contribution to the predominantly experimental EngD thesis. A current time domain model has been further developed to incorporate SVSS and ball end mill geometry.

Finally, implementation of variable speed in industrial environment has been researched. A further knowledge gap is identified in the implementation of variable speed in commercial milling machines, as most research up to date has been realized either theoretically or in laboratory conditions. In response to this need, a new method has been developed to be able to implement variable spindle speed and variable feed straight forwardly in a wide range of commercial milling machines. To end up with, a machine characterisation has been completed in order to identify the working window to apply the Variable Spindle Speed (VSS) method, and experimental trials have been carried out to demonstrate the capability of this approach.

This thesis starts presenting a case study of IBRs with the need to improve current finish machining strategies and delivers new solutions from various perspectives, complementing each other and readily available to implement in the industry environment.

ACKNOWLEDGEMENTS

“Don’t be embarrassed by your failures, learn from them and start again”- Richard Branson.

This has been the most difficult work in my life, with many bumps in the road and very difficult personal circumstances in which the easiest thing to do was throwing in the towel. I have suffered from anxiety and pressure, and I had constant thoughts that I was failing. But somehow, I have never given up and my mindset has always been that I can do better than what I have done so far. This attitude has pushed me through the thesis completion.

I would like to thank to my family, especially Leire, my wife, who came to live to the UK supporting my doctorate studies, and we created a beautiful family with our children Unax and Kaila. It has not been easy to grow a family abroad on our own, but Leire has been very strong all this time to overcome the challenges that life has put us.

I cannot forget mum and dad, who always supported my studies and encouraged me to work hard on this path. Without them, I would have never travelled to the UK pursuing my academic career. This year I almost lost dad in a work accident and that event changed my mindset of what is important in life. It helped me handling mental health issues and converting it into positive energy towards work.

Finally, I have words of gratitude for my supervisors Prof. Neil Sims and Dr. Dave Curtis. Their guidance has been essential to complete this work. I will never forget their support when I had to deal with difficult personal circumstances. I appreciate their honest advice and most importantly their attitude to help me always.

Thank you.

CONTENTS

CONTENTS

CHAPTER 1. INTRODUCTION.....	1
1.1 Background	1
1.2 Engineering context	3
1.2.1 IBR Manufacturing process.....	4
1.2.2 Machining time distribution	6
1.3 Challenge of the finish milling process	7
1.3 Summary	8
CHAPTER 2. EFFECT OF CUTTING VARIABLES ON SURFACE INTEGRITY	10
2.1 Introduction	10
2.2 Background on surface integrity.....	11
2.2.1 Surface roughness.....	11
2.2.2 Residual stress.....	13
2.2.3 Microhardness	15
2.2.4 Microstructure	17
2.2.5 Benchmark on cutting variables	18
2.2.6 Summary of literature.....	21
2.3 Experimental approach.....	21
2.3.1 Method	23
Machine, cutting tool and coolant.....	23
Workpiece	23
Machine set-up	24
Cutting approach	25
Cutting variables	25

CONTENTS

Cutting force measurement.....	27
2.3.2 Results.....	27
Tool wear	27
Cutting force analysis.....	29
Surface roughness.....	33
Part topography.....	37
Micro-hardness	41
Sub-surface deformation	45
2.3.3 Conclusions	51
2.4 Summary	53
CHAPTER 3. TOOL AND COMPONENT DYNAMIC ANALYSIS	55
3.1 Introduction	55
3.2 Tool dynamic analysis	55
3.3 Component dynamic analysis	58
3.4 Summary	61
CHAPTER 4. BLADE OPTIMIZATION FOR FINISH MILLING OPERATION	62
4.1 Introduction	62
4.2 Methodology.....	63
4.2.1 Model geometry	63
4.2.2 Ansys workbench preliminary analysis	65
4.2.3 Ansys Mechanical.....	66
4.2.3.1 Geometry	66
4.2.3.2 Coordinate systems	67
4.2.3.3 Contacts	67
4.2.3.4 Mesh	68
4.2.3.5 Mesh edit	69

CONTENTS

4.2.3.6 Supports	69
4.2.3.7 Solution	70
4.2.3.8 Additional remarks.....	70
4.2.4 Ansys workbench abridged analysis	70
4.2.5 Direct optimization	72
4.2.6 Topographical variation	74
4.3 Results.....	76
4.4 Conclusions	80
4.5 Summary	80
CHAPTER 5. LITERATURE REVIEW ON CHATTER MITIGATION.....	82
5.1 Introduction	82
5.2 Process damping	82
5.2.1. Effect of cutting parameters on process damping	83
5.2.2 Process damping modelling.....	86
5.3 Modelling of chatter	89
5.3.1 Historical overview	89
5.3.2 Chatter mitigation methods	95
5.3.3 Frequency domain models	96
5.3.4 Time domain models	97
5.3.4.1 Time domain chatter criteria	98
5.3.5 Experimental methods.....	99
5.4 Ball-end mill tool geometry modelling	100
5.5 Flexible part modelling	103
5.6 Variable speed milling.....	104
5.6.1 Adaptive spindle speed variation	105
5.6.2 Modulated spindle speed variation	109

CONTENTS

5.7 Summary	119
CHAPTER 6. CNC IMPLEMENTATION OF SINUSOIDAL SPEED AND FEED.....	123
6.1 Introduction	123
6.2 Method.....	124
6.2.1 Machine specifications	125
6.2.2 Data acquisition	127
6.2.3 Automated overrides	127
6.3 Experimental work.....	129
6.3.1 Sinusoidal signal simulation	129
6.3.2 Experimental machine testing	131
6.4 Results and discussion	132
6.4.1 Spindle speed vs. RVF	132
6.4.2 Feed vs. RVF	135
6.4.3 Repeatability tests	136
6.4.4 Frequency response for magnitude and phase	138
6.5 Conclusions	142
6.6 Summary	143
CHAPTER 7. TIME DOMAIN MODEL FOR BALL END TOOL AND SINUSOIDAL VARIABLE SPINDLE SPEED (SVSS)	145
7.1 Introduction	145
7.2 Model formulation.....	146
7.3 Milling kinematics	148
7.3.1 Identify current tooth position	150
7.3.2 Define the workpiece arc surface points	152
7.3.3 Calculate dimensions of the intercept segment geometry	152
7.3.4 Update the intercept segment radius.....	154

CONTENTS

7.4 Milling forces.....	155
7.5 System dynamics.....	159
7.6 Summary	163
CHAPTER 8. CONCLUSIONS AND FUTURE WORK	165
8.1 Summary of thesis	165
8.2 Conclusions	167
8.3 Contributions	168
8.4 Future work.....	169
REFERENCES	172

LIST OF FIGURES

Figure 1. Most recent aircrafts; Boeing 787 Dreamliner (left) [1] and Airbus A350 WXB (right) [2]. 1

Figure 2. Section view of the turbofan engine PW1000G from Pratt & Whitney [7]. 2

Figure 3. Integrally Bladed Rotor (IBR) component. 4

Figure 4. 5 axis roughing strategy to mill the blades. 5

Figure 5. 5 axis finishing strategy carried out to mill the blades. 5

Figure 6. Distribution of the cutting time employed to machine IBRs. Data collected from CNC programs as well as from the production line of the component analysed in this work. 6

Figure 7. Samples of the sub-surface microstructure obtained from the case study component after milling (left) and turning (right) processes. 11

Figure 8. Hermle C50 five axis milling machine. 23

Figure 9. Workpiece fixed and ready for the machining trial. 24

Figure 10. Set up of the trials. Machine’s A axis rotated at 90° and angle plate fixed to the bed also at 90° in order to hold the dynamometer and the part in a horizontal initial position. ... 25

Figure 11. Tool wear after the completion of the cutting trial at different cutting conditions. 28

Figure 12. Cutting force (left side) and feed force (right side) plotted for two variables; Surface speed and feed per tooth. 29

Figure 13. Set of plots showing the evolution of forces (cutting force and feed force) for step over and cutting depth variations. Plots on the top of the figure show the cutting force and feed force for the step over variable while the plots on the bottom show the forces for the cutting depth variable. 31

Figure 14. Cutting force and feed force for the two tested materials (custom forging and forged billet) for lowest test condition (left hand side) and highest condition (right hand side). 33

Figure 15. Set up of the surface roughness measurement test. Workpiece held in a small vice and the machined face looking upwards while the roughness tester analyses the surface generated. 33

LIST OF FIGURES

Figure 16. Roughness in the step over direction (left hand side graph) and feed direction (right hand side) plotted for two variables; Surface speed and feed per tooth.	34
Figure 17. Set of graphs showing the evolution of surface roughness in step over and feed direction for cutting depth and step over variations. Graphs on the top of the figure show the surface roughness for the cutting depth variable while the graphs on the bottom show the roughness for the step over variable.	36
Figure 18. Surface roughness in step over and feed direction for the two tested materials (custom forging and forged billet) for lowest test condition (left hand side) and highest condition (right hand side).....	37
Figure 19. Sub-surface micro hardness profile graphs showing the influence of surface speed for different feed per tooth values (top left, $f_z=0.05\text{mm}$; top right, $f_z=0.1\text{mm}$; bottom left, $f_z=0.2\text{mm}$; bottom right, $f_z=0.3\text{mm}$).	42
Figure 20. Sub-surface micro hardness profile graphs showing the influence of feed per tooth for different surface speed values (top left, $v_c=60\text{m/min}$; top right, $v_c=170\text{m/min}$; bottom left, $v_c=240\text{m/min}$).	43
Figure 21. Sub-surface micro hardness profile graphs showing the influence of cutting depth (top left and top right) and step over (bottom left and bottom right) for different surface speed and feed per tooth values).	44
Figure 22. Sub-surface micro hardness profile graphs showing the influence of the workpiece material (custom forging and forged billet) at lowest and highest parameter combinations.	45
Figure 23. Drawing of the tapered ball end mill.	56
Figure 24. Stability diagram of the cutting tool. Blue dots show the location of the four different surface speeds tested in Chapter 2.	57
Figure 25. Tap test points within the blade.	59
Figure 26. IBR milling fixture.	64
Figure 27. Split body geometry, solid (left) & surface (right).	65
Figure 28. Cylindrical coordinate system orientation.	67
Figure 29. Mesh structure.	69
Figure 30. Model setup.	70
Figure 31. Simplified IBR model setup.	71

LIST OF FIGURES

Figure 32. Optimization. Parameter setup.	73
Figure 33. Overview of resulting candidate point schematic.	74
Figure 34. Sketch of an individual split stock cross-section.....	75
Figure 35. Parametrized construction of IBR blade.	75
Figure 36. Simplified model showing baseline first flap frequency.....	76
Figure 37. Optimized stock layout.	77
Figure 38. Optimal stock layout.	77
Figure 39. Smoothed model.....	78
Figure 40. Total deformation and first flap frequency results for topographical (left) and linear (right) variation.	79
Figure 41. Chatter avoidance/suppression method classification	96
Figure 52. Starrag NB251 machine and axis layout.	126
Figure 53. Example of sinusoidal signal simulated in matlab and measured in the machine.	130
Figure 54. Typical example of feed failure error.....	131
Figure 55. Feed failure for $RVA=0.1$ and $F=400\text{mm}/\text{min}$	132
Figure 56. Working area for $RVA=0.1$ and $F=400\text{mm}/\text{min}$	133
Figure 57. Feed failure for both $RVA=0.1$ and $RVA=0.2$ and $F=400\text{mm}/\text{min}$	134
Figure 58. Working area for $RVA=0.2$ and $F=400\text{mm}/\text{min}$	135
Figure 59. Feed failure for variable feed rate and fixed $RVA=0.1$ and $S=1000\text{rpm}$	136
Figure 60. Repeatability test for X and Y axis at fixed parameters $S=3500$, $F=400$, $RVA=0.1$, $RVF=0.125$	137
Figure 61. Repeatability test for X and Y axis at fixed parameters $S=3500$, $F=400$, $RVA=0.1$, $RVF=0.125$ (peak zoom).	138
Figure 62. Speed and feed magnitude for variable spindle speed.	139
Figure 63. Speed and feed magnitude for variable feed rate.....	140
Figure 64. Speed and feed pahse delay for variable spindle speed.	141
Figure 65. Speed and feed phase delay for variable feed rate.	141
Figure 42. Simulink diagram for time domain simulation.	147
Figure 43. Simulation flow chart.....	149
Figure 44. Diagram for the calculation of θt	151

LIST OF FIGURES

Figure 45. Milling dynamic model for up or conventional milling.....	151
Figure 46. Geometry of the uncut chip thickness during the milling process.....	155
Figure 47. Detail of the ball type tool geometry and sketch for discretized depth, d_b calculation.....	158
Figure 48. Cutting force diagram built in Simulink	159
Figure 49. Sinusoidal Variable Spindle Speed (SVSS).....	161
Figure 50. Simulink diagram to generate the instantaneous spindle speed (n) in SVSS.	161
Figure 51. System dynamics block for the equation of motion in y direction.....	162

LIST OF TABLES

Table 1. Comparison of the cutting parameters employed in this case study against the cutting parameters employed by different authors in their research studies.20

Table 2. Composition of the two tested materials: custom forging currently employed and a forged billet.....24

Table 3. Mechanical properties of the tested material.24

Table 4. Selection of variable parameters and total number of conditions tested in the machining trials.....26

Table 5. Range of variable cutting parameters tested.26

Table 6. Variation in force level from lowest to highest feed per tooth conditions.30

Table 7. Variation in force level from lowest to highest surface speed conditions.31

Table 8. Variation in force level from lowest to highest step over conditions.32

Table 9. Variation in force level from lowest to highest step over conditions.32

Table 10. Variation in roughness from lowest to highest surface speed conditions.35

Table 11. Variation in roughness from lowest to highest feed per tooth conditions.35

Table 12. Variation in roughness from lowest to highest cutting depth conditions.36

Table 13. Variation in roughness from lowest to highest step over conditions.....37

Table 14. Topography of the machined surface for each tested cutting conditions.38

Table 15. Evaluation of sub-surface damage and grain directionality caused by the machining effect for the tested conditions.46

Table 16. Two main natural frequencies and the stiffness of the tool.....57

Table 17. Frequencies of the main vibration modes for different areas of the blade.59

Table 18. Advanced geometry options.66

Table 19. NB251 technical data.126

Table 20. Automated override NC program example.....128

NOMENCLATURE AND ABBREVIATIONS

A

a_e Radial depth of cut

a_p Axial depth of cut

B

b Axial width of cut

BEA Blue Etch Anodize

b_{lim} Critical width of cut

Blisk Bladed Disk

C

c Damping coefficient

CAD Computer Aided Design

CMM Co-ordinate Measuring Machine

CNC Computerized Numerical Control

CSS Constant Spindle Speed

CSSV Continuous Spindle Speed Variation

D

db Arc length

DDE Delay Differential Equation

DDS Dynamic Data System

dz Depth of discretized tool layer

E

EFS Elastic Foundation Stiffness

EngD Engineering Doctorate

F

f Feed

NOMENCLATURE AND ABBREVIATION

F_a	Axial force
F_r	Radial force
F_t	Tangential force
FEA	Finite Element Analysis
FFT	Fast Fourier Transform
FPI	Fluorescent Penetrant Inspection
FRF	Frequency Response Function
f_z	Feed per tooth
H	
h	Chip thickness
I	
IBR	Integrally Bladed Rotor
K	
k	Spring constant
k'	Angle between the tool centre axis and higher point of db
k_{ac}	Axial cutting stiffness
k_{rc}	Radial cutting stiffness
k_{tc}	Tangential cutting stiffness
L	
l	Current axial layer
LE	Leading Edge
M	
m	Mass
$MISQP$	Mixed Integer Sequential Quadratic Programming
MRR	Material Removal Rate
$MSLD$	Multidimensional Stability Lobes Diagram
N	
n	Instantaneous spindle speed

NOMENCLATURE AND ABBREVIATION

n_l	Total number of axial discretization layers
NDT	Non Destructive inspection Technique
P	
PCD	Poly Crystalline Diamond
PTP	Peak to Peak
R	
r_s	Intercept segment radius
r_t	Tool radius
R_a	Average Roughness
$RCSA$	Receptance Coupling Substructure Analysis
RMS	Root Mean Square
RSM	Remote Solve Manager
RVA	Speed Variation Amplitude Ratio
RVF	Speed Variation Frequency Ratio
S	
S_a	Surface arc point
S_{ap}	Surface arc point (present tooth)
S_{ap-1}	Surface arc point (previous tooth)
S_{atx}, S_{aty}	Instantaneous tooth position coordinates
S_{ax0}, S_{ay0}	Tooth position in global coordinates
S -Function	System Function
SLD	Stability Lobes Diagram
S_q	Root Mean Square Roughness
$SSSV$	Sinusoidal Spindle Speed Variation
STL	Stereolitographic
SVC	Support Vector Classification
$SVSS$	Sinusoidal Variable Spindle Speed
T	
T	Period

NOMENCLATURE AND ABBREVIATION

<i>TE</i>	Trailing Edge
<i>V</i>	
v_c	Surface Speed
<i>VSM</i>	Variable Speed Machining
<i>W</i>	
<i>WC/Co</i>	Composite of tungsten carbide and cobalt
<i>X</i>	
<i>XRD</i>	X-Ray Diffraction
<i>Greek</i>	
<i>Symbols</i>	
\mathcal{E}	Phase Shift
ϑ	Angle formed by lower and higher points of db with tool centre
θ_t	Angular position of cutting tool
θ_{t-1}	Previous angular position of the tooth
θ_{a0}, θ_{a1}	Angular position in global coordinates
θ_u	Instantaneous tooth angle
λ	Helix angle
σ_{11}	Normal Residual Stress (feed direction)
σ_{12}	Shear Residual Stress
σ_{22}	Normal Residual Stress (cutting direction)
τ_t	Number of tool revolutions
φ	Reference tooth angle
Ω	Spindle speed
ω_0	Average spindle speed
ω_A	Amplitude of average spindle speed

CHAPTER 1. INTRODUCTION

1.1 Background

Aircraft engine parts have been manufactured using different materials and techniques throughout history. The need for providing enough power supply for increasingly economic and ecological aircrafts have resulted in both reducing the weight of the engine, and increasing its efficiency. In order to achieve demanding weight reduction requirements, higher strength to weight ratio materials need to be used. Composite materials are becoming more and more popular due to their exceptional strength to weight ratio and even if the use of composite materials is being increased in the airframes of the newest aircrafts such as the Boeing 787 Dreamliner or the Airbus A350 XWB (Figure 1), the use of those materials is very limited in engine critical parts, due to the temperature and fatigue life requirements. In order to improve the efficiency of the engines, higher temperature resistance materials need to be used.



Figure 1. Most recent aircrafts; Boeing 787 Dreamliner (left) [1] and Airbus A350 WXB (right) [2].

Titanium alloys are the most popular alloys for compressor stages in the aircraft engine (Figure 2), due to their very good strength to weight ratio and its performance in high temperatures. The most popular titanium alloy in aerospace is Ti-6%Al-4%V, which covers more than 45% of the total production worldwide [3]. This alloy, which is an $\alpha+\beta$ alloy, is so popular because of its high strength to weight ratio at elevated temperatures together with corrosion and fracture resistance [4], [5], and can be used in blades which work at temperatures up to 400°C [3]. However, titanium alloy Ti 6-4 is considered to be a difficult to cut material, due to various reasons:

- Low thermal conductivity, which leads to high temperatures in the cutting zone (i.e. next to the cutting edge of the tool)
- High chemical reactivity at high temperatures with many cutting tool materials, originating diffusion wear
- High strength at elevated temperatures [5], [6].

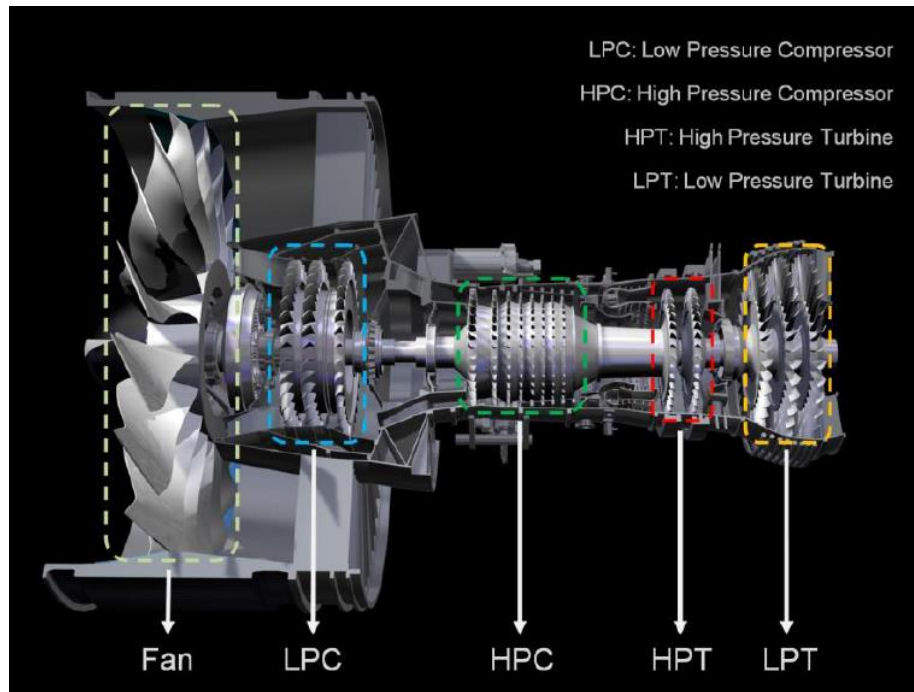


Figure 2. Section view of the turbofan engine PW1000G from Pratt & Whitney [7].

Titanium alloy products are expensive because of the complexity of the extraction process, the difficulty of melting and also due to the added cost related to low machinability [8]. Therefore, titanium components are used only when high reliability and performance are needed. During the machining process, the heat generated tends to damage the material on the surface and sub-surface, creating plastic deformation, cracks, phase transformations and residual stress effects [6]. In order to keep under control the fatigue life of the components, it is highly important to assure a high end surface integrity in the machined components. While big effort has been made to reduce the machining times of those difficult to cut materials, lower attention has been paid to the surface integrity, which includes surface roughness, residual stress, surface and sub-surface microstructure and microhardness analysis [5]. In fact, any proposed improvement in terms of productivity in machining should be assessed by the resultant surface integrity in order to introduce it in flying parts.

1.2 Engineering context

IBRs (Integrally Bladed Rotors) or Blisks, shown in Figure 3, are parts which are located in the compressor stages of the aero-engine turbines. The name of this part comes from the particularity of integrating both the disk and the blades in a single part, compared to the traditional assembled configuration of disk and attached blades. The main benefit of IBRs compared to the disk-blade assembly is the weight saving, which can be up to 30%. This weight saving comes from the single component nature of IBRs as opposed to the original assembly of disk + blades, which requires more material in the joints. This weight saving improves the performance of the engine. The main disadvantages compared to the traditional configuration are the higher cost involved in manufacturing the part and also the cost involved in repairing any damage suffered by the blades. As a result of the research work carried out in the field, the manufacturing process of the IBRs has improved and also the technology and costs related to the blade repairs. Therefore, IBRs are nowadays the preferred option of the aero-engine manufacturers for the compressor stages.

Different materials are used to manufacture IBRs depending on the mechanical and thermal properties required for each case. For the low pressure compressor stages titanium alloys are employed, whereas for the high pressure compressor stages, where the temperatures are higher, nickel alloys are employed [9]. The current research is based in the case study of the machining process of a particular IBR manufactured in Titanium alloy.

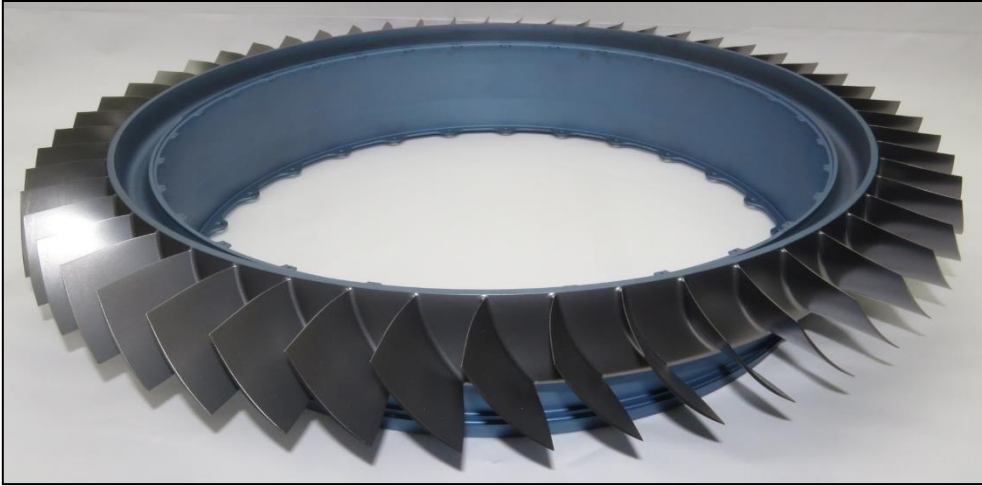


Figure 3. Integrally Bladed Rotor (IBR) component.

1.2.1 IBR Manufacturing process

The manufacturing process starts from melting the alloy following a triple melting process and getting the desired chemical and mechanical properties. The wrought alloy is then forged to the pre-form of the part and heat treated to the specifications.

The first machining operation is the turning of the body or disk which is carried out in 2 different steps; roughing and finishing. A Computer Numerical Control (CNC) lathe is employed for that purpose. The roughing operation comprises two different fixtures to machine the forward side and the afterward side of the part, same as the finish turning.

The next step is to mill the blades of the part. To do so, a 5 axis milling machine is employed. First of all, rough milling is carried out, in which the pre-form of the blades is created (Figure 4). The tool creates slots between the blades using slot milling strategy and the finish stock material is left in the walls for the finishing.

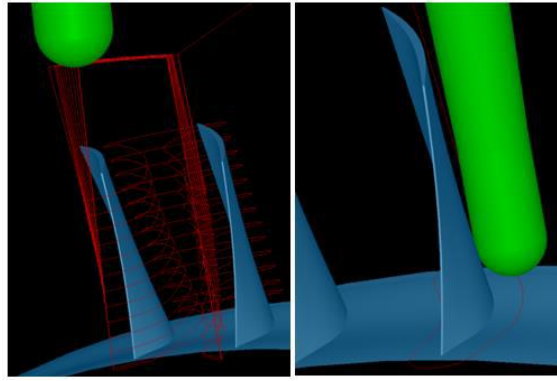


Figure 4. 5 axis roughing strategy to mill the blades.

Blades and platform are finished following a contouring point milling technique, as shown in Figure 5.

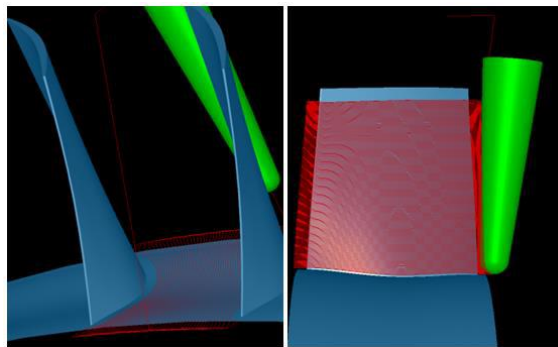


Figure 5. 5 axis finishing strategy carried out to mill the blades.

Complementary milling operations, such as hole drilling, scallop and casellation milling are carried out to end the material removal processes.

Some handwork operations are required as well. Deburring operations are carried out when necessary, followed by breaking sharp edges. Finally, blades are polished to meet surface roughness requirements, according to drawing requirements.

After finishing all the operations stated above, the part is visually inspected and Co-ordinate Measuring Machine (CMM) measurement is performed. The balance of the part is checked and if there is any unbalanced area, material is removed from the indicated areas to meet the specified requirements.

Then, Non Destructive inspection Techniques (NDTs) are carried out to check the quality of the part, Blue Etch Anodize (BEA) technique to detect abusive surface discontinuities and

abnormalities caused by machining, such as abusive machining and Fluorescent Penetrant Inspection (FPI) to detect defects like cracks.

Finally the part is shot peened according to the standard specifications in order to create higher compressive residual stresses and increase the fatigue life of the component and after visually inspecting, the part it is ready to be delivered.

1.2.2 Machining time distribution

As a starting point for this work, cutting times for the different operations were identified (Figure 6) and the results showed that finish milling process is the most time spending machining process, taking the 49% of the total machining time. From the finish milling operation, blade finishing is, by far, the longest feature in terms of cutting time, which indicates that it is the most strategic operation to improve.

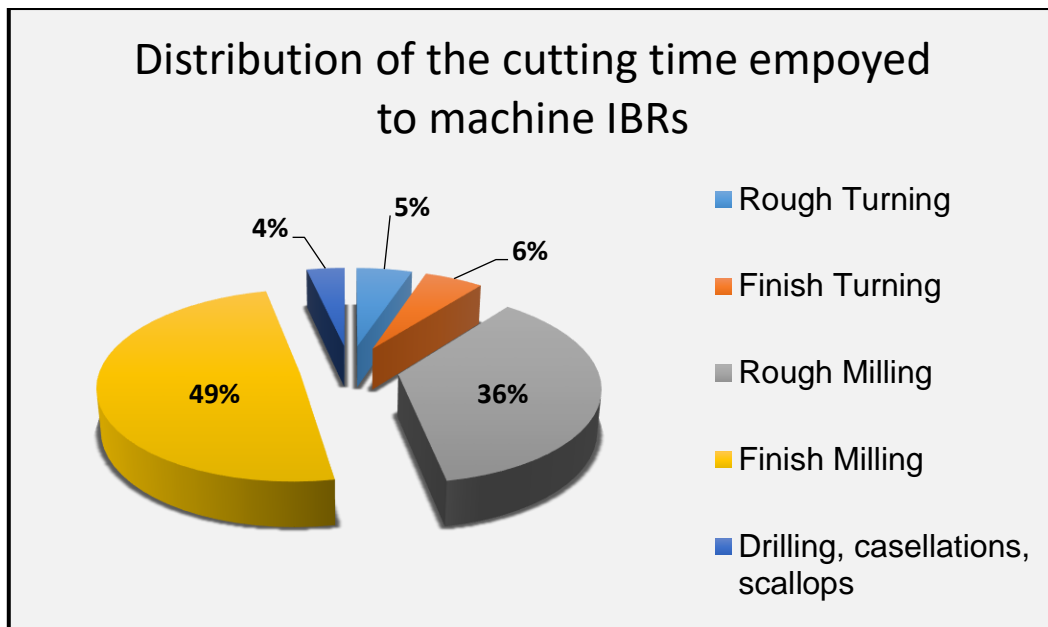


Figure 6. Distribution of the cutting time employed to machine IBRs. Data collected from CNC programs as well as from the production line of the component analysed in this work.

However, the optimisation of the blade finish milling operation involves the understanding and assessment of the damage generated in the sub-surface region and the quality of the machined surface, which is considered in general as the surface integrity of the material. In other words, the optimisation of the finish machining processes requires joint knowledge of the machining process and the behaviour of the material.

1.3 Challenge of the finish milling process

Blade finish milling of an IBR is a complex operation for various reasons, but mainly due to the workpiece material, geometry of the blades and the low stiffness of the tool/workpiece combination. The material employed in the low pressure compressor stage of the IBRs is Titanium 6-4, the most widely used and studied material out of the titanium alloys. Although this alloy is used in the industry since the 1950's it is still considered a hard to cut material and the material removal rate (MRR) in machining processes is low. When too high cutting parameters are employed, tool wear develops quickly while the workpiece material can be damaged due to the heat generated in the process.

The geometry of the blade is complex due to its 3D free form curved surface and requires a five axis milling machine to perform the finish milling operation. There are different approaches to machine such blades, but the most widely employed technique consists of slot milling the gap between the blades and then contour milling the blades from the tip to the root, descending in a helical movement. This approach is carried out with point milling, a high precision strategy which is performed by variants of ball end mills. The tool has a tilt and a lead angle which are constantly changing across the blade so that the relative position between the tool and the workpiece is constant. The understanding of the strategy summarised above and the contact point between the tool and the workpiece is important to predict the behaviour of the cutting process.

Last but not least, the low stiffness of the tool/workpiece combination makes the process dynamically very unstable, leading to regenerative vibration or chatter issues which affects negatively to the surface integrity of the part and also to the tool life. For general machining operations, chatter issues are related to the flexibility of the tool; In order to solve this problem, it is enough to analyse the dynamic behaviour of the tool and find stable machining regions (parameters) for that particular tool. However, in the case of blade finish milling, the flexible blades, together with the flexible tool generate a coupled dynamic response, which is more complex to understand. Besides, the blade's flexibility and therefore dynamic response changes across the blade, from leading to trailing edge and from tip to root, creating a variable and difficult to predict dynamic behaviour of the system. For the reasons given above, it is a big challenge to find stable cutting conditions across the blade.

The three aspects mentioned above, related to the material's behaviour to be machined, the complex geometry and therefore complex milling strategy and the coupled dynamics of the tool/workpiece flexible system represent the main challenges that are explored in this thesis.

The aim of this EngD thesis is to develop new insights into these challenges, so as to improve productivity of IBR manufacture. The specific objectives are:

- 1) Understand the manufacturing process of an IBR and identify the key machining operation to improve productivity.
- 2) Select a parameter working window based on literature as well as own experience, and evaluate the effects on surface integrity.
- 3) Perform a dynamic analysis of the system and identify main vibration modes and frequencies.
- 4) Develop a method to optimize stock geometry to improve the stability of the component.
- 5) Carry out a detailed literature review on chatter mitigation methods. Identify the most suitable method for this particular case and find modelling gaps.
- 6) Develop an existing chatter model, filling the gaps for the specific needs of the selected method.
- 7) Investigate the industrial implementation of the chatter mitigation method proposed.

1.3 Summary

The manufacturing process of an IBR has been proposed as a case study for this EngD thesis, in which increasing the machining productivity is the ultimate aim. Following a logical path, first the background of aircraft components has been presented. This has been followed up with the engineering context, which are machining difficulties associated to this particular part.

After the brief introduction to the topic, IBR manufacturing process has been reviewed and machining times of different operations have been obtained. Finish milling and more specifically blade finish milling process has been identified as the most time-consuming

operation, with 49% of the total machining time. This is used as an indicator to focus the research work of the following chapter to improve blade finish milling.

Finally, specific objectives have been established to achieve the ultimate aim of increasing machining productivity of an IBR component through a novel approach. Each objective is aligned with a chapter in this thesis, in an effort to create a clear and easy to read document.

CHAPTER 2. EFFECT OF CUTTING VARIABLES ON SURFACE INTEGRITY

2.1 Introduction

Increasing research efforts are being done in the field of surface integrity. It is of vital importance to assure that the material keeps the required properties after the machining operations are performed, avoiding changes in the microstructure or other type of damage to the material. Titanium alloys are especially sensitive to machining effects on the material so even higher attention is required for finishing operations when machining titanium alloys. It is of great interest to explore the effect of different cutting tools or parameters on the surface integrity of the machined material in order to understand the behaviour of the material.

Surface integrity assessment is typically carried out by the combination of microstructure analysis of the material, residual stress, surface roughness and micro-hardness test. It is very important to ensure a high end surface integrity in critical parts of an aircraft due to their fatigue requirements, which are reduced if a good surface integrity has not maintained. Generally, this high-end surface integrity is defined from a baseline condition analysed in a rig test, in which a single component or the whole assembly are experimentally exposed to real flying conditions with security margins.

Figure 7 shows baseline representative sub-surface microstructures of turned and milled surfaces and sub-surfaces from the case study IBR. These samples are used to validate any modifications in milling and turning finishing operations, after the component has been rig tested to fatigue and other flying conditions.

Samples in Figure 7 have been obtained from a real full scale development test part, manufactured for the component validation. This was done as part of the EngD training in the sponsor company. Both samples in Figure 7 show a very continuous microstructure through the surface and sub-surface of the material. Grains near the surface of the material are not

excessively aligned to the cut direction, which means that both milling and turning operations were gentle to the material. Typical signs of a damaged material due to abusive machining such as phase transformation, white layer, plastic deformation or cracks were not observed in the samples of Figure 7 above.



Figure 7. Samples of the sub-surface microstructure obtained from the case study component after milling (left) and turning (right) processes.

2.2 Background on surface integrity

As mentioned in section 2.1, surface integrity is generally evaluated as a sum of various measurable surface and sub-surface tests. Those are surface roughness, residual stress, micro-hardness and most importantly sub-surface microstructure. In this section, a literature search is carried out on those tests, with the objective to correlate test outcomes to the cutting parameters employed. In addition, a benchmark comparison is made between the cutting parameters found in the literature and those currently used in the manufacture of the IBR analysed in this work.

2.2.1 Surface roughness

Surface finish requirements for the IBR analysed on this case study are $R_a=0.8\mu\text{m}$ for blades and holes, whereas for the rest of the part the rejection criteria is $R_a=1.6\mu\text{m}$. These limits are established in the component drawing notes, which means that any part needs to comply with these limits in order to ship to the customer. Current finish turning operations achieve the requirements of $R_a=1.6\mu\text{m}$ but blade end milling operation does not generally reach to the requirement of $R_a=0.8\mu\text{m}$. This is due to the complexity of the blade shape coupled with the

very low thickness walls, which produce vibration issues and increase the roughness values up to $R_a=1.8\mu\text{m}$. In order to improve the surface roughness to the required limit, a costly polishing operation needs to be performed to the blades. In the following paragraphs, the effect of different parameters on the surface roughness is reviewed.

Mhamdi et al. [10] analysed the surface integrity of Ti 6-4 in ball end milling. The similarity with the process of the present study is that both use ball end mill cutters and the machined surface is concave. Regarding the surface roughness, they found that the worst area was the top of the concave surface, with a S_q roughness value of $4.7\mu\text{m}$ where the effective cutting speed was zero or near zero. In the other areas the S_q surface roughness was found to be around $3\mu\text{m}$. Another finding was the relationship between the surface roughness and the speed-feed (relative linear speed of the part with respect to the tool), where an increase from $300\text{mm}\cdot\text{min}^{-1}$ to $600\text{mm}\cdot\text{min}^{-1}$ and $900\text{mm}\cdot\text{min}^{-1}$ of the speed-feed led to a S_q value of $2.8\mu\text{m}$, $3.4\mu\text{m}$ and $4.7\mu\text{m}$ respectively.

Sun et al. [5], studied the surface integrity in end milling Ti 6-4. They proved the anisotropic nature of the surface roughness in milling and the effect of the radial depth of cut as well as the feed on the surface roughness. For the increases of 0.02mm in feed per tooth, the roughness increased generally $0.1\mu\text{m}$ in an almost linear behaviour. As for the radial depth of cut, an increase from 2mm to 6mm led to an increase of $0.6\mu\text{m}$ to $0.95\mu\text{m}$ in feed direction and $0.7\mu\text{m}$ to $0.85\mu\text{m}$ in the cutting direction. More complex seemed to be the surface speed influence on the surface roughness, which did not show any clear pattern.

The effect of the tool wear on surface roughness was analysed by Rao et al. [4], and they did not see any significant change in the roughness for different cutting speeds as the tool was wearing out (always below the rejection criteria of average flank wear less than 0.025mm). Ezugwu et al. [11] found out the same in their research work.

Nurul et al. [12] compared WC/Co inserts with PCD inserts in finish milling of Ti 6-4 as one of the points of their research focused on the evolution of surface roughness for different cutting speeds. It was observed that an increase in cutting speed from 40 to $250\text{m}\cdot\text{min}^{-1}$ produced an increase in the roughness of 0.25 to $0.75\mu\text{m}$ for both insert materials tested. The increase in roughness was reported to be due to the chatter affecting to titanium alloy machining, which was higher in the case of carbide tools comparing to PCD tools.

Che-Haron et al. [6] analysed the roughness towards the tool life and concluded that the surface finish tends to become smoother when the tool is arriving to the end of life, and then suddenly increases when the tool fails. According to the authors, the smoothing effect was probably created due to adhered material covering the cutting edge.

It can be concluded, from the comparison of different research works, that the surface roughness is negatively affected by the increase of the feed and radial depth of cut, whereas it is not very clear how it relates to the surface speed. The only clear trend showing the negative effect of surface roughness when increasing the surface speed was reported to be due to the chatter effect, which tends to appear in titanium alloy machining. If this is not taken into consideration, it is very difficult to assess the effect of the surface speed. Regarding the tool life, it was reported to have a negligible effect on the surface roughness at tools wear levels below the tool rejection criteria, showing a small improvement in surface roughness towards the end of the tool life, probably due to adhered material to the cutting edge.

2.2.2 Residual stress

J. Sun et al. [5], analysed the effect of cutting speed and feed rate on residual stresses when finish milling with solid TiAlN coated carbide tools. Surface residual stress was measured through X-Ray Diffraction (XRD) and $\sin^2\Psi$ method. They found, both for feed direction (σ_{11}) and cutting direction (σ_{22}) an increasing normal compressive residual stress up to a speed of $80\text{m}\cdot\text{min}^{-1}$, with a maximum of -350MPa for σ_{11} and -300MPa for σ_{22} . For higher speeds the compressive normal residual stress obtained was lower. The shear stress (σ_{12}) changed from tension to compression by increasing the speed, in a range from 50MPa to -50MPa , a lower magnitude comparing to the previous values. Regarding the effect of the feed, they observed that the feed (σ_{11}) and cutting (σ_{22}) direction normal residual stresses became less compressive when the feed was increased, whereas the shear residual stress (σ_{12}) became more compressive in those conditions, but in a lower magnitude than in the case of the feed and cutting directions.

The conclusions of Sun et al. [5] were that the residual stress is affected by the combined effect of the mechanical and thermal deformations, so that the compressive residual stress would increase generally with the cutting speed. However, when the cutting speed is high

(over $80\text{m}\cdot\text{min}^{-1}$) the effect of the temperature becomes higher and induces thermal deformations which leads to reduce the compressive residual stress or even to create tensile stress in high speed machining.

Rao et al. [4] based part of their research on studying the tangential component of the residual stresses in Ti 6-4 milling with uncoated carbide tools. They measured the surface and sub-surface residual stresses by X-Ray Diffraction (XRD) and $\sin^2\Psi$ method. Apart from measuring the effect of surface speed and feed, they analysed the effect of the depth of cut and the evolution of the residual stress at different depth levels of the material. As observed by Sun et al. [5], when the surface speed was increased at levels above $75\text{m}\cdot\text{min}^{-1}$ the residual stress effect was negligible given the error of measurement. The feed effect, though, gave an opposite result of that obtained by Sun et al. [5], as an increase of feed resulted in an increase of compressive residual stress. According to the authors, the increase in compressive stress happened due to the lower values of the frictional component of specific cutting pressure with increasing feed, which coupled with the cooling action resulted in a lower heat generation and, thus, led to higher compressive stresses.

Rao et al. [4] observed that when the depth of cut was increased, the residual stress became less compressive. In terms of the effect of the depth of the surface, it was observed that it was extended around $40\mu\text{m}$ below the surface of the machined part, progressively reaching to an area where the material did not suffer any stress alteration.

Another contribution of Rao et al. [4] was to analyse the effect of tool wear on the residual stresses. They found out that there was a reduction of the compressive residual stress value when the tool was gradually wearing out. According to Rao et al., this is attributed to the increasing influx of heat energy into the machined surface with increasing flank wear.

Puerta Velasquez et al. [13] conducted high speed turning tests to analyse the effect of the cutting speed on surface residual stresses. The measurements were done by Wide XRD technique, using Pearson VII functions. They found out that the normal stresses (σ_{11} and σ_{22}) were compressive up to a point around $100\text{m}\cdot\text{min}^{-1}$ and then suffered a big step to become tensile stresses for higher speeds.

In general, it is observed that residual stress is more compressive as the surface speed is increased, up to a point around 75-100m·min⁻¹ in which the thermal effect might interfere and a reduction in the compressive layer is observed or even becomes tensile stress. However, there is no clear consensus regarding the effect of the feed, which might have an important thermal component in its behaviour. Finally, depth of cut and tool wear have a negative effect in compressive stresses, as both higher depths of cut and tool wear tend to decrease the compressive layer. It is concluded that thermal energy generated in the cut is responsible of reducing compressive residual stress or even generating tensile stress.

2.2.3 Microhardness

Sun et al. [5] studied end milling and showed an increase in the hardness on the surface of the machined part (1350-1500HK) followed by a lower hardness than the bulk material in the first measurement below the surface (5µm below surface) with a stable bulk hardness of around 800HK. Even if the trend that they observed is likely to be correct, the absolute values are much higher than the typical hardness values obtained for titanium alloys, so there must be an error at some point of the study. Apart from this, they showed the effect of the temperature in the softening of the surface at high speeds, as lower hardness values were recorded for higher surface speeds.

C.H. Che-Haron et al. [6] observed a similar trend in their rough turning tests. They carried out microhardness measurements in the first 0.5mm sub-surface depth, with Vickers hardness scale, for different feed rates and obtained a very similar shaped curve but in different scales. They reported that the highest hardness value was obtained at 0.005mm beneath the surface; whereas at 0.02mm beneath the surface the hardness was lower than the average hardness, due to over aging process according to the researchers. At 0.07mm beneath the surface they observed another hardening point and then the values became lower progressively. In the finish milling tests, the hardness was very similar to the hardness of the bulk material at a depth of around 20µm. However, in the case of the rough turning, the hardness became similar to the bulk material hardness at a depth of around 0.5mm. From this data, it can be confirmed how the roughing operations affect much more than the finishing operations to the properties of the sub-surface material. This happens because the

roughing operation creates a deeper heat affected zone and there is a work hardening effect as well.

From the data provided by Che-Haron et al. [6], the hardness was very similar when the feed value was increased from $0.25\text{mm}\cdot\text{rev}^{-1}$ to $0.35\text{mm}\cdot\text{rev}^{-1}$, but the effect of the wear made a bigger difference; significantly more hardening (e.g. 30HV increase for the worn out tool at 0.08mm below the surface) was suffered when machining was carried out with worn out tools.

Ezugwu et al. [11] carried out microhardness measurements in their finish turning study with PCD tools at high cutting speeds. They analysed the effect of using high pressure coolant on different aspects of the surface integrity and they pointed out the benefits of the high pressure in machining titanium alloys. Conventional flood coolant was compared to through tool coolant at pressures of 11 MPa and 20MPa.

Results showed that there is a hardening effect of the surface when using conventional coolant supply, which is minimized when the applied coolant pressure is increased. They reported that the hardening effect was due to high plastic flow rate combined with heat generation at the primary shear zone and suggested that an efficient coolant supply condition lead to a lower heat generation and therefore lower plastic flow. They also mentioned the softening effect that other authors stated especially in the tests carried out with high pressure coolant supply, which they explained to be due probably to the tempering effect at the cutting interface.

Summarising, machining operations create a hardening effect on the surface of the machined layer, followed by a softening immediately below the surface and then reaching to the bulk hardness deeper on the material. Sub-surface softening is not desired as material properties decrease. Here, cutting conditions determine the severity in terms of the affected depth and hardness reduction of this effect. Thermal input to the material is reported to be a key factor in the surface hardening followed by subsurface softening. From this perspective, high pressure coolant has proved to be beneficial due to its higher cooling capacity compared to flood coolant.

2.2.4 Microstructure

Mhamdi et al. [10], after dry milling with a TiAlN coated carbide ball-end mill at a surface speed of $150\text{m}\cdot\text{min}^{-1}$, with a feed per tooth range from $0.05\text{--}0.15\text{mm}/\text{tooth}$ and depth of cut of 0.5mm in both axial and radial direction, observed a layer of plastically deformed material or surface drag of about $50\mu\text{m}$ in the worst case, which was registered at the top of the concave surface machined.

Sun et al. [5] observed the microstructure of Ti 6-4 after milling with TiAlN coated carbide end mill, with fresh tips at different cutting speeds. They fixed the feed ($f_z=0.08\text{mm}/\text{tooth}$) and depths of cut ($a_e=4\text{mm}$, $a_p=1.5\text{mm}$) while varying surface speeds, from $50\text{m}\cdot\text{min}^{-1}$ to $110\text{m}\cdot\text{min}^{-1}$. In general terms, the sub-surface was in good condition (free from white layer, phase transformations or distorted layers) although they reported a deformation in β phase and a lower β phase level when the tested speed was $80\text{m}\cdot\text{min}^{-1}$ and higher.

Part of the work done by Puerta Velasquez et al. [13] was focused on the microstructure evaluation of high speed turned Ti 6-4 surface. They observed an affected material zone for extremely low and high surface speeds tested ($20\text{m}\cdot\text{min}^{-1}$ and $260\text{m}\cdot\text{min}^{-1}$). They tried to differentiate three areas in the sub-surface of the material in order to assess the sub-surface of the material; an area called P3 which is clearly distorted, followed by a second area P2 which is a transition area with slightly distorted layer and finally P1 area, which has the properties of the bulk material. For both cutting speeds, the P3 area showed a heavy surface drag, elongating and aligning the grains parallel to the surface. They reported that the P3 area could take a depth between $1\text{--}5\mu\text{m}$. The P2 area was reported to be $5\text{--}60\mu\text{m}$ in depth following to the P3 and both tested cutting speed showed an orientation of the grains in the cutting direction. They suggested that the affected area (P3+P2) is higher as the cutting speed is increased.

In another study, microstructure was analysed after rough turning in dry cutting conditions and using uncoated carbides [6]. Two tests were carried out; the first at a surface speed of $V_c=45\text{m}\cdot\text{min}^{-1}$ and a feed of $f=0.35\text{mm}\cdot\text{rev}^{-1}$ and the second at $100\text{m}\cdot\text{min}^{-1}$ and a feed rate of $0.25\text{mm}\cdot\text{rev}^{-1}$. Pictures of the microstructure were taken when the tools were fresh and when the tools were nearly worn out.

The authors reported that when turning was carried out under dry conditions, a thin layer of plastically deformed layer of around $1\mu\text{m}$ to $2\mu\text{m}$ was formed immediately underneath the machined surface.

Ezugwu et al. [11] finish turned Ti 6-4 using PCD tools at a feed rate of $0.15\text{mm}\cdot\text{rev}^{-1}$, depth of cut of 0.5mm and surface speed range of $175\text{-}250\text{m}\cdot\text{min}^{-1}$, employing higher coolant pressure as the surface speed was increased. The resultant microstructure, revealed no evidence of sub-surface defects such as cracks, laps, tearing or plastic deformation.

Although research studies reviewed in the literature were Ti6-4 alloy, microstructure variations are expected due to the manufacturing process of the raw material. However, a general detrimental effect in sub-surface microstructure is observed for higher surface speeds as well as for higher feeds. The temperature generated in the cutting zone is reported to be responsible for the sub-surface deformation as it shows the fact that using high pressure coolant can counteract the heat generated due to higher surface speed and reduce sub-surface damage.

2.2.5 Benchmark on cutting variables

Lopez de lacalle et al. [14] studied the effect of surface speed, feed, depth of cut and clearance angle on tool life, using uncoated carbide solid tools. Different tests were carried out with one variable parameter in each test and simulating a rough milling operation; The first test was performed with a fixed feed value ($0.15\text{mm}/\text{tooth}$), a tool diameter of 20mm , three teeth, a_e of 5mm and a_p of 3mm . Different surface speeds were tested ($40\text{m}\cdot\text{min}^{-1}$ – $80\text{m}\cdot\text{min}^{-1}$) and it was found out that the speed was between $60\text{m}\cdot\text{min}^{-1}$ and $70\text{m}\cdot\text{min}^{-1}$ in order to cut for about 15 minutes before reaching tool life rejection criteria.

For the next test, different feed values were tested ($0.08\text{mm}/\text{tooth}$ – $0.25\text{mm}/\text{tooth}$) and three surface speeds ($40, 50, 60\text{m}\cdot\text{min}^{-1}$). It was observed that the optimum feed for all the speeds was very close to $0.12\text{mm}/\text{tooth}$. So, according to the research, surface speeds of no more than $60\text{-}65\text{m}\cdot\text{min}^{-1}$ would be required to get a tool life of at least 15 minutes. This could be combined with a feed of $0.12\text{mm}/\text{tooth}$, three teeth, diameter= 20mm , $a_e=5\text{mm}$ and $a_p=3\text{mm}$.

An interesting contribution was done by Rao et al. [4] regarding the finish milling cutting parameters. They carried out a face milling operation with a single uncoated carbide insert mounted in the face milling tool, a light feed of 0.05mm/tooth, an a_p of 0.76mm and full radial engagement. Surface speeds were tested from 76.2m·min⁻¹ to 182.9m·min⁻¹. Acceptable tool life was obtained at the speed of 99.1m·min⁻¹, which worked below 0.02mm flank wear for slightly more than 30 minutes.

As mentioned above, it is complicated to compare milling operations taking into account that the research is generally performed in straight cuts, whether in face milling or shoulder milling operations. The machining behaviour is much more complex when milling components in a 5 axis milling strategy. In addition, stiffness of the base material has to be taken into account when milling compressor blades, which changes at different depths and this introduces another variable to the process.

The closest research work to the current case study was performed by Kuljanic et al. [15], who analysed the performance of end milling Ti 6-4 compressor blades. However, they only used PCD cutters in their test compared to the WC/Co (Carbide) tools used in the production of the case study IBR. Another difference is that they used an inserted tool, comparing to the custom solid tool used in the case studied IBR. After some initial speed, feed and depth of cut tuning tests, all the time using the same tool (end milling cutter with 3 PCD inserts), they chose the following parameters; Surface speed ($V_c=108\text{m}\cdot\text{min}^{-1}$), feed per tooth ($f_z=0.135\text{mm}$), axial depth of cut ($a_p=0.2\text{mm}$) and radial depth of cut ($a_e=5\text{mm}$). Setting the blade surface roughness requirement as the tool rejection criteria, they achieved a tool life of 381min.

Providing that both blade milling cases are end milling operations and they are of very similar shape, the best indication of the performance can be obtained by comparing the MRR (Material Removal Rate) which is the time in which a certain volume of the material is cut in the machining process. Regarding to the research work carried out by Kuljanic et al. [15], the material removal rate they machined at was 0.44cm³/min. This number comes from multiplying the cross section of the cut with the table feed or part's relative speed to the tool. For the current end blade milling process, the MRR obtained was 0.31cm³/min. A very significant difference in MRR was achieved, so that the process in the case study is lower in terms of performance. Taking into account only the depth of cut that the tool is moved from

pass to pass in the same blade, the results were the following; $21.75\text{cm}^2/\text{min}$ for the research study and $2.09\text{cm}^2/\text{min}$ for the end milling process in the case study. This means, if both processes would leave the same stock material for the last pass, then the productivity of the research study would be ten times higher. Even if a huge difference was found between the two processes, it has to be pointed out that the research work was probably carried out in parts formed just by blades, which gives higher accessibility to the tools comparing to the IBRs.

Table 1 shows the summary of the cutting parameters for milling and turning discussed in section 2.2:

Table 1. Comparison of the cutting parameters employed in this case study against the cutting parameters employed by different authors in their research studies.

Source	Tool type	Surface speed ($\text{m}\cdot\text{min}^{-1}$)	Feed ($\text{mm}\cdot\text{rev}^{-1}$) or (mm/tooth)	DoC (mm)	Cutting distance /time
Turning					
Roughing					
Case study IBR	Various	40-60	0.2-0.3	1-2	15-30 min
Mann and Taylor [9]	CNMG uncoated carbide	72	0.1	2	15 min
Che-Haron et al.[4]	CNMG uncoated carbide	45	0.25	2	27 min
Finishing					
Case study IBR	Various	35-60	0.1-0.3	0.25-0.5	10-30 min
Ribeiro et al.[3]	VBMT coated carbide	90	0.1	0.5	300meters
Ezugwu et al. [17]	PCD	200	0.15	0.5	50 min
Milling					
Roughing					
Case study IBR	$\varnothing 25\text{mm}$ inserted, 2 flutes, coated carbide	51	0.19	$a_p=5$; $a_e=$ fully engaged	175 min
Finishing					
Case study IBR - blades	$\varnothing 6.35\text{mm}$ solid, 4 flutes, coated carbide	32-80	0.11	$a_p=0.3$; $a_e=1.5$	522 min
Lopez de lacalle et al. [13]	$\varnothing 20\text{mm}$ solid, 3 flutes, uncoated carbide	60-65	0.15	$a_p=3$; $a_e= 5$	15 min
Rao et al. [2]	inserted, 1 flute, uncoated carbide	99	0.05	$a_p=0.76$; $a_e=$ fully engaged	30 min
Kuljanic et al. [7]	$\varnothing 32\text{mm}$ inserted, 3 flutes, PCD	108	0.135	$a_p=0.2$; $a_e= 5$	381 min

2.2.6 Summary of literature

A literature search has been conducted about the effect of different cutting parameters on the main indicators of surface integrity, which are surface roughness, residual stress, microhardness, and microstructure. As cutting parameters such as surface speed, feed, depth of cut are increased, generally surface integrity suffers deterioration. Moreover, surface integrity is particularly affected by the heat generated in the cutting zone. In this respect, improved cooling methods, such as the use of high-pressure coolant and also cutting with enhanced wear resistant tools, help towards keeping the condition of the surface and sub-surface of the machined material.

There are not much research works in the literature suitable for a benchmark comparison, especially for a back-to-back comparison with the case study IBR. However, information searched about experimental work carried out on Ti6-4 and especially on blade finishing operations, shows the following:

- Feed per tooth in the case study is generally within the literature tested feed region.
- There is a wide range in surface speed, but literature shows some experimental work carried out at considerably higher surface speeds compared to the baseline case study.
- Baseline depth of cut in turning is within the range found in literature, although finish milling is carried out with much lower depths of cut. This is partly due to the geometry requirements of the blades, which limits to use higher depth of cut techniques. This also affects to the MRR, which is much lower compared to a blade finish milling operation from other research work, although probably because it is not so restricted from blade geometry. In this respect, tool life or cutting time achieved per tool is higher for the case study IBR finish milling.

2.3 Experimental approach

In Section 2.2, a literature review about the effects of different cutting parameters on the surface integrity has been carried out, and a benchmark study comparing baseline parameters with the state of the art. Results suggest that the surface speed used in the case study IBR is

in the lower end of the typical range found in literature. Same happens with the depth of cut, although as mentioned in Section 2.2, this is partly limited due to the cutting strategy. As far as feed per tooth is concerned, baseline parameters are within the typical range, although testing top of the range values is considered very interesting due to the potential MRR gains associated to high feed per tooth.

An experimental approach is followed to better understand the finish milling process and its relation to the surface integrity of the finished part [16]. The reason to carry out an experimental testing is the sensitivity of the surface integrity found in literature, which is affected by the cutting zone temperature, related not only to the parameters but also to the tool material, tool wear or coolant delivery method. Therefore, It has been decided to analyse the effects of a given set of representative variable parameters on the surface integrity of the workpiece material to observe the limitations of the process. Cutting parameters used in current blade finish milling have been selected together with a range of higher cutting parameters, which have been chosen based on a literature review of surface integrity in milling operations [17] as well as the limits established by the machine and the milling process.

The aim is to keep the trials as similar to the blade finish milling process as possible; this is achieved by using the same tool, material, tool path strategy, machine and cutting fluid conditions of those used in current blade finish milling process. However, it has been decided to use a rigid workpiece at this stage, instead of machining directly into a blade shape. This is done in order to remove the dynamic behaviour of the flexible part, so that the relationship between the cutting parameters and the surface integrity is easier to identify. A rounded, oval shaped part has been used to machine each condition, during enough time to create a surface which allows access to a portable surface roughness measurement device and provides a big enough surface to cut and prepare metallographic samples. Cutting times are ranging from 70 to 340 seconds depending on the surface speed and feed employed for a given condition. The milling machine is a Hermle C50 five axis milling centre. The outputs from the experimental testing are those focused to understand the process and the relationship between the cutting parameters and the surface integrity. To do so, cutting forces, tool wear, topography, surface roughness, micro hardness and sub surface microstructure are measured. Residual stresses are not in the scope of this preliminary study because more

affordable tests are valid to understand the overall surface integrity condition. In any case, surface integrity can be fairly good assessed with the rest of the tests carried out in this study.

2.3.1 Method

This section explains the method followed to carry out the experimental tests.

Machine, cutting tool and coolant

A five axis Hermle C50 CNC milling machine (Figure 8) is used to perform the trials. The machine provides a maximum spindle speed of 18000 rpm and high pressure through tool coolant capacity. The selected tool is a $\varnothing 6.35$ mm coated carbide tapered ball end mill containing four flutes and a 55° helix angle design, coupled with an HSK 100 tool holder. A combination of high pressure and flood coolant are applied to the cutting zone, replicating the method used in the IBR finish milling. High pressure coolant is applied through tool directly to the flutes of the tool with a pressure of 70 bar coming out from the pump and flood coolant is also directed to the tool tip.



Figure 8. Hermle C50 five axis milling machine.

Workpiece

Small blocks of Ti 6-4 in solution treated and annealed condition are used as a workpiece, with the size of 70x30x22mm (*lengthxwidthxheight*) and oval shape (Figure 9). They are cut by EDM from a bigger forging part and three holes are drilled in order to bolt them to the dynamometer.



Figure 9. Workpiece fixed and ready for the machining trial.

Two sources of material are used in the machining trials; from one side, a custom forging (which is used as raw material to manufacture blisks) and from the other side a forged billet. Both supplied by different companies but following the same heat treatment process; solution treated and annealed. Table 2 and Table 3 show the chemical composition and mechanical properties of both materials, respectively.

Table 2. Composition of the two tested materials: custom forging currently employed and a forged billet.

		Content of elements (%)										
		Al	V	Fe	Si	O	C	Cu	N	H	B	Y
Custom forging	Top ingot	6.54	4.02	0.21	0.015	0.188	0.004	0.0053	0.003	0.0012	<0.001	<0.001
	Bottom ingot	6.50	4.04	0.21	0.015	0.2	0.003	0.0055	0.002	0.001	<0.001	<0.001
Forged billet	Ingot	%	%	ppm	ppm	ppm	ppm	ppm	ppm	ppm	ppm	ppm
	Value	6.23	3.83	1448		1847	155		52			10

Table 3. Mechanical properties of the tested material.

	Mechanical properties	
	Custom forging	Forged billet
Ultimate tensile strength (MPa)	1004.35	948.4
Yield strength (MPa)	918.01	860.3
Elongation (%)	16.19	14.25

Machine set-up

The set-up of the machine for the trials is as similar as possible to the set up used for blade finish milling when manufacturing blisks. The bed of the machining centre is turned 90° in A axis and a 90° angle plate is fixed to the bed so that the dynamometer can sit on the angle

plate while keeping parallel position to the floor, as it is shown in Figure 10. The workpiece is then fixed and positioned to the dynamometer with three bolts.



Figure 10. Set up of the trials. Machine's A axis rotated at 90° and angle plate fixed to the bed also at 90° in order to hold the dynamometer and the part in a horizontal initial position.

Due to the A and C axis rotational movement during the cut, the cables coming out from the dynamometer have to be carefully handled in order to avoid any cable damage caused by the extension of the cables. Therefore, cables are tied around the bed and the angle plate creating a proper configuration for strain relieving and then they are passed through the door, to the outside of the machine to connect to the rest of the hardware.

Cutting approach

Point milling strategy is performed in order to simulate the cutting path of a blade. The tool is positioned with a lead angle of 30° and a tilt angle of -20° relative to the workpiece and the toolpath follows the oval shape of the workpiece moving downwards in vertical direction following a helical path. After the initial engagement to the material, the tool continues engaged in the cut until a minimum of 5mm of vertical machined surface is created (this is the minimum space required to perform the sub-surface microstructure analysis).

Each workpiece take two machining conditions; after the first condition is machined, the workpiece is turned around and a new condition is machined.

Cutting variables

A total of 24 conditions are machined, including as variable parameters the surface speed (V_c), feed per tooth (f_z), the step over (s) the cutting depth (a_p), the material and the wear level of the tool (worn out tool meaning tool reaches to the end of life according to current process). Table 4 shows the experimental sheet:

CHAPTER 2. EFFECT OF CUTTING VARIABLES ON SURFACE INTEGRITY

Table 4. Selection of variable parameters and total number of conditions tested in the machining trials.

Order	Vc (m/min)	fz (mm/tooth)	s (mm)	a (mm)	Tool wear	Material
1	32	0.109	0.3	1.5	Brand new	Custom forging
2	32	0.109	0.3	1.5	Worn out	Custom forging
3	32	0.109	0.3	1.5	Brand new	Forged billet
4	32	0.109	0.3	1.5	Worn out	Forged billet
5	60	0.058	0.3	1.5	Brand new	Custom forging
6	60	0.109	0.3	1.5	Brand new	Custom forging
7	60	0.2	0.3	1.5	Brand new	Custom forging
8	60	0.3	0.3	1.5	Brand new	Custom forging
9	170	0.058	0.3	1.5	Brand new	Custom forging
10	170	0.109	0.3	1.5	Brand new	Custom forging
11	170	0.2	0.3	1.5	Brand new	Custom forging
12	170	0.3	0.3	1.5	Brand new	Custom forging
13	240	0.058	0.3	1.5	Brand new	Custom forging
14	240	0.109	0.3	1.5	Brand new	Custom forging
15	240	0.2	0.3	1.5	Brand new	Custom forging
16	240	0.3	0.3	1.5	Brand new	Custom forging
17	240	0.3	0.3	1.5	Brand new	Forged billet
18	170	0.109	0.1	1.5	Brand new	Custom forging
19	170	0.2	0.1	1.5	Brand new	Custom forging
20	240	0.109	0.1	1.5	Brand new	Custom forging
21	240	0.2	0.1	1.5	Brand new	Custom forging
22	170	0.109	0.3	0.5	Brand new	Custom forging
23	170	0.2	0.3	0.5	Brand new	Custom forging
24	240	0.109	0.3	0.5	Brand new	Custom forging

The ranges of the variable parameters selected for the tests are different in each case, which means that the comparisons can't be made back to back. For any comparison to be made, the contribution of each variable to the material removal rate (MRR) is considered. Table 5 shows the contribution of each parameter to the increment of the baseline MRR.

Table 5. Range of variable cutting parameters tested.

Variable parameter	Minimum range	Maximum range	MRR (x times)
f _z (mm/tooth)	0.058	0.3	5.17
V _c (m/min)	60	240	4
s (mm)	0.1	0.3	3
a (mm)	0.5	1.5	3

In Table 5, it can be observed that the feed per tooth is the variable that most contributes to increase the productivity when the highest value of its range is selected. Following to the feed, the surface speed is the next in terms of MRR increment and finally both depths of cut at the same rate.

Cutting force measurement

Cutting forces are measured during the machining time. In order to do so, a three component (F_x , F_y , F_z) dynamometer, KISTLER 9257B is used. The data is collected connecting the dynamometer to the charge amplifier KISTLER 5070 and this to the data acquisition system KISTLER 5697 to transfer the information to the PC.

2.3.2 Results

Tool wear

Tool wear has been analysed for each condition at the end of the cutting test. A brand new tool has been used for each cutting condition (except the three conditions performed with worn out tool). Flank face has been evaluated and pictures of it taken in a Stemi Zeiss optical microscope, to measure tool wear. The minimum industrial requirement in the finish milling process for the tool is to last at least one complete blade before it reaching to the wear limit. This is to avoid mismatches in the finished blade geometry. A very low or even no wear after these tests is not very representative, due to the cutting time being very short compared to the time employed to finish mill a blade. However, if a tool shows a considerable wear or damage after the completion of the test, that means, this particular tool together with the given cutting parameters is not capable of machining at least one blade under the required conditions.

Figure 11 shows tool wear for a selection of representative cutting conditions:

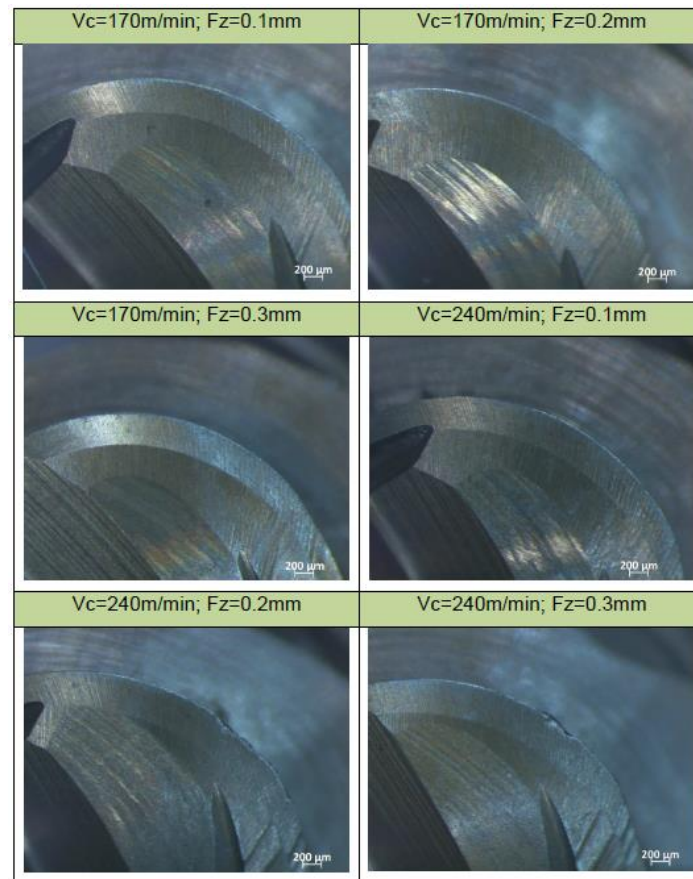


Figure 11. Tool wear after the completion of the cutting trial at different cutting conditions.

Figure 11 shows six images of the flank of a tooth, each image corresponding to different cutting conditions and therefore different tools. It can be clearly appreciated that the first four images show a very similar flank wear, which goes from $11\mu\text{m}$ to $13\mu\text{m}$. That is a very low wear, which develops soon after starting to cut at almost any cutting conditions. The rest of the conditions which employ lower parameters are also analysed and the wear level is very similar to the first four pictures shown in Figure 11. As mentioned before, wear level does not give much information, considering the short cutting time of the tests compared to the requirements to machine at least one complete blade. However, a significantly higher tool wear has been found in the images shown at the bottom of Figure 11, which belong to the two most demanding cutting conditions tested; the image at the bottom left corresponds to a surface speed of 240m/min and a feed per tooth of 0.2mm . A flank wear of $75\mu\text{m}$ has been measured whereas the image at the bottom right corresponds to a surface speed of 240m/min and a feed per tooth of 0.3mm in which a maximum wear of $72\mu\text{m}$ has been measured after 67 seconds machining time. Looking at the wear patterns, it looks like a notch

wear is developing; especially for the latter case, and this wear type is very prejudicial to finish milling operations as they produce uneven surfaces.

It is clear, from the tool wear point of view, that the highest cutting conditions tested and referred in the paragraph above are not capable of finish milling one or more blades within an acceptable tool edge condition, so that lower cutting parameters need to be employed in the finish milling process.

Cutting force analysis

Maximum cutting forces are found for each condition tested and the variations in the cutting forces for different variable parameters are collected. A comparison has been made and the effect of each variable is evaluated.

Force signal is collected for the length of the whole cut for each condition, which means that the oval shape of the workpiece is recorded for several cycles. It is found that the machine has limitations to keep the feed constant while cornering through the oval shape, so it has been decided to analyse the cutting force data obtained from the middle of one of the straight lines, for five different cycles after the tool is completely engaged, and calculate the average of the maximum values found in each cycle. The results are plotted showing the effect of the different variables in the maximum forces.

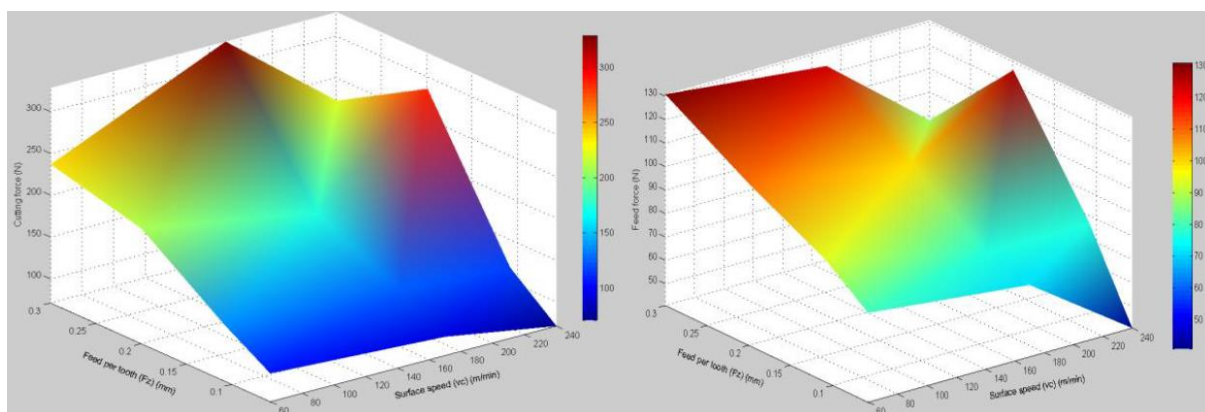


Figure 12. Cutting force (left side) and feed force (right side) plotted for two variables; Surface speed and feed per tooth.

Each of the graphs plotted in Figure 12 show a set of twelve data points, plotted on a 3D surface type graph. The plot on the left hand side shows the cutting force, whereas the plot

on the right hand side shows the feed force. Surface speed (60m/min, 170m/min, 240m/min) and feed (0.058mm, 0.109mm, 0.2mm, 0.3mm) are compared in both plots.

The first fact is that cutting force is always higher than the feed force for all conditions tested. Analysing the effect of the feed per tooth, a clear ascending trend in forces is observed for higher feed values. There is one data point which does not follow this trend; the peak observed at 0.2mm feed per tooth at the highest speed. This peak clearly breaks the general trend for both, the cutting force and the feed force. Percentages of the force increase, from lowest to highest values of feed can be seen in Table 6. Cutting force is increased in the range of (126% - 251%) whereas the feed force is increased in the range of (66% - 116%).

Table 6. Variation in force level from lowest to highest feed per tooth conditions.

Effect of Fz in forces when increasing from 0.058 to 0.3mm						
Vc	Cutting force			Feed force		
	Fz-0.058	Fz-0.3	diff. (%)	Fz-0.058	Fz-0.3	diff. (%)
60	104.87	236.79	125.79	78.86	130.69	65.72
170	93.48	328.24	251.13	71.46	123.44	72.74
240	71.14	222.6	212.90	40.87	88.15	115.68

Observing the evolution of the force for different surface speeds, it can be noticed that generally forces decrease slightly as surface speed is increased although the effect is small compared to that produced by the feed per tooth. There are two exceptions that don't follow this trend; at 170m/min when the feed is 0.3mm (which shows an increase only in the cutting force) and at 240m/min when the feed is 0.2mm (increase in both cutting force and feed force). The mentioned exception points are easily recognizable through the two peaks in the cutting force graph and the peak in the feed force graph. As in the previous case, the data obtained for these points is very consistent, which means that it is not likely to be a measurement error. Table 7 shows the percentage difference in forces when the Vc is increased from the min. to the max. value. If the unexpected data point is not considered, the cutting force drops (6% - 32%) and the feed force drops (17% - 48%).

CHAPTER 2. EFFECT OF CUTTING VARIABLES ON SURFACE INTEGRITY

Table 7. Variation in force level from lowest to highest surface speed conditions.

Effect of Vc in forces when increasing from 60 to 240m/min						
	Cutting force			Feed force		
Fz	Vc-60	Vc-240	diff. (%)	Vc-60	Vc-240	diff. (%)
0.058	104.87	71.14	-32.16	78.85	40.87	-48.17
0.1	138.67	116.28	-16.15	92.92	76.73	-17.42
0.2	208.77	285.39	36.70	109.59	126.45	15.38
0.3	236.79	222.6	-5.99	130.69	88.15	-32.55

The effect of depth of cut has also been analysed; from one side the total cutting depth and from the other side the step over depth for each pass. The two plots on the top of Figure 13 show the effect of the step over in the forces, whereas the two graphs on the bottom of Figure 13 show the effect of the cutting depth over the forces.

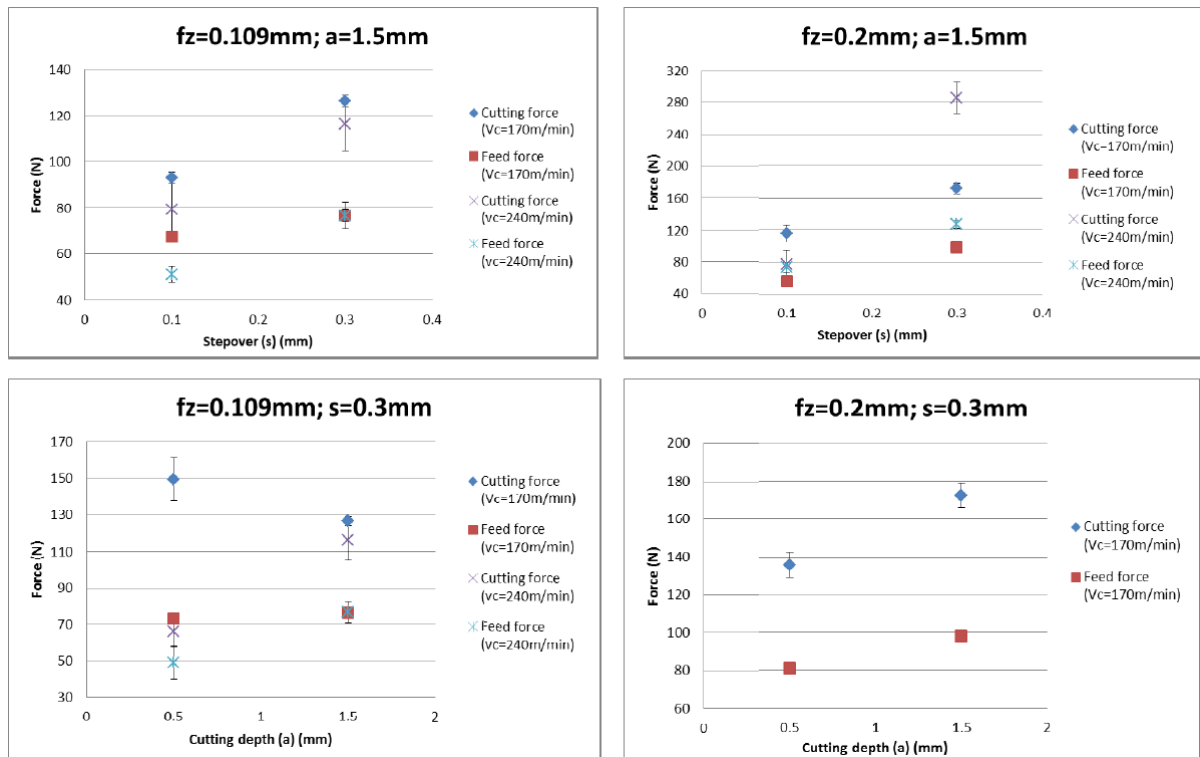


Figure 13. Set of plots showing the evolution of forces (cutting force and feed force) for step over and cutting depth variations. Plots on the top of the figure show the cutting force and feed force for the step over variable while the plots on the bottom show the forces for the cutting depth variable.

Starting with the step over, for all different conditions tested, the higher the step over, the higher the forces are. This can be seen in Table 8; the cutting force is increased in a range of (36% - 50%) and the feed force is increased in a range of (13% - 77%). Same happens with the cutting depth, with the exception of the cutting force observed at 0.5mm cutting depth and 170m/min, in the bottom left hand side graph, in Figure 13. Table 9 shows that cutting force

grows (27% - 76%) while the feed force grows (21% - 57%). The percentage gaps show general trends, but the gaps are too wide for most of the variables to make any specific conclusions.

Table 8. Variation in force level from lowest to highest step over conditions.

Effect of step over (s) in forces when increasing from 0.1 to 0.3mm						
	Cutting force			Feed force		
Vc/Fz	SO-0.1	SO-0.3	diff. (%)	SO-0.1	SO-0.3	diff. (%)
170/0.1	93.02	126.4	35.88	67.49	76.58	13.47
240/0.1	79.46	116.28	46.34	51.08	76.73	50.22
170/0.2	114.9	172.5	50.13	55.72	98.43	76.65
240/0.2	77.59	285.39	267.82	73.35	126.45	72.39

Table 9. Variation in force level from lowest to highest step over conditions.

Effect of cutting depth (a) in forces when increasing from 0.5 to 1.5mm						
	Cutting force			Feed force		
Vc/Fz	CD-0.5	CD-1.5	diff. (%)	CD-0.5	CD-1.5	diff. (%)
170/0.1	149.64	126.4	-15.53	73.29	76.58	4.49
240/0.1	66.11	116.28	75.89	48.94	76.73	56.78
170/0.2	135.86	172.5	26.97	81.09	98.43	21.38

The trends observed in Figure 12, related to the effect of the surface speed and feed per tooth are also confirmed here, although the surface speed shows a couple of exceptions in the top right plot of Figure 13; one is the cutting force at 240m/min and 0.3mm step over and the other one is the feed force trend, which is higher for 170m/min in comparison to 240m/min.

Cutting forces have also been analysed in order to compare both tested materials. Only two conditions have been compared, the higher and the lower ends of the speed / feed combinations (Figure 14). Both materials perform similarly in terms of cutting and feed forces, although the forged billet requires slightly less forces to be machined. This result is in correlation with the mechanical properties presented above, as the forged billet has a lower yield strength compared to the custom forging.

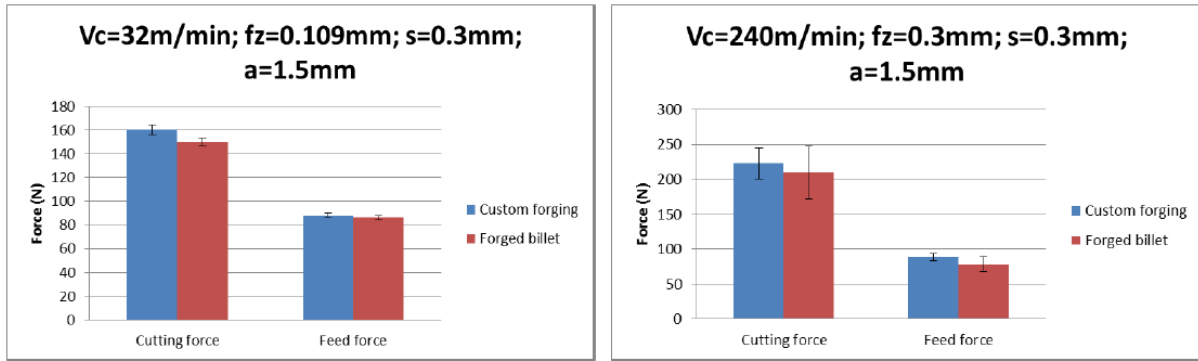


Figure 14. Cutting force and feed force for the two tested materials (custom forging and forged billet) for lowest test condition (left hand side) and highest condition (right hand side).

The plots in Figure 14 show a decrease in cutting forces of 6.3% and 5.9% for the lowest and the highest parameters respectively, where the forged billet is the material that shows the lowest force values, as commented in the paragraph above. The same happens for the feed force, although in this case the cutting forces are 1.6% and 11.3% lower when machining the forged billet, for the lowest and highest parameters respectively.

Surface roughness

Surface roughness has been measured on the machined surface of all conditions. A portable MITUTOYO roughness measurement device has been employed and a set of six measurements have been taken to obtain the average and standard deviation values. Measurements are carried out in both, feed direction and step over direction. Figure 15 shows the set-up of the surface roughness measurement.



Figure 15. Set up of the surface roughness measurement test. Workpiece held in a small vice and the machined face looking upwards while the roughness tester analyses the surface generated.

Roughness results are analysed in a similar way to the cutting force results, plotting the effects of surface speed and feed in a 3D graph and 2D graphs showing the effects of cutting depth

and step over. Overall, very high surface roughness values are obtained for a finish milling operation; Recorded roughness (R_a) values are in the range of $0.76\mu\text{m}$ and $4.19\mu\text{m}$ for the step over direction and in the range of $0.73\mu\text{m}$ and $3.13\mu\text{m}$ for the feed direction. IBR blades are typically limited to $0.8\mu\text{m}$ R_a value, which is usually reached through hand polishing or vibro-finishing methods. However, it is not productive to hand polish or vibro-finish from high surface roughness values (i.e. more than $R_a 1.6\mu\text{m}$). This means that most of the readings obtained in this project would be above the roughness limit criteria. Understanding the reason why the roughness levels are so high and reducing those to acceptable limits while productivity is increased is be one of the keys for the success of the finish milling operation in IBR blades.

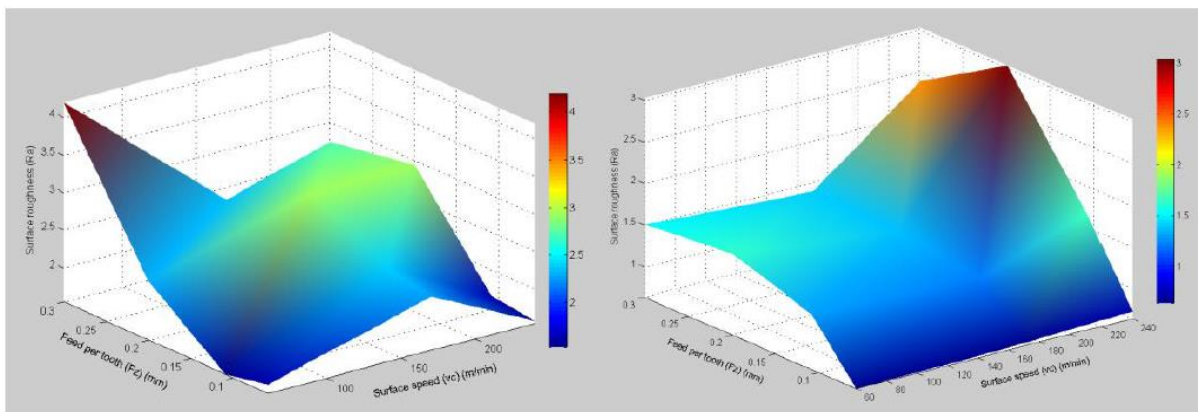


Figure 16. Roughness in the step over direction (left hand side graph) and feed direction (right hand side) plotted for two variables; Surface speed and feed per tooth.

The plots in Figure 16 show the evolution of the surface roughness for various surface speed and feed per tooth conditions; the plot on the left hand side collects the information of the step over direction, whereas the plot on the right hand side collects the information of the feed direction.

Analysing the step over direction it is difficult to obtain any conclusion; a very high peak of $R_a=4.19\mu\text{m}$ can be observed at the lowest speed and highest feed combination. The surface speed and the feed should not have an important effect in the step over direction, as this is mainly regulated by the amount of vertical displacement of the tool. Apart from the high peak mentioned before, it can be observed that the lowest feed values are the best in terms of roughness in step over direction, independently of the surface speed combination.

Roughness in feed direction is plotted in the right hand side graph of Figure 16. For low and medium speeds, a clear trend can be observed; from 0.058mm to 0.1mm the roughness is increased considerably, but for the following steps in feed (from 0.1 to 0.2 and from 0.2 to 0.3) this increase is less pronounced. These results suggest optimum performance when lowest feed and highest surface speed are employed. The graph also shows two big peaks and a third point which is higher than expected; those three points, which correspond to the surface speed of 240m/min, are in the same tooth pass frequency. This can be an indicative that the mentioned tooth pass frequency might be interfering with one of the tool’s modes of vibration, by producing resonance or it could also be due to the chatter effect.

Table 10. Variation in roughness from lowest to highest surface speed conditions.

Effect of Vc in roughness when increasing from 60 to 240m/min						
	Step over direction			Feed direction		
Fz	Vc-60	Vc-240	diff. (%)	Vc-60	Vc-240	diff. (%)
0.058	1.66	1.57	-5.42	0.64	0.73	14.06
0.1	1.54	1.64	6.49	1.3	1.67	28.46
0.2	2.32	2.93	26.29	1.62	3.03	87.04
0.3	4.19	2.74	-34.61	1.51	2.39	58.28

Table 10 shows the percentage increase or decrease that the surface speed produces in the surface roughness. Step over direction is not showing any response to the Vc, as sometimes it increases the roughness and sometimes it decreases (-35% to 26%). However, the roughness in feed direction increases clearly with the Vc (14% to 87%).

In terms of the feed, Table 11 confirms that feed has a bigger effect than Vc. Surface roughness is increased (4% to 152%) in step over direction whereas a bigger increase can be seen in the feed direction (109% to 227%).

Table 11. Variation in roughness from lowest to highest feed per tooth conditions.

Effect of Feed per tooth in roughness when increasing from 0.058 to 0.3mm						
	Step over direction			Feed direction		
Vc	Fz-0.058	Fz-0.3	diff. (%)	Fz-0.058	Fz-0.3	diff. (%)
60	1.66	4.19	152.41	0.64	1.51	135.94
170	2.25	2.33	3.56	0.67	1.4	108.96
240	1.57	2.74	74.52	0.73	2.39	227.40

Cutting depth follows an unexpected trend for all but one condition, as it can be seen in both graphs on the top of Figure 17. Higher cutting depths result in a lower roughness in both, step over and feed direction. The only condition in which the opposite trend is observed belongs

to the step over direction when machined at $V_c=170\text{m/min}$ with $f_z=0.109\text{mm}$. This unexpected trend is analysed in the discussion section below.

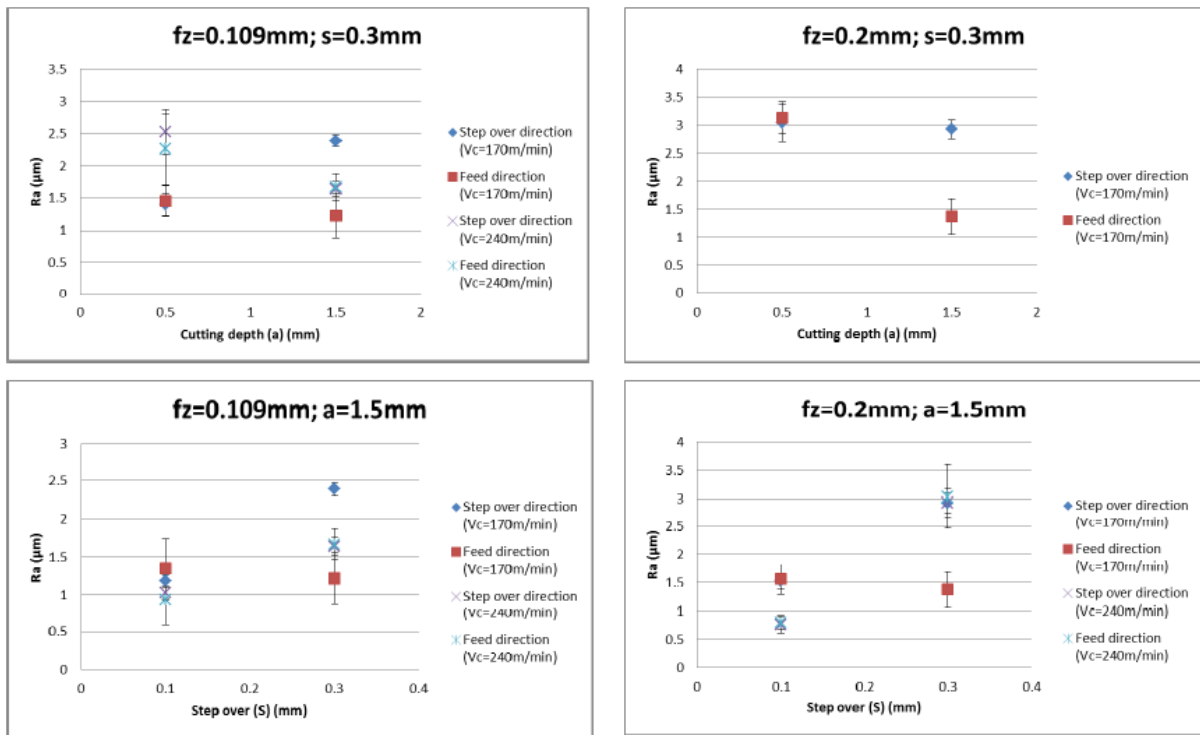


Figure 17. Set of graphs showing the evolution of surface roughness in step over and feed direction for cutting depth and step over variations. Graphs on the top of the figure show the surface roughness for the cutting depth variable while the graphs on the bottom show the roughness for the step over variable.

Table 12 shows a decrease in roughness when a higher cutting depth is employed; (-4% to -35%) for step over direction, with the exception of the previously mentioned condition, and a reduction (-16% to -56%) for feed direction.

Table 12. Variation in roughness from lowest to highest cutting depth conditions.

Effect of cutting depth in roughness when increasing from 0.5 to 1.5mm						
	Step over direction			Feed direction		
V_c/F_z	CD-0.5	CD-1.5	diff. (%)	CD-0.5	CD-1.5	diff. (%)
170/0.1	1.4	2.39	70.71	1.45	1.22	-15.86
240/0.1	2.53	1.64	-35.18	2.26	1.67	-26.11
170/0.2	3.04	2.92	-3.95	3.13	1.37	-56.23

When the step over parameter is increased, the roughness gets higher values in step over direction but not always in feed direction (bottom graphs, Figure 17). Table 13 shows the percentage increase/decrease recorded when the step over is changed from 0.1mm to 0.3mm. In step over direction a clear increase can be seen (59% to 286%) whereas the feed does not provide any clear picture (-10% to 279%).

CHAPTER 2. EFFECT OF CUTTING VARIABLES ON SURFACE INTEGRITY

Table 13. Variation in roughness from lowest to highest step over conditions.

Effect of step over in roughness when increasing from 0.1 to 0.3mm						
Vc/Fz	Step over direction			Feed direction		
	SO-0.1	SO-0.3	diff. (%)	SO-0.1	SO-0.3	diff. (%)
170/0.1	1.19	2.39	100.84	1.35	1.22	-9.63
240/0.1	1.03	1.64	59.22	0.94	1.67	77.66
170/0.2	1.52	2.92	92.11	1.56	1.37	-12.18
240/0.2	0.76	2.93	285.53	0.8	3.03	278.75

Regarding to the material comparison, the graphs in Figure 18 show that the roughness in both, step over and feed direction follows the same trend observed with the forces; the forged billet, which requires lower forces to be machined, also show a lower surface roughness. Looking at the percentages, a variation from 12.9% to 8.8% is recorded in step over direction between the two materials and a variation from 24.4% to 1.3% in feed direction. Highest percentages in both cases belong to the lowest parameter condition; however, more than just four data points are needed to see if this is a real trend.

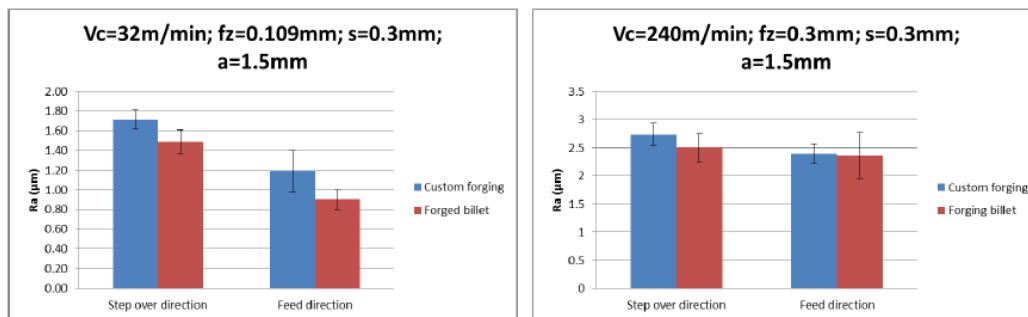


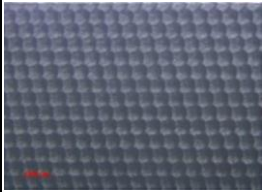
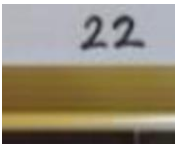
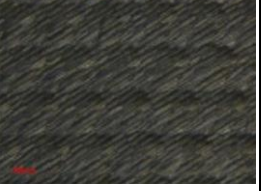
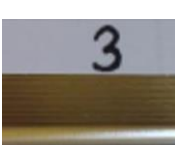
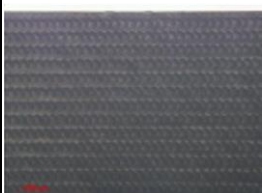
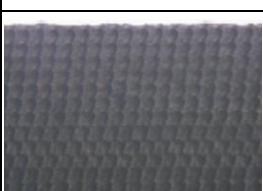
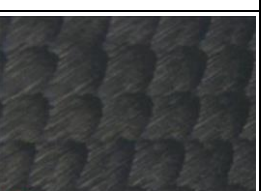
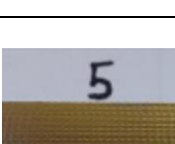
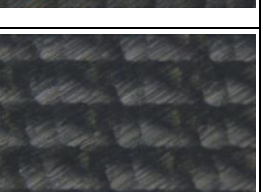
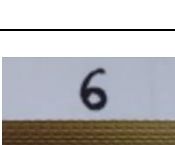
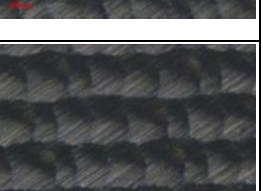
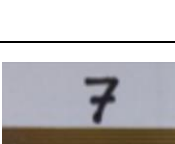
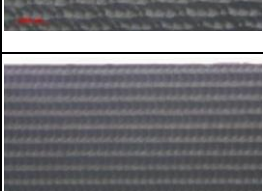
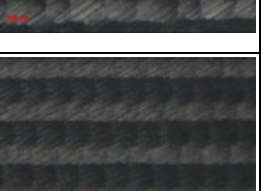
Figure 18. Surface roughness in step over and feed direction for the two tested materials (custom forging and forged billet) for lowest test condition (left hand side) and highest condition (right hand side).

Part topography

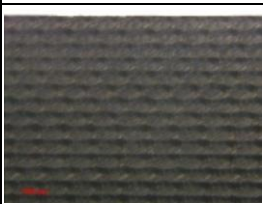
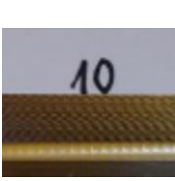
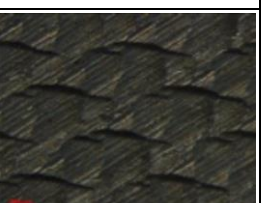
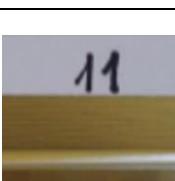
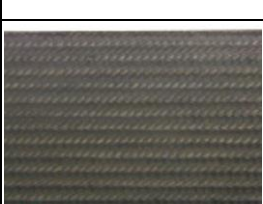
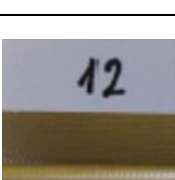
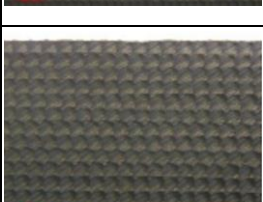
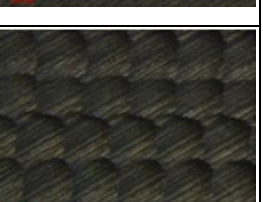
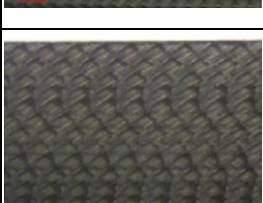
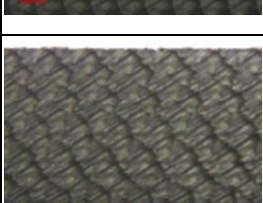
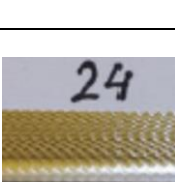
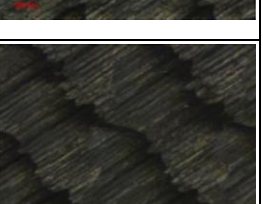
The topography of the surface has been analysed qualitatively, from pictures obtained with a conventional camera and also by using a ZEISS STEMI 508 zoom microscope to get amplified pictures of the surface, in which the tooth pass marks can be observed. The idea of this analysis is to find evidence of irregular surfaces and the conditions in which these irregularities occur. Table 14 shows the images for different tested conditions.

CHAPTER 2. EFFECT OF CUTTING VARIABLES ON SURFACE INTEGRITY

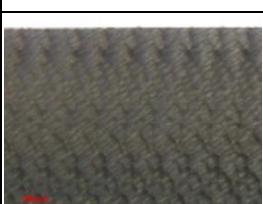
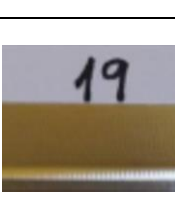
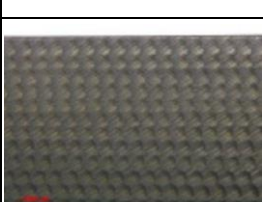
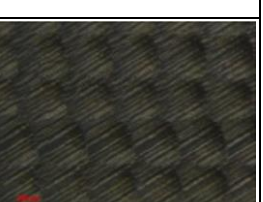
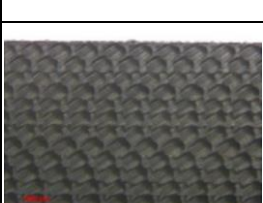
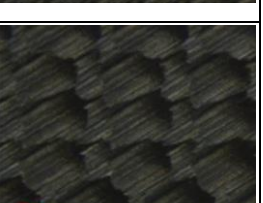
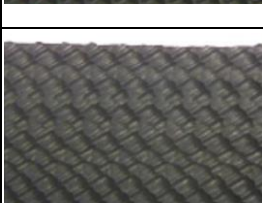
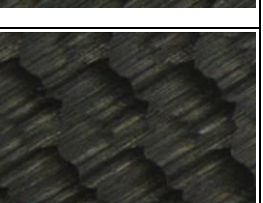
Table 14. Topography of the machined surface for each tested cutting conditions.

Vc (m/min)	Fz (mm/tooth)	s (mm)	a (mm)	Material	Overview image	Zoom 1	Zoom 2
32	0.109	0.3	1.5	Custom forging			
32	0.109	0.3	1.5	Forged billet			
60	0.058	0.3	1.5	Custom forging			
60	0.109	0.3	1.5	Custom forging			
60	0.2	0.3	1.5	Custom forging			
60	0.3	0.3	1.5	Custom forging			
170	0.058	0.3	1.5	Custom forging			

CHAPTER 2. EFFECT OF CUTTING VARIABLES ON SURFACE INTEGRITY

170	0.109	0.3	1.5	Custom forging			
170	0.2	0.3	1.5	Custom forging			
170	0.3	0.3	1.5	Custom forging			
240	0.058	0.3	1.5	Custom forging			
240	0.109	0.3	1.5	Custom forging			
240	0.2	0.3	1.5	Custom forging			
240	0.3	0.3	1.5	Custom forging			
240	0.3	0.3	1.5	Forged billet			

CHAPTER 2. EFFECT OF CUTTING VARIABLES ON SURFACE INTEGRITY

170	0.109	0.1	1.5	Custom forging			
170	0.2	0.1	1.5	Custom forging			
240	0.109	0.1	1.5	Custom forging			
240	0.2	0.1	1.5	Custom forging			
170	0.109	0.3	0.5	Custom forging			
170	0.2	0.3	0.5	Custom forging			
240	0.109	0.3	0.5	Custom forging			

Current cutting conditions can be found in the overview images 1 and 3 in Table 14. Both surfaces show a regular tooth pass, indicating clearly the area of the material removed by each tooth. Even if the material removal rate is the same in both cases, the pattern created in the surface is slightly different. Looking at the rest of the conditions, tooth-pass can be

generally recognized with regular marks on the surface for the feed per tooth values up to 0.1mm but for the higher feed per tooth values ($f_z=0.2\text{mm}$ and $f_z=0.3\text{mm}$) the tooth-pass can't be recognized and the surface appears distorted. This is due to a rubbing effect of the tool against the workpiece which could be due to the geometry of the tool that can't evacuate the chip properly or due to chatter instability conditions. However, at the low surface speed of 60m/min this does not occur, and the tooth-pass is recognizable even at the highest feed values. Surface speed looks to be independent of the topography created in the tested window, since regular surface marks can be found even at high speeds.

For the lowest step over value tested ($s=0.1\text{mm}$) it looks like the tooth-passes are overlapped and this creates a distorted surface. However, it has been previously observed that the surface roughness is better for the lowest step over value, so having a regular and recognizable tooth-pass in the surface doesn't mean that the roughness is lower.

Cutting depth appears to be independent of the topography in the tested ($0.5\text{mm}<a<1.5\text{mm}$) window. Finally, in some particular cases, a tooth-mark is shorter than the rest of the marks created by the rest of the teeth in a given cut. It is believed that runout (which has not been measured in the trials) causes this pattern. For future experimental tests it is very important to consider the possible effects of the runout and therefore it will be measured.

In terms of the topography observation for the different materials, the results are very similar for the most demanding parameter set but considerably different for the lowest parameters tested as it is very difficult to recognise the tooth-pass for the forged billet. This might be related to the lower cutting forces and surface roughness observed in the part coming from the forged billet.

The topography analysis reveals a generally worse condition as the feed is increased and this does not exactly match with the surface roughness analysis, in which the roughness (specially in feed direction) is generally lower for $f_z=0.3\text{mm}$ compared to $f_z=0.2\text{mm}$.

Micro-hardness

Metallographic samples have been prepared from each of the machined parts, including the step-over and feed direction samples. After grinding and polishing the samples, a sub-surface micro-hardness analysis has been carried out in the in the feed direction samples. Ten

different sub-surface distances have been measured, with eight repetitions for each point. The reason for doing eight repetitions is the typical high scatter seen in micro-hardness measurement of Ti6-4, due to the alpha and beta grains present in this alloy, which have different hardness. Apart from these measurements, another twelve measurements have been carried out in order to obtain the bulk hardness in each sample. The graphs in Figure 19 are ordered to show the influence of the different parameters in the micro-hardness profile. The bulk hardness line shown in the graphs is the average of the bulk hardness obtained from the totality of the samples.

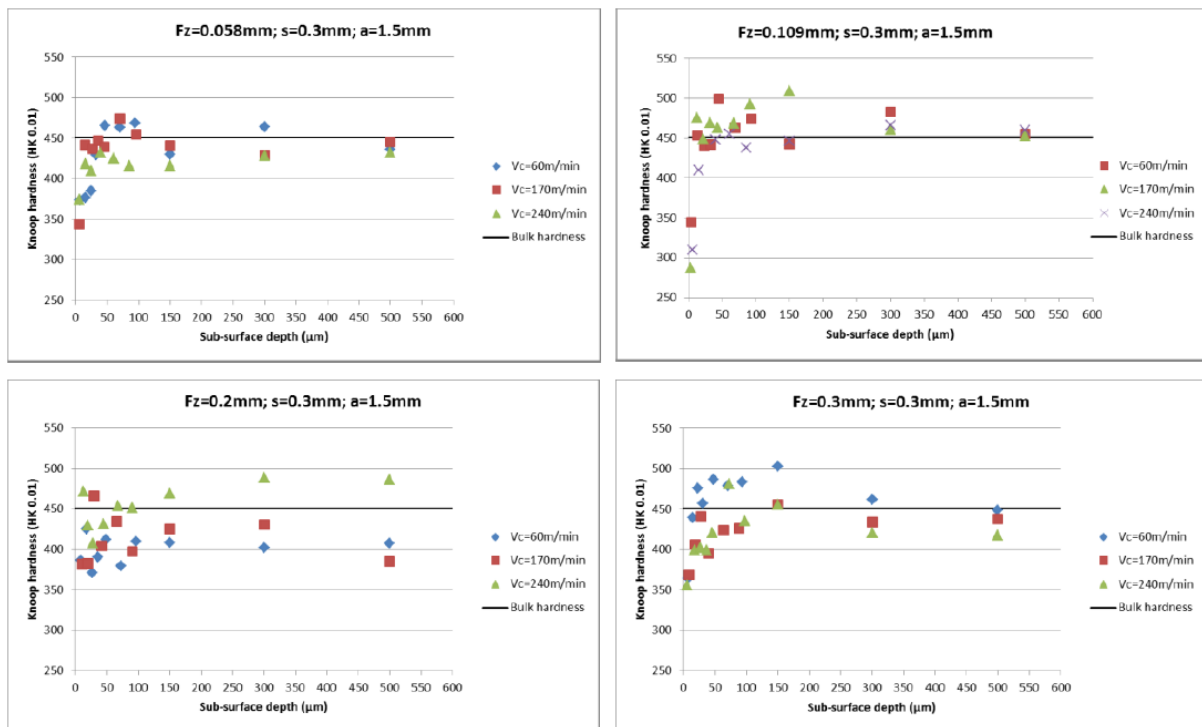


Figure 19. Sub-surface micro hardness profile graphs showing the influence of surface speed for different feed per tooth values (top left, $f_z=0.05\text{mm}$; top right, $f_z=0.1\text{mm}$; bottom left, $f_z=0.2\text{mm}$; bottom right, $f_z=0.3\text{mm}$).

In the plots of Figure 19, it can be observed the effect of the surface speed in the micro-hardness profile at different feed values. The first observation is that there is not an important hardening effect in the samples analysed. The maximum values obtained in the measurement are in the range of 500HK which is 50HK above the bulk hardness. However, in many cases the hardness is hardly above the bulk hardness, independently of the surface speed. This is usually a sign of the material not being abusively machined.

Something that can be observed in all the samples analysed is the softening effect for the first 10-20µm below the surface. The closer to the surface the lower are the hardness

measurements recorded. Even if some of the measurements points are too close to the surface to comply with the ASTM standards, (generally those points under $10\mu\text{m}$ below the surface) the reliability and repeatability of such measurements is very similar to the rest of the points, so, the softening effect seen in the initial microns below the surface can be trusted as the rest of the hardness data recorded.

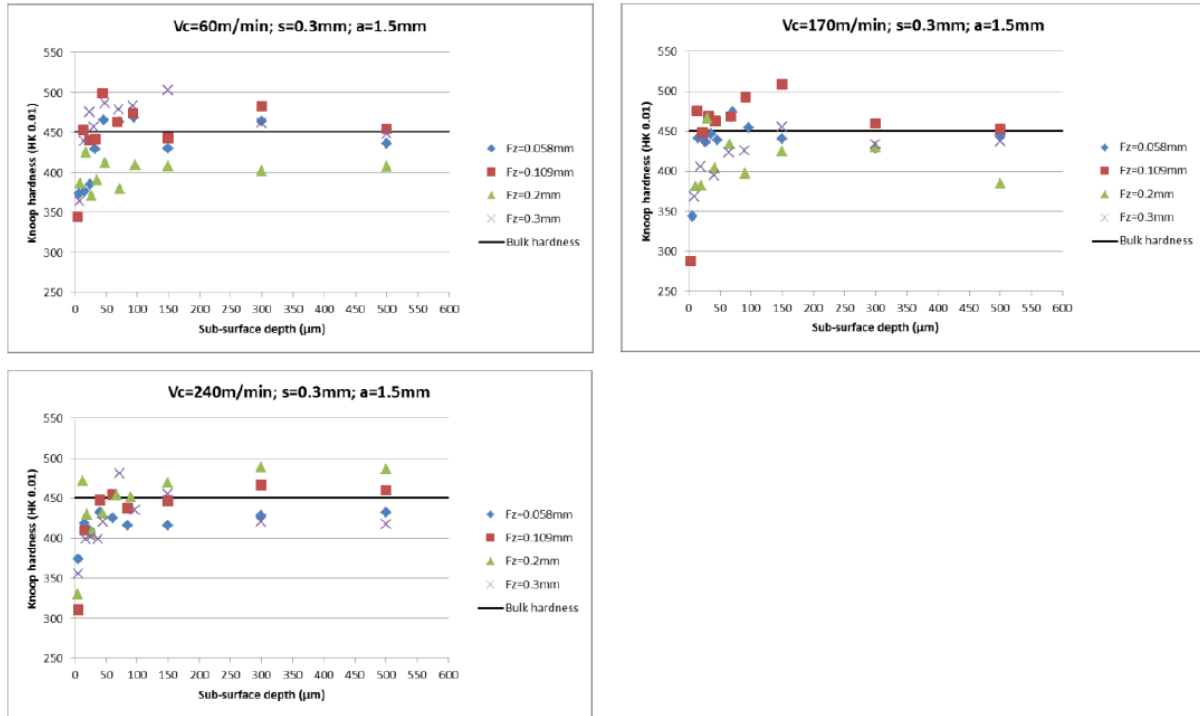


Figure 20. Sub-surface micro hardness profile graphs showing the influence of feed per tooth for different surface speed values (top left, $v_c=60\text{m/min}$; top right, $v_c=170\text{m/min}$; bottom left, $v_c=240\text{m/min}$).

Regarding to the effect of the feed per tooth (graphs in Figure 20), which proofs to be the most influencing parameter in the forces, the surface roughness and the topography, the only conclusion that can be made is that the feed in the tested range is not contributing to any particular worsening (i.e. increase in hardening) in the micro-hardness profile.

Similarly, the graphs in Figure 21 show that the step over and the cutting depth are not influencing the micro-hardness profile obtained through the sub-surface of the machined faces. Lowest and highest values of the graphs are randomly distributed and this is probably due to the high deviation or scatter previously mentioned but most importantly due to the low effect of those parameter ranges in the tested process window.

CHAPTER 2. EFFECT OF CUTTING VARIABLES ON SURFACE INTEGRITY

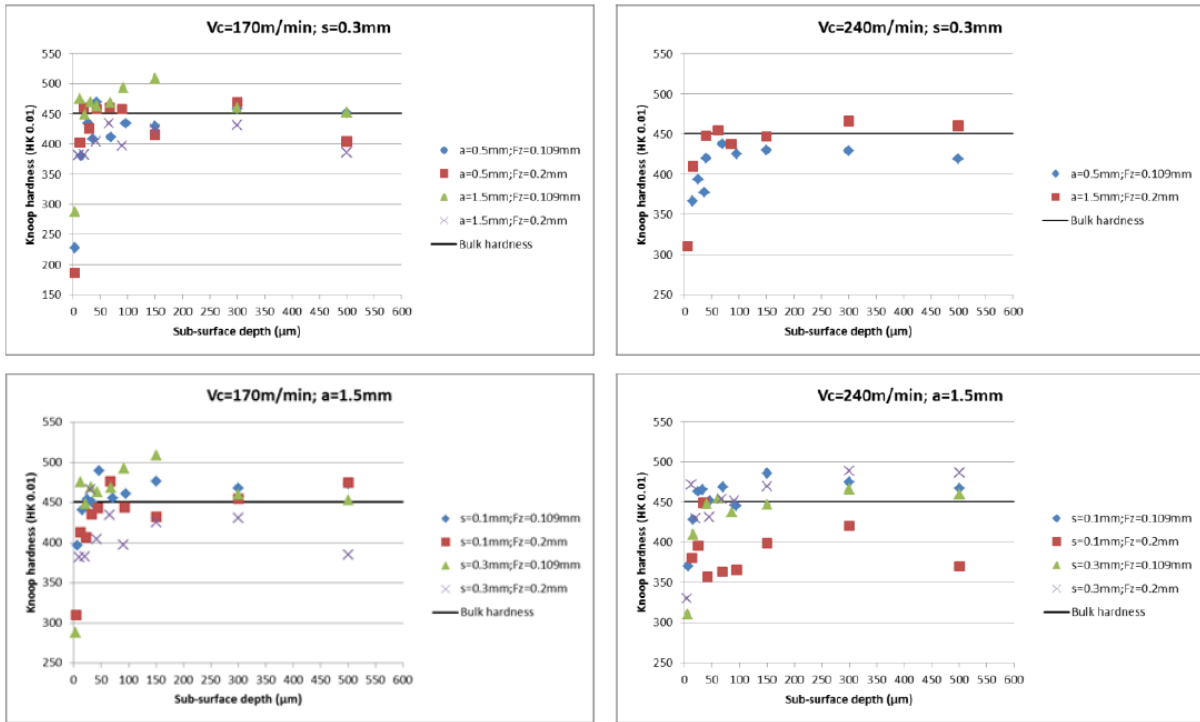


Figure 21. Sub-surface micro hardness profile graphs showing the influence of cutting depth (top left and top right) and step over (bottom left and bottom right) for different surface speed and feed per tooth values.

Finally, and following the order set in the previous sections, the comparison between the custom forging and the forged billet has been made. Figure 22 shows that the forged billet is softer than the custom forging through the sub-surface profile. This observation goes in the same line of the cutting force data and the surface roughness, which also records lower values for the forged billet. However, no influence is found between the current (lowest) parameters and the highest parameters tested for each material, as seen in the previously commented graphs.

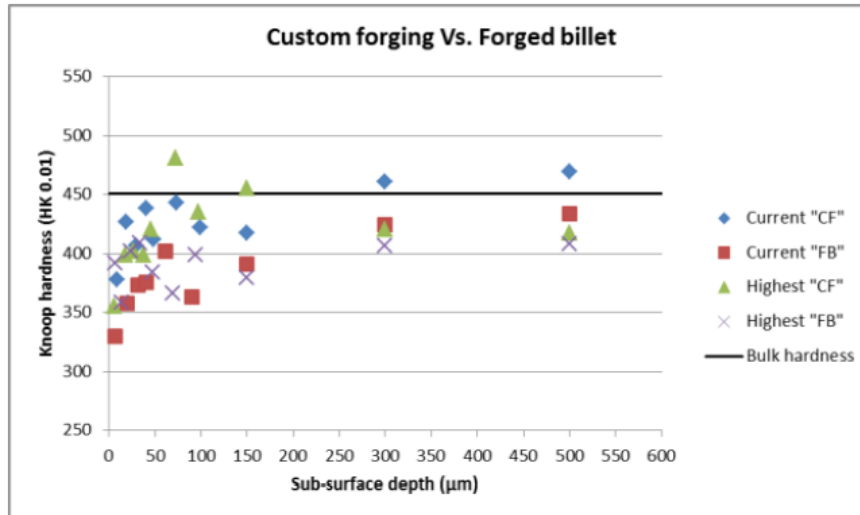


Figure 22. Sub-surface micro hardness profile graphs showing the influence of the workpiece material (custom forging and forged billet) at lowest and highest parameter combinations.

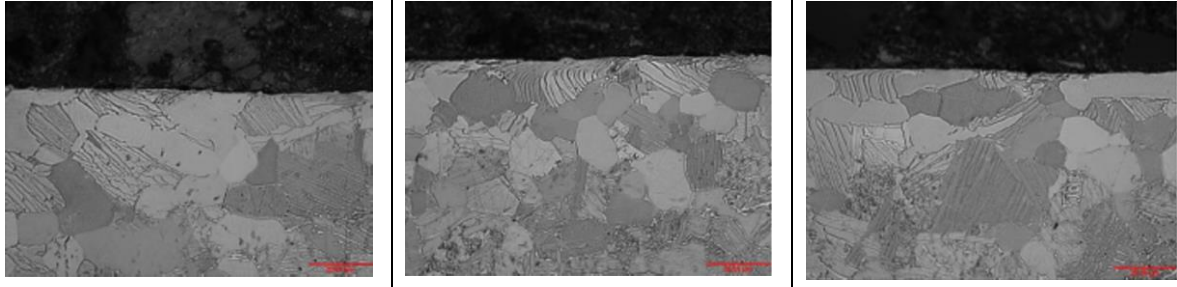
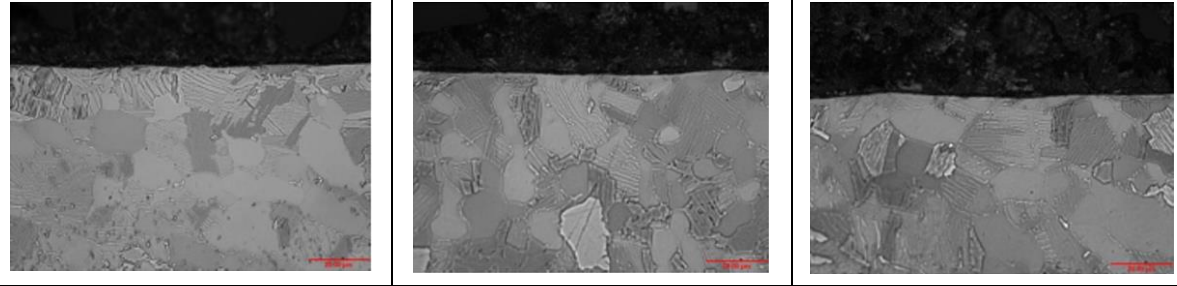
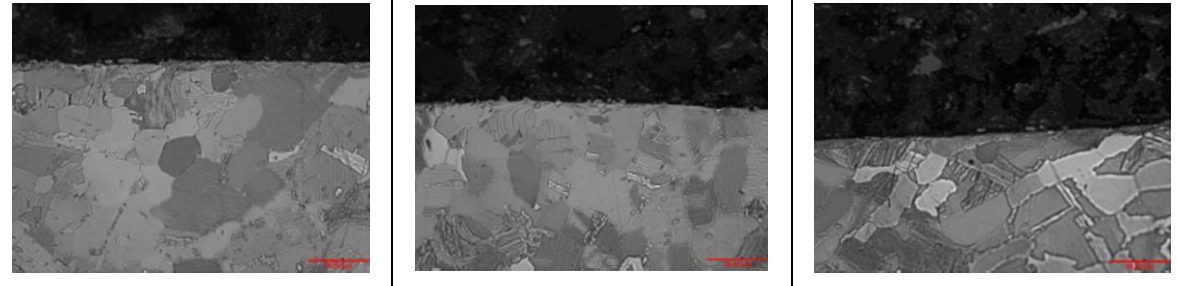
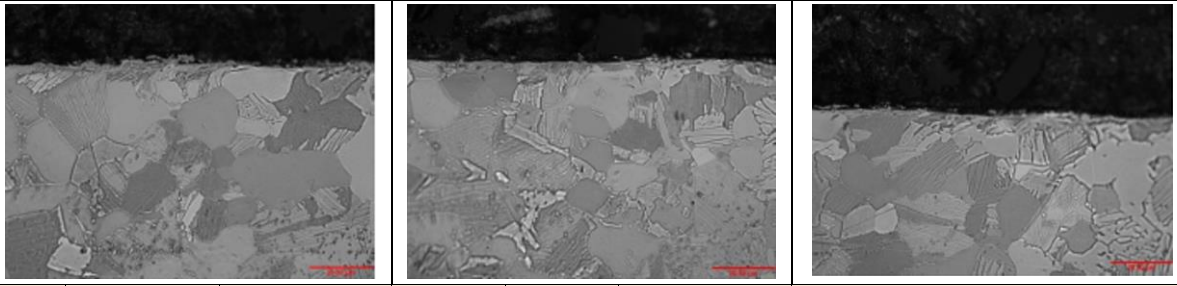
Sub-surface deformation

After indenting the metallographic samples to plot the micro-hardness profiles, those have been re-grinded and polished prior to etching to reveal the microstructure. Up to ten pictures have been taken from each sample showing the biggest deformations found through the feed direction. Table 15 shows the three most significant images for each sample (condition); highest deformations based in the grain directionality have been measured and the average of those measurements has been listed for each condition. Note that the following analysis is based in the sub-surface deformation and not in the surface defects. A more specific analysis and evaluation should be made in order to see the effect of the tested parameters in the level of defects or irregularities created on the surface.

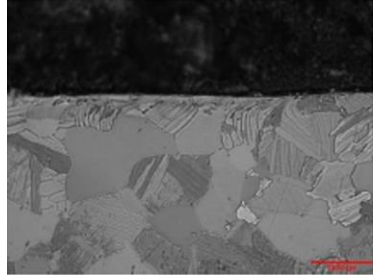
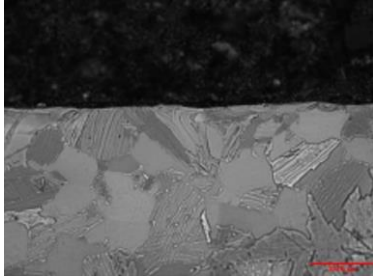
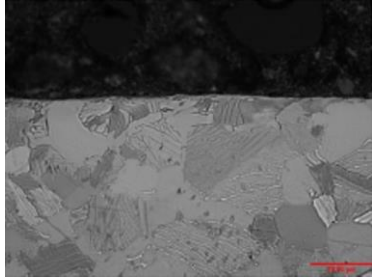
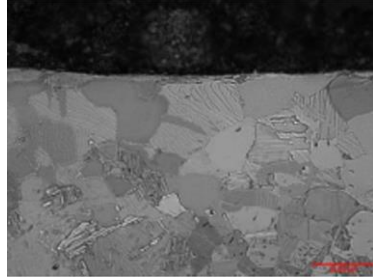
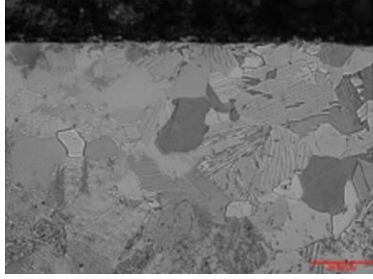
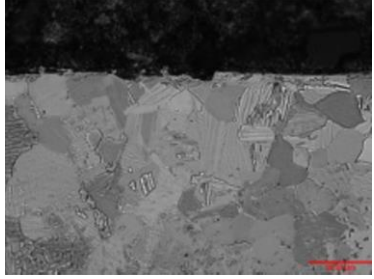
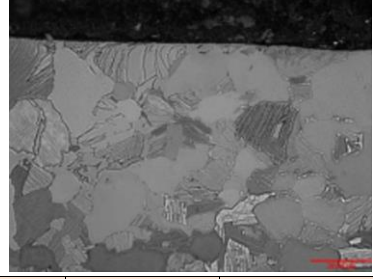
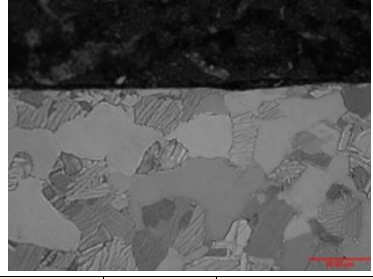
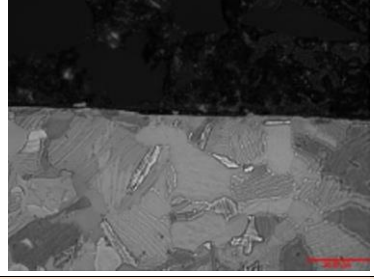
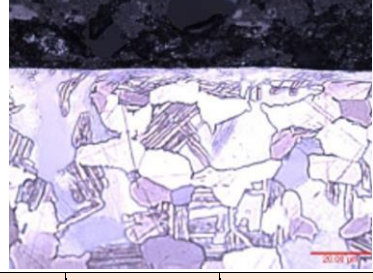
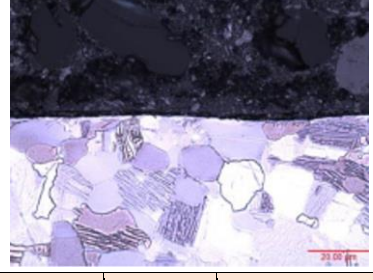
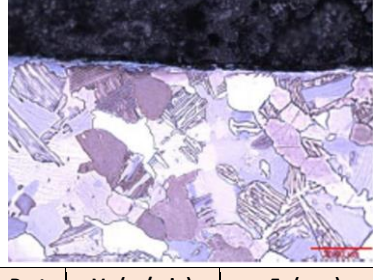
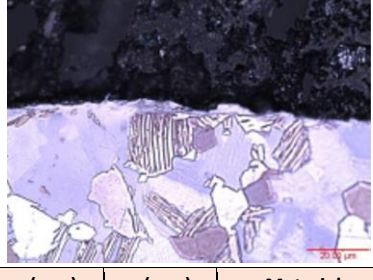
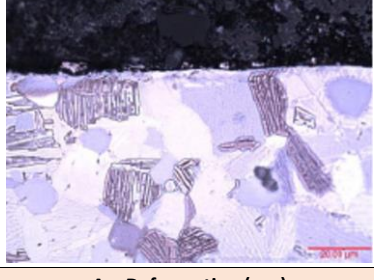
Also, due to the etching process, some samples are not as well revealed as others, but it has been possible to measure the deformed layer in most of them. The exception in this case is the forged billet material, which has responded differently to the etching process and has not revealed the two phases of Ti6-4. Therefore, no sub-surface deformation analysis has been done with the samples coming from the forged billet.

CHAPTER 2. EFFECT OF CUTTING VARIABLES ON SURFACE INTEGRITY

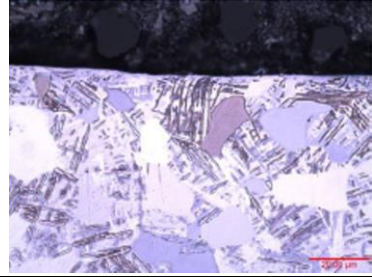
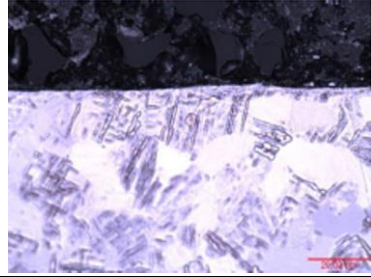
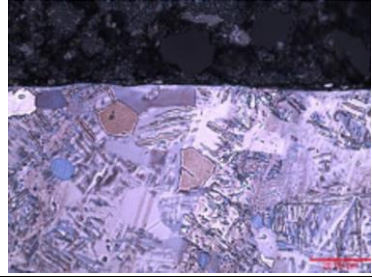
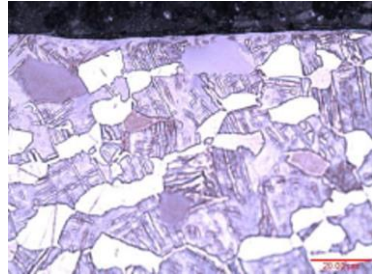
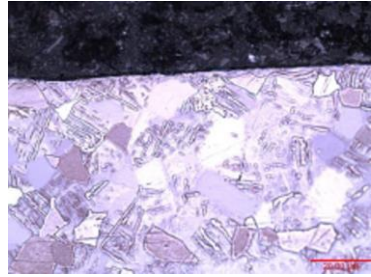
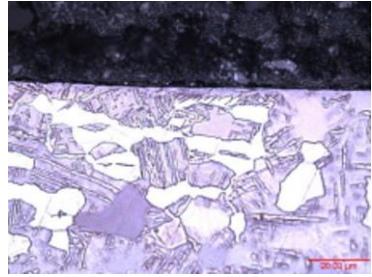
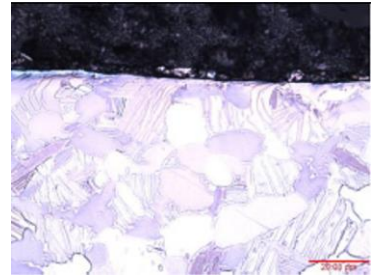
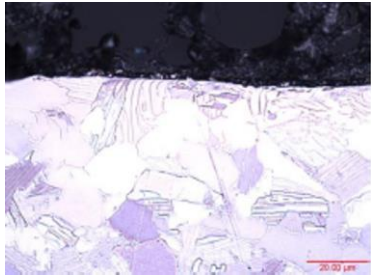
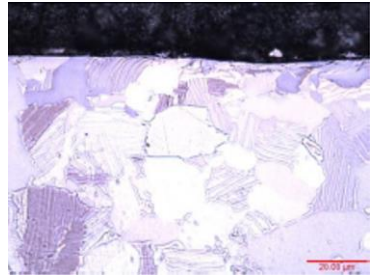
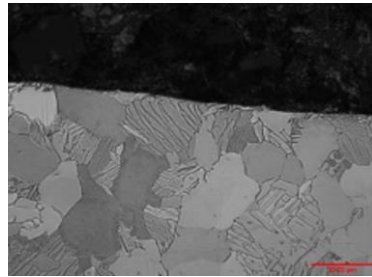
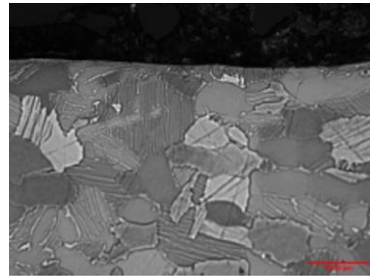
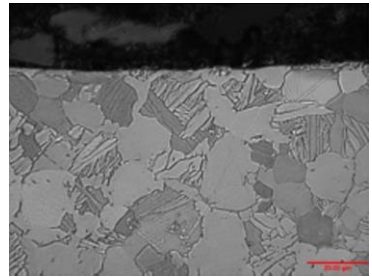
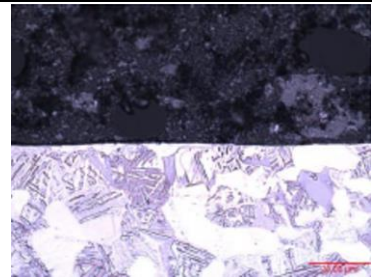
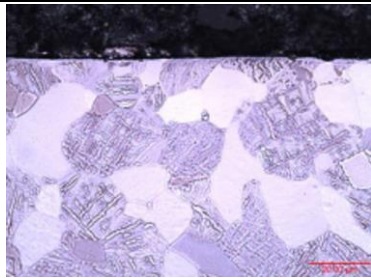
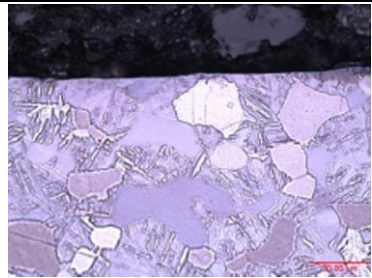
Table 15. Evaluation of sub-surface damage and grain directionality caused by the machining effect for the tested conditions.

Part	Vc (m/min)	Fz (mm)	s (mm)	a (mm)	Material	Av. Deformation (μm)
1	32	0.109	0.3	1.5	Custom forging	5.64
						
Part	Vc (m/min)	Fz (mm)	s (mm)	a (mm)	Material	Av. Deformation (μm)
3	60	0.058	0.3	1.5	Custom forging	5.14
						
Part	Vc (m/min)	Fz (mm)	s (mm)	a (mm)	Material	Av. Deformation (μm)
4	60	0.109	0.3	1.5	Custom forging	5.67
						
Part	Vc (m/min)	Fz (mm)	s (mm)	a (mm)	Material	Av. Deformation (μm)
5	60	0.2	0.3	1.5	Custom forging	6.07
						
Part	Vc (m/min)	Fz (mm)	s (mm)	a (mm)	Material	Av. Deformation (μm)
6	60	0.3	0.3	1.5	Custom forging	5.87

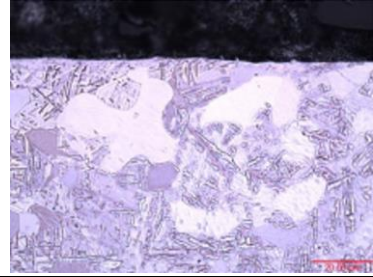
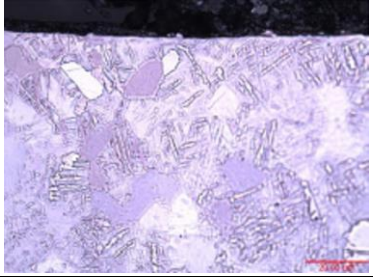
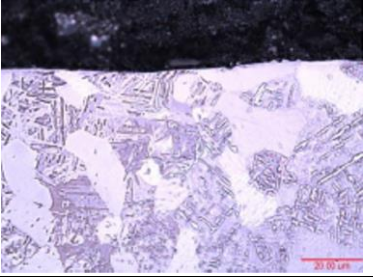
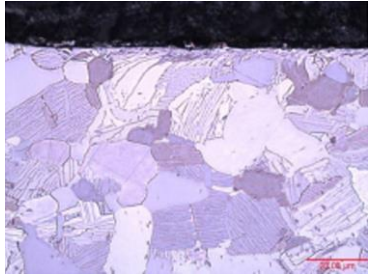
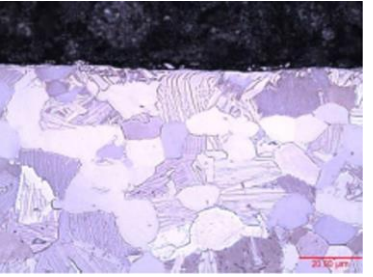
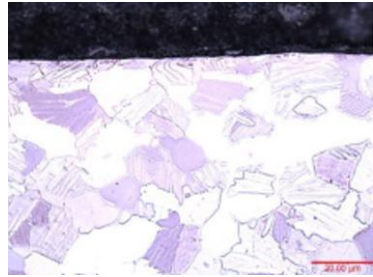
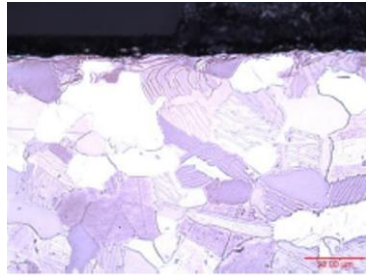
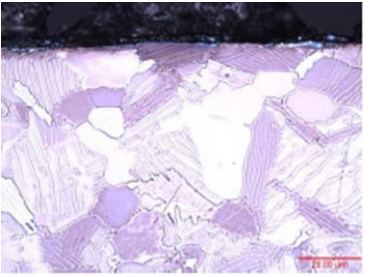
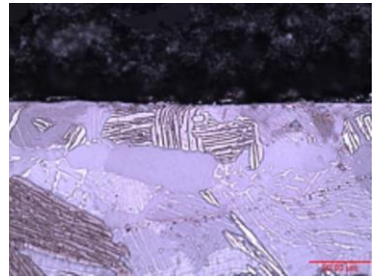
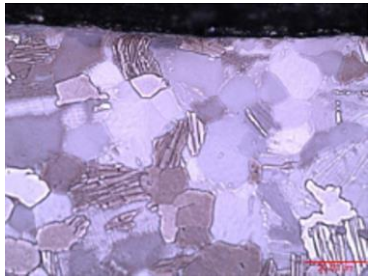
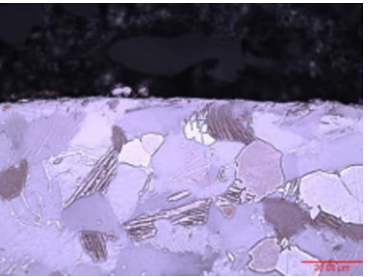
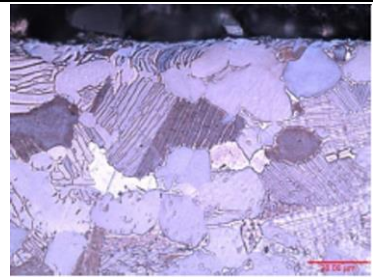
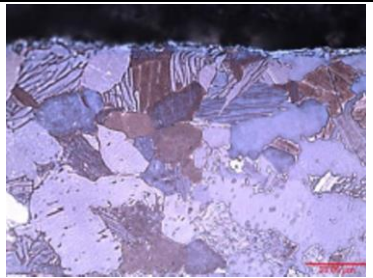
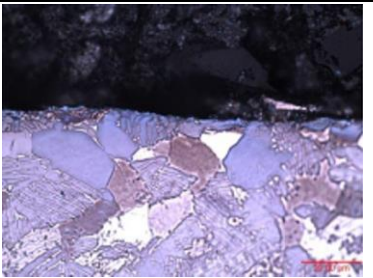
CHAPTER 2. EFFECT OF CUTTING VARIABLES ON SURFACE INTEGRITY

						
Part	Vc (m/min)	Fz (mm)	s (mm)	a (mm)	Material	Av. Deformation (μm)
7	170	0.058	0.3	1.5	Custom forging	5.91
						
Part	Vc (m/min)	Fz (mm)	s (mm)	a (mm)	Material	Av. Deformation (μm)
8	170	0.109	0.3	1.5	Custom forging	6.12
						
Part	Vc (m/min)	Fz (mm)	s (mm)	a (mm)	Material	Av. Deformation (μm)
9	170	0.2	0.3	1.5	Custom forging	5.76
						
Part	Vc (m/min)	Fz (mm)	s (mm)	a (mm)	Material	Av. Deformation (μm)
10	170	0.3	0.3	1.5	Custom forging	6.33
						
Part	Vc (m/min)	Fz (mm)	s (mm)	a (mm)	Material	Av. Deformation (μm)
11	240	0.058	0.3	1.5	Custom forging	1.5

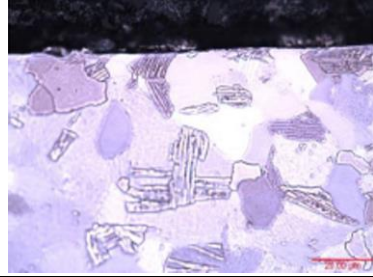
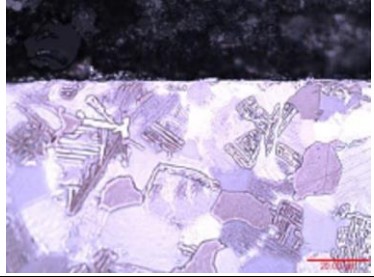
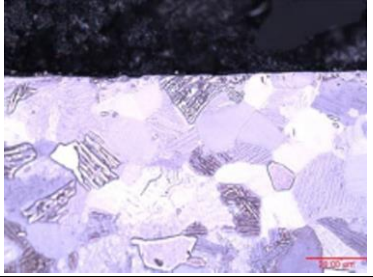
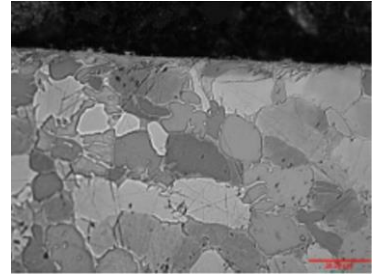
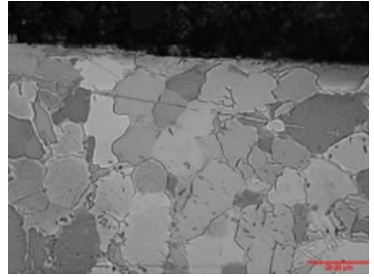
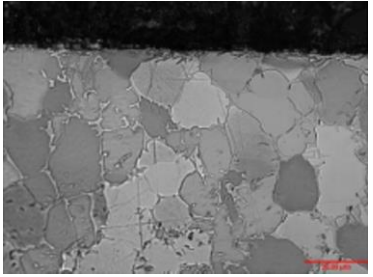
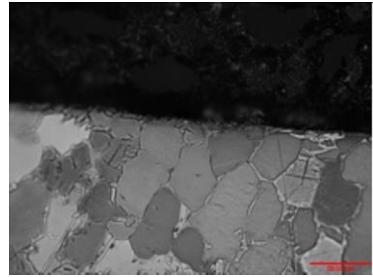
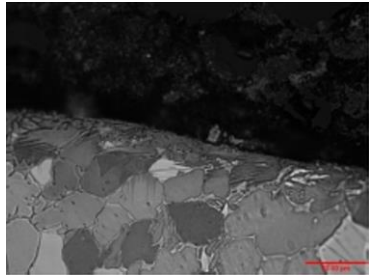
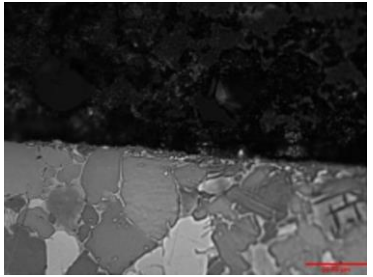
CHAPTER 2. EFFECT OF CUTTING VARIABLES ON SURFACE INTEGRITY

						
Part	Vc (m/min)	Fz (mm)	s (mm)	a (mm)	Material	Av. Deformation (µm)
12	240	0.109	0.3	1.5	Custom forging	4.09
						
Part	Vc (m/min)	Fz (mm)	s (mm)	a (mm)	Material	Av. Deformation (µm)
13	240	0.2	0.3	1.5	Custom forging	8.19
						
Part	Vc (m/min)	Fz (mm)	s (mm)	a (mm)	Material	Av. Deformation (µm)
14	240	0.3	0.3	1.5	Custom forging	5.97
						
Part	Vc (m/min)	Fz (mm)	s (mm)	a (mm)	Material	Av. Deformation (µm)
15	170	0.109	0.1	1.5	Custom forging	4.60
						
Part	Vc (m/min)	Fz (mm)	s (mm)	a (mm)	Material	Av. Deformation (µm)
16	170	0.2	0.1	1.5	Custom forging	5.36

CHAPTER 2. EFFECT OF CUTTING VARIABLES ON SURFACE INTEGRITY

						
Part	Vc (m/min)	Fz (mm)	s (mm)	a (mm)	Material	Av. Deformation (μm)
17	240	0.109	0.1	1.5	Custom forging	8.68
						
Part	Vc (m/min)	Fz (mm)	s (mm)	a (mm)	Material	Av. Deformation (μm)
18	240	0.2	0.1	1.5	Custom forging	6.26
						
Part	Vc (m/min)	Fz (mm)	s (mm)	a (mm)	Material	Av. Deformation (μm)
19	170	0.109	0.3	0.5	Custom forging	7.03
						
Part	Vc (m/min)	Fz (mm)	s (mm)	a (mm)	Material	Av. Deformation (μm)
20	170	0.2	0.3	0.5	Custom forging	7.37
						
Part	Vc (m/min)	Fz (mm)	s (mm)	a (mm)	Material	Av. Deformation (μm)
21	240	0.109	0.3	0.5	Custom forging	4.74

CHAPTER 2. EFFECT OF CUTTING VARIABLES ON SURFACE INTEGRITY

						
Part	Vc (m/min)	Fz (mm)	s (mm)	a (mm)	Material	Av. Deformation (μm)
22	32	0.109	0.3	1.5	Forged billet	
						
Part	Vc (m/min)	Fz (mm)	s (mm)	a (mm)	Material	Av. Deformation (μm)
24	240	0.3	0.3	1.5	Forged billet	
						

The sub-surface deformation level goes from $1.5\mu\text{m}$ to $8.7\mu\text{m}$ for the different conditions. No white layer or phase transformation is found through the analysed samples, which means that the machining operation has not affected in an aggressive way the subsurface region of the workpiece. Looking at the conditions and the deformation level, it is very difficult to make any conclusion, as the highest machining conditions don't always match with the highest deformed sub-surface regions. For example, the lowest deformation level is found for the highest surface speed and the lowest feed combination. Low surface speed / low feed combinations do not show better results than the opposite conditions, which shows that the tested parameter window is not big enough to see the negative effects of the more aggressive parameters. However, it has to be pointed out that one of the most deformed sample is machined at $V_c=240\text{m/min}$ and $F_z=0.2\text{mm}$, which shows the worst results in cutting forces and also in surface roughness.

The level of deformed sub-surface layer observed is generally independent of the cutting parameters, according to the results obtained for this particular parameter window. This means that, sub-surface deformation level is not a limitation for the material for the tested conditions, as opposed to the surface roughness, for example.

2.3.3 Conclusions

An initial surface integrity analysis has been carried out through the evaluation of the surface roughness, topography, micro-hardness and sub-surface deformation. In addition to this, cutting forces have been measured to understand the behaviour and dynamic response of the machining operation. Cutting force analysis shows that the cutting process is not very demanding power-wise, as the forces are in the range of (40N-330N) for different conditions over the tested window. Differences in cutting forces are mainly due to the increase in feed per tooth, whereas higher surface speed contributes to obtain lower forces. As opposed to expected, some force values are higher than others, especially those at feed per tooth values of 0.2mm compared to 0.3mm respectively. The reason why this happens could be due to a process damping effect appearing in the cut at higher feed per tooth values.

Results that strengthen the previous hypothesis are found in the surface roughness analysis; roughness values increase gradually up to $f_z=0.2\text{mm}$ and then are reduced for $f_z=0.3\text{mm}$. A similar trend is found in the cutting depth, as the roughness is decreased when the cutting depth is increased three-fold. These findings are thought to have a connection with the process damping effect. In general, the trends are similar to those found in the force analysis, feed per tooth being the most influencing parameter for the outputs.

However, surface speed does not show any particular trend, as opposed to the force analysis. An important aspect to consider about the surface roughness obtained in the machining tests is that values are higher to those obtained in blade finish milling for the same cutting conditions (same parameters). Machine and cutting fluid delivery system are the same as for the component machining, but the shape of the workpiece (rigid block instead of thin walled blades) and the cutting program (created from different software packages) are different. Further research needs to be carried out in order to find the root cause of higher surface roughness in the machining trials compared to that in manufactured component's blades.

According to the topography of the machined parts, tooth-pass marks are easily recognizable for some of the cutting parameters although at high speed / high feed combinations the tooth-pass marks become unrecognizable due to a rubbing effect between the tool and the workpiece. The reasons of this to happen could be the influence of chatter at those conditions as well as the tool geometry, which is not particularly designed to perform at the highest tested parameters, and could lead to a different chip formation. For future testing, chips should be collected to obtain information about chip formation and to have evidence to explain why the topography becomes so different and tooth-pass cannot be recognized under some circumstances.

Topography analysis of the machined parts also reveals irregular patterns in the tooth-pass marks which can be attributed to the runout effect, as it happens randomly across different conditions. Runout has not been measured for the tests, but it should be considered for the next machining trials of the research project.

Micro hardness analysis does not show differences within the tested parameter window. The nature of this analysis in a two-phase material is very uncertain, due to grains having different hardness previous to any machining induced effect. In order to minimize the high scatter, up to eight repetitions have been done per indent in a given depth below surface. No differences are appreciated, so the conclusion is that the scatter produced by grains of different phase has a bigger impact than the effect produced by changing the parameters in the tested window. Even if no difference can be seen for the variation of the parameters, a softening is appreciated in the first 10-20 μm below the surface followed by a light hardening effect.

Finally, results obtained from the optical microscope reveal that sub-surface regions of the machined blocks are not affected by the tested parameter window, as deformation and directionality of the grains are not consistent with the surface speed and feed increments. No white layer or phase transformation is found in the analysed samples and the measured depth of the directionality of the grains is between 1 μm -8 μm . Sub-surface analysis carried out for the test is not extensive and therefore machining induced damage is not analysed. This is an important area for the component quality assessment, as it has influence in the fatigue life of the component.

2.4 Summary

This chapter evaluates the effect of cutting variables in surface integrity. The need for carrying out this analysis comes from the case study presented in Chapter 1, where finish milling has been identified as the key operation to improve. Any modifications done to the finishing operations of critical parts like IBRs need to undergo through surface integrity validation. That is the reason of tackling the surface and sub-surface material condition first.

After looking into literature about the background on surface integrity, a test parameter window has been proposed and a range of cutting parameters have been performed in point finish milling, replicating the finish milling strategy for IBR blades, but providing a rigid workpiece instead of slender blades. The objective has been to analyse the effect of the tested parameter window in the surface integrity obtained, by analysing some of the outputs which assess the surface integrity, such as surface roughness, topography, micro-hardness or sub-surface microstructural deformation.

Results show that tool induced chatter might have happened in the highest speed ranges tested, although more data would be needed to confirm this end. This can alter the results, especially the ones related to roughness and topography, which are poor in general, probably due to the cutting program post processing being different of that used in manufacturing real components, but especially worsened for the high speed / high feed conditions. It might be useful to further analyse the causes to get so high surface roughness values, accompanied with distorted topography, in order to gain a better understanding of the process.

Sub-surface regions of the material do not appear to be particularly damaged, as micro-hardness results are very similar to both, the lowest and highest conditions and only a small hardening effect is found through the different conditions. According to the sub-surface damage, no white layer is generated (typical sign of abusive machining) and the grain deformation range is below $8\mu\text{m}$ in all cases. The highest deformation levels do not always correspond to the highest parameters tested, which confirms a very little effect of the tested parameter window in terms of sub-surface damage produced. This means that the material can withstand the whole parameter set tested in its sub-surface region, although it might not be acceptable due to the poor surface generated at some particular conditions.

This chapter concludes that surface integrity, apart from surface roughness, which can be corrected through polishing operations, is not a limiting factor in the parameter window tested. In this respect, chatter effect, which is suspected to appear at the most demanding cutting conditions tested is a concern, as IBR finish milling process is most likely affected by chatter, especially if higher MRR is pursued.

In the next chapter, a dynamic analysis of the tool/workpiece system has been carried out in order to understand how does chatter affect to the machining process of blade finish milling. New strategies proposed for the improvement of this manufacturing process will therefore require the understanding of the system dynamics and the objective will be to propose chatter mitigation techniques as a path to increase productivity.

CHAPTER 3. TOOL AND COMPONENT DYNAMIC ANALYSIS

ANALYSIS

3.1 Introduction

Results obtained from the experimental testing carried out in chapter 2 show that sub-surface condition is not severely affected, no matter which cutting parameters from the selected working window are employed. However, the high surface roughness obtained for some conditions indicate that chatter effect is likely to be present within the selected cutting parameters, especially considering the low stiffness of the IBR blades, which was not reproduced in the experimental test of chapter 2.

Therefore, once the surface integrity is not considered a limiting factor, improvement of the finish milling process has to come from the understanding of the chatter effect and the solutions developed both to mitigate chatter and increase productivity, which is the ultimate objective of this study.

In this respect, the first step is the dynamic analysis of the tool/workpiece system. An experimental approach has been followed to measure natural vibration frequencies, due to the access to semi-finished as well as finished IBR components as well as tool set up and fixturing within the production machine.

This chapter will give an insight of the dynamics of the system and it will help to take further decisions to improve productivity while tackling the chatter effect.

3.2 Tool dynamic analysis

The tool selected for the analysis is a solid coated carbide tapered ball end mill, which contains four flutes and constant lead helix angle of 55° . The ball diameter is $\varnothing=6.35\text{mm}$ and the shank diameter $\varnothing=20\text{mm}$. Taper angle is 8° and the overhang of the tool is 110mm (Figure 23). The reason of using a taper geometry is the clearance needed to machine the blades, and the ball-

end geometry is one of the options that allow to run a point milling strategy. This is the tool used for the finish milling operation of the case study IBR.

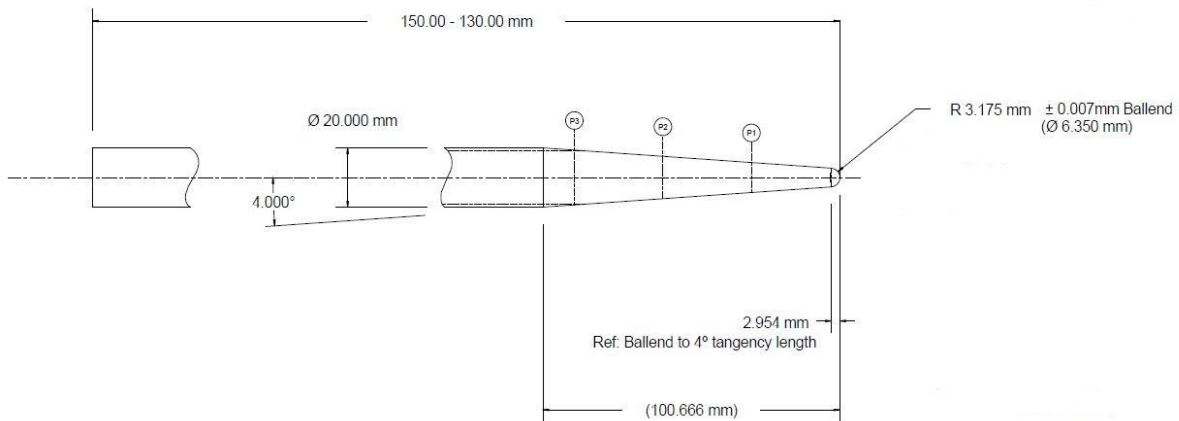


Figure 23. Drawing of the tapered ball end mill.

A tap testing has been performed to the machine/tool system and vibration modes as well as the stiffness of the system have been obtained. MetalMax software, together with a hardware composed by a tuned hammer, an accelerometer and a data acquisition box, have been used to perform the analysis. The accelerometer is stuck with wax to one of the flutes and the system is excited with the hammer from the opposite side.

The hammer is instrumented with a force sensor which generates a voltage signal proportional to excitation force so that the excitation force is measured during the test. The structure is excited and the excitation is measured, as well as the response. The accelerometer converts electronic signal into acceleration and measures it. Then the signal is process through a data acquisition system to convert signal into frequency domain. Frequency Response Function (FRF) is computed from two signals, response (output) and excitation (input). The FRF describes the ratio of one signal with respect to another signal over a frequency range and natural frequencies as well as stiffness and damping coefficients are obtained.

Results are shown in Table 16:

Table 16. Two main natural frequencies and the stiffness of the tool.

Mode	Frequency (Hz)	Stiffness (N/m)
1	1056	$2.97 \cdot 10^6$
2	1206	$7.87 \cdot 10^6$

The natural frequency of the first mode of vibration is 1056Hz with a stiffness of $2.97 \cdot 10^6$ N/m whereas the second mode vibrates at 1206Hz with a stiffness of $7.87 \cdot 10^6$ N/m. From the high natural frequencies measured, it can be said that both vibration modes correspond to the tool, as the modes corresponding to the machine are of lower frequency. Measurements on the tool are taken in both axis x and y to see if there are differences on both axis. The results show a very similar behaviour for both axes.

Stability lobes for the tool are calculated from both vibration modes measured above, using MetalMax software [18]. The result is shown in Figure 24. Blue dots are marked for the positions in the graph that have been experimentally tested.

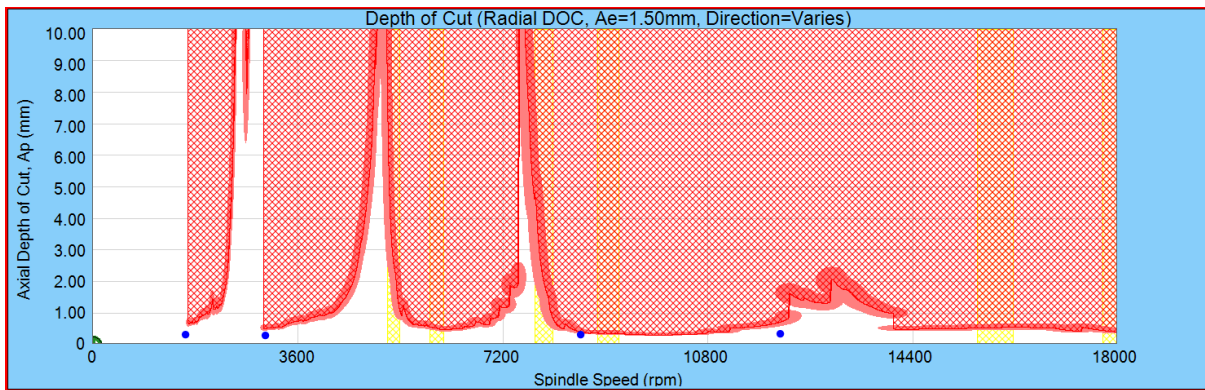


Figure 24. Stability diagram of the cutting tool. Blue dots show the location of the four different surface speeds tested in Chapter 2.

The graph, first of all shows that the critical depth of cut is very low, in the region of 0.3mm. As it was predicted, it is very difficult to improve cutting performance through high surface speed and low feed combination, especially for complex shape feature machining, such as blades, as the very low depth of cut required, together with the small feed per tooth limits the productivity considerably. The four blue dots (corresponding to $V_c=32$ m/min, $V_c=60$ m/min, $V_c=170$ m/min and $V_c=240$ m/min, from Chapter 2 tested conditions) are very close or in the limit of unstable cut. It is hard to predict if the dots are in the stable or unstable

region because the stability lobes diagram is a prediction of the process dynamics and the tested set of points are in the chatter borderline region. The vertical bands in yellow show the resonant vibration harmonics of the spindle speed; cutting close to the resonance bands can lead to higher vibration levels, although less than those amplitudes found with chatter. Finally, the stable regions at higher depths of cut could be further investigated to avoid chatter in the cutting process, although high depths of cut are a limiting factor in the blade geometry. Therefore, cutting conditions with higher depths of cut are not analysed and looking at the current depth of cut, the graph above shows a borderline region with chatter.

3.3 Component dynamic analysis

Together with the tool analysis, a dynamic analysis of the part has been performed. As described in the introduction chapter, the blades are machined through an initial roughing operation, which consists of slot milling the gaps between blades and creating a semi-finished stock, followed by a finishing operation employing a 5 axis point milling technique through a helical path from tip to root.

The aim of the dynamic analysis is to check the modes of vibration of the blade in two conditions; semi-finished and finished stages. The reason to check both semi-finished and finished stages is that for the first part of the cut, close to the tip of the blade, the part vibrates according very close to the semi-finishing modes. This is due to the mass of the blade, which is almost the mass of the semi-finished blade. However, when the tool is close to the root, the part vibrates very close to the finishing modes for the same reason of the mass approaching to the finished blade mass. By finding the boundary vibration conditions, it is possible to specify the range of natural frequencies for each area within the blade.

The tap testing has been carried out at nine different areas of the blade, as shown in Figure 25; three points in the tip (leading edge, middle and trailing edge), three points in the middle section and the last three points in the root. The accelerometer is positioned in the convex side and the part is hit from the concave side, opposite to the accelerometer. Then, the accelerometer and the hammer are turned to repeat measurements from the other side. For some of the tap tested areas it has not been possible to obtain a response; this is due to the sensitivity of the hammer.

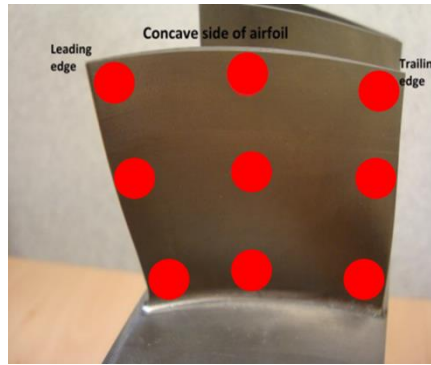


Figure 25. Tap test points within the blade.

Table 17 shows the main frequencies of the modes of vibrations obtained for different areas within blade, at semi-finished condition and finished condition.

Table 17. Frequencies of the main vibration modes for different areas of the blade.

Tap test area	Vibration mode 1 (Hz)	Vibration mode 2 (Hz)	Vibration mode 3 (Hz)	Vibration mode 4 (Hz)
Finished blade				
Concave tip mid	985	-	3959	4720
Convex tip mid	985	2037	3949	4692
Concave central mid	1017	2040	3980	-
Concave central LE	1020	2026	3973	4609
Concave central TE	1013	2037	3907	4682
Convex central LE	1017	2037	3831	-
Convex central TE	1020	2019	3963	4592
Concave root mid	1020	2040	4015	4734
Convex root mid	1020	2040	4021	4737
Average	1011	2035	3955	4681
Semi-finished blade				
Concave tip mid	1266	-	-	-
Convex tip mid	1266	-	-	-
Concave central mid	1272	2804	-	-

CHAPTER 3. TOOL AND COMPONENT DYNAMIC ANALYSIS

Concave central LE	1272	2801	-	-
Concave central TE	1276	2794	-	-
Convex central mid	1269	2808	-	-
Convex central LE	1272	2801	-	-
Convex central TE	1272	2801	-	-
Concave root mid	1276	2801	-	-
Convex root mid	1276	2808	-	-
Average	1272	2802		

Table 17 shows the frequencies of the different modes of vibration measured on the blade both in semi-finished and finished conditions. From one side, it can be observed that the vibration frequencies for a given mode of vibration change slightly across the different areas of the blade. This might be the effect of the mass loading from the accelerometer, when located at different areas. The most considerable differences are found in the tip region, especially for the finished condition. This is probably due to the higher impact of the accelerometer mass in comparison with the finished blade mass.

However, the biggest differences are found from the semi-finished condition to the finished condition of the blade; the difference in the mass of the blade is now more important compared to the mass added by the accelerometer. This leads to a shift in the vibration frequencies. As an average, the main vibration mode shifts from 1272Hz to 1011Hz whereas the second vibration mode shifts from 2802Hz to 2035Hz. From the results above, it is deduced that during the finish milling process of the blade, the natural vibration frequencies are located between the upper and lower ranges stated above, depending on how much material is left to cut on the blade.

When dynamic behaviour of tool and part are compared, it looks like the natural frequencies of the tool and the part will be coincident at some point, and this is something that needs to be further investigated to better understand the cutting dynamics of the blades. This behaviour adds complexity to the system dynamics and it should only affect at a certain section of the blade, due to its shifting frequencies as material is being removed.

An alternative to avoid interaction between tool and workpiece is to either modify the tool or modify the blade. As mentioned in Section 3.2, the tool is fixed due to access issues and

the strategy carried out. However, vibration modes of the blade can be modified by adding or reducing mass at strategical points prior to the finishing pass.

3.4 Summary

Chapter 3 briefly looks into the dynamics of the tool and workpiece system. With the main objective of increasing the manufacturing productivity, after surface integrity is not considered a limitation and observing potential chatter and process damping effects, research efforts are now directed to understand the dynamics of the system.

Therefore, tool and workpiece tap testing has been carried out and dominant vibration modes have been identified and their vibration frequencies recorded. From one side, there is a shift in frequency from semi-finished stage to finish stage of the blade. This defines a range of frequencies the blade will undergo at different moments of the finishing cut.

It is expected that the blade finishing operation will see both tool and workpiece vibration frequencies match at some point. This is something of interest for further research, although a different approach can be considered, which is modifying the stock material of the blade prior to the finishing operation, by adding or removing material intentionally to increase the main vibration frequency, avoid interference with tool's natural frequency and improve overall dynamic response of the blade.

This second approach not only avoids coupling dynamics, but also has the potential to increase stiffness of the blade and ultimately machining productivity as chatter is less critical. In chapter 4 this approach is developed in a strategy called blade stock optimization.

CHAPTER 4. BLADE OPTIMIZATION FOR FINISH MILLING OPERATION

4.1 Introduction

In Chapter 1, manufacturing process of IBRs has been analysed and blade finish milling has been identified as the most time-consuming machining operation. This is due to the combination of material and geometry, which makes it difficult to increase productivity. In Chapter 2, after carrying out a literature review and experimental work, it has been concluded that surface integrity for the tested working window, with typical variable parameters, is not a limiting factor. Meanwhile, surface roughness, which can be considered part of surface integrity but not necessarily affecting to the sub-surface region of the material, is considerably affected for some cutting conditions. This, and cutting force behaviour suggests the existence of chatter and possibly some degree of process damping.

Therefore, chatter mitigation is considered as the most effective path to improve finish milling productivity of IBR blades. Chatter phenomena is closely related to the geometry of the feature to be machined and for this reason, geometry optimization is analysed before dealing directly with chatter. In other words, it means creating the most stable structure before tackling chatter. It is considered that an optimized stock geometry has the potential to make the blades more stable against chatter. In addition, Chapter 5 investigates chatter mitigation techniques in detail.

A route to improve finish milling of IBR blades is the optimization of the blade geometry in the semi finishing operation aiming to produce an improved geometry for the last finishing operation. The optimization proposed here is based on simulating vibration modes of IBR blades using FEA (Finite Element Analysis) and analysing different finish milling stock layouts in order to optimize natural frequency of the main vibration mode. The FEA analysis work has been carried out in Ansys workbench software, and support from Unigraphics CAD software is used to create the geometries and smooth surfaces. The final objective is to achieve a

natural frequency of the blade which is larger than the excitation frequencies (107Hz-802Hz for the tested range of speeds) and their harmonics, and also larger than tool's natural frequency, producing a stiffer blade envelope and a better response to chatter.

Sections 4.2 to 4.8 below explain the steps of followed with FEA, explaining the process carried out to create the simulation model and analysing the results obtained.

4.2 Methodology

4.2.1 Model geometry

The FEA model has been created considering stock limits from a manufacturing point of view and the constraints set by the fixturing of the part within its machine set up. The stock window for finish milling operation is defined from the machining experience for ball-end mill tools. A minimum of 0.1mm is used to avoid causing push off, and a maximum of 2.5mm from a surface integrity and machinability point of view. Fillet radius is set to 8mm following the semi finishing tool used for this feature.

The wedge angle of the model has been modified to achieve a 7.66° ($360^\circ/47$) angle, since the IBR studied in this work comprises of 47 blades. A curved wedge cut has been generated to accommodate the full fillet radius and create the segment.

Fixturing of the part has been analysed in order to set boundary conditions for the FEA analysis, as shown in Figure 26. The component is clamped between a top and bottom plate on the forward and afterward faces highlighted in red and clamping force alone prevents rotation of the component in the fixture. Six bolts, equi-spaced, are used to clamp the part highlighted in blue. The forward flange of the component, highlighted in green is not constrained in the fixture during blade milling.

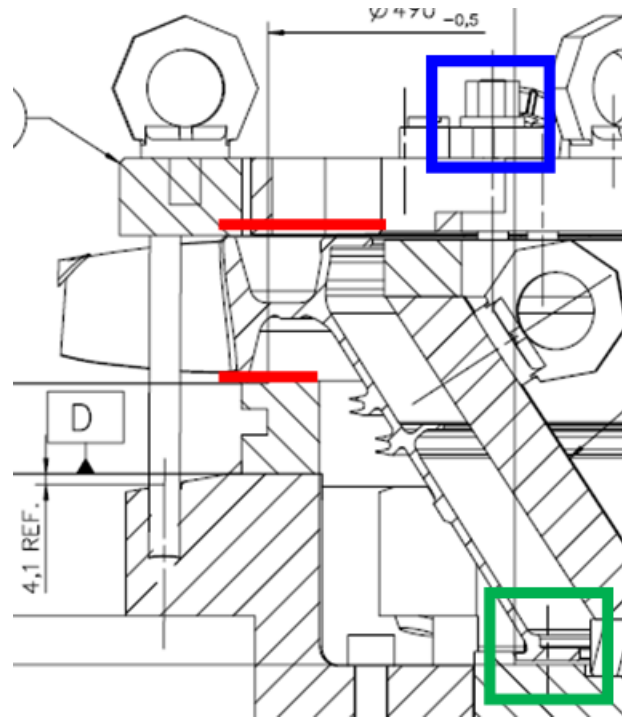


Figure 26. IBR milling fixture.

The analysis, completed as part of this research work, is intended to identify the first flap mode of vibration for the geometry described above and, through suitable analysis of the vibrations, provide an optimized geometry to maximise the frequency of this mode whilst controlling the amount of material added to the blade stock. This approach will create a stiffer blade geometry in the semi-finished state, reducing milling chatter for a given machine setup. Appropriate boundary conditions are applied to the model to ensure the clamping of the component to the machine table is replicated.

The stock offset for the blade is set to 0mm and the blade surface created is extracted as a face chain before a blend is added to the blade root. Datum planes are added in the XZ-plane and the YZ-plane such that the extracted blade surface can be subdivided into smaller sections. The resolution chosen here can greatly affect the computational time for optimisation to be achieved. Initially a 7x7 split is picked as it provides sufficient variables to perform a detailed optimisation analysis in a few hours without requiring immense computing power (Figure 27). The two YZ-planes created closest to the blade leading and trailing edges are also used to split the solid blade body into three, to aid with meshing during the analysis.

The split is performed after the fillet has been added and the planes must flow continuously from root to tip as shown in Figure 27.

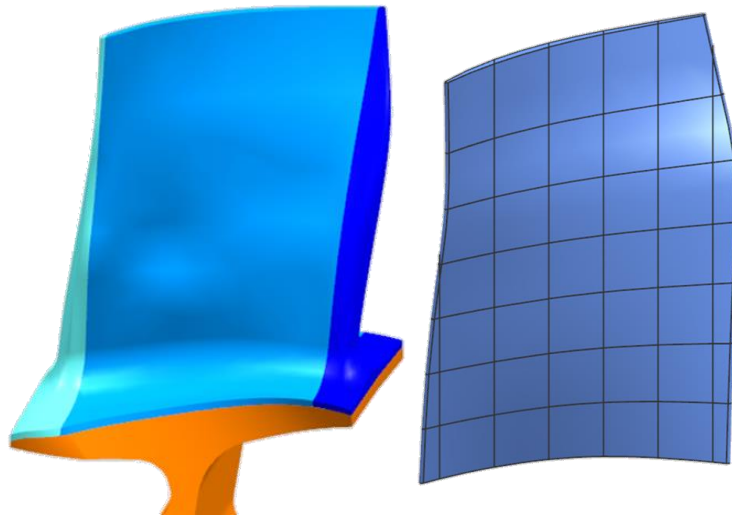


Figure 27. Split body geometry, solid (left) & surface (right).

Figure 27 is also split at the blade root. This can be achieved using the extract geometry command prior to uniting the blade and disc. Selecting the disk's outside surface as a face chain provides the planar geometry required to perform this split. The split shown has an additional offset of 0.05" (1.27mm) though this is not strictly necessary.

4.2.2 Ansys workbench preliminary analysis

This section describes the steps followed to prepare the FEA model. It starts from adding a modal analysis to the project schematic in workbench, and importing the reference model geometry either directly as a Unigraphics .prt file or as an exported parasolid file (.x_t).

Using a .prt file offers the additional benefit of enabling the user to subsequently modify the geometry in NX (Unigraphics). Workbench is able to recognise the change and update the model/mesh accordingly. In this work a .prt file is selected as NX is used back and forth to work with geometry changes. In order to successfully import both solid and surface bodies, the following settings are selected:

Table 18. Advanced geometry options.

Analysis Type	3D
Use Associativity	<input checked="" type="checkbox"/>
Import Coordinate Systems	<input type="checkbox"/>
Import Work Points	<input type="checkbox"/>
Reader Mode Saves Updated File	<input type="checkbox"/>
Import Using Instances	<input checked="" type="checkbox"/>
Smart CAD Update	<input checked="" type="checkbox"/>
Compare Parts On Update	No
Enclosure and Symmetry Processing	<input checked="" type="checkbox"/>
Decompose Disjoint Geometry	<input checked="" type="checkbox"/>
Mixed Import Resolution	Solid and Surface

Connection between the two applications must be maintained throughout the analysis; and therefore, closing NX/ANSYS before results are saved may cause the modal analysis to fail. It is important to select the appropriate material for the analysis, which in this case is Ti6-4 Forging Disks. This material needs to be assigned as the default solid material for the model.

4.2.3 Ansys Mechanical

This section explains how the model is set in Ansys mechanical.

4.2.3.1 Geometry

When the model has been attached, the 'Geometry' section reveals 4 solid bodies and multiple sheet bodies. These sheet bodies need a defined thickness. This thickness is entered as a value between the maximum and minimum stock limits. To confirm that the model can solve for the most extreme profile, maximum stock limit is tested as the sheet thickness.

4.2.3.2 Coordinate systems

After defining the thickness, a cylindrical coordinate system is created. The origin of the coordinate system is defined by Global Coordinates and the orientation of each axis is manipulated to create a radial y-axis that defines the rotational axis of the blisk as shown in Figure 28.



Figure 28. Cylindrical coordinate system orientation.

4.2.3.3 Contacts

By importing the geometry directly into Workbench, the contacts between each split body are automatically generated as 'Contact Regions'. These bonded contacts are displayed each corresponding to a pair of faces. Additional manual bonded contacts need to be added between the solid blade body and each sheet at the blade root that is concealed by a solid body.

4.2.3.4 Mesh

Once the contacts have been specified, a mesh is created. In this case, for the fundamental blade mesh a 'Curvature' size function is preferred with 'Coarse' relevance center, 'Medium' smoothing and 'Fast' transition. This settings have been selected from experience obtained with the software in this and other projects, and the knowledge shared with specialists in modelling.

The size selection is most critical in reducing computational time. The values selected for the mesh are:

- 'Min Size' = 0.5mm,
- 'Max Face Size' = 2.0mm
- 'Max Tet Size' = 4.0mm.

A coarser mesh can be generated; however radii for LE and TE tends to become jagged with regions disappearing. Since the tetrahedrons are forced to occupy a larger area, many are generated with high Jacobian values. Resulting frequency results are therefore more erratic.

Element mid-side nodes are kept for this analysis and the free face mesh type is set to 'Quad/Tri' to generate a stable mesh.

A hex dominant mesh is applied to the disc segment and central blade body. Using hex elements in the model, the number of elements required to generate a smooth mesh are reduced. They also avoid generation of misleading stiffness results that can be produced when using very large tetrahedral elements.

Figure 29 shows an example of the resulting mesh structure.

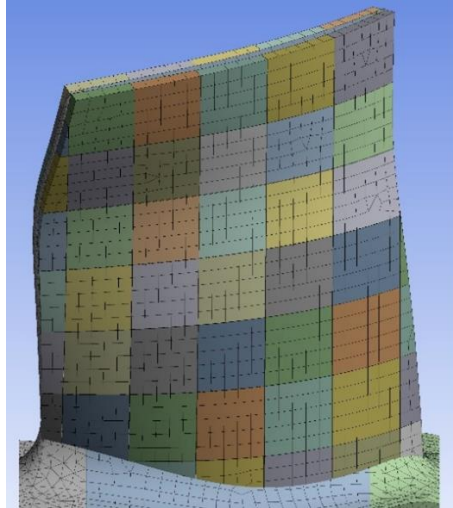


Figure 29. Mesh structure.

4.2.3.5 Mesh edit

A 'Node Merge Group' is applied to the sheet bodies to ensure that the same nodes are used at each sheet body interface. Nodes are merged 'Face-Face' and 'Face-Edge' and a tolerance value of less than 0.1mm avoids excessive merging.

4.2.3.6 Supports

The component is clamped between a top and bottom plate on the forward and afterward faces highlighted as 'A' in Figure 30. Clamping force alone prevents rotation of the component in the fixture.

For the Modal analysis, a fixed support is added to these faces. Since the model is only representative of a 47th segment of the overall IBR structure; a fixed displacement is applied to the wedge boundary faces 'B' (Figure 30), to simulate the radial rigidity of the IBR.

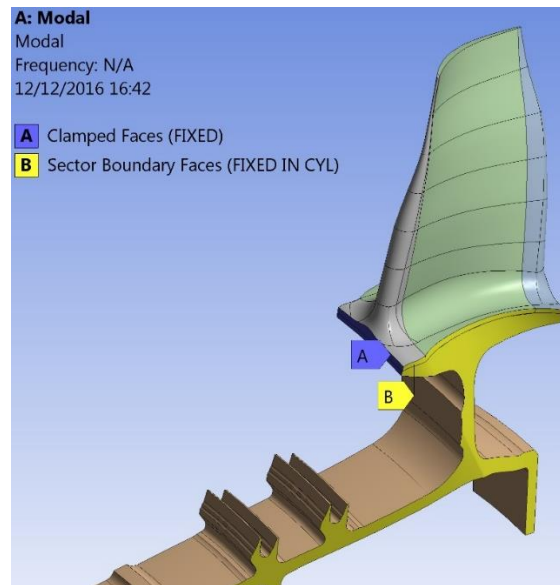


Figure 30. Model setup.

4.2.3.7 Solution

Since the disc is only clamped at the blade root, the first frequency is typically a lateral disc mode which oscillates about the IBR neck (immediately below the blade). This mode has little adverse effect on the blade and hence focus is centred on first flap frequency, which is typically Mode 2.

The solver typically takes around 30 seconds to complete and the result file is no larger than 30MB.

4.2.3.8 Additional remarks

A pre-stress can be applied perpendicular to the tip of the blade to represent the force applied by the cutting tool. However, this force has negligible effect on the solution and therefore is omitted for simplicity.

4.2.4 Ansys workbench abridged analysis

Using the results from the preliminary IBR modal analysis, it is possible to further simplify the geometry and therefore greatly reduce computational time. This step is vital to enable the efficient use of the direct optimisation tools which require high computational time.

This is done by further splitting the IBR wedge immediately below the root of the blade to reduce mesh complexity and computing time (see Figure 31). This leaves a planar surface which can still be fully constrained to model the milling fixture.

Coming from the preliminary analysis described in section 4.2.2, coordinate systems, contacts and mesh subsections do not require any modification.

In order to simulate the properties of the disc segment in the modal analysis, an additional constraint is required. An elastic support is added to the lower surface of the blade root. The ‘Foundation Stiffness’ value is dependent on the surface area.

Instead of deriving foundation stiffness from first principles it is possible to iterate the solver to achieve an approximate Elastic Foundation Stiffness (EFS) value. Since the first flap frequency value has been determined in the preliminary analysis, the foundation stiffness value can be adjusted to achieve an identical frequency value.

For this particular IBR, splitted through the disc section, a value of 1600 N/mm^3 has been applied (see Figure 31). Splitting the IBR at blade root reduces cross-sectional area; thus a far greater foundation stiffness value is required.

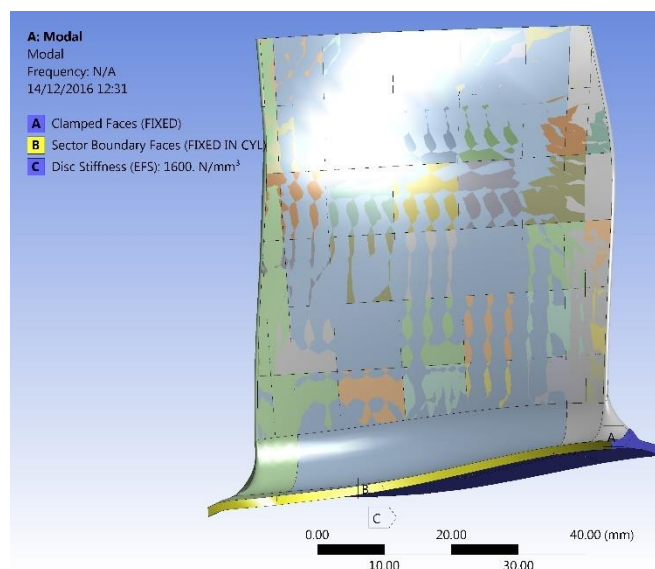


Figure 31. Simplified IBR model setup.

This approximation reduces nodes and element count for the model, reducing the result file and computational time by approximately 50%.

By suppressing the disc body, the deformation modes that are generated change. Mode 1 now displays the first flap frequency and therefore it is defined as the mode of interest. It is important at this stage to confirm that the frequency generated is identical to the preliminary analysis.

4.2.5 Direct optimization

So far, the preliminary analysis has been described and a further simplification has been carried out by suppressing the disk body and adding a foundation stiffness instead. Computational time is reduced and the model is ready to work with the direct optimization tool available in Ansys software. Section 4.2.4 describes the work carried out in order to obtain geometry optimization results targeting the increment of the blade's flap frequency.

In Ansys Mechanical, thickness is parametrized. Blade mass is also parametrised to allow the monitoring of overall stock level per iteration. Mass can be set as a limit or objective for the optimisation process if it is considered critical for manufacture, although at this point it is only used for monitoring purpose.

The direct optimization tool is dropped to the project schematic window, so that it links to the analysis system. This is done after the thickness and mass options are parametrized.

Initially, the method type is set to 'MISQP'. Within this method, Initial Finite Difference Delta is defined, which determines the rate of change of each variable between iterations. Increasing the delta generates data points near to the upper and lower bounds swiftly to produce a holistic analysis of the stock thickness. If a stock profile has already been established for the blade, the difference delta can be reduced along with the allowable convergence percentage to fine-tune results and verify global convergence.

To ensure that the solver converges, maximum number of iterations is set to 200 (20 is default) and maximum number of candidates option is reduced to 1.

Within the option of objectives and constraints, geometry mass and total deformation reported frequency are selected with an objective to maximize the frequency parameter. The solver optimization process can be aided further by specifying a constraint (i.e $\geq 2200\text{Hz}$).

This helps with establishing an absolute maximum frequency for the model and is therefore only used as a verification tool.

In order to reduce the computational effort for the initial stock assessment, manufacturing values option is selected. This setting is enabled with discrete values for all thickness parameters simultaneously. Lower and upper bounds of 0.1mm and 2.5mm are established respectively, based on current knowledge and experience. Step, range and starting values are modified to suit desired thickness requirements. These values are then pasted directly into the input parameters section of the table of schematic window.

Once successfully generated manufactural values for the model, the input parameters are displayed as shown in Figure 32.

Table of Schematic C2: Optimization				
	A	B	C	D
1	Input Parameters			
2	Name	Lower Bound	Upper Bound	Starting Value
3	P1 - Blisk trial10B-prt3\A0 Thickness (mm)	0.1	2.5	2
4	P2 - Blisk trial10B-prt3\A1 Thickness (mm)	0.1	2.5	2
5	P3 - Blisk trial10B-prt3\A2 Thickness (mm)	0.1	2.5	2
6	P4 - Blisk trial10B-prt3\A3 Thickness (mm)	0.1	2.5	2
7	P5 - Blisk trial10B-prt3\A4 Thickness (mm)	0.1	2.5	2
8	P6 - Blisk trial10B-prt3\A5 Thickness (mm)	0.1	2.5	2
9	P7 - Blisk trial10B-prt3\A6 Thickness (mm)	0.1	2.5	2
10	P8 - Blisk trial10B-prt3\A7 Thickness (mm)	0.1	2.5	2
11	P9 - Blisk trial10B-prt3\A8 Thickness (mm)	0.1	2.5	2
12	P10 - Blisk trial10B-prt3\A9 Thickness (mm)	0.1	2.5	2
13	P11 - Blisk trial10B-prt3\A10 Thickness (mm)	0.1	2.5	2
14	P12 - Blisk trial10B-prt3\A11 Thickness (mm)	0.1	2.5	2
15	P13 - Blisk trial10B-prt3\A12 Thickness (mm)	0.1	2.5	2
16	P14 - Blisk trial10B-prt3\A13 Thickness (mm)	0.1	2.5	2

Figure 32. Optimization. Parameter setup.

At this stage the optimization process is solved. Typical run time for this analysis to converge is approximately 150 hours. However, execution time is greatly reduced through the use of ANSYS Workbench’s parallel solving method ‘RSM’. This is enables multiple design points to be solved simultaneously.

After the optimization has converged, the maximum frequency value determined is highlighted as candidate point 1 in the resulting table. A side-by-side comparison with the starting values is attained to reveal the benefits of the optimisation. (Figure 33)

CHAPTER 4. BLADE OPTIMIZATION FOR FINISH MILLING OPERATION

Outline of Schematic C2: Optimization			
	A	B	C
1		Enabled	Monitoring
90	P83 - Blisk trial10B-prt3\G3 Thickness	<input checked="" type="checkbox"/>	
91	P84 - Blisk trial10B-prt3\G4 Thickness	<input checked="" type="checkbox"/>	
92	P85 - Blisk trial10B-prt3\G5 Thickness	<input checked="" type="checkbox"/>	
93	P86 - Blisk trial10B-prt3\G6 Thickness	<input checked="" type="checkbox"/>	
94	P87 - Blisk trial10B-prt3\G7 Thickness	<input checked="" type="checkbox"/>	
95	P88 - Blisk trial10B-prt3\G8 Thickness	<input checked="" type="checkbox"/>	
96	P89 - Blisk trial10B-prt3\G9 Thickness	<input checked="" type="checkbox"/>	
97	P90 - Blisk trial10B-prt3\G10 Thickness	<input checked="" type="checkbox"/>	
98	P91 - Blisk trial10B-prt3\G11 Thickness	<input checked="" type="checkbox"/>	
99	P92 - Blisk trial10B-prt3\G12 Thickness	<input checked="" type="checkbox"/>	
100	Parameter Relationships		
101	<input checked="" type="checkbox"/> Raw Optimization Data		
102	<input checked="" type="checkbox"/> Convergence Criteria		
103	Results		
104	<input checked="" type="checkbox"/> Candidate Points		
105	<input checked="" type="checkbox"/> Tradeoff		
106	<input checked="" type="checkbox"/> Samples		

CQ	CR	CS
P93 - Geometry Mass (kg)	P94 - Total Deformation Reported Frequency (Hz)	
	Parameter Value	Variation from Reference
0.11915	★★ 1460.7	0.00 %
0.097544	★★★ 2279.8	56.08 %

Figure 33. Overview of resulting candidate point schematic.

4.2.6 Topographical variation

The split stock optimization method carried out in section 4.2.4 allows the user to determine the highest stiffness blade shape possible on the assumption that each section is of a uniform stock thickness. Reducing the size of each section leads to a more refined shape however the increase in variables means that vast computational resources are required. In addition, the stock thicknesses can only be varied in the XY and YZ planes.

Entering the initial optimization results back into the NX CAD model, the utilisation of smoothing tools to allow the stock to be varied topographically is enabled. Returning to the split stock blade model, the edge of each horizontal blade band is extracted to produce a series of parallel composite curves (from blade root to tip). Each curve is then imported into its own sketch whilst maintaining associativity. Using each of these curves as a guide (shown as grey construction line), minimum and maximum stock thickness offsets are formed as shown in cyan in Figure 34. The red curve in Figure 34 is produced by inserting a spline that intersects the endpoint of a series of perpendicular offset thicknesses from the midpoint of each split section.

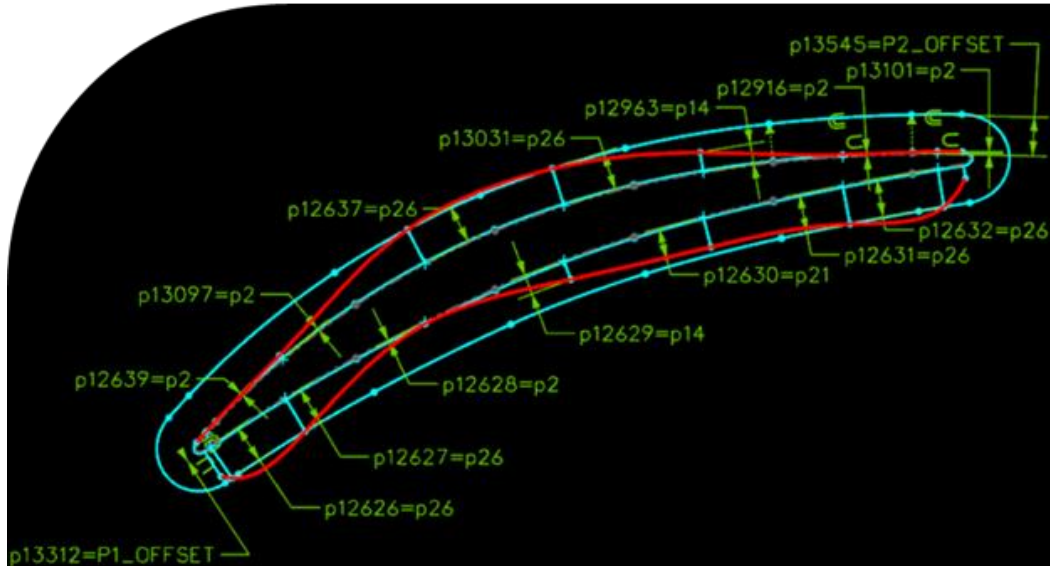


Figure 34. Sketch of an individual split stock cross-section.

Figure 35 shows the sum of each parallel curve from sections one to seven, from tip (left) to root (right). Purple lines show the topographical variation that shapes the optimized stock blade using smoothing tools.

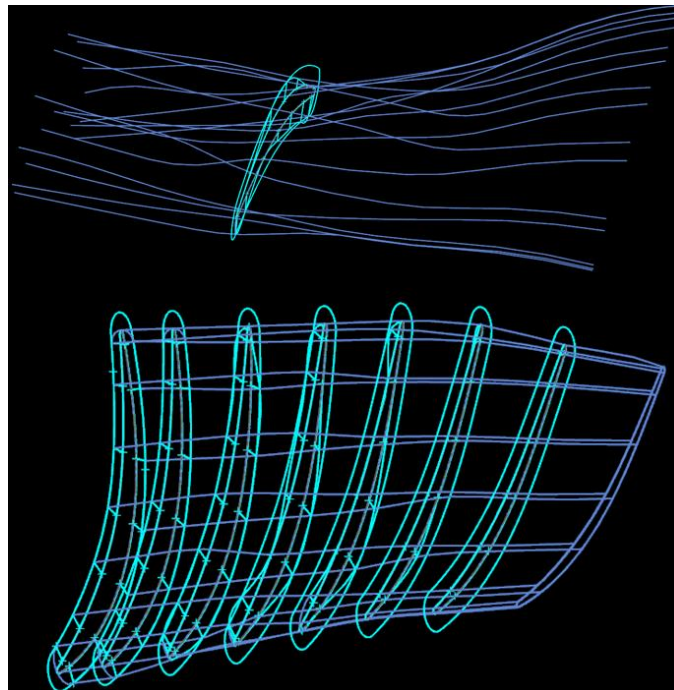


Figure 35. Parametrized construction of IBR blade.

4.3 Results

Previous sections in this chapter describe the process of generating an FEA model and the process to run the analysis in order to optimize the first flap frequency, main vibration mode of the blade. Now results obtained in the analysis are discussed.

Initial FEA model for the preliminary analysis is simplified with a new model by suppressing the disk body and applying a stiffness value of 1600 N/mm^3 . This stiffness value is selected so that the first flap frequency (main vibration mode) is replicated from the complete blade and disk section analysis (Figure 36).

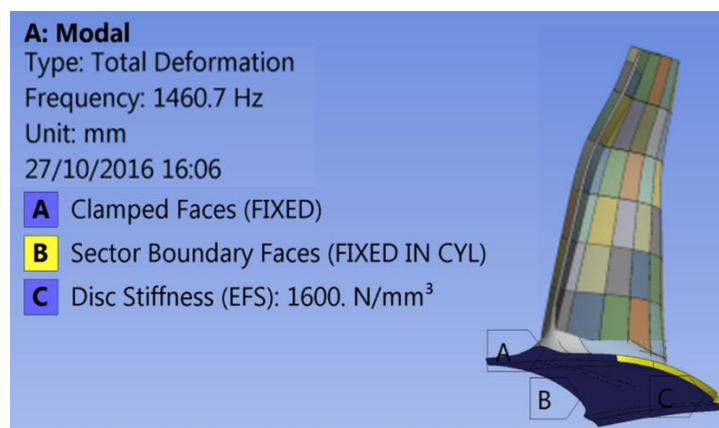


Figure 36. Simplified model showing baseline first flap frequency

Both the preliminary model and the simplified model are analysed with an initial stock of 2mm over the entire concave and convex surfaces. This replicates current stock for the finishing operation. The mode 1, which is the first flap frequency, gives a frequency of 1460.7Hz. This is the baseline frequency and it compares to 1272Hz obtained in the experimental tap test carried out in chapter 3. There is a difference of 189Hz, which is acceptable for the purpose of this study.

Figure 37 shows the optimization result for a 7x7 split stock. The first flap frequency obtained is now 2281.3Hz, an increment of 56% in respect to the baseline. As it can be observed in Figure 37, blade finishing stock is optimized by adding material in the root up to the manufacturing limits and reducing material in the tip down to the manufacturing limits, in this case 2.5mm and 0.1mm stock respectively.

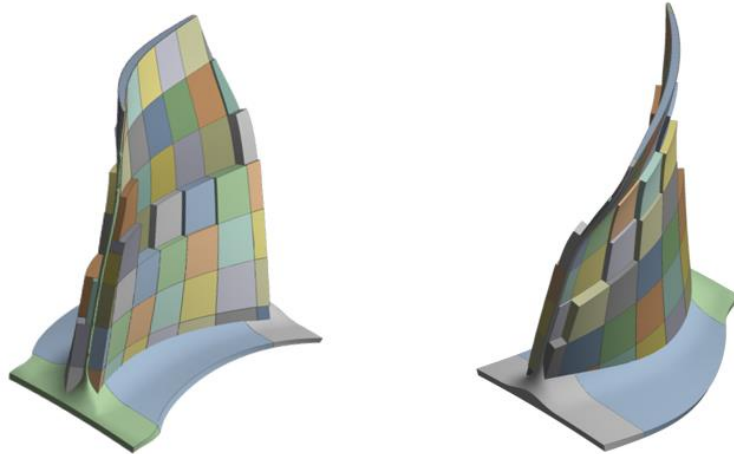


Figure 37. Optimized stock layout.

Figure 38 below shows optimal stock simulated for each section A to G and 0 to 13. This layout is not considering the difficulties of the roughing or semi-finishing tool to create this geometry and it is clear that such abrupt changes in stock are not achievable in the semi finishing stage.

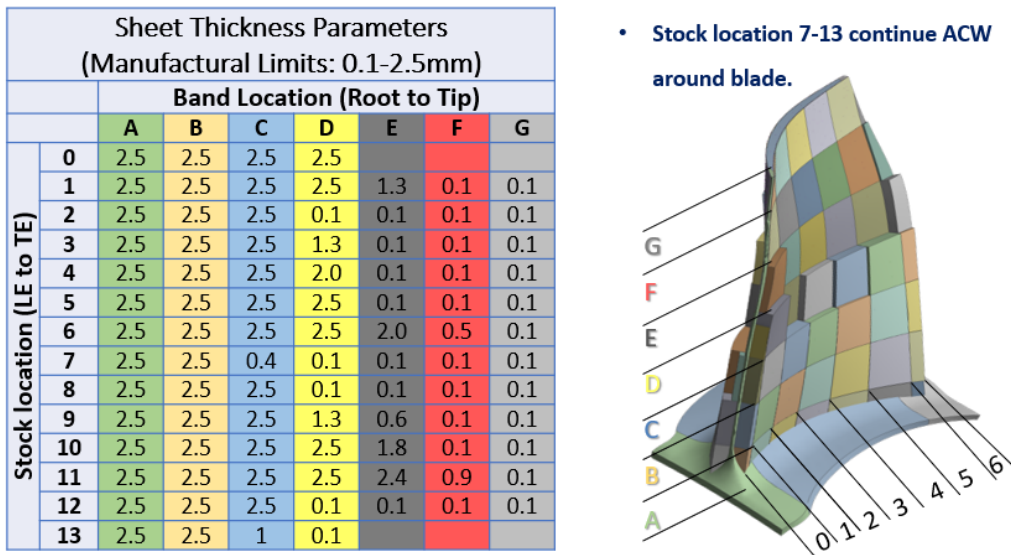


Figure 38. Optimal stock layout.

Therefore, this result needs to be reshaped through NX CAD software smoothing tools to achieve tangency between adjacent points and new iterations are done in order to obtain an

optimized stock with manufacturable transitions. Result from smoothing action is observed in Figure 39. Results are given in inches.

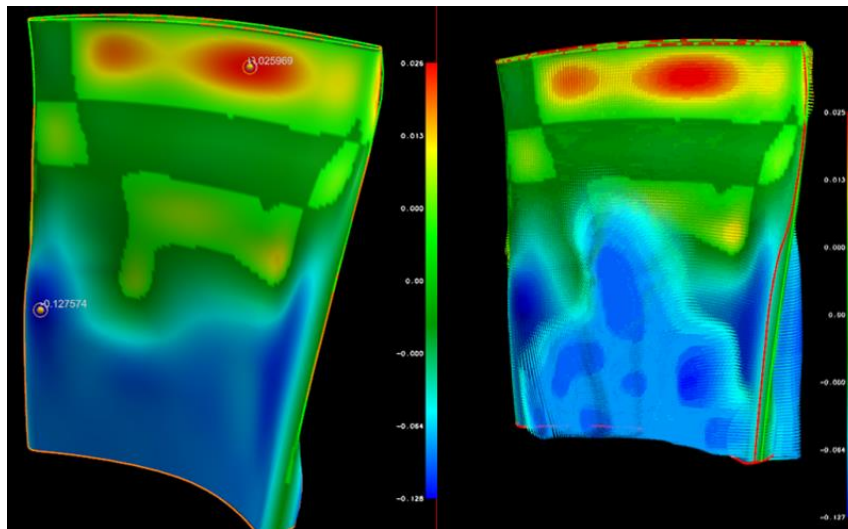


Figure 39. Smoothed model.

A maximum value of 0.1276 inches (3.24mm) is obtained and a minimum value of -0.0259 inches (-0.56mm). Note that zero is considered the minimum stock of 0.1mm. Those max. and min. values are outside the manufacturable range established previously from manufacturing experience. A localised maximum could be achievable, but minimum stock is under the finished stock, and further smoothing needs to be carried out before analysing the results of the optimized geometry. Therefore, a smoothing action to the resultant geometry has been performed both with a topographical variation through the whole blade and with a linear variation between horizontal sections.

Total deformation and main vibration mode frequencies are shown in Figure 40. Picture on the left shows a smoothed topographical variation model, whereas picture on the right shows a smoothed linear variation model. Both approaches greatly improve the target frequency of 1460.7Hz. Topographical variation model achieves a frequency of 2538.7Hz while the linear variation model achieves a frequency of 2913.4Hz. These are percentual improvements of 73.8% and 99.5% respectively.

The difference between the experimentally obtained frequency (1272Hz) and modelled baseline frequency (1460.7Hz) is low comparing to the gains obtained with the topographical (2538.7Hz) and linear (2913.4Hz) variation models respect to the baseline frequency.

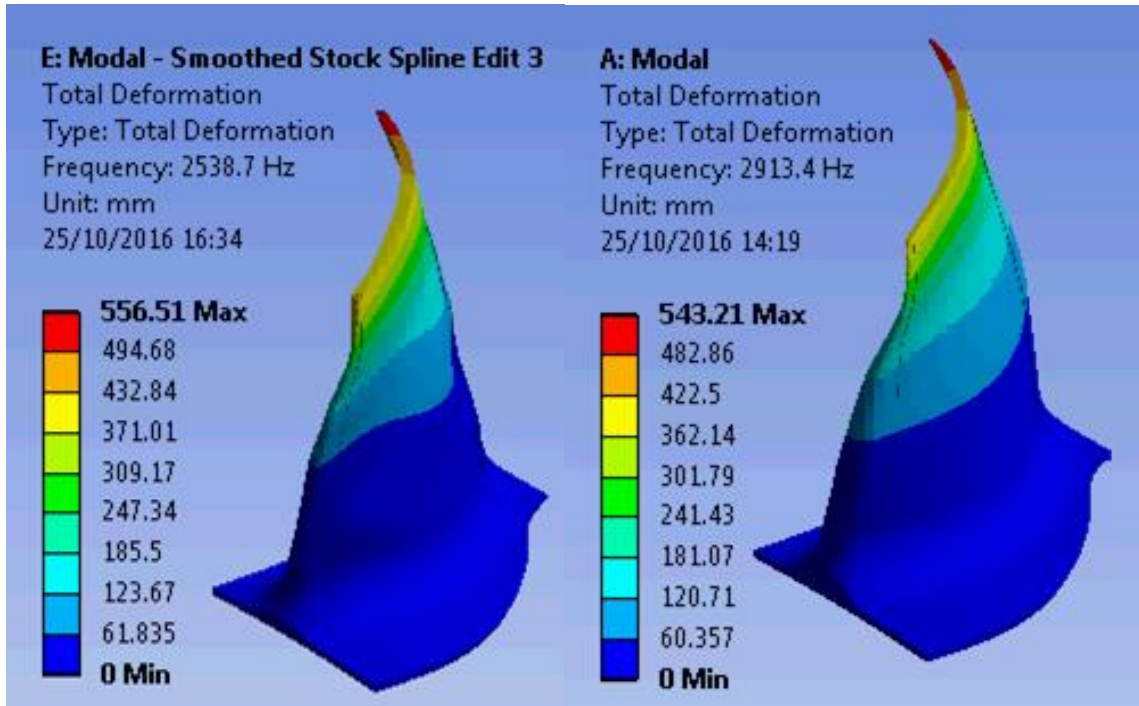


Figure 40. Total deformation and first flap frequency results for topographical (left) and linear (right) variation.

There are important differences between the topographical model in which the stock variation occurs in 2 axis or the linear model in which the stock variation occurs in a single axis. Linear variation achieves a higher frequency (and a lower deformation). This is due to adding mass across the blade, mainly in the bottom half of the blade. This is expected to have some impact in tool life for the finishing operation. From the other side, the topographical variation model has a more complex curvature geometry which could be difficult to machine with the bigger ball-end semi finishing or roughing tools due to limiting tool radius. Overall, topographical optimization model provides a 10% lighter blade for semi-finished stock condition comparing to the linear model, but manual adjustments of the geometry are needed to adhere to min/max stock limits, as shown in Figure 39.

4.4 Conclusions

IBR blade finish milling stock optimization process has been explained and analysed in this section. Initially, model geometry, supports, mesh and set up details have been explained. An optimization method has been outlined and different results have been compared for topographical stock variation and linear stock variation.

The main objective of this work is to optimize stock to achieve maximum frequency for the main vibration mode of the blade. The method that offers the best result is the linear variation stock model, which raises 99.5% the baseline frequency. This comes at the cost of a higher mass across the blade, which might have some impact in tool life, but also a simpler geometry to achieve in the semi-finishing operation. This solution is preferred over the topographical stock variation overall.

The modelled baseline dominant frequency differs in 189Hz respect to the experimental results from the tap test described in chapter 3. Material properties applied to the model and the contacts as well as the mesh are likely to cause the difference between them. This could be reduced by further adjusting the contacts, mesh and material properties, but it is acceptable for the current exercise, especially comparing the frequency gains obtained with optimised stock geometries.

This work is an initial stock optimization approach towards a more stable and efficient finish milling operation for IBR blades. However, future work in blade stiffness when final cutting is in progress could add great value to this study. In the same line, a more in deep analysis to other vibration modes occurring during the finish machining of the IBR blades might be of interest.

4.5 Summary

This chapter focuses on how the finish milling stock can improve IBR blade vibration response. This EngD thesis is a journey towards the optimization of finish milling of IBR blades. The need for this particular study has been identified in Chapter 2, in which surface integrity for the

typical finish milling working window for IBR blades has been analysed and found not to be a limiting factor compared to chatter effect.

This leads to directing the research towards chatter mitigation strategies. There are many different approaches to tackle this issue but optimizing the initial stock geometry is arguably the best starting point. The result of the work described in this chapter is a 99.5% increase in the main vibration mode frequency compared to current manufacturing method baseline. This has been achieved within a min. and max. manufacturing stock values of 0.1mm and 2.5mm respectively. This enhances greatly the stability of the IBR blade prior to finish milling operation and therefore improves its response to vibrations.

Tool excitation frequencies from the tested window (32m/min to 240m/min) are 107Hz to 802Hz. Hence, increasing the natural frequencies further away from the excitation frequencies is favourable for a stable cutting process. Nevertheless, harmonics of the excitation frequencies could still interact with the component frequencies producing resonance, and they should be considered in a future cutting parameter selection.

The stock geometry optimization work is justified from the huge step forward in blade stiffness obtained and clearly shows that the traditionally employed constant finish milling stock is a deficient strategy for this type of structures. Additionally, this optimization allows to separate natural frequencies of the tool and the IBR blade, which were in conflict before.

Further work in geometry optimization could be done, especially considering blade stiffness while finish milling cutting is in progress, as well as studying the effect of other secondary vibration modes.

Overall, semi-finished shape optimization has helped to improve dynamic properties of the system but in order to seek further productivity gains, it is now important to perform a more detailed review of existing techniques for chatter mitigation. Therefore, this is the focus of Chapter 5.

CHAPTER 5. LITERATURE REVIEW ON CHATTER MITIGATION

5.1 Introduction

An IBR case study has been presented with the objective of improving productivity of the component. A preliminary experimental work has been conducted, observing that surface integrity is not a limiting factor for the tested working window. Instead, high surface roughness and the evaluation of the cutting forces suggest that both chatter and process damping are likely to occur, especially when the real dynamics of the blade are considered as opposed to the experimental work, which was completed in a rigid workpiece.

Therefore, a new strategy has been followed through the understanding of the tool and workpiece dynamics, followed by an optimization of the blade stock to overcome possible issues of the tool and workpiece matching vibration frequencies, and most importantly improving the dynamic stability of the semi-finished blade.

Although this improvement alone is expected to increase blade finish milling productivity, it is considered that further benefits can be obtained by understanding chatter phenomena and applying new strategies which are compatible with blade stock optimization.

At this stage, a thorough literature review is carried out, covering both process damping and chatter. This is very important, in order to find the most appropriate chatter mitigation strategy and also to find current knowledge gaps and provide solutions which not only improve the manufacturing process of an IBR, but also contributes to the state of the art of this research field.

5.2 Process damping

Process damping is the nonlinear effect of the penetration of the tool in the wavy surface generated in previous passes due to the regenerative vibration or chatter. This penetration

creates forces in the opposite direction of the forces that generate chatter vibration. If the penetration between the tool and the wavy surface is big enough, generated forces are able to counteract the forces that generate chatter, by limiting the negative effects of the latter, which means to limit the vibration amplitude. This is the simplest way to explain process damping, although it is more complex to explain all the aspects that control the generation of the process damping forces. In fact, even if the first attempts to understand the process damping effect were carried out more than three decades ago, still it is not fully understood.

5.2.1. Effect of cutting parameters on process damping

J. Tlustý and F. Ismail [19], in a theoretical approach, stated that process damping occurs due to the interference of flank of the tooth with the slope of its motion in the cut. According to this, relative clearance between the tool and surface is different when the tool is moving upwards and downwards in the previously generated waves. In downwards position, when the slope of the wave reaches or exceeds the relief angle, interference is created between the tool and the surface which produces process damping forces. The slope of the wave is proportional to the amplitude of vibration and the ratio of vibration frequency and cutting speed. Therefore, they concluded that for low cutting speeds and high vibration frequencies the process damping is high. Also, from their theoretical explanation it can be easily recognized that the smaller the relief angle, the higher the process damping will be.

Y. Altintas et al. [20] analysed the effect of the tool wear on the process damping in a turning process. To do so, they carried out dynamic cutting tests on stainless steel to obtain the dynamic cutting force coefficients but ignored the curvature term which they found difficult to identify. Experimentally, they found that the process damping coefficient increased almost linearly with the tool wear. After, they predicted a stability lobe diagram both, for a new tool and a tool with a flank wear of 0.080mm, and the stability area was incremented from 1000rpm to 3000rpm for the worn tool. This was then experimentally tested by machining in different points within the predicted stability lobes diagram. The experimental results agreed well with the stability lobes predicted, confirming the great influence of the flank wear on the process damping.

L.T. Tunc and E. Budak [21] applied the energy analysis in their mathematical model to determine the indentation coefficient from the experimentally identified process damping coefficient. Their work is probably the most extensive up to date analysing the effects of cutting parameters on the process damping. After simulating different cutting parameters, they obtained the following results for milling Ti6-4; The lower the clearance angle, the higher the process damping coefficient. In a variation from 6° to 20° clearance angle, the differences were significant at cutting speeds lower than 100m/min. Similar results were obtained for the edge radius in a range from 10µm to 50µm; in this case, increasing the edge radius also increased the process damping coefficient. Flank type was also analysed and cylindrical flank provided higher process damping compared to the planar flank. Both, lower vibration frequencies and higher vibration amplitudes generated higher process damping forces as well. When quarter and half radial immersion were compared, the bigger radial immersion proved to provide a more stable cut. Finally, tools with different number of flutes were compared and the less flutes in the tool proved to be better for chatter stability in general.

C.M. Taylor et al. [22] studied how tool's edge condition combine with the relief angle to affect process damping in a turning process. They created an analytical model for the case of high width of cut and high specific ploughing force of the workpiece. The model was based in Tlustý's process damping theory that related surface speed and vibration frequency to the vibration wavelength and added geometrical contact produced by the relief angle and the edge radius. Their model predicted that the edge radius dominates the process damping for low vibration wavelengths or low surface speeds, while the tool flank dominates the process damping for higher surface speed. A two-section composite curve was predicted with an edge-dominated wavelength region followed by a flank dominated higher wavelength region. For simulations at lower widths of cut (less than 3.5 times b_{crit}) vibration amplitude was dominated by the edge radius within the stability threshold set at 5µm peak vibration amplitude. To confirm this, they carried out an experimental turning test in 230M07 steel, with a 20µm edge radius and 7° relief angle tool. Results confirmed that below the surface speed of 200m/min the maximum vibration amplitude was dominated by the tool with the edge preparation, compared to the theoretical flank driven vibration amplitude obtained with a sharp tool. In summary, the work of C.M. Taylor et al. proved that edge radius has a bigger impact in process damping compared to the relief angle, for certain circumstances.

The time domain model developed by N.D. Sims and M.S. Turner [23] considered process damping forces in milling due to interference between the tool flank and the surface generated by the previous tooth. They did not include the edge geometry features to the model, but they recognised the influence of the edge geometry and suggested to be introduced in a further development of the model. They used a vibration amplitude based threshold to define the acceptable process damped, chatter stability. The main finding of the simulations was that the process damping wavelength (corresponding to the threshold for vibration amplitude) increased as the feed per tooth or the maximum chip thickness was increased. They compared simulation results to experimental tests and the results agreed qualitatively, despite the fact that the process damping coefficients were not properly calibrated.

V. Sellmeier and B. Denkena [24] investigated the process damping theoretically and experimentally for dynamic milling processes, focussing on the effect of cutting edge chamfers. To do so, they combined the cutting force model of Friedrich with the process damping model of Wu. They found that the stability limit increases significantly with the width of the cutting edge chamfer, in the analysed range of 0-0.2mm, with a chamfer angle of 1° and clearance angle of 14° . Their main finding was that the mentioned stability limit increase was not limited to the low spindle speed range, but rather occurred across the whole range of spindle speeds. For example, in slotting tests carried out with an aluminium alloy and at a spindle speed of 10000 rpm, they found that the end mill without chamfer became unstable at $a_p = 6mm$ whereas the end mill with a chamfer length of 0.2mm was still stable at $a_p = 15mm$. They also found that the process damping coefficients were not constant but decreased with increasing the width of chamfer, which they believed that happened due to an increase in temperature of the workpiece that led to a softening of the workpiece material. The reasons of such behaviour of process damping at high surface speeds were thought to be the increase in chatter vibration frequency at higher spindle speeds and also the low clearance angle of the cutting edge chamfer. Such a low clearance, together with the elasto-plastic behaviour of the workpiece material, is believed to rub along the cutting edge chamfer even if the inner modulation is zero and thus creating process damping even if the slope of the vibration waves is very small. However, according to the authors, the main reason for the high speed process damping was some kind of mode interaction between the lower and

higher frequency modes, as they proved that the system stability varied significantly when the study was done with one and two eigenmodes. The fact that in many previous studies the structural dynamics were simplified to a system with only one eigenmode would explain the novelty of the finding.

In general, it is widely recognised the effect of the cutting tool geometry on process damping. Flank type of the tool and clearance angle have demonstrated to be very important together with the cutting edge radius in the successful appearance of this phenomena. Similarly, surface speed and feed per tooth have an impact on the generation of the process damping. Therefore, successful modelling of this phenomena needs to consider detailed geometry of the tool including the effect of the tool wear, and the effect of cutting parameters such as surface speed and feed per tooth. Section 5.2.2 looks into the modelling work carried out by other researchers.

5.2.2 Process damping modelling

J. Tlustý and F. Ismail [25] considered in a predictive model the basic nonlinearity of process when the tool jumps out of the cut for part of the cycle. They saw that the chatter amplitude was limited by this effect and they created a time domain simulation that included the jump of the tool out of the workpiece material for part of the cycle when the chatter amplitude was big enough for this effect to happen. In another research paper, these researchers discussed the nonlinearity created by the process damping effect [19]. They explained process damping as a cause of the interference of the flank of the tooth with the slope of its motion in the cut. Also, they analysed the slope of the wave σ and related it with the chatter frequency and the surface speed (eq. 5.1).

$$\sigma_{max} = 2\pi A \frac{f_c}{V_c} \quad (5.1)$$

They illustrated graphically how the relative position of the tool and the slope of the wave together with the relief angle of the tool generate the process damping effect and also stated that process damping was enhanced when chatter frequency was high and surface speed low. However, they did not include this nonlinearity in their simulation model.

D.W. Wu and C.R. Liu [26] created a mathematical model of machining chatter in which they developed the dynamic cutting force. This model considered the ploughing force on the tool nose to explain the positive damping that limits the chatter amplitude vibration. In order to obtain the ploughing force, damping coefficient had to be obtained from complicated dynamic cutting tests, so they suggested estimating from an existing stability chart, created with an arbitrary feed [27]. This model confirmed that the ploughing force acting on the tool nose dominates the low-speed stability whereas the cutting force acting in the rake face dominates the high-speed stability.

S.C. Lin et al. [28] proposed a method to estimate the process damping from data collected during working conditions without having to remove the effect of the regenerative vibration to do so. They employed a modified Dynamic Data System (DDS) approach to estimate the cutting process damping which was based in characterizing the data obtained in a stochastic process using a differential equation and modified for not having to physically remove the effect of regeneration. However the model poorly estimated process damping when chatter occurred.

I. Minis et al. [29] developed a milling specific mathematical model, which improved the previous milling dynamic models such as the model developed by Shridar et al. [30] which was specific for milling but did not include nonlinear effects. I. Minis et al. used a two degree of freedom system, as proposed by Shridar et al. that became linear if each tooth remained in contact with the workpiece along the length of the machined arc; however no process damping effect was considered in the model.

Y. Altintas et al. [20] developed a cutting force model to include three dynamic cutting force coefficients, related to regenerative chip thickness and the process damping related velocity and acceleration (curvature) terms which govern the flank/tool contact. The dynamic cutting force coefficients were obtained from orthogonal cutting tests in a controlled experiment with a fast tool servo which was oscillated at the desired frequency. The tool oscillating frequency and the spindle speed were synchronised to obtain in phase inner and outer modulations that removed the regenerative effect to identify process damping coefficient. They improved the prediction of the chatter stability at low speeds due to the consideration of the tool flank / wave contact which was not included in previous research works.

E. Budak and L. Tunc [31] stated that process damping modelled in the past through dynamic cutting force coefficients proved to be very difficult to measure and led to inconsistency in the obtained data. Instead, they proposed the cutting force coefficient to be identified directly with chatter test where the contact force modelling to generalize the data was based on an energy analysis. They demonstrated that the presented method could be used to predict process damping accurately for very different conditions to those used in the identification tests. Once the indentation force was identified the process damping coefficients and the stability limits for other cases could be predicted without having to do more testing.

Parallel in time, N.D Sims and S.T Turner [23] developed a time domain model to simulate process damping in milling. The model was created to explore the relationships between the cutting conditions and the amplitude of chatter vibrations. Their model was formulated by using the length of contact of the flank with the wavy surface to calculate the cutting forces. They acknowledged the important effect of the edge force coefficients in the vibration amplitude but their analysis assumed the cutting edge force coefficients as zero, while they suggested to properly calibrating them for the future.

As a general conclusion, no model was found that properly integrate process damping with a flexible workpiece and ball end mill tool. A model which integrates those aspects of the milling process would be required to develop in order to understand and apply the optimized solutions for stable cut in IBR blade finishing operation.

However, developing a chatter model that integrates process damping for ball-end mill tool and flexible workpiece might take considerable research and development work. Experimental work carried out in Chapter 2 suggests existence of process damping, which might be occurring when the feed per tooth is increased. However, main benefits from process damping effect are obtained when big depth of cut is employed. This is a limiting factor in the case of IBR blade finish milling, due to the geometrical requirements of the blade shape. Therefore, low depths of cut are used in point milling strategy, and this prevents process damping from obtaining the big benefits in productivity associated to high depths of cut.

For this reason, an approach of developing a process damping related strategy is not considered. Instead, efforts are directed to map all the existing chatter mitigation strategies and discuss which method might be the most beneficial for the particularities present in IBR finish milling operation. This is carried out in section 5.3 below.

5.3 Modelling of chatter

5.3.1 Historical overview

Chatter has been a problem faced by the machinist from long time ago. Initial mentions of chatter in machining were reported at the beginning of the 20th century. It was Taylor [32] who stated that chatter was the “most obscure and delicate of all problems facing the machinist”. However it was not until the late 1950’s when the first theories about regenerative chatter were developed. Tobias and Fishwick [33] published in 1958 the first theory about regenerative chatter, which was later called the T-F method. They first outlined the efforts carried out in the past to investigate machine tool chatter but argued that they were of little use for production engineer and machine tool designers due to mainly three reasons; theoretical recommendations being contrary to practical experience, large number of parameters involved in chatter phenomena, which made complex to understand and use in the industry and the lack of a general theory that would cover different cases. Known as the first big step in the understanding of regenerative chatter, Tobias and Fishwick developed the first analytical approach of the phenomena. They proposed the concept of instantaneous chip thickness affected by current and previous revolutions/teeth and variable forces feeding the dynamic system. Natural frequency, stiffness and damping ratio were determined by resonance tests. They developed the equations of motion with a harmonic type solution and presented the first stability charts plotting non dimensional rotational speed multiplied by the number of teeth (abscissa) and the effective amplification factor (ordinate). For a given set of conditions, the chart would show a stable, critical or unstable region.

Doi and Kato [34] carried out experimental testing in a turning process and observed that when a lathe tool oscillates radially (normal to the machined surface), the normal cutting force component variation lags behind the harmonic motion of the tool.

Research work carried out by Smith and Tobias [35] did a review of the relationship between the cutting forces and chip thickness observed by other researchers, including Doi and Kato, which was causing controversy whether if the change in chip thickness was leading to the change in force or the other way around. Based on experimental data, they concluded that for low frequencies, the cutting forces lag behind the chip thickness whereas for higher oscillation frequencies there is a phase change and cutting force leads against the chip thickness.

Tlusty and Polacek [36] developed a theory for the regenerative chatter which was named as T-P method. Their method was suitable for the investigation of the stability of a cutting process in cases where the structural modes are close to each other, but this method ignored the effects of the cutting speed and the rate of penetration.

Tobias [37] published a state of the art in machine tool vibration research in 1961 and estimated that with the introduction of stainless steel and other materials difficult to machine for aircraft construction, the machining capacity of the aircraft industry would have to be increased by 4 to 10 times.

In the early 1960's, Gurney and Tobias [38], further developed Tobias' theory including other researchers inputs, and presented a graphical method for the investigation of regenerative chatter. The method was based on the harmonic response of the tool and allowed the determination of stable and unstable cutting speed ranges. They considered both the chip thickness variation effect and the penetration rate effect. Unlike with the T-F method, the stability of different modes could be investigated simultaneously.

In the next decade, a step forward in the research of machining chatter was made when Hanna and Tobias [39] presented a theory of nonlinear regenerative chatter. According to the linear theory of chatter, the amplitude of vibration ought to increase indefinitely once the width of cut exceeds a certain critical value and the process becomes unstable. However, this does not happen in practice, as the vibration amplitude stabilizes at a finite level. The stabilization phenomenon was explained to be due to nonlinearities in the system but without specifying where did they come from. Hanna and Tobias created a mathematical theory representing the structure by an equivalent single degree of freedom system with nonlinear stiffness characteristics and the cutting force by a third degree polynomial of the chip

thickness. The model led to a second order differential equation with nonlinear stiffness and nonlinear time delay terms from which the conditions of steady state chatter were derived.

Smith and Tlusty [40] carried out a review in the different numerical time domain models employed at the time, from the most simple approach to the more accurate approach. They defined four different models. The first model, named as “Average Rigid Force, Static Deflection Model” computed force based on average power (which led to an average force) and the deflection of the tool did not play any role in force calculation. This method is erroneous when more than one tooth gets simultaneously in the cut, as the force in the leading tooth causes a deflection on the tool. A more realistic computation of the cutting force was provided by the “Instantaneous Rigid Force” model. This model did not consider the force produced on the cutter to be simply proportional to the average power, but rather computed the instantaneous force on incremental sections of the helical cutting edge. The total force in the cutter was obtained as the vector sum of the tangential and radial forces on all elements cutting. This model did not consider that the deflection of the cutter in response to the force makes any change in the force. An extension of the previous model, named as “Instantaneous Rigid Force, Static Deflection Model”, computed the forces in the same way but also giving an indication of the cutter deflection and the surface generated. However, the deflection of the cutter was taken simply proportional to the force, with no effect in the force calculation. The model called “Instantaneous Force With Static Deflection Feedback” improved the previously mentioned models because the deflection of the cutter was not only computed based on the force, but also was fed-back to have an influence in the force. However, this model was not complete yet because the surface generated by the previous tooth was not included to determine the instantaneous chip thickness. The last model “Regenerative Force, Dynamic Deflection Model” was created to include the effect of the instantaneous chip thickness due to the previous tooth pass.

Tlusty and Ismail [25], [41] defined the analytical chatter theory that would be widely used in the research field. They addressed the nonlinearity caused when the tool jumped out of the cut (force equal to zero). The analytical solution was defined by solving the obstacle of the time dependence of the cutting force direction. This was done using the average tooth angle approach, and therefore, an average force direction. They then used the directional

orientation factors to first project this force into the x and y mode directions and second, project these results onto the surface normal.

Minis and Yanushevsky [42] proposed an analytical method to solve the dynamic milling model. They applied the theory of differential – difference equations with time varying periodic coefficients. The stability of the system was examined using Fourier analysis.

Altintas and Budak [43] developed a new method for the analytical prediction of stability lobes in milling. They transformed the dynamic milling equations into a time invariant, but radial immersion dependent system. Similar to Tlustý and Ismail, they approximated the time dependent cutting forces by an average value, but instead of using the average angle of the tooth in the cut, the time varying coefficients were expanded into a Fourier series and the series was truncated to include only the average component. Called zero order solution, when the average of periodic directional factors are used, the stability solution is reduced to direct evaluation of spindle speed and depth of cut. This prediction is accurate when the radial immersion is not very low (immersions larger than a quarter of the cutter diameter) and tooth passing frequencies are not beyond the natural modes of the structure.

Schmitz and Smith published “machining dynamics” book [44] and they compared accuracy of Tlustý’s average tooth angle approach versus the Fourier series zero order approach from Altintas and Budak. Both approaches showed close agreement for a 20% radial immersion cut but the Fourier series approach was more accurate for a full immersion slotting case. This is due to the orthogonality between the average surface normal and y direction in slotting, which causes the directional orientation factor for the y direction to be zero and the contribution of the dynamics in the y direction to be neglected.

In 1998, Budak and Altintas [45]–[47] expanded their analytical method to predict stability lobes using the Fourier series multi frequency approach, which provides improved prediction when the process is highly intermittent at small radial immersions. They also extended their model to peripheral milling of a cantilevered thin web (flexible workpiece). In their work, it was shown that when a single frequency is considered in representing the dynamic response of the milling system, it is possible to obtain an analytical solution for the stability lobes. In fact, it was demonstrated that the analytical single frequency solution gives almost identical

results to the multi frequency solutions for the cases in which the radial immersion was not very low.

Altintas and Weck [48] reviewed the dynamic modelling and chatter stability of milling by comparing various analytical models with the time domain solution. In their comparison, the method employed by Budak and Altintas showed generally the best fit to the time domain solution.

Inspeger and Stepan [49] were the first in developing the semi-discretization method for solving the stability of linear delayed systems. The method is based on a special kind of discretization technique with respect to the past effect only. The resulting approximate system is delayed and also time periodic, but still, it can be transformed analytically into a high-dimensional linear discrete system. The method is applied to determine the stability charts of the Mathieu equation with continuous time delay.

Butcher et al [50] proposed a new technique for studying the stability properties of dynamic systems modelled by delay-differential equations (DDEs) with time periodic parameters. By employing a shifted Chebyshev polynomial approximation in each time interval with length equal to the delay and parametric excitation period, the dynamic system can be reduced to a set of linear difference equations for the Chebyshev expansion coefficients of the state vector in the previous and current intervals. This defines a linear map which is the “infinite-dimensional Floquet transition matrix”.

Le Lan et al. [51] presented a new stability prediction tool based on the dynamic behaviour of both the milling tool and the workpiece by using finite element method. Dynamics of both tool and workpiece were expressed under the form of a transfer matrix, linking modulation to cutting force and following the approach of Budak and Altintas. Their addition was the calculation of a new transfer matrix at each node and therefore, a stability lobe for each node along the toolpath. This method can only be used if the distance between two nodes is not too small comparing to the chatter wavelength, and it can be suitable as a quick indication of chatter in design phases, in order to avoid expensive prototyping.

Ding et al [52], [53] proposed a full discretization method to predict the milling stability based on direct integration. The model is represented in integral form, the time period is equally

discretized into a finite set of intervals and the full-discretization method is developed to handle the integration term of the system. On each small time interval, the second-degree Lagrange polynomial is employed to interpolate the state item, and the linear interpolation is utilized to approximate the time-periodic and time-delay items, respectively. They did a comparison of zero order, 1st order semi-discretization and 1st order, 2nd order full-discretization methods rate of convergence and showed that the second-order full-discretization converges faster than others. The algorithm is computationally efficient because the involved matrix exponentials are calculated only in the outer loop for sweeping the range of spindle speed, and not needed to be updated in the inner loop for sweeping the range of the depth of cut. According to the authors, this method can reduce the computation time by about 60% compared to the semi-discretization methods.

Mann and Patel [54] described a new approach to examine the stability of delay differential equations that builds upon prior work using temporal finite element analysis. In contrast to previous analyses, which could only be applied to second order delay differential equations, the given approach developed an method which could be applied to a broader class of systems which may be written in the form of a state space model.

Friedrich et al. [55] presented a new approach to assess the process stability based on measured acceleration signals. The idea was to estimate the stability lobe diagrams in milling with continuous learning algorithms. The multidimensional stability lobe diagram (MSLD) which includes both cutting depth and width of cut as well as spindle speed, are derived during the production using two new continuously learning algorithms. The first approach uses an extended Support Vector Classification (SVC) which is able to perform continuous learning. Thus the training data can be collected over time and the algorithm is able to deal with time variant systems. The learned MSLD based on the measured information is similar to the analytically calculated MSLD. The second approach is based on an artificial neural network, which is trained by a Kalman Filter with a multi-input extension. For the MSLD with spindle speed, cutting depth and width of cut, the artificial neural network shows the best results.

To summarize, from the 1950's big efforts have been to understand chatter phenomena and help engineers and machinists face this particular problem with new and improved tools that

could predict how and when chatter occurs, as well as providing solutions to overcome this problem and increase productivity of machining operations. New chatter models have been developed in this time, and the wide research interest in the topic has aided the evolution of more detailed theories. Non-linearities are better understood and implemented and even machine learning algorithms are being used to obtain feedback from the system in real time and respond accordingly.

It is not easy to create mind map only by reading the historical background in chatter theories, as there are different methods involved and different paths followed that often obtain similar results. In an effort to map the state of the art in chatter modelling, a classification of chatter mitigation methods has been created as part of this thesis in section 5.3.2 below.

5.3.2 Chatter mitigation methods

Many chatter mitigation or suppression methods and models have been developed since the 1950's and there are different ways of classifying them. One option to classify them is differentiating the methods using the lobbing effect from the methods which change the system behaviour. System behaviour can be changed in an active or passive way. From the methods using the lobbing effect, a differentiation can be made between in-process and out-of-process methods (see Figure 41). Out of process methods are based in predicting the system behaviour by dynamic models, closely followed by experimental tests to validate models. These models are divided in analytical models and numerical models. Analytical models, which use the frequency domain to show a picture of the dynamic behaviour of the system, include the average tooth angle approach, fourier transform, semi and full discretization methods, Chevyshev polynomial approach time-finite element analysis. Numerical methods are the ones which simulate the process in small time steps and are named as time domain models.

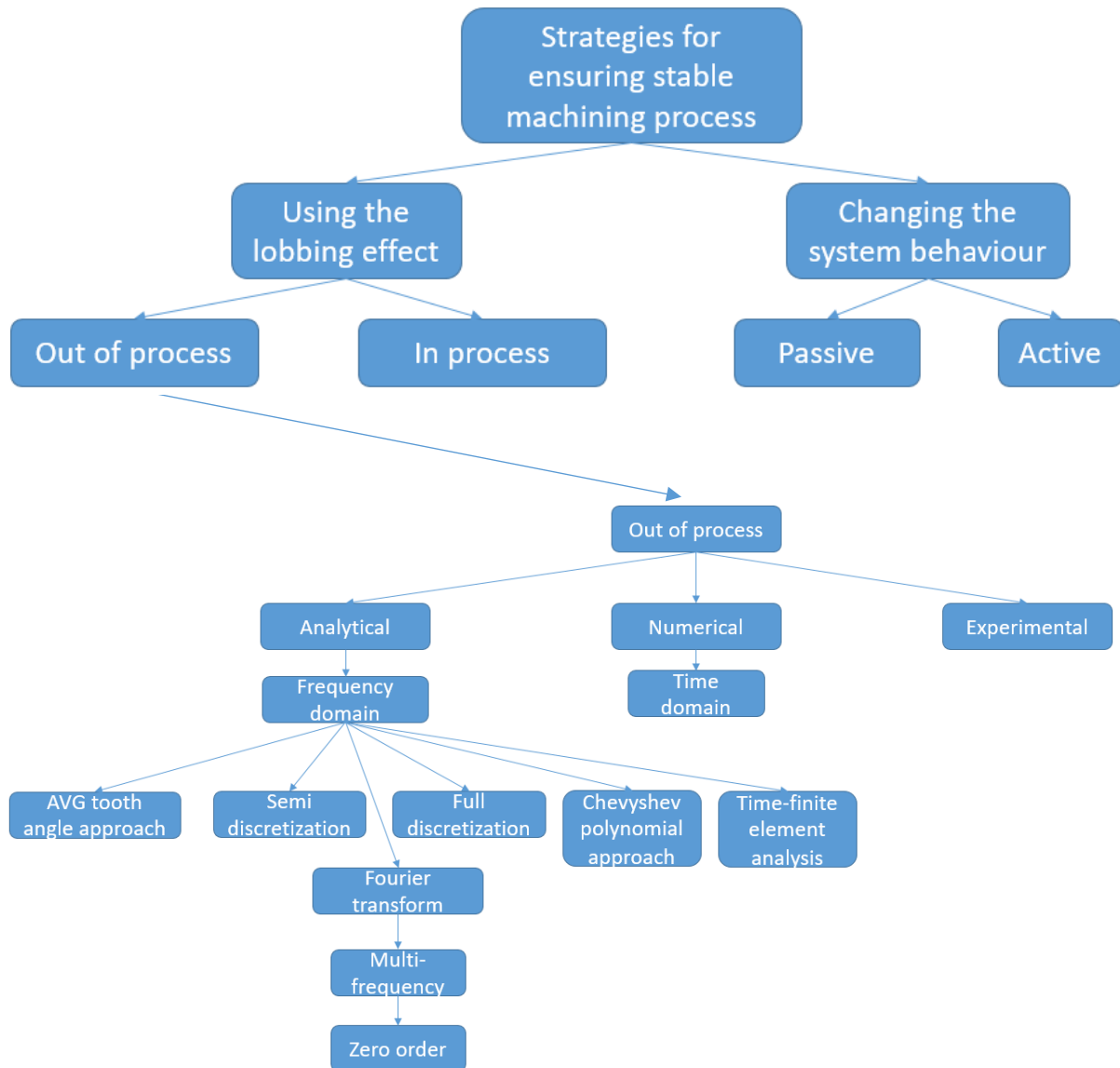


Figure 41. Chatter avoidance/suppression method classification

5.3.3 Frequency domain models

Frequency domain models are the most simple and quick for chatter detection. The methods based on frequency domain, model the cutting forces acting in the cut and therefore the chip thickness which is time dependent. The regenerative effect of the chip thickness and cutting forces is considered and using different approaches, the system is converted to become time invariant. The system can then be presented in the frequency domain and stability lobes can be obtained, usually in two dimensions by plotting spindle speed and width of cut, or in three dimensions by adding a third cutting parameter. The main problem of the frequency domain models is that they don't consider many non-linearities which happen in the cutting process

and therefore in certain circumstances the error level of the model is not negligible. In addition, a frequency domain model gives an overall picture of the dynamic system, but fails to catch changing dynamic systems as it happens in complex part machining, in which the stiffness of the part could be constantly changing.

The steps followed to generate stability lobes diagram are the following:

- 1- Determine oriented FRF and identify valid chatter frequency ranges. This happens when the Real part of the FRF is negative
- 2- Solve for ϵ , phase between current and previous tooth vibration for valid frequency ranges
- 3- Find average number of teeth in the cut for the selected radial immersion
- 4- Calculate b_{lim} over the valid frequency ranges
- 5- Select an N value (integer number of waves between teeth) and calculate associated spindle speeds over valid frequency ranges
- 6- Plot Ω vs. b_{lim} for each N value (N=0, N=1, N=2, etc.)

There are different methods to transform the dynamic milling equations into a time invariant, but radial immersion dependent system. Those methods are the average tooth angle approach, which was first developed, Fourier transform technique, such as the multi-frequency or simplified zeroth order approach, semi and full discretization methods, Chebyshev polynomial approach or time-finite element analysis.

5.3.4 Time domain models

Time domain is a numerical simulation model which solves the dynamic equation of motion by numerical integration. This method gives local force and vibration levels for a selected cutting condition and differs from the frequency domain models in the level of detail obtained. However, in order to create stability lobe diagrams, a numerous set of simulations need to be carried out, which are more time consuming and requires bigger computational efforts.

The simulation generally follows the following steps:

- 1- The instantaneous chip thickness is determined using current/previous vibrations

- 2- Cutting force is calculated
- 3- Force is used to find new displacement
- 4- Process is repeated in small time steps

Thrust [25], [56] was the pioneer in creating a time domain model which included the basic non-linearity of cutting tool and workpiece separation. Based on thrust's model, other researchers have improved and added more nonlinearities to the time domain simulation. Smith and Thrust [57] determined dynamic cutting limits in the form of constant Peak to Peak (PTP) force plots. Montgomery and Altintas [58] represented the tool and workpiece by digitized surfaces and managed to model more accurately the trochoidal tool path and regeneration of waviness. Altintas and Lee [59] further developed the time domain model of Montgomery and Altintas, and included the ball-end geometry, although the model was restricted to full and half radial immersions of the tool. This restriction was overcome by Campomanes and Altintas [60] in an improved model capable of simulating very small radial depths of cut. Their model consisted in discretized tool and workpiece kinematics and dynamic model to represent the exact trochoidal movement of the tool. This model has been widely used by other researchers in the last decade.

5.3.4.1 Time domain chatter criteria

A time domain model doesn't show an overall stability picture as the frequency domain models do, instead, numerous simulation runs are needed to build a Stability Lobes Diagram (SLD). Although more detailed than a frequency domain diagram, time domain simulations need a chatter criteria in order to establish the limit between the stable and unstable conditions. Different methods have been proposed to detect the chatter onset in time domain models. The first time domain model of Smith and Thrust [61] based the chatter identification criteria in Peak to Peak (PTP) forces method. It consisted in plotting PTP forces in a diagram with given increments and chatter stability would correspond to a sharp variation in PTP force which indicated chatter onset. Campomanes and Altintas [60] presented the non-dimensional chatter coefficient as the method to identify the onset of chatter. The coefficient was a division between the maximum uncut chip thickness during a dynamic time domain simulation and the maximum uncut chip thickness during a time domain simulation in which the workpiece and tool remain rigid. They set a threshold of 1.25 and any value above that

would be triggering chatter. Li et al. [62] proposed that the ratio of the predicted maximum dynamic cutting force to the predicted maximum static cutting force could be used as a criterion for the chatter stability. Bayly et al. [63] suggested a statistical variance of tool displacement signal of periodic 1/tooth samples to determine chatter in a time domain simulation as well as in experimental tests. Sims [64] used a time domain simulation developed by Campomanes and Altintas with some modifications in order to improve the chatter detection time. He proposed the self-excitation damping ratio as a chatter detection criteria. The damping ratio is related to the amplitude of two successive oscillations by a logarithmic decrement and it gives immediate indication of the level of damping from just a few vibration cycles. A positive damping ratio indicates a stable cut while a negative damping ratio indicates an unstable cut. This method allows to improve the computational time required to detect chatter in a simulation.

5.3.5 Experimental methods

Various experimental methods have been used in order to compare and validate simulation results obtained from both frequency domain models and time domain models. The general purpose of the experimental methods is to measure the self-excited and/or forced vibrations on-line with purposely designed cutting conditions to evaluate the accuracy of the simulation models proposed. Methods to measure experimental outputs and chatter detection criteria are key in order to obtain an accurate comparison of methods.

Weingaertner et al. [65] used a microphone to obtain sound signal in experimental cuts and evaluate the accuracy of both frequency domain model and time domain model against the empirical test. For roughing operation, both analytical and time domain simulations were practically the same and showed good agreement with experimental tests. However, for finishing operation with low radial depth of cut, there were small differences between the two models but discrepancies were found respect to the experimental results, especially for conditions close to resonance.

Wu et al. [66] developed an experimental method to define chatter stability nonlinear criterion. They obtained vibration signals using accelerometers from a thin part milling and analysed the vibration signal of different processing parameters based on the phase plane

method, Poincare method and spectral analysis. Then, the relationship between the maximum Lyapunov exponent and the spindle speed and milling depth changes was discussed. Finally, taking the largest Lyapunov exponent as the criterion, the study determined the chatter stability domain of milling by using contour method. For this experimental method up to 121 experimental cuts were carried out.

In this section, a classification of the different chatter mitigation methods has been done. This helps mapping each method within the global picture of chatter mitigation. The following sections focus on the specific aspects of the machining dynamic models required to simulate the conditions found in an IBR component.

5.4 Ball-end mill tool geometry modelling

Free-form blade features of the IBRs are generally finish milled with high precision ball end mills which have a lead and a tilt angle relative to the blade when machining. It is important to consider the particular coordinates of the tool in the cut while developing a model for this process. In this section research works which included ball end mill geometry for their milling models are mentioned.

After the first approach to modelling tapered mills done by T.C Ramaraj and E. Eleftheriou [67], Y. Altintas and P. Lee [68] developed a general mechanics and dynamics time domain model for helical end mills. The cutting forces at each cutting edge point were determined by orthogonal to oblique mechanics transformation and the total cutting forces were evaluated by digitally integrating the contribution of all cutting edge points along the flutes in the cut. Chip thickness was calculated by modelling the true trochoidal motion with the true kinematics of milling, in which the static displacements, forced and chatter vibrations were included. This model was capable of predicting dimensional form errors left on the generated surface as well as chatter stability lobes. However, no process damping effect or workpiece flexibility was taken into account and the cutter-spindle assembly was assumed to be rigid in axial direction. S. Engin and Y. Altintas [69] improved the previous helical end mill model of Altintas by including the structural vibrations of both cutter and workpiece in the chip thickness evaluation. The geometric model was parametrized as a generic helical end mill and different equations were presented to identify the coordinates of the local cutting edge

geometry depending on the type of end mill. Dynamic chip thickness, cutting forces, vibrations, surface finish, torque and moments generated were simulated in time domain, whereas chatter stability lobes were predicted using both time domain and frequency domain analytical solutions.

Liu et al. [70] presented a theoretical Dynamic cutting force model for ball end milling. The three dimensional instantaneous cutting forces acting on a single flute of a helical ball end mill were integrated from the differential cutting force components on sliced elements of the flute along the cutter axis direction. They found reasonable agreement between measured and simulated dynamic cutting forces.

K. Akazawa and E. Shamoto [71] integrated ball end mill geometry with inclination in feed direction and workpiece flexibility in an analytical model, as mentioned before. The cutting force was calculated by dividing each tooth into infinitesimal edges and expressing their location in polar coordinates. The self-exciting force was then evaluated by averaging the cutting force increment during one rotation or tooth pass period. Finally, the average force increment caused by unit displacement was calculated and the resultant average cutting force constant was obtained. The critical depth of cut was derived as for the orthogonal case in turning process, because they assumed that the system was flexible only in the through-thickness direction. The difference was that they used the average cutting force constant instead of the product of critical depth of cut and specific cutting force of the orthogonal case.

Guang Liang et al. [72] created a chip thickness model for 5 axis ball end finish milling. A combination of a three dimensional trochoidal tooth trajectory model and engagement boundary chip model was developed to determine instantaneous chip thickness in 5 axis ball end finish milling.

E. Ozturk in his PhD [73] and published together with E. Budak [74] carried out probably the most detailed analysis of the milling dynamics with a ball end mill done so far. They presented a model that included the 3D dynamics of five axis ball end milling and included the effects of the lead and tilt angle. Single and multi-frequency solutions were presented as well as a time domain model. Three coordinate systems were used in order to position a local point in the cutting edge, a Cartesian tool coordinate system at the ball centre, a fixed X,Y,Z machine coordinate system and a coordinate system representing feed, cross-feed and normal

directions. The variations of the cutting force coefficients were handled by dividing the tool in disk sections along Z axis, instead of averaging, which would lead to higher errors. After, the stability problem was formulated; the relations for the dynamic displacements were substituted into the cutting force equations, obtaining an eigenvalue problem. Finally, single and multi-frequency solutions were used to solve the problem. As for the time domain model, each discrete time for a given cutting condition was related to the immersion angle of the tool. At each immersion angle, dynamic cutting forces and resulting dynamic displacement vector were calculated, which were solved with the Runge-Kutta method. Interesting results were obtained from the simulations; from one side, it was observed that there was a little difference between single and multi-frequency solutions compared to the difference found for a three axis flat end milling in other studies. This was explained by the ratio of the time spent in cutting to noncutting in five axis ball end milling, which is not very short, even for small radial depths. From the other side, it was observed that the lead and tilt angles have a considerable effect in the absolute stability limit, which was confirmed with experimental results.

Wei et al. [75] modelled the geometry of cross section parameters of chamfered cutting edge on a ball end mill of solid carbide.

Tunc [76] created an analytical model to predict the frequency response functions on tool tip, for geometries such as ball end or taper end mills. He used a receptance coupling substructure analysis (RCSA) with a stereolithographic (STL) slicing algorithm to enable the exact calculation of cross-sectional properties of the cutting tool from its 3D model. Experimental results show more accuracy than existing arc approximation methods and FEM solutions in terms of computation time and compromise between computation accuracy and performance.

Dai et al. [77] studied chatter stability prediction for five axis ball end milling. The differential dynamic equation considering regenerative chatter effect was derived from an ideal cutting model.

This review on ball-end geometry modelling shows that different attempts have been made to include this feature within the general milling chatter modelling. Although there might exist some applications for straight ball-end mill tool, it is more common to see cutting operations

with certain lead and or tilt angles. More advanced applications, those machined with 5 axis strategies, require the implementation of both lead and tilt angles at the same time. This has been done in detail by E. Ozturk, developing the most detailed five axis chatter simulation model up to now.

5.5 Flexible part modelling

Most of the dynamic milling models developed so far only considers the dynamic behaviour of the tool, while considering the workpiece rigid. This can be useful for general applications in which the tool is more flexible than the workpiece. However, for processes such as IBR blade finish milling, the workpiece has to be considered, because it is even more flexible than the tool. A few existing dynamic milling models that include the effect of flexible parts are mentioned in the following section.

F.J Campa et al. [78] presented a three dimensional frequency domain model for the calculation of the stability lobes of low rigidity parts. They used the three dimensional model previously developed by Y. Altintas [79] who included a third axis in the vertical direction to accurately represent variable component of the chip thickness when ball end, bull nose or inclined cutting edges were employed. F.J Campa et al. included the flexibility of the workpiece by calculating the dynamic displacement between the tool and the workpiece, adding the Frequency Response Function (FRF) matrixes of the tool and the workpiece. A mono-frequency solution was adopted in order to solve the force model equation. The stability diagrams obtained from the model were then experimentally validated, with 87% of the tested points successfully predicted. However, the model did not consider process damping.

K. Akazawa and E. Shamoto [71] also developed an analytical model to predict stable cutting conditions when ball end milling flexible workpieces. They considered the tool inclination because the ball end mills are usually inclined to the workpiece in practice. The inclination of the tool was considered in the feed direction only and the flexibility of the workpiece in the through-thickness direction. In order to calculate the critical depth of cut and the spindle period, the real and imaginary parts of the workpiece transfer function were used. The predicted stability lobes agreed qualitatively with experimental results.

E. Budak et al. [80] followed a different approach to analyse workpiece dynamics in flexible part milling operations. They argued that the workpiece dynamics are difficult to add to the analysis as they are continuously changing due to the mass removal and variation of the cutter contact. Therefore, they presented a methodology for prediction of in-process workpiece dynamics, based on a structural dynamic modification using the FE model of the workpiece. The method consisted on obtaining the FRF of the workpiece only once and then continuously modifying it by considering the removed material volume during the cycle. This was carried out by generating the mesh of the workpiece, determining the removed elements for each tool location and finally updating the FRF by matrix inversion method. They proved in blades, both by simulating and experimentally that the natural frequencies vary with material removal and suggested the multi-level machining as an alternative to reduce machining time.

Most of the dynamic milling models that consider part flexibility are analytical, but M.L. Campomanes and Y. Altintas [60] developed a time domain model combining methods used by other authors and included the flexibility of the part in the model. Dynamic characteristics of the cutter and workpiece were determined experimentally and the cutting surface was modelled using a discretized kinematics algorithm. Many non-linear effects were considered, as the radial immersion change due to deflections/vibrations, effect of edge forces and the effect of forced vibrations on chatter stability, but not process damping.

The research works analysed in this section show how to consider the workpiece flexibility in dynamic milling models. Generally, the analytical models include the part flexibility as a combined FRF tool/workpiece, but it can also be considered in a time domain model.

5.6 Variable speed milling

Variable speed milling could be a good solution for chatter avoidance in complex geometry blisk milling based on the wide research carried out in the topic and the benefits it shows in many cases over the constant spindle speed. The main difficulty of finish milling blisk blades, apart from the complex geometry, is that, the stiffness and dynamic response of the tool/part is constantly varying while the tool is removing material. Therefore, chatter behaviour is constantly changing and stable/unstable regions are constantly shifting in the stability lobes.

Chatter avoidance by varying spindle speed has been a wide research topic. Investigation has been carried out both as adaptive spindle speed variation and modulation of spindle speed. Adaptive spindle speed approach is to shift the spindle speed (ramp up or ramp down) in order to remain in the stable regions of the stability lobe diagram. Spindle speed modulation is a technique developed to avoid chatter, in which the spindle speed is oscillated around a mean value. This technique consists on a continuous variation of the tooth pass frequency, yielding a continuous variation of the phase between the tool-workpiece relative displacement and the tooth passing cycle, which prevents chatter from growing up.

5.6.1 Adaptive spindle speed variation

The nature of this approach consists in adapting the spindle speed to the system's changing dynamics in order to remain in a stable region within the stability lobe diagram. It is a technique which targets the high speed machining region, due to the wider gaps between the stability lobes. In contrast, it is difficult to apply in the lower speed regions, unless the system dynamics are very stable. Both out-of-process and in-process approaches have been studied for adaptive spindle speed variation with most research work focusing on the high speed machining region.

Delio et al. [81] compared various sensors for the in-process chatter detection, concluding that the use of a microphone was more suitable than other sensors, such as cutting force or displacement measurements, especially when flexible workpiece and tooling were involved in the milling process. However, they also outlined the limitations of the microphone, such as directional considerations, frequency response, and environmental sensitivity. In parallel [82], [83], they developed a control system which based on the data collected from the microphone, automatically adjusted the spindle speed and the feed rate so as to achieve stable milling. The system iteratively adjusted the tooth pass frequency to the dominant chatter frequency in the sensor output, which led to a minimization of the phase between the inner and outer modulations in a different approach comparing to the sinusoidal spindle speed variation strategy studied by other authors. The main problem of this method is the typical chatter frequency of a milling operation being too high, which would require high spindle speeds, valid only for high speed machining.

Tarng and Li [84] presented a spindle speed change method based on the features of the cutting-force spectrum obtained from the Fast Fourier Transform (FFT) for the avoidance of chatter in milling operations. They removed chatter by selecting a spindle speed which is a small integer ratio of the chatter frequency divided by the number of teeth, adjusting the phase shift ϵ to be equal to zero. Liao and Young [85] proposed a very similar approach too, collecting the cutting forces and obtaining the FFT, from which the chatter frequency was identified when the intensity at a given frequency exceeded a critical value. The system would then shift the spindle speed to adjust the phase shift.

Soliman and Ismail [86] also presented a new control system for chatter avoidance, they did so by ramping up the spindle speed when chatter was detected. For the chatter criteria they used the “R” value obtained from force signal as proposed by Ismail and Kubica. The control system collected the dynamic and static components of the cutting force data and saved them in arrays to calculate the “R” value. Then, using an algorithm, a spindle speed ramp rate was selected based on the “R” value pattern. Finally, spindle speed data was generated and sent to the data acquisition processor. This would be repeated until the system reached to a stable region and the control system stopped the ramping up process. This approach has some problems, starting that chatter marks are found until the ramping up reaches to a stable region, which is directly proportional to the ramp up speed. Also, this control system only considers ramping up speed until chatter is removed, but not ramping down or stopping the process to find a better speed for the cases when ramping up is out of the process limits.

Ismail and Ziaei [87] extended the control system developed by Soliman and Ismail for its application in chatter suppression in 5 axis of flexible parts, using both off-line and on-line measures. Off-line measure consisted in increasing the feed rate when the rotary axes were undergoing large increments in order to maintain the chip thickness, while on-line measure consisted in the spindle speed ramping controller developed by Soliman and Ismail, although with speed ramping down capability too. They used sound intensity level criteria to identify chatter. A combined system of both measures was found to be the most effective. It was only tested at low spindle speeds and feed rates and the need of a fast responding spindle drive was outlined as the main problem for its industrial implementation.

T. Schmitz [88]–[90] developed a method to detect chatter on-line using sound signal but instead of filtering to frequency signal through FFT, the method consisted in a statistical evaluation of the synchronously sampled audio signal through Poincare mapping technique, which requires less computational effort, only one sample per spindle revolution versus the tens of kilohertz sampling rates necessary to avoid aliasing in the FFT analysis.

Tsai et al. [91], [92] proposed an in-process adaptive spindle speed tuning algorithm by feedback of an acoustic cutting signal. A pair of microphones perpendicular to each other were used to acquire the acoustic cutting signal resulting from milling chatter. A real time feedback control loop was constructed based on the analytical approach of Solis to establish the stability boundaries for spindle speed compensation in such a way to ensure the milling process to be within the stability zone of the stability lobe diagram. The spindle speed compensation strategy was based on the input from the chatter acoustic signal and based on the signal level and the current spindle speed either no compensation, ± 100 rpm or ± 200 rpm compensation would be applied depending on the chatter acoustic signal being stable, moderate or severe respectively. They verified experimentally the algorithm and concluded that it was an inexpensive, simple and suitable to apply in practice, although inappropriate to be employed in a noisy environment.

Van Dijk et al. [93] presented an online chatter detection analytical algorithm that automatically detects chatter in an online fashion and in a premature phase such that no visible marks on the workpiece are present. They proposed two control strategies that guarantee a chatter free high speed milling operation by automatic adaptation of spindle speed and feed. After comparing different sensors (microphone, accelerometers at the spindle housing, eddy current sensors and a dynamometer), they concluded that the accelerometer was the best option from performance (early chatter onset detection) and cost effectiveness point of view. The first control strategy avoided chatter occurrence by setting the tooth passing frequency equal to the chatter frequency resulting in a zero phase difference between two subsequent teeth motion. The second control strategy lowered the total perturbation vibrations and maintained robustness of performance by adapting the spindle speed and feed.

Kalinski and Galewski [94] developed a chatter surveillance method for milling with ball-end mill. They did a dynamic analysis of the milling process and they presented dynamics of controlled closed loop system with time-delay. From there, they developed the method of vibration surveillance by the spindle speed optimal-linear control. This is an out of process method in which simulations are used to propose a spindle speed variation strategy for the implementation in the CNC program before the cutting is performed. Later, Kalinski and Galewski [95] applied the surveillance method to flexible part milling with ball-end mill. They matched the spindle speed to optimal phase shift and in case of having various dominant natural frequencies across the process, optimal spindle speeds should be calculated for each zone separately. This was not evaluated in their work.

Campa et al. [96] developed an analytical model in order to avoid chatter by predicting stable spindle speed across the tool path of thin floors while milling with bull-nose end mills. They first discretized the tool path (initial part geometry, removed material, geometry of the tool, and radial/axial depths selected) to generate the geometry for the FEM analysis. FRF's were obtained from FEM modal analysis and effective stiffness calculation, together with the damping obtained from experimental impact tests. Then a FRF matrix could be assembled from modal frequency, effective stiffness and damping coefficient of the n main modes. Finally a three dimensional stability plot was created, having the tool path as the third dimension. Because the depth of cut is fixed, the stability diagram could be simplified to a 2D spindle speed vs. tool path which allows to program a variable spindle speeds across the tool path in advance of starting the physical cut. The authors recognized errors attributed to the analytical nature of the process modelling, tool path discretization and the input parameters, although a considerable improvement in surface roughness (from $1.49\mu\text{m}$ to $0.4\mu\text{m}$ was obtained in experimental validation tests. This method would be most reliable for milling in the low order lobe regions, which are wide enough to be affected by the uncertainties of the method.

Friedrich et al. [55] developed two continuous learning algorithms capable of simulating Multidimensional Stability Lobe Diagrams (MSLD). The algorithms collect input data from changing cutting conditions and using a learning method provides stability diagrams including depth of cut, width of cut, and spindle speed. They used a time domain simulation which included information about depth and width of cut, the spindle speed and the process

stability, to feed the learning algorithm. Although not covered in the simulation model, they suggest that spindle speed or depths of cut could be changed along the cut to adapt to the sweet spots of the instantaneous MSLD, as well as implement the algorithms to real production for on-line chatter detection and suppression.

Summarizing, adaptive spindle speed variation is a chatter mitigation technique with big potential but also with some limitations. The concept behind adaptive speed variation is to evaluate a SLD constantly during the cut, which can be done while cutting (in-process) or through previous analysis of the tool path via simulations (out of process). It is specially indicated for the low order lobes, in high-speed machining, because it is easier to find the stable gaps. However, there are limitations, specially to apply this technique to constantly changing scenarios, case of blade finish milling. Another problem is the need of advanced equipment such as microphones, dynamometers, accelerometers, eddy current sensors, etc. which are common in research environment but not in industrial applications, in which engineers and machinists are not often prepared for using this equipment. Besides, in-process techniques are often reactive, which means chatter is developed before speed is adapted. Regarding to out of process techniques, they also have great potential, although they require a unique solution for each part. Unfortunately, this technique is not ready to be applied in general industrial environment yet due to the complicated analysis and simulation work required by specialist researchers.

5.6.2 Modulated spindle speed variation

Spindle speed modulation has captured the interest of many research activities in the recent years. Although it has some known limitations on the modulation parameter limits set by the machine spindle, it has shown clear benefits in respect to the constant spindle speed for chatter avoidance or suppression. Modulated speed has become in an extended research topic compared to the adaptive speed, due to its relatively easy application and its success over the low-mid spindle speed regions, in which modulation technique is beneficial over the constant spindle speed. Research has mainly focused in identifying the best modulation form, how to optimize modulation parameters (amplitude and frequency variation) and the integration of the modulation in existing and new dynamic models. Although most of the work done is for out-of process chatter avoidance, there are some researchers who have studied

in-process application to suppress chatter by modulating the spindle speed only when required.

Canniere et al. [97] focused their work contrasting the initial variable spindle speed research carried out by Takemura and later on by Sexton. Early work suggested that increase in the stability of the cutting process could be obtained by continuously varying the spindle speed. They used the techniques of perturbation calculus to construct a non-periodic approximate solution to the delayed differential equation and confirmed that variable spindle speed machining could enhance the stability of the dynamic system.

Rahman and Ito [98] mentioned the need to detect the onset of chatter accurately in order to avoid it in-process. They proposed a method to determine chatter threshold through the in-process measurement of the horizontal deflection of the workpiece measured by means of eddy current type displacement pick-ups in a turning operation. Chatter could be identified before the chatter marks developed.

Lin et al. [99] studied the effects of variable speed cutting on vibration control in face milling, and carried out both simulation and experimental tests to confirm that the self-excited vibrations which occur during constant speed machining can be suppressed by continuously varying the spindle speed. They examined the shape of the variable speed trajectory and found that a sinusoidal wave could be tracked more precisely than other type of periodic waves (smaller tracking error) due to its acceleration and jerk characteristics. Finally they showed the importance of selecting adequate ratios of frequency and amplitude variation, and confirmed an improved chatter suppression ability for increased frequency and amplitude variations, although that could cause problems with the spindle and controller of the machines.

Tsao et al. [100] represented the system dynamics in the angle domain to make numerical simulation and stability analysis much simpler, also considering a one degree-of-freedom model modified for a simple face milling example. Using a central finite difference approximation and matrix theory, they developed a stability analysis tool based on spectral radius. However, their simulation and experimental results did not completely match, which was attributed to nonlinearities and mode interaction in unstable cutting.

Altintas and Chan [101] developed a detailed time domain model, including runout, variable spindle speed, flank interference and tool wear. A sinusoidal speed was introduced in the simulation model by choosing two inputs, the amplitude of speed variation and frequency of speed variation. An in-process chatter detection and suppression method was created using sound signal. First, the user inputs (chatter threshold factor for the sound spectrum, nominal speed, amplitude and frequency of speed variation) were introduced. The FFT of the collected sound signal was processed and its maximum magnitude and frequency were determined. Chatter was assumed to be present when the maximum magnitude exceeded the low frequency spectrum average by a factor greater than the threshold factor. A new iteration would start as soon as the initial data acquisition was completed. The time domain model would send the necessary control signals to the variable spindle drive. If chatter was detected from the previous signal processing, then speed variation signals would be sent to the spindle speed controller, otherwise a constant speed signal would be sent. Their research work showed that if the spindle speed was sufficiently oscillated, the wave regeneration mechanism was disturbed and chatter vibrations could be suppressed. However, the method required a high performance, high torque delivery spindle drive which deliver speed oscillations with a wide range of amplitude and frequency in a short time interval.

Ismail and Kubica [102], [103] also found variable speed modulation a useful research topic. They highlighted that the spindle speed modulation may not be suitable for an entire job and the static force variation resulting from the modulated feed per tooth could produce undesirable effects where constant cutting speed could suffice, therefore showing the need of a control system. The first part of their research consisted in developing a measurable chatter indicator. Previous studies from other researchers were based on vibration level measurement (accelerometer, microphone, etc.) and Peak To Peak (PTP) chatter detection from the frequency spectrum obtained. The chatter threshold with this method was dependent on machine, workpiece, and parameters. Ismail and Kubica proposed a new method with a lower sensitivity to cutting conditions; they proposed the “R” value which was a ratio obtained from dividing the Root Mean Square (RMS) of the dynamic with the static RMS components of the cutting forces over one spindle revolution. A threshold was still needed but this was not as cutting conditions dependent. Results of measurement showed magnitude differences in “R” value comparing to simulated results; this was attributed to

nonlinearities and runouts. The second part of the research proposed a method for the on-line chatter control and spindle speed modulation using fuzzy logic control. The method was based in a single input, double output controller without a derived or empirical relation between the cutting status and the control parameter. The input was the chatter indicator, “R” value, while the outputs were the amplitude and frequency of the sinusoidal modulation of the spindle speed. The controller activated the modulated spindle speed when the depth of cut was changed so that the “R” value reached to the threshold.

Soliman and Ismail [104] investigated a new method for in-process chatter detection with the “R” value proposed by Ismail and Kubica but using the spindle drive current signal instead of cutting force. Both the simulation results as well as the experimental results showed that current signals can transmit chatter frequencies reliably. Although this method required less hardware to be applied, it had problems to evaluate the sensitivity of the reduced current signals at high frequencies.

Pakdemirli and Ulsoy [105] studied the variation of spindle speed to avoid chatter using perturbation analysis. They used the angle of revolution as the independent coordinate for maintaining a constant delay in the equation in a simplified one degree of freedom model and considering a harmonically varying spindle speed. An approximate analytical solution was obtained and stability lobes were presented for the variable speed. Small increases in stability regions were found with speed fluctuations not exceeding 2% of the mean spindle speed. However, numerical results of other work predicted that for larger gains in stability, fluctuations of 20% were needed, which were too high to get accurate results with the perturbation approach presented.

Radulescu et al. [106] used a mechanistic dynamic model to simulate variable spindle speed in sinusoidal form applied to face milling. They evaluated processes with one and multiple modes of vibration as well as changing dominant modes. For cutting processes having one dominant mode of vibration, the model predicted that variable speed machining is especially effective over constant speed machining when the tool-work system changes its dominant mode of vibration throughout the cut, or when the tool-work system has several modes of vibration coming from component parts that are cut in the same time. For cutting processes having multiple dominant modes of vibration, the model predicted that variable speed

machining is especially effective over constant speed machining when the tool-work modes of vibration are unequal and moderately coupled to each other.

Jayaram et al. [107] developed an analytical model to predict chatter stability of variable spindle speed machining, based on transforming the linear differential equations with time varying delay to the solution of an infinite order characteristic equation. This method was developed for the turning process.

Sastry et al. [108] proposed a solution based on a discrete time approach for the chatter stability in variable sinusoidal spindle speed in face milling. They described the process dynamics by a set of differential-difference equations with time varying periodic coefficients and time delay. Although their solution was applicable to systems with multiple vibration modes, computational difficulties in evaluating the eigenvalues of the state transition matrix of very large order limited its application to simple low degree of freedom systems.

Namachchivaya and Beddini [109] studied variable spindle speed for chatter avoidance, using a perturbative method to obtain finite dimensional equations. They adapted Hanna and Tobias' one degree of freedom model for turning process. They observed that the transient vibrations often attained very large amplitudes before decaying, which were increased with increased width of cut. Hence, in the presence of spindle speed variation, the stability boundary from the linear model provided an improved chatter threshold only if the delayed bifurcation was supercritical. If it was subcritical, then the stabilization due to spindle speed variation would not be significant because small disturbances could cause oscillations to jump from small to large amplitudes.

Al Regib et al. [110] developed a new method for programming optimized spindle speed variation for online chatter suppression. The method was based in minimizing the energy input of the cutting process. They solved numerically the work done by the cutting force during sinusoidal spindle speed variation over a wide range of spindle speeds and generated charts to select the optimum amplitude ratio. They also proposed a heuristic criteria for selecting the frequency of the speed variation. They used a single degree of freedom turning model to develop the method and found limitations for high speed machining due to the high amplitude variations required.

A three dimensional time domain model was used by Bediaga et al. [111] adapted to simulate variable spindle speed to suppress chatter. They used Sinusoidal Spindle Speed Variation (SSSV) technique to optimise the relationship between the chatter frequency and the tooth pass frequency. They proposed a method based in limiting the amplitude of the speed variation according to the feed per tooth limitations for overwearing and overloading. With the amplitude limitations, several time domain simulations were carried out with different amplitude and frequency parameters. The severity of the vibration was measured instead of the vibration amplitude of the chatter peak, since the SSSV excites more frequencies than the normal machining, which could lead to a mistaken conclusion. They confirmed, as other authors had done previously, that SSSV is not an appropriate method to suppress chatter at low order stability lobes ($K=0$ or $K=1$) from high speed machining.

Zatarain et al. [112] presented a theory to evaluate the Continuous Spindle Speed Variation (CSSV) in frequency domain. Their approach was based in Budak and Altintas' multifrequency method but adding the variability component to the spindle speed. Instead of using the typical SLD, they plotted the limit depth of cut for different frequencies and amplitudes of sinusoidal (or triangular) speed variation. From these graphs they could select the speed variation parameters most adequate for the cutting conditions required. One of the problems they found was that for highest variation amplitudes frequencies of the CSSV, the spindle was not able to reach the requested speed variation, which could limit the possibilities of CSSV. This method is capable of optimizing the speed variation amplitude and frequency, but the applicability to changing dynamic conditions during the cut was not covered in the study.

Bediaga et al. [113] also studied CSSV in a very similar format as they did with SSSV, but using different forms of speed variation. They added a semi-discretization model to simulate CSSV and compared to the frequency domain model from Zatarain et al. Stability was plotted for amplitude, frequency and inverted eigenvalue and in order to save computational time, plots were representing a defined axial depth of cut. Similar results were obtained from frequency and semi-discretization methods compared. The semidiscretization method proposed could also analyse the dynamic changes of the system, by tracking the evolution of the transition matrix created. The latter was not analysed and developed though.

Zhang and Ni [114] proposed an internal energy based analysis on the mechanism of spindle speed variation for chatter control, using a nonlinear delay differential equation in a single degree of freedom model. This approach allowed to find speed variation parameters (amplitude and frequency) which would suppress chatter immediately. The minimum speed variation amplitude was obtained from the delta between the net work done by the dynamic cutting force and the threshold of the damping structure being negative or equal to zero. They also considered the application of this method into a closed loop control to integrate into CNC machining system to cope with changing system dynamics.

Long and Balachandran [115] studied variable spindle speed for chatter suppression in both up and down milling. They used a semi discretization scheme to discretize the system over one period and reduced the infinite-dimensional transition matrix to a finite-dimensional matrix. Eigenvalues of this matrix are used to examine the stability. Instead of having a criteria to select the best amplitudes and frequencies, a set of simulations were carried out with different combinations. Results obtained from their study showed a pronounced improvement in stable axial depth of cut when the ratio of tooth pass frequency to the first natural frequency of the system is low. In addition, variable spindle speed showed a better improvement in stability when up-milling, compared to down-milling.

Seguy et al. [116] analysed the effect of the spindle speed variation in high speed milling process, after previous studies suggested that variable spindle speed was not viable due to the high performance spindle requirements and the wide shape of the low order stability lobes. They used a semi discretization method to compute optimal amplitudes and frequencies, from a set of simulated values. Triangular speed variation was selected, based on the fact that for a given spindle characteristic, the triangular modulation provides larger amplitudes and frequencies than the sinusoidal or the square wave modulation. They targeted spindle speeds corresponding to the first flip and to the first Hopf lobes. The results showed that the efficiency of the variable spindle speed in high speed region is diverse; For the area of the first flip lobe, the critical depth of cut could be increased comparing to constant spindle speed. However, for the area of the first Hopf lobe, no significant gains in the depth of cut could be achieved. As highlighted by other researchers, they observed that the improvements depend mostly on the amplitude of speed variation, while the dependence on frequency is low.

Seguy et al. [117] further analysed the variable spindle speed in high speed milling process, in this case at the spindle speeds where the constant speed cutting results in period doubling chatter. The stability analysis was carried out for both triangular and sinusoidal speed modulations using the semi discretization method. They found that the sinusoidal shaped modulation is more effective than the triangular one, for the same amplitude and frequency parameters, although for a given spindle characteristics, the triangular shape allows larger modulation amplitude.

Xie et al. [118] developed an improved semi discretization algorithm for the prediction of milling with varying spindle speed. The dynamics of the milling system were described by a linear time periodic system with varying time delays, including the regenerative effect and the algorithm was implemented based on Floquet theory. They compared the accuracy and efficiency of their developed semi discretization method against Inspeger's widely accepted semi discretization method. The new method demonstrated a higher computational efficiency. Xie et al. [119] also extended the improved semi discretization method to analyse variable spindle speed with helix angle. Based on tool geometry and machining theory, the cutting region was divided into five different cases to calculate the cutting force. The influences of radial immersion rate and modulation parameters relative to variable spindle speed milling were explored, and results showed that the high radial immersion rate was more likely to cause chatter than the low radial immersion rate.

Saleh and Sims [120] modified a Simulink model that can predict regenerative chatter in milling to enable its use under variable spindle speed conditions. They achieved this by re-writing the equations of motion in non-dimensional time where the non-dimensional is representative of the number of simulated tool revolutions.

Totis et al. [121] developed an innovative and fast algorithm for chatter prediction in milling with variable spindle speed, based on the Chevyshev Collocation Method, with a two degree of freedom model. This algorithm provided much faster convergence times, from one to three orders of magnitude compared to the semi-discretization method, therefore overcoming the convergence problems which may affect to the semi discretization method.

Ding et al. [122] presented a semi-analytical method for stability analysis of milling with variable spindle speed. They reformulated the Delay Differential Equation obtained from the

milling dynamic model in an integral equation form, by dividing one time period into a series of subintervals. They did not consider the loss-of-contact effect as well as the multiple regenerative effect. With the aid of constant step numerical integration, the transition matrix over one time period was obtained to determine the milling stability by using Floquet theory. Unlike for constant speed machining, the time delay was determined by an integral transcendental equation, calculated accurately by an Ordinary Differential Equation based method. They applied the method for a two degree of freedom milling model and compared satisfactorily to semi discretization and time domain simulations with less computational effort.

Niu et al. [123] studied a variation of the method used by Ding et al. in order to further improve the computational times achieved by the constant-step numerical integration method. They used two degree of freedom milling dynamic system, and did not consider the loss-of contact and the multiple regenerative effect too. They adopted the Fourier series to unify all kinds of periodic spindle speed modulation schemes. In the unified framework, the time varying delay was derived implicitly and then calculated accurately using an Ordinary Differential Equation based method. Then, a Floquet theory based variable-step numerical integration method was proposed for the stability analysis. The results showed that this method was more computationally efficient than the semi discretization method and the constant-step numerical integration method proposed by Ding et al. Different modulation schemes were compared and the sinusoidal modulation could achieve higher stable productivity, while the triangular modulation permitted larger modulation parameter options.

Jin et al. [124] developed a milling dynamic model for the combined milling system with variable pitch cutter and spindle speed variation. They constructed a milling dynamic model which could take into account simultaneously the effects of the variation of the cutter pitch angles and the variation of the spindle speed. Then, linear stability analyses were carried out based on an updated semi discretization method. The method predicted stability lobes of milling processes with both variable pitch angles and variable spindle speed together. Although not experimental work was carried out, simulation results showed that the combination of the variable pitch angle and variable spindle speed had a bigger chatter suppression capability than each of them separately for low-medium spindle speed regions.

These results suggested further research in combining other methods too, like variable helix angles, serrated flutes or other spindle speed modulation forms.

Albertelli et al. [125] developed an online chatter detection algorithm suitable for variable spindle speed milling. The cutting stability assessment was performed in the spindle angular domain, and carried out through the real time computation of a normalized chatter indicator based on the cyclostationary theory. Before computing the chatter indicator, the order tracking and the synchronous averaging methodologies were adopted for pre-processing the vibrational signals and the data coming from the spindle encoder. The chatter indicator was successfully tested in different machining conditions and it showed a good performance in terms of reliability and capability of dealing with fast evolving cutting conditions.

Wang et al. [126] investigated the transient vibration behavior in milling with variable spindle speed. They constructed a discrete dynamical map of variable spindle speed milling, so that the response to initial conditions and the response to external forcing could fully describe the milling dynamics. Two transient vibration growth phenomena were found and proved that strong transient vibrations are induced by the transient growth of response to initial conditions or response to external forcing. The proposed method adopted the transient stability and receptivity analyses to evaluate the response to initial conditions and response to external forcing respectively. Compared to other methods, this gave a stability criterion based on both eigenvalues and non-normal eigenvectors and considered the transient behavior to external excitation. Experimental results showed good agreement with simulation results.

Wang et al. [127] proposed the multi harmonic spindle speed variation to improve the stability in high speed milling regions. The dynamic equations with multi harmonic spindle speed variation including the phase factor were derived to describe the milling process and the stability analysis was completed with a semi discretized method. The speed variation function could be described by some finite parameters and then the genetic algorithm was used to optimize these parameters. As a result, the optimized milling process had a higher stability limit, especially in the high speed zone. Numerical simulations were carried out and the correctness of the proposed method was verified.

Dong and Zhang [128] proposed the reconstructed semi discretization method to analyze the stability of the delay differential equations with varying delay term established based on the milling process with variable spindle speed. Firstly the modulation period was discretized and the time periodic delay term in varying delay differential equation was approximated at the discrete intervals based on the Shannon orthogonal basis. Then, the transition matrix was constructed and the Floquet theory was used to build the stability boundary of the milling system. This method was compared to the well accepted semi discretization method and demonstrated a higher computational efficiency. Results showed that the approximation of the time delay term with sinusoidal law could be used when the variation amplitude is small.

Summarizing, overall, modulated speed variation is a very interesting chatter mitigation technique, useful for some particular conditions in which other techniques present difficulties to work. An aspect that modulated speed outperforms adaptive speed is the conditions at low spindle speeds in which stability lobes are close one from the other. In this scenario it might be difficult to find the right spot continuously. However, modulated speed can be set so that chatter build-up is constantly suppressed. For this reason, modulated speed variation is considered a promising technique for the ultimate objective of chatter mitigation and therefore achieving an increase in machining productivity.

This technique has an important obstacle like other techniques reviewed in this chapter, which is the industrial implementation. Modulated speed has the potential to offer an easy to apply solution for the industry. However, so far the objective was to develop a method, and lab based hardware, or modified machines were used for that purpose. A challenge for the industrialization of modulated speed is to investigate machine programming and to develop a solution which can be executed by commercial milling machines.

5.7 Summary

Extensive research has been carried out since the 1950's in order to solve one of the biggest and most difficult to understand problems related to machining, the self-excited vibrations or chatter. Different models have been developed and improved along the years, including analytical models which provide a quick overview of the stability in frequency domain, time domain models which require a bigger computational effort but are capable of simulating

non-linearities that happen in the process, and finally experimental methods which are not time and cost effective but are the most reliable methods to identify chatter in real working conditions and are used extensively to validate simulation models developed in many of the research works carried out in this topic.

The objective of the current study is to solve an industrial problem affecting to the finish milling of aeroengine IBRs, which is complex due to the difficult to cut material, a titanium alloy, the geometry of the blades which require a five-axis contour or point milling technique with a ball-end mill or similar type of tool and the low stiffness of the thin walls of the blades. In addition to the above-mentioned complexities, the dynamic behaviour of the tool/workpiece system is constantly changing as the tool path moves from tip to root of the blade as the material is removed in the machining process. This particular situation makes some chatter avoidance methods not suitable for this application.

There are different strategies to optimize the finish milling process for this application. From defining and enhancing the process damped region in the low spindle speed range, to machining with a working window below the limiting width of cut or finding out regions between the stability lobes and predicting/reacting to the dynamic behaviour of the system to adapt the cutting parameters along the machining process to remain in stable conditions.

Using the process damped region has some limitations involving the detailed modelling of the non-linearities and especially the geometric and roughness limitations to use big widths of cut. Adapting the cutting parameters to remain within the stability lobes is another possible approach. The main problem to apply this approach is the complexity of the dynamic system, due to the five axis ball-end contour milling and the flexibility of the workpiece which contributes to changing dynamics of the system as material is being removed. Also, it is known that the adaptive spindle speed is most suitable for high speed regions due to the bigger stability areas present at high speed, and finish milling titanium blisks is difficult to apply at high speed milling, left alone in complex geometries like blades. The last option to improve machining performance is to suppress chatter through the spindle speed modulation technique. This technique looks the most suitable for the speed regions usually employed for cutting titanium in difficult-to-cut features such as blisk blades.

The literature review shows a considerable amount of work carried out developing spindle speed modulation technique and work has been mainly focused in finding the most beneficial modulation form (ie. Sinusoidal, triangular, square) as well as optimizing the modulation parameters with the objective of finding the best combination for chatter avoidance/suppression. Different models have been tested, such as time domain models, semi discretization models and frequency domain models, together with some new models, trying to predict spindle speed modulation stability accurately with the less computational effort possible. Another research focus is its applicability, as an out-of-process method or as an in-process method. Easiest to apply in a production environment is the out-of-process method because it does not require specialist knowledge or specific hardware and software in the factory, although depending on the optimization level, it could be more complicated to develop than in-process methods. It could be possible to combine both approaches, or even develop an out-of-process method optimised through in-process feedback.

However, very little has been covered in the literature about applying these methods in real life products with complex system dynamics as it is the case of IBRs. Radulescu et al. [106] considered complex dynamics for variable spindle speed modelling, but no references could be found of dynamic models including spindle speed modulation which considers ball-end tool geometry and flexibility of the workpiece. In the past, models were developed for the combination of ball-end tool geometry and flexible workpiece but they were considering constant spindle speed. Similarly, the latter have been considered in a couple of research works in adaptive spindle speed machining models, but none for modulated spindle speed.

A gap in the literature has been found in developing a dynamic model for sinusoidal modulated spindle speed variation which considers the ball-end tool geometry and workpiece flexibility. Both current time domain and semi-discretized or frequency domain models could be adapted to include the effects mentioned above, in order to propose an optimized speed modulation technique for IBR and similar complexity component milling.

A further gap found in the literature is the industrial implementation of the modulated speed technique. Research studies up to date employ lab based equipment or modified machines to produce modulated signal. However, industrialization of these techniques require the

implementation in commercial machines without complex equipment or hardware/software modifications.

Now that gaps in literature have been identified, following chapters focus on developing novel solutions to fill those gaps. In particular, a new method to produce modulated speed and feed in commercial machines and a time domain model, which already exists but adds new features to simulate modulated speed and feed in ball-end geometry tools.

Chapter 6 investigates the machine characterization aspect for the industrial implementation of the sinusoidal variable spindle speed and Chapter 7 develops a time domain model for ball-end tool and sinusoidal variable spindle speed.

CHAPTER 6. CNC IMPLEMENTATION OF SINUSOIDAL SPEED AND FEED

6.1 Introduction

Variable Speed Machining (VSM) requires a machine capable of producing variable signal both for spindle speed and feed (in order to keep constant uncut chip thickness while varying target spindle speed). This is one of the main difficulties encountered to apply this technique simple and efficiently in industry. Most milling machines and their control systems are not prepared for varying the speed smoothly around a mean speed value, e.g., following a sinusoidal wave. This might be one of the reasons why most of the work done in research environment about variable spindle speed is theoretical, without complementary experimental work [57], [107], [114], [122], [128].

As a first approach, a line-by-line NC code could be created with small distance steps in each with its corresponding spindle speed and feed. However, the result is not acceptable producing errors in the execution.

Research in other work carried out using variable speed shows that generally complex solutions had to be adopted involving hard changes in the software of the control system or the kernel [111]–[113], which provided valid solutions but at the same time difficult to apply in industrial environments. Xie et al. [119] proposed a semi-discretization algorithm to predict chatter with variable spindle speed milling. No experimental tests were carried out but theoretically, they concluded that selection of RVA plays a very important role enhancing the stability region when a sufficiently high value is selected. This was proposed to be $RVA=0.1$ (10% amplitude variation). For $RVA=0.05$ no noticeable impact in stability was found. Frequency variation rate was selected from RVF 0.1 to 0.5 and it was found that the stability gradually increased. Kalinski and Galewski [94], in their research about chatter vibration surveillance by optimal linear spindle speed control, used a triangular spindle speed variation method. They found considerable limitations on the machine to produce the desired signal.

The machine was capable to produce variable spindle speed variation not exceeding 2000rpm without having a feed drop failure. Also, they saw that changes in spindle speed had to be done over 0.3sec. to reach desired speeds. The method to achieve the triangular speed variation was not presented, but they stated that they used a standard CNC control to achieve the speed variation, although they used a fixed feed rate, therefore altering the chip load while cutting. Ding et al. [122] proposed a numerical integration method for stability analysis with variable spindle speed but with no experimental work involved. The simulations they carried out showed an increase in axial stability from 0.8 to 3mm and this was mostly affected by RVA in comparison to RVF. Wang et al. [126] analysed the transient behaviour of milling with triangular variable speed. Experimental tests were carried out with a Siemens 840D control but no details of the method to achieve variable speed were given. Maximum RVA of 0.2 was used with low RVF values between 0.003 and 0.005.

In this research work a method has been used prioritising a possible industrial implementation. This was applied successfully by Seguy et al. [116] for a triangular speed variation, with a difference between input and measured speed trajectories below 0.5%. The method consists in automating both speed and feed overrides for a given set of mean speed and feed (note that this has been tested in a Starrag NB251 machine with Siemens 840D control, but it should be applicable to at least overall machines run by Siemens 840D control). This method has an important limitation, which is the maximum amplitude variation, given by the control override limits. Although overrides could be limited to values of 80-120% (which means a maximum of 20% amplitude variation), this is a range which according to other studies most benefits are obtained from the variable speed. The advantage is clear with the option to apply the method directly with a commercial control system in a very few NC code lines.

6.2 Method

Before implementing variable speed/feed into machining trials, it is necessary to carry out a machine characterization. This characterization aims to find the limits of the machine regarding its capability to produce a sinusoidal signal around a mean speed and feed value. The method consists in producing air cuts at different parameters and recording the actual

signal produced by the machine. These will then be compared with the simulated signals generated in Matlab and conclusions will be obtained whether the proposed method is valid, and if so, the limitations it has and the working window for further machining trials using variable speed/feed with automated overrides.

A set of different parameters have been selected for the characterization. Main variables have been identified as spindle speed, feed, amplitude variation rate (RVA) and frequency variation rate (RVF). From those variables, RVA is limited by the machine override, generally up to a 20% maximum. This means that a maximum amplitude variation of 20% is possible to obtain. However, as mentioned before, research data suggests that the range between 10-20% might be the best for chatter suppression.

Regarding to speed and feed limitations, it is expected to be influenced by the RVA and RVF combinations, together with the dynamics of the spindle and/or the table feed to keep up with the requested variation speed.

For every combination selected, an air cut of 200mm has been carried out. By default, machine's x axis has been used for travel, but a repeatability test has been done with y axis travel to confirm feed travel axis is not influencing the results. Initially, both feed rate and RVA are fixed and limits are found for a range of spindle speeds in relation to the maximum RVF achieved. Once this has been mapped, influence of the feed is analysed by increasing the feed rate and fixing the rest of parameters. Finally, the influence of RVA is analysed by replicating speed-RVF curves for a maximum amplitude of 20%.

The conclusions of the testing mentioned above provide a working window for the automated override speed/feed variation method. This is going to be the main limitation for industrial implementation, and the concept for chatter suppression will be discussed in next chapters within regions of the working area obtained in the characterization test.

6.2.1 Machine specifications

The machine selected for this characterization is the Starrag NB251 (), a blisk manufacturing dedicated machining center. The particularities of this machine are the vertical table, which rotates in A axis and travels in X and Y axis and the spindle head which apart from the typical spindle rotation along Z axis, it also rotates in B axis and travels in Y axis.

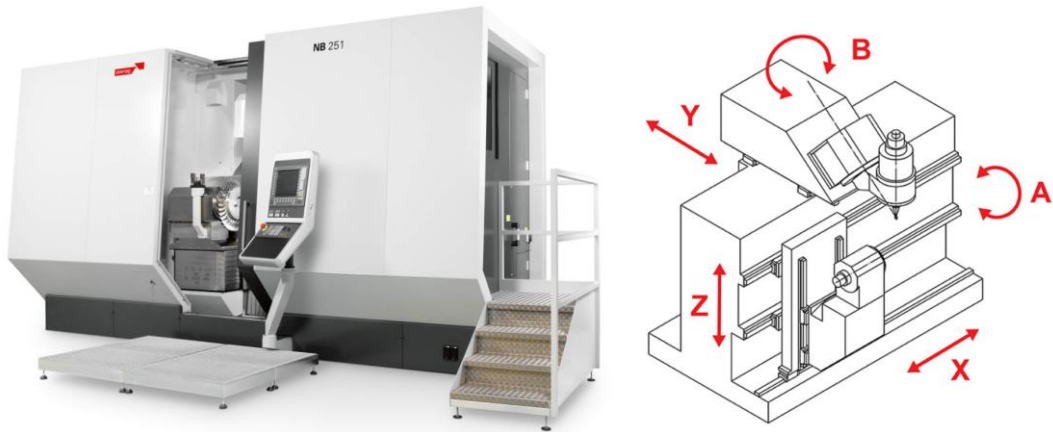


Figure 42. Starrag NB251 machine and axis layout.

lists the main technical data of the machine.

Table 19. NB251 technical data.

Travel X axis	700mm
Travel Y axis	400mm
Travel Z axis	400mm
Rotation A axis	360 degrees endless
Rotation B axis	+/- 87 degrees
Linear X/Y/Z axis traverse	62m/min
Rotary A axis feed	200U/min
Rotary B axis feed	60U/min
Motor spindle speed	18000U/min
Power motor spindle at 100% load	28kW
Torque motor spindle at 100% load	181Nm
Tool taper	HSK-A63 (A80)
CNC control	Siemens 840D

6.2.2 Data acquisition

Machine characterization is based on the comparison of the signals obtained from Matlab simulation (target signal), the nominal signal commanded by the control system and the actual signal recorded. This data is collected by Siemens Industrial SINUMERIK Edge monitoring system, a commercial solution from Siemens which includes ready-to-use software for exploiting machine data locally and in real time at the machine or globally across machines via the latest information technology.

Monitored data includes spindle speed, feed rate, axis positions and time, as well as other outputs which are not considered in this work. Recorded data is stored in the cloud and this can be accessed from a computer, even remotely, using siemens edge software. Although data is not in a straightforward readable format, a simple coding in Matlab helps obtaining a readable format, from where nominal and actual signals can be plotted against previously simulated signals.

A very important characteristic in any data acquisition system is the sampling rate. SINUMERIK Edge records data at a frequency of 500Hz. Following the Nyquist criterion, recorded signal's frequency should not be more than half the sampling rate provided by the data acquisition system. In other words, sinusoidal signals up to a frequency of 250Hz are capable to measure accurately with the Edge device. The above sampling frequency is capable to record up to a spindle speed of 15000rpm at once per revolution. This is not a limitation for the current project as shortest sine wave periods are of 0.15 seconds, which gives a frequency of 6.6Hz.

6.2.3 Automated overrides

Although considerable research has been carried out with variable speed approaches, machining centers have not been designed for its industrial implementation yet. Most research work done in variable speed have used complex solutions modifying the software of the controller or the kernel, which is a limitation for industrial implementation. For this reason, even if variable speed has shown potential to suppress chatter and improve machining productivity, it has not been widely implemented.

The solution proposed here is a simple but effective way of varying speed and feed in any commercial machine run by the popular Siemens 840D control (note that other control systems might work too in a similar way). The concept is to use the overrides of the control system but instead of the typical operator based manual handling, automating them via CNC program.

For this purpose, Siemens Synchronous Actions is used. A simple CNC code is written where some initial values are specified, the initial and final travel points and the trigonometric function desired. See below in an example of the override automation.

Table 20. Automated override NC program example.

```
G54 G90;
T1;
L700;
D1;
M03 S1000;
R40=0.1; %RVA
R41=0.1; %RVF
R42=1000; %Mean spindle speed
R43=0.0024; %K NC time-position conversion constant
ID=1 WHENEVER $AA_IW[X]>0 DO
$AA_OVR[S1]=100*(1+R40*SIN(360*R41*R42*R43*$AA_IW[X]));
ID=2 WHENEVER $AA_IW[X]>0 DO $AC_OVR=0.4*$AA_OVR[S1];
GO X-20 Y0;
G01 X200 F400;
M30;
```

The NC code above follows a simple instruction which activates when the position in X axis reaches to zero value and the action commanded is a sine wave along a mean spindle speed value with the indicated frequency and amplitude variation rates. Feed rate sinusoidal wave is proportional to the spindle speed's sinusoidal wave, so when the position in X axis reaches to zero value a percentage of the the current value of spindle speed is commanded.

6.3 Experimental work

Machine characterization has been carried out by experimental tests combined with computer simulations. The tests consist in simulating the speed and feed variation for a given set of parameters (speed, feed, RVA and RVF) and produce the same signal on the machine. Both signals are then compared and frequency response functions are plotted for magnitude and phase. This is done first by selecting spindle speed as a variable and fixing feed and RVA. Then, spindle speed and RVA are fixed and feed is set as a variable. Finally the effect of RVA is evaluated by repeating the first set of parameters for a higher RVA. Last but not least, repeatability tests have been carried out, reproducing a given signal repeatedly and also changing the feed travel from X to Y axis.

6.3.1 Sinusoidal signal simulation

A sinusoidal signal is created in Matlab to compare with machine monitored results. This is a straightforward task by simply producing a sine function for the speed and feed:

$$S(t) = S_0 \left[1 + RVA \cdot \sin \left(RVF \cdot S_0 t \cdot \frac{2\pi}{60} \right) \right] \quad (7.1)$$

$$F(t) = f_t \cdot n \cdot S(t) \quad (7.2)$$

Where,

$$S(t) = \text{Current spindle speed}$$

$$S_0 = \text{Mean spindle speed}$$

$$F(t) = \text{Current feed rate}$$

$$f_t = \text{Feed per tooth}$$

$$n = \text{Number of flutes}$$

The equations above show time based sinusoidal signals for both spindle speed and feed. One difference between this signal and the signal produced by Synchronous Actions automated overrides is that the latter is generated position based instead of time based due to NC code requirements. This is done by defining a constant value K at a given time in the simulation,

$$K = \frac{t}{x} \quad (7.3)$$

Where,

$K = NC \text{ time} - \text{position conversion constant}$

$x = \text{position}$

By knowing both time and position from the simulated signal, K is obtained and introduced in the NC program as a constant multiplying current X position inside the sine. Although this approach is not identical, it is valid to compare both simulated and machine's produced signal. Below, an example of a signal simulated is plotted against CNC's nominal signal and the actual signal produced.

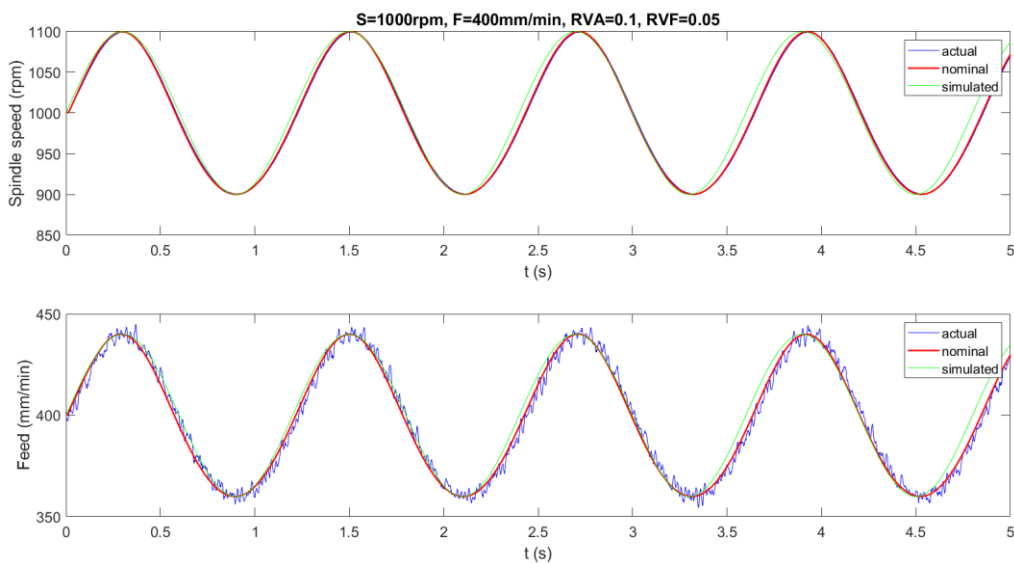


Figure 43. Example of sinusoidal signal simulated in matlab and measured in the machine.

The example of shows how the signals are overlapped with a very accurate magnitude in spindle speed and a slight shift phase in both spindle speed and feed. Also, some noise is found in the actual feed, although it is very small. Magnitude, phase shift and noise are dependent on the parameters used to create the signal. The higher RVA or RVF the more demanding should be for the machine to produce the requested signal. The same could happen as the spindle speed or the feed are increased. This will be evaluated below.

6.3.2 Experimental machine testing

Following the method described above, some initial tests have been carried out to obtain an insight of the machine's capability to produce the requested signal following a sinusoidal wave shape. At some conditions, such as the parameters shown in the plot above, the nominal and current signals follow well the target shape. However, when the requested conditions are harder to achieve, sudden feed drops are detected.

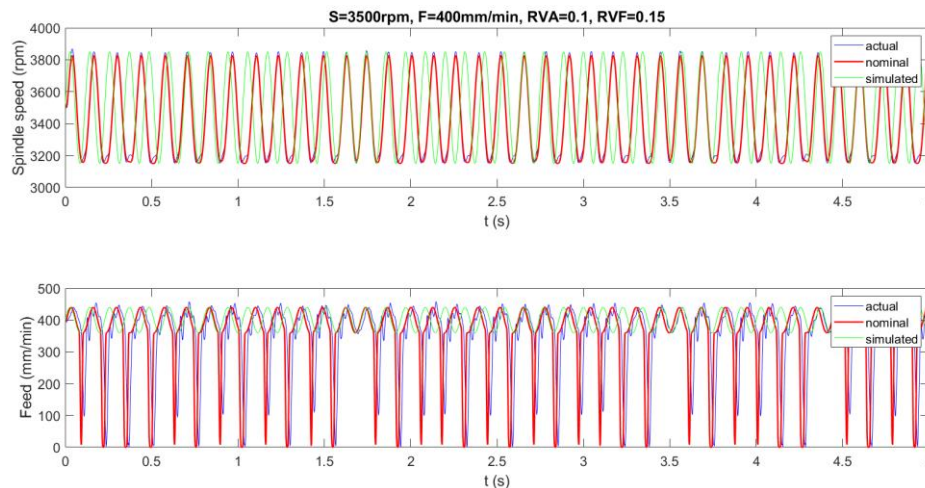


Figure 44. Typical example of feed failure error.

The feed drops identified in are considered the most important limitation for implementing this technique in further machining trials. Therefore, the following machine characterization is done with a feed failure criteria. When feed failure happens, generally it can be observed directly on the CNC controller screen, as an error light flashes while the program keeps running. The objective of the experimental testing is to understand when does the above failure happen as well as to define a working window for further machining trials.

Tests have been carried out in the following order:

- For a range of spindle speeds, RVF is varied until a feed failure is identified (fixed feed $F=400\text{mm/min}$ and $RVA=0.1$)
- For a range of spindle speeds, RVF is varied until a feed failure is identified (fixed feed $F=400\text{mm/min}$ and $RVA=0.2$)
- For a range of feed rates, RVF is varied until a feed failure is identified (fixed spindle speed $S=1000\text{rpm}$ and $RVA=0.1$)

Additional tests have been performed for the following purposes:

- Parameter repeatability test (fixed all parameters)
- Axis repeatability test (fixed all parameters except travel in different axis)

Although feed failure criteria is the most important to define the working window, other criteria like the frequency response for the magnitude and phase of the signal for both spindle speed and feed are considered and discussed.

6.4 Results and discussion

In this section, results from the various tests summarized above are analysed. Initially, feed failure criteria is applied for a range of spindle speeds and a range of RVA. Then, the same criteria is applied to a range of feed rates. Finally, additional tests have been performed in order to verify the repeatability of the parameters and different axis.

6.4.1 Spindle speed vs. RVF

First, spindle speed is tested against RVF until feed failure has been observed. Spindle speeds range between 1000-6000rpm have been tested. For each spindle speed starting at 1000rpm, different RVF values are tested until feed failure happens.

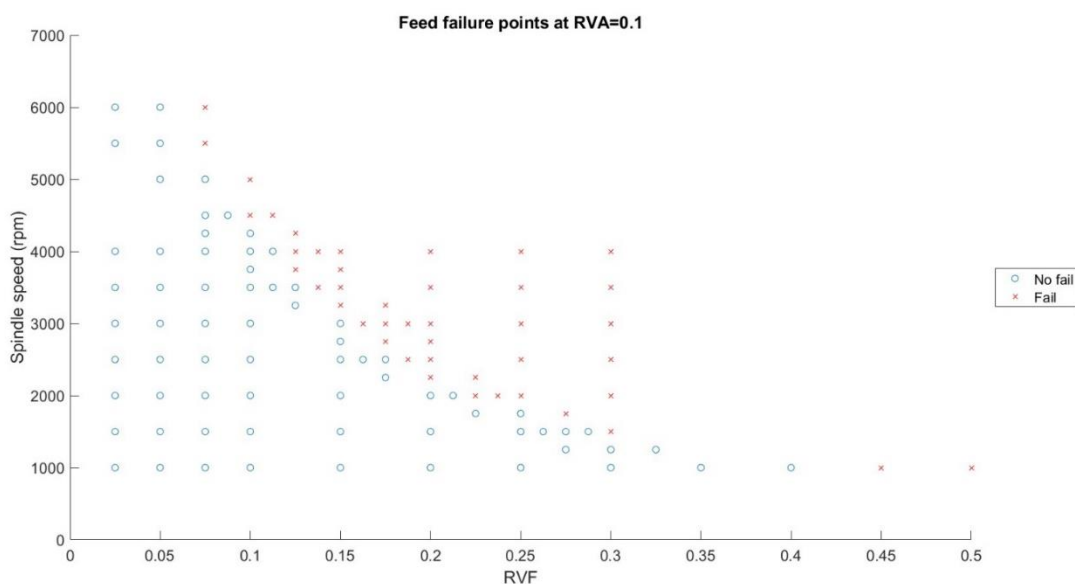


Figure 45. Feed failure for RVA=0.1 and F=400mm/min.

shows a plot of spindle speed vs. RVF. A total number of 112 tests have been run in order to complete this graph. Blue circles represent a correct sinusoidal path followed by the feed, while the red crosses represent a feed failure condition.

Observing the graph in the Figure above, a relationship is easily identified between the spindle speed and RVF. The higher RVF value is and the higher the spindle speed is, the more likelihood for a feed failure to happen. In fact, a fictitious line drawn between no failing and failing points follows an hyperbolic curve in the region tested of up to an spindle speed of 6000rpm and an RVF of up to 0.5. Every point below this curve will fit the no feed fail criteria.

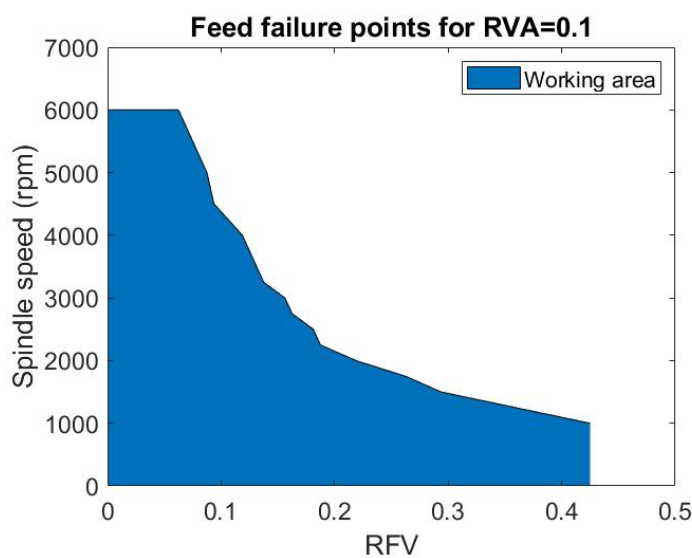


Figure 46. Working area for RVA=0.1 and F=400mm/min.

shows a blue coloured representation of the working area based on the feed failure criteria for a constant value of RVA=0.1 or in other words, a 10% of amplitude variation.

As discussed above in method section, most machines are limited to an override of 20%. This is a machine limitation and it affects to the maximum amplitude variation. The maximum value for RVA is therefore 0.2 (20% amplitude variation) and this top of the range value has been evaluated following the same procedure as above.

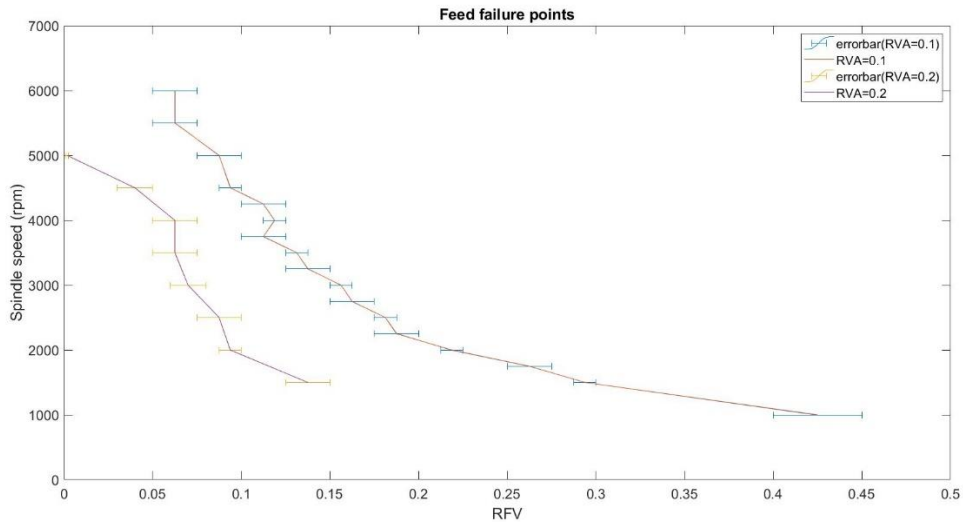


Figure 47. Feed failure for both RVA=0.1 and RVA=0.2 and F=400mm/min.

shows a comparison for the feed failure criteria between a 10% and a 20% amplitude variation, as this is the range of RVA which will be analysed in the machining trials. Instead of plotting the graph using circles and crosses, in this case error bars have been used, representing a no fail and fail condition each side respectively, and a line joining every middle point.

The first observation is that the amplitude variation rate has a negative effect on the feed failure related error. For a higher RVA value, the limitation in RfV is bigger for a given spindle speed value. Or similarly, for a fixed RfV, it is possible to use a higher spindle speed without incurring in feed failure error.

Although the range tested for a 20% amplitude variation is slightly narrower (due to time limitations in machine usage), spindle speeds from 1500-5000rpm are good enough to see a correlation between RVA=0.1 and RVA=0.2. Both curves are very similar in shape and the lower amplitude variation rate is shifted to the right in RfV axis.

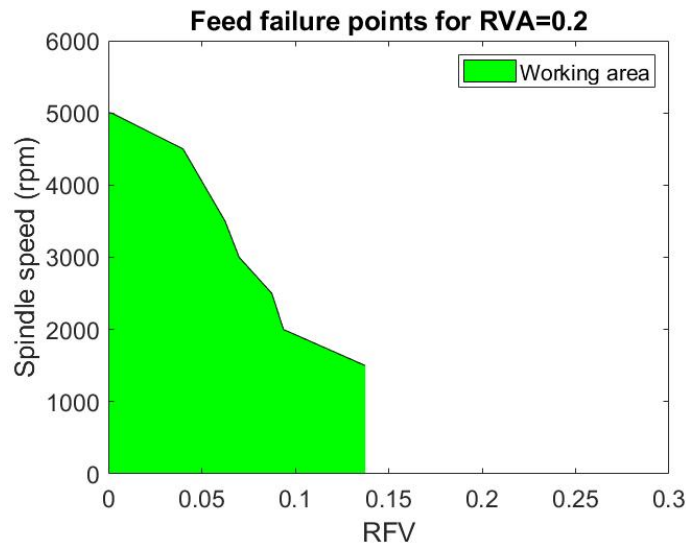


Figure 48. Working area for RVA=0.2 and F=400mm/min.

shows a green coloured representation of the working area based on the feed failure criteria for a constant value of RVA=0.2 or in other words, a 20% of amplitude variation.

Both area graphs shown in the figures above define the working area for the feed failure criteria and the correlation between them completely defines the parameters which can be tested in further machining trials safely avoiding feed failure to happen. However, there is a middle step that needs to be verified. This curves have been produced running air cuts, so some cutting checks will be carried out to confirm cutting load is not adding an extra limitation.

6.4.2 Feed vs. RVF

Next phase in machine characterization is to evaluate the potential effect feed rate might have in feed failure error. In order to do so, a range of feed rates between 400-10000mm/min has been tested while fixing both spindle speed and RVA.

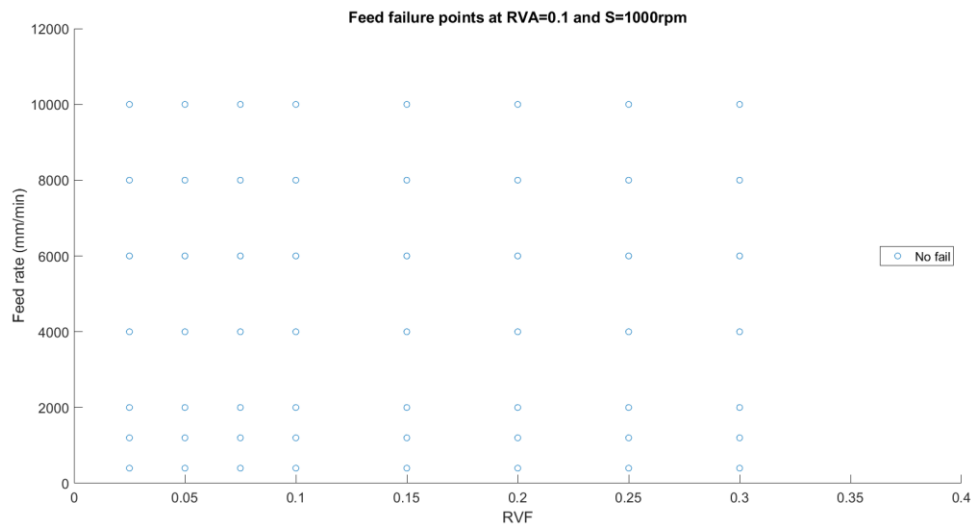


Figure 49. Feed failure for variable feed rate and fixed $RVA=0.1$ and $S=1000rpm$.

shows that for a range of variable frequency rates, an increasing feed rate is not producing the feed failure error observed in the sections above. This result differs from the result obtained at variable spindle speed, as no boundary point can be found even for considerably high feed rates.

These results suggest that unlike spindle speed, RVA or RVF , feed failure error is not triggered by the feed rate variable. However, this does not necessarily mean that feed rate will not have an impact in frequency response magnitude and phase. This will be evaluated in the next sections. In order to understand the different behaviour of spindle speed and feed rate, it must be considered that both are under a different dynamic system. Spindle speed has a variable rotational speed; meanwhile, feed has a variable linear speed. Also, with synchronous actions, feed reacts to the sinusoidal signal originally created for the spindle speed.

6.4.3 Repeatability tests

It is important to carry out a simple repeatability test to confirm the validity of the characterization tests. Repeatability has been performed for parameters and also different table axis (e.g. X and Y).

A given set of fixed parameters have been selected and five repetitions have been recorded back to back. Then, another five repetitions have been carried out with the same fixed

parameters but travelling in a different axis (e.g. Y instead of X). This will demonstrate if both axis are equivalent for the working window definition.

A borderline condition but stable (no feed failure) has been selected; Spindle speed of 3500rpm with a feed rate of 400mm/min, RVA of 0.1 and RVF of 0.125. First five repetitions travelling in X axis and last five repetitions travelling in Y axis.

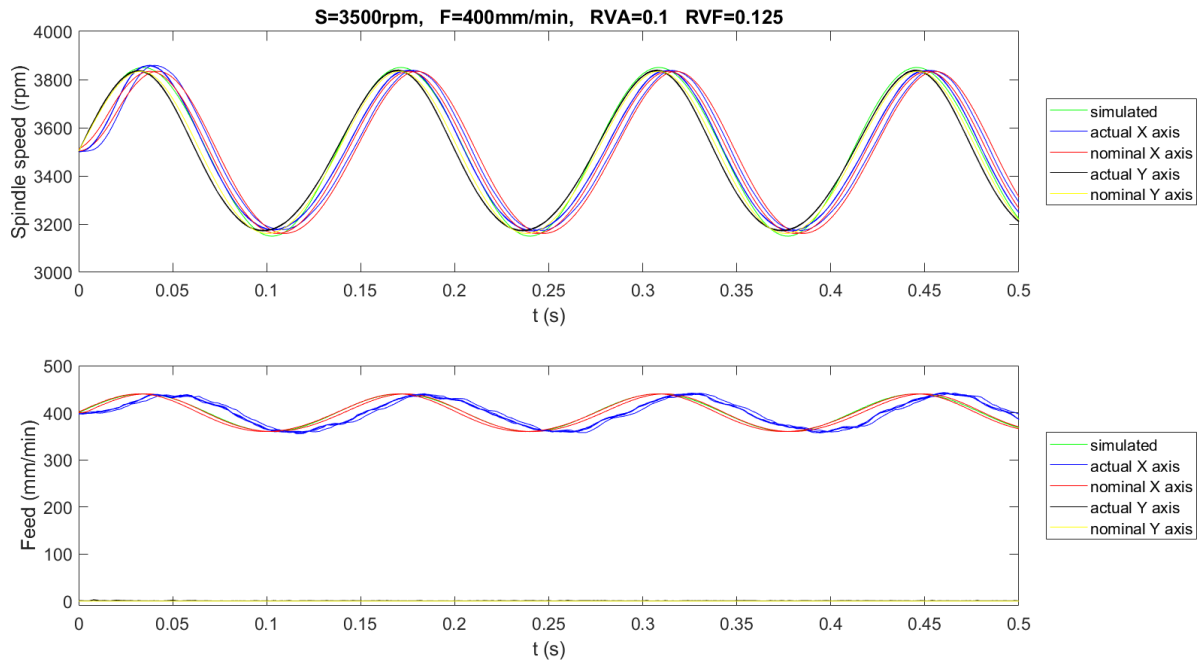


Figure 50. Repeatability test for X and Y axis at fixed parameters $S=3500$, $F=400$, $RVA=0.1$, $RVF=0.125$.

Results from show repeatability for constant parameters in two different axis. X axis is linked to a table linear movement and Y axis is linked to a spindle head linear movement.

In a general view observed at , it can be concluded that both X and Y axis tests approach well to the simulated signal in terms of spindle speed and feed, although for the latter there is a phase shift between nominal and actual.

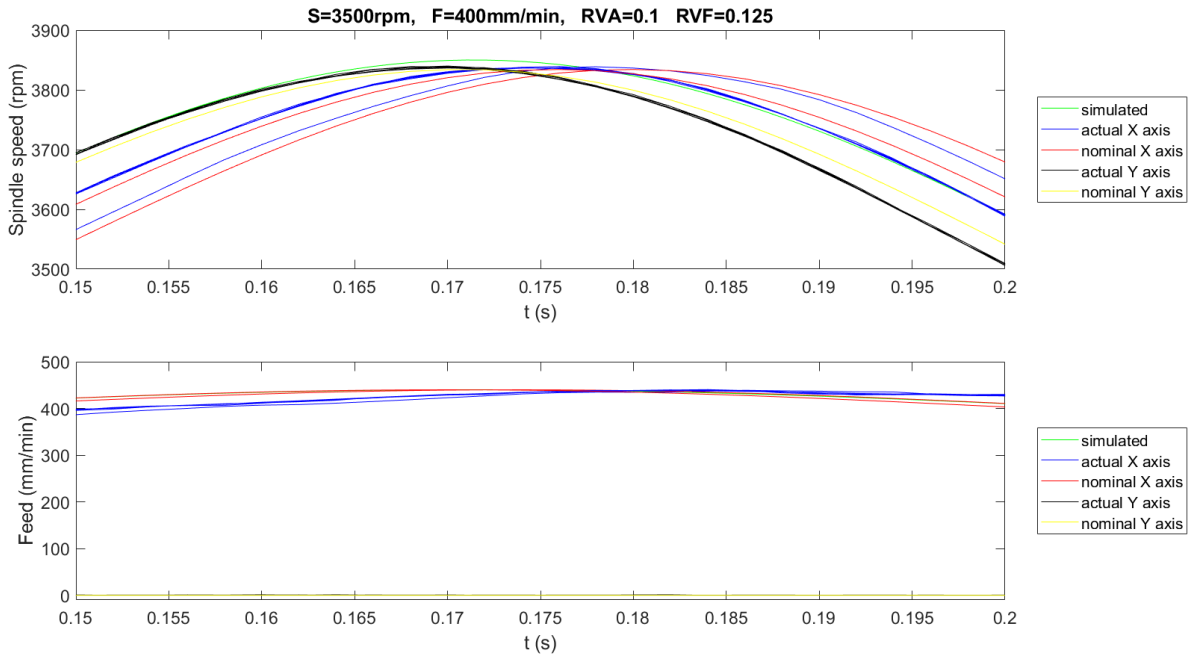


Figure 51. Repeatability test for X and Y axis at fixed parameters $S=3500$, $F=400$, $RVA=0.1$, $RVF=0.125$ (peak zoom).

A closer look from shows Y axis performing closer to the simulated signal in both nominal and actual recordings, in comparison to X axis, which is more scattered. Regarding the feed, results from X axis are approaching well to the simulation; However, Y axis is not moving as it records a feed rate around zero. This is likely due to a typing error during programming travel in Y axis and this should be confirmed before running machining cuts in Y axis direction.

In any case, providing there has been a typing error during Y axis programming, repeatability is considered good enough for the purpose of this study.

6.4.4 Frequency response for magnitude and phase

After the most critical feed failure and repeatability have been analysed, a more detailed observation of the sinusoidal signal is carried out. For this purpose, frequency response has been analysed for both magnitude and phase for spindle speed and feed rate.

Initially, spindle speed is selected as a variable for a range of RVF. Spindle speed ranging from 1000rpm to 4000rpm has been plotted against a RVF from 0.025 to 0.3.

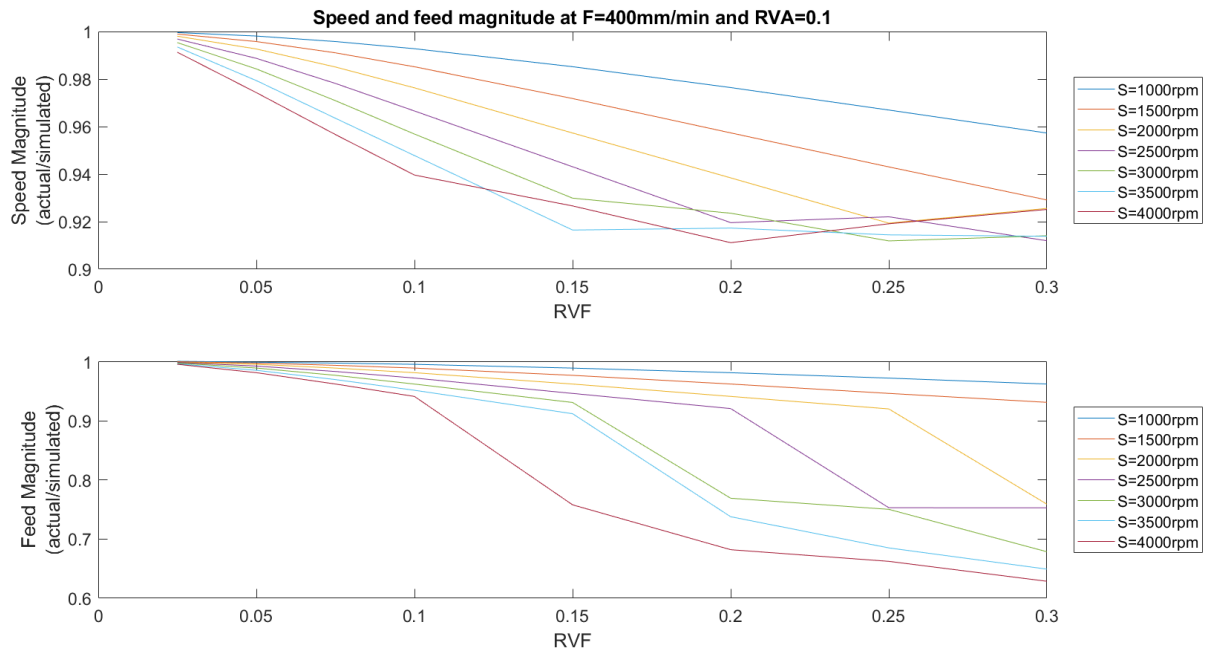


Figure 52. Speed and feed magnitude for variable spindle speed.

Looking at the magnitude in , it is observed that both for speed and feed, magnitude drops as the frequency variation rate is increased. The same happens when the speed is increased, as magnitude profile drops for both speed and feed. When speed and feed magnitudes are compared, a bigger drop is observed for feed rate; While magnitude remains above 90% for speed, it drops under 70% for the feed for certain combinations of speed and RVF. Based on the figure above a 90% magnitude acceptability criteria seems a good criteria considering that below this level, feed magnitude drops considerably.

After evaluating the frequency response to the spindle speed, the process is followed for the feed rate. Speed and feed magnitudes are now plotted for a frequency response of the feed rate. A range of feed rates from 400mm/min to 10000mm/min has been tested with a RVF ranging from 0.025 to 0.3.

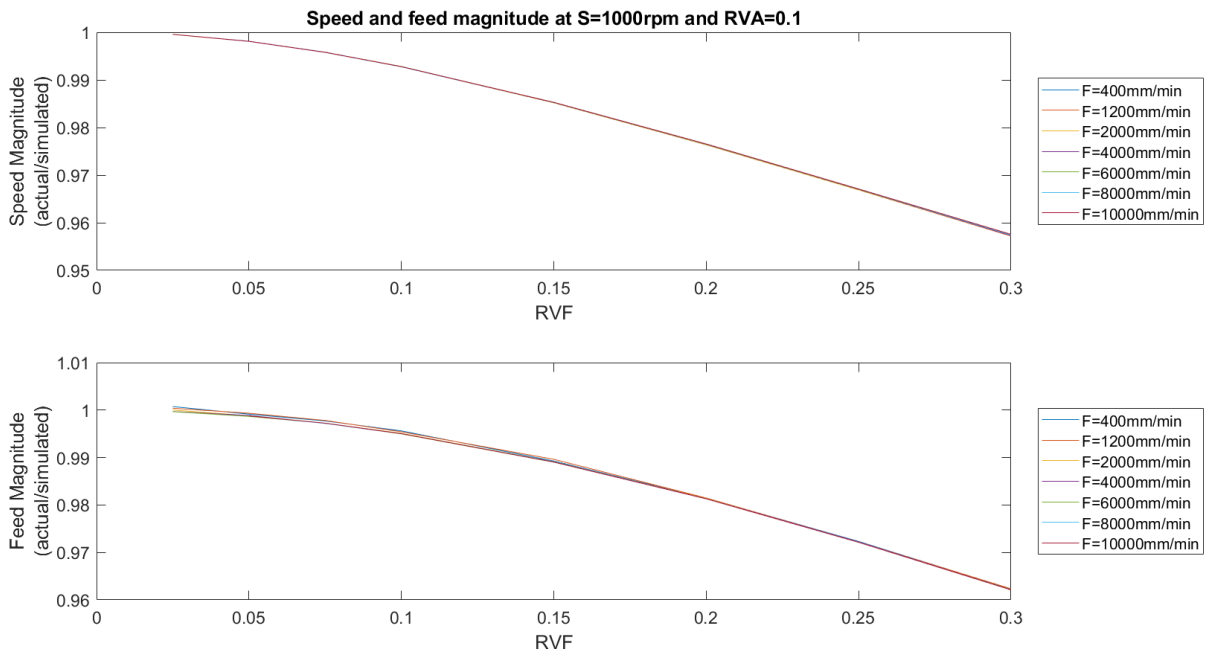


Figure 53. Speed and feed magnitude for variable feed rate.

The results from show a magnitude drop as the frequency variation rate is increased. This drop is lower in comparison to the drop observed for the spindle speed variation, as the tested range keeps a magnitude over 96% for both speed and feed.

An important finding is that curves produced by a range of different feed rates are a very close match, which means that feed rate does not have any impact in speed and feed magnitude. This agrees with the finding above in which the feed rate variable was not related to the feed failure error.

Finally, phase delay is analysed when spindle speed is set as a variable and also when feed rate is set as a variable. Following the same format as above, first a spindle speed ranging from 1000 to 4000rpm is evaluated and later a feed rate ranging from 400 to 10000mm/min is analysed.

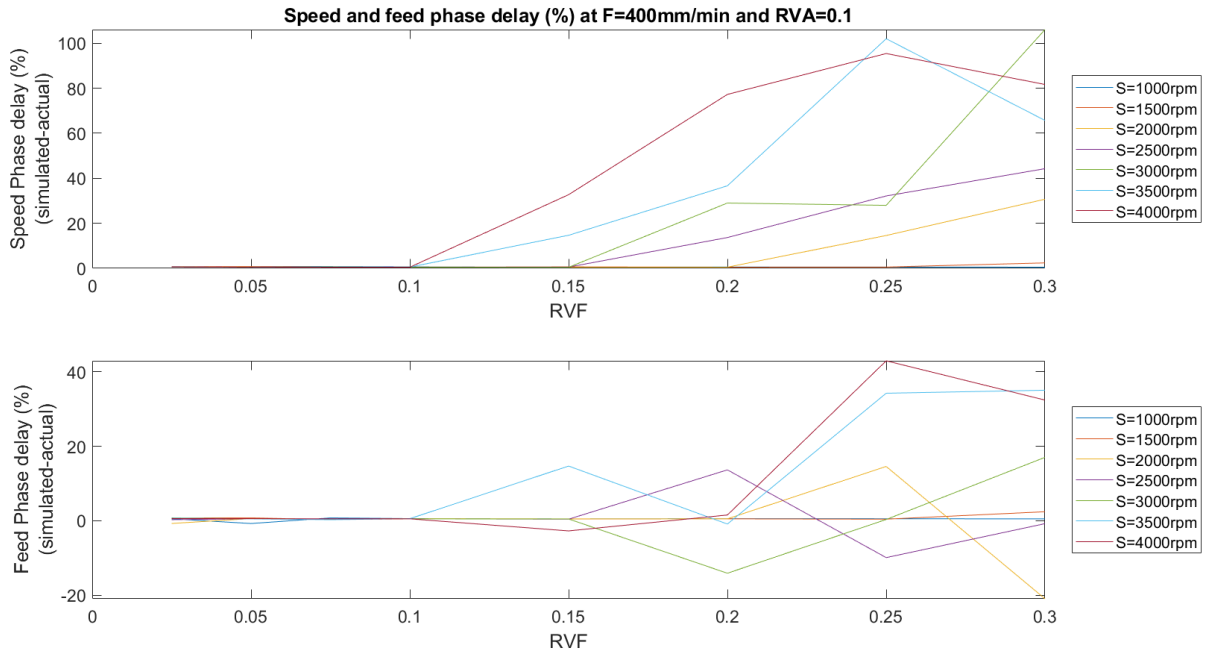


Figure 54. Speed and feed phase delay for variable spindle speed.

Looking at , it can be observed that speed phase delay starts being considerable earlier (at lower RVF) as the spindle speed is increased. Phase delays are particularly high at level over 60% for speeds over 3000rpm and RVF over 0.2.

Feed phase delay has been plotted too, but in this case results are closely related to the feed failure errors producing feed drops and therefore creating false phase delays.

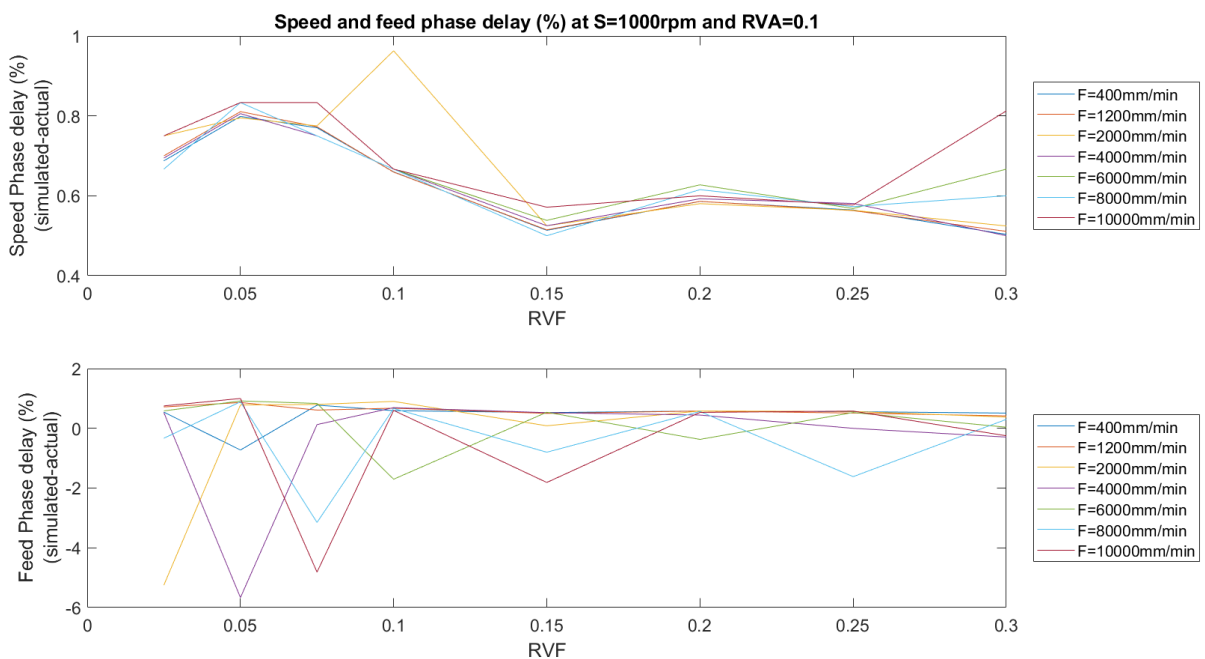


Figure 55. Speed and feed phase delay for variable feed rate.

Finally phase delays have been plotted for varying feed rates. Here speed phase delay is very similar and low for any of the tested feed rates and the phase delay does not show a clear worsening effect as the frequency variation rate is increased, as observed in . Feed phase delay does not show any clear trend for the feed variation across a range of RVF values

6.5 Conclusions

A machine characterization has been done for the NB251 machining center. The purpose of this characterization is to evaluate machine's capability and limits to produce a sinusoidal variable speed and feed signal while assuring that data can be monitored with sufficient accuracy.

Siemens Edge monitoring system has proved to be accurate enough for machine data recording. It's sample rate of 500Hz, is capable to record spindle speeds up to 15000rpm at once per revolution rate. This is more than enough for this work because the sample rate needed for the speed variation is much lower.

An experimental machine testing has been carried out to learn machine's working range when variable speed and feed are applied. A machine limitation has been found which has been named as "feed failure" and a working window has been identified for a range of cutting parameters and speed/feed variation parameters. From the cutting parameters, i.e. spindle speed and feed, only the former has shown a considerable effect on the feed failure. Both frequency and amplitude variations have an effect too. Spindle speed and frequency variation rate (RVF) follow a hyperbolic curve which defines feed failure. A very similar curve is defined by a higher amplitude variation rate but shifted. The higher the spindle speed, RVF or RVA, the closer feed failure to happen.

Repeatability of parameters and axis has been studied too and in general a good enough repeatability has been observed for the purpose of this work. However, there is a result of concern when Y axis is selected, as the feed is around zero and no travel occurs. This is likely due to a typing error in the NC code, but a further evaluation is needed to confirm this.

Sinusoidal signal has been compared between the simulated and the machine nominal/actual response. A frequency response has been evaluated for magnitude and phase shift, both for spindle speed and feed. Here, feed rate's effect is negligible comparing to the spindle speed. For the spindle speed range tested, the speed's magnitude keeps over 90% but feed rate's magnitude shows a considerable drop below 90%. This is considered to be a limitation criteria for the magnitude.

Finally, phase delays are increasing with spindle speed and RVF and they are particularly high (at levels over 60%) for speeds over 3000rpm and RVF over 0.2. Higher amplitude variation is expected to increase phase delay too, although this has not been evaluated. However, feed rate has a little effect on phase delay, as it has been confirmed in the rest of the tests.

6.6 Summary

Chapter 6 analyses the experimental machine implementation of sinusoidal variable speed. Although research efforts are often directed to develop theoretical solutions, not always theoretical studies end up being applicable to the industrial context. Modulated variable speed is an example. From a variety of research work carried out on the theoretical side of the problem, there is no one clearly offering a solution that can be implemented into commercial machines. The work presented in Chapter 6 is an attempt to fill this gap.

Initially, a CNC code has been created, which is easily manipulated by any machinist, and works on standard milling machines. Then, an experimental characterization work has been carried out, to learn about the limits imposed by the machine when a modulated speed and feed (to keep feed per tooth constant) is required. A data monitoring system built in the machine has been used to record outputs of speed and feed in response to the input signal.

Characterization work has been carried out with a range of variable parameters, which are, amplitude and frequency variation ratios, spindle speed and feed. A machine limitation has been found as the feed per tooth suddenly drops to zero for high spindle speeds. Although a reason for the so called "feed failure" has not been defined, a valid working window has been created for the machine. Apart from the issues to process the feed per tooth variation, the

tested milling machine struggles keeping high speed frequency and amplitude variation ratios outside the valid working window.

There is remaining work to do in order to understand machine's physical limitations and checking how these limitations compare to the limitations of other machines. However, this is a proven method to implement sinusoidally modulated speed and feed within a particular working window in standard milling machine.

Overall, there are different limitations that apply to the particular case of IBR blades to mitigate chatter. From one side, limitations regarding the depth of cut, which is limited by the complex geometry to 0.3mm. From the other side the spindle speed, which can be sinusoidally varied up to 4000rpm with an effective variation rate of 10% for both frequency and amplitude. For the studied tool, this means $V_c=80\text{m/min}$ and $F_z=0.3\text{mm/tooth}$. The implementation of optimized stock geometry and variable speed technique are expected to increase stability and therefore produce a chatter free surface at the maximum cutting conditions proposed above. The potential benefit of this strategy is not only the machining time reduction (approximately a third of the current time based on feed per tooth increment from $F_z=0.109\text{mm/tooth}$ to $F_z=0.3\text{mm/tooth}$), but also reduction or avoidance of blade polishing operation which comes later in the manufacturing process.

CHAPTER 7. TIME DOMAIN MODEL FOR BALL END TOOL AND SINUSOIDAL VARIABLE SPINDLE SPEED (SVSS)

7.1 Introduction

Time domain models have been developed in the past in order to simulate cutting conditions and obtain outputs such as cutting forces, displacements, chip thicknesses, etc. without performing machine trials [56]–[60]. The simulation process in a time domain model is generally computationally demanding, especially if multiple conditions are tested in order to recreate the well established stability lobes diagram. However, numerical simulation methods, compared to analytical models have other advantages like the capacity to include non-linearities to the model with relative ease. Also, the level of detail is higher in a time domain model, as it provides local force and vibration levels for a selected cutting condition.

The objective of this chapter is to develop a time domain model capable of simulating a specific cutting method, which has the potential to improve the finish milling performance of complex geometry and difficult-to-cut parts, such as blisks, often finish milled by using a contouring strategy with ball-end geometry tools. The particularity of the model presented below is that apart from capturing the ball-end geometry of the tool, it is capable of simulating a sinusoidal variable spindle speed (SVSS), a unique combination on the state of the art of modelling and therefore with potential to explore the benefits attributed to the variable spindle speed into this particular cutting method.

The model developed in this chapter is based on the time domain model proposed by Campomanes and Altintas [60], who used a discretized kinematics algorithm to model the surface, providing a realistic representation of how the cutter and workpiece interact. This model was later adapted and simplified by Sims [64] in a MatLab – Simulink environment with the purpose of presenting a new chatter detection criteria for helical geometry tools and constant spindle speed (CSS). The same Simulink platform was used and further developed by Saleh and Sims [120] to consider variable spindle speed in the form of triangular variation.

The current model takes the already developed Simulink model and further develops to integrate ball-end geometry and sinusoidal variable spindle speed (SVSS).

This chapter describes the simulation model originally created by Sims [64] and further developed for the purpose of this research study. A general overview of the model is presented in order to explain the basic concepts of the program and then the different parts of the model are analysed in more detail for the full understanding of the reader.

7.2 Model formulation

Figure 56 shows an overview of the simulation model. This model has already been developed by N.D. Sims and the new contributions to the model are the development of ball-end geometry and variable spindle speed. Below the model is presented with own figures and diagrams created for this thesis, although the first part is just a description of the existing model.

The model consists of three different blocks built in Simulink, named milling kinematics, milling forces and system dynamics, which are connected into a loop for each step in the simulation.

CHAPTER 7. TIME DOMAIN MODEL FOR BALL END TOOL AND SINUSOIDAL VARIABLE SPINDLE SPEED (SVSS)

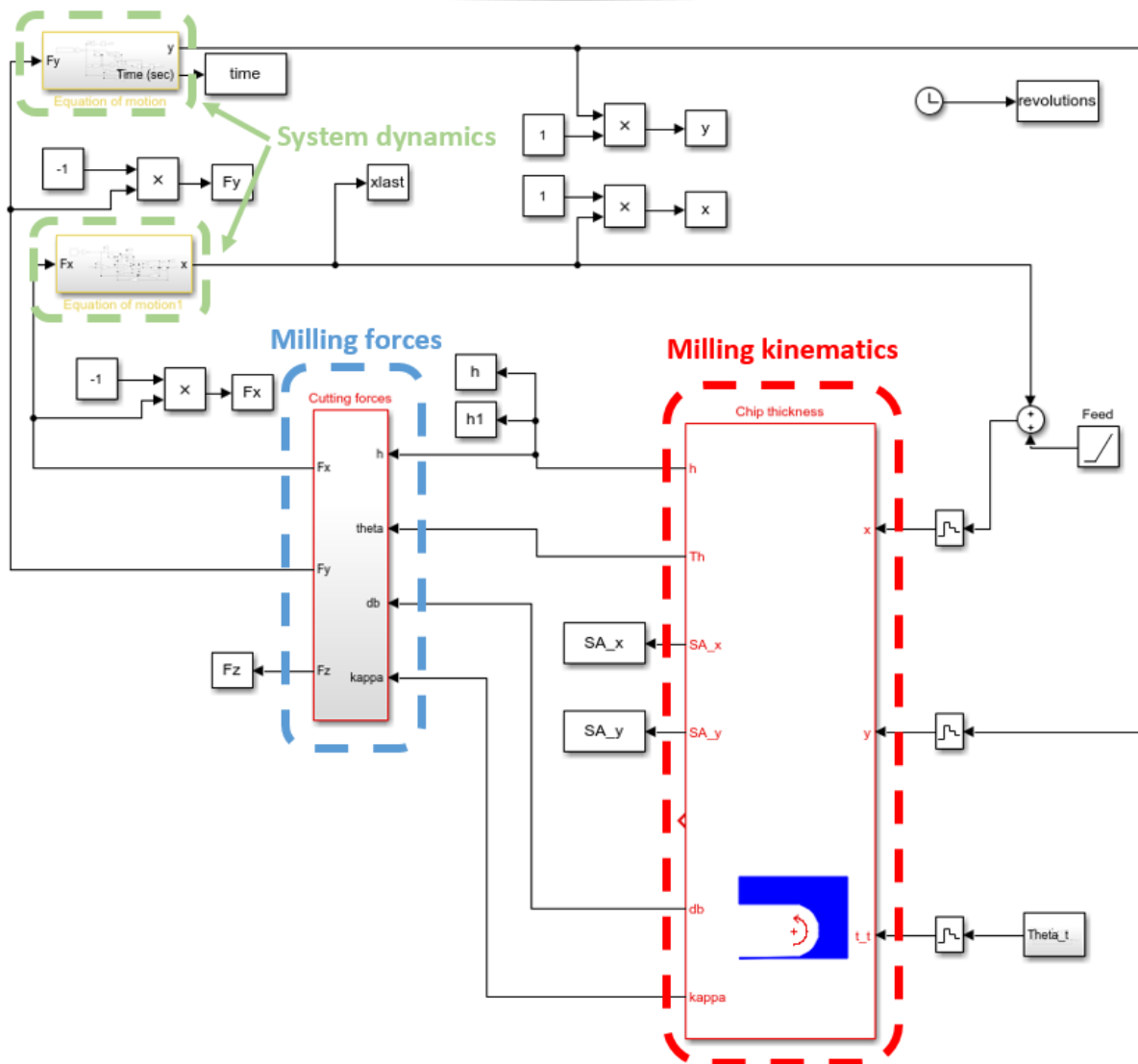


Figure 56. Simulink diagram for time domain simulation.

The calculations start in the milling kinematics block. This block is created by an S-Function (System Function) written in C language. The tool is divided into discrete axial slices and the geometry of the tool and workpiece is calculated within each slice. Radial coordinates are used to calculate tool geometry and Cartesian coordinates are used to calculate workpiece geometry. Then the relative displacement of the workpiece and tool is established, accounting for the feed and vibrations in x and y directions. An array S_a with a length of one revolution is created for each tooth in each axial slice, which defines the surface of the workpiece produced by the tooth. This array is updated for every revolution of the simulation.

For each revolution step, the following steps are carried out:

- Calculate tooth position based on current simulation time and spindle speed
 - Update workpiece surface array for the present tooth S_{ap}
 - Calculate instantaneous chip thickness for the present tooth based on current tooth position and the surface array for the preceding tooth. $S_{ap} - S_{ap-1}$
- (*) If tooth tip does not intersect the surface array generated by the preceding tooth (S_{ap-1}), then the surface array for (S_{ap}) is updated by interpolation between data points in (S_{ap-1}). In this case, the workpiece remains unchanged and the chip thickness is zero.

The instantaneous chip thickness calculated in the kinematics block is used to calculate cutting forces. For each tooth and axial slice, radial, tangential and axial forces are calculated, with the instantaneous chip thickness, cutting stiffness coefficients and the axial slice thickness.

$$F_r = k_{rc} \cdot h \cdot db \quad (6.1)$$

$$F_t = k_{tc} \cdot h \cdot db \quad (6.2)$$

$$F_a = k_{ac} \cdot h \cdot db \quad (6.3)$$

The forces in radial and tangential direction are then transformed to Cartesian (x, y) coordinates.

Finally, in the system dynamics block, for each time step calculated cutting forces are used together with modal parameters (m, k, c) to obtain displacements in x and y direction through a transfer function. x and y positions are then used to update the kinematics block for the following time step calculation.

7.3 Milling kinematics

The milling kinematics block makes calculations for each revolution step, based on the instantaneous tooth angle and the position in x and y axis, which is given by the feed and the relative position between the tool and the workpiece. The output of the block is the uncut

CHAPTER 7. TIME DOMAIN MODEL FOR BALL END TOOL AND SINUSOIDAL VARIABLE SPINDLE SPEED (SVSS)

chip thickness h , the chip width for the ball geometry and the arc surface for each revolution step in the calculation. Figure 57 shows a flow chart of the milling kinematics block.

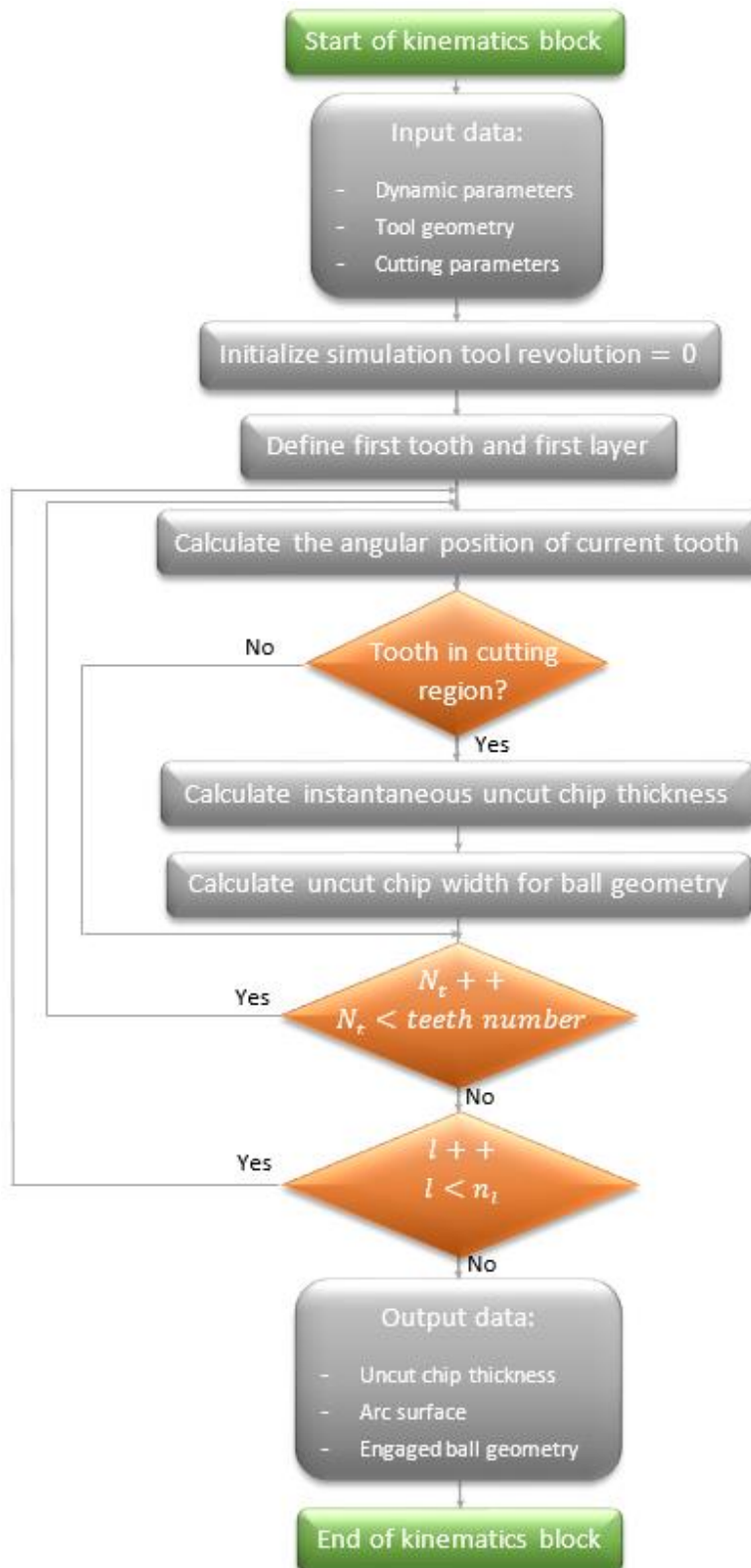


Figure 57. Simulation flow chart.

Below, the calculations to obtain the uncut chip thickness are explained.

7.3.1 Identify current tooth position

The first calculation in the milling kinematics block is to identify the instantaneous tooth position coordinates S_{atx}, S_{aty} . These coordinates are obtained from the tool radius r_t and the instantaneous tooth angle θ_u within the cutting area. The instantaneous tooth angle is calculated from the angular position of the cutting tool θ_t , the angular position of each tooth i relative to the reference tooth φ , the current axial layer l , the total number of axial discretization layers n_l , the axial depth of cut b , the tool radius r_t and the helix angle λ , as:

$$\theta_u = \theta_t + \varphi - \frac{(1+l)b \tan(\lambda)}{n_l r_t} \quad (6.4)$$

The angular position of the tool θ_t , varies according to the input signal in the Sinusoidal Variable Spindle Speed (SVSS). Compared to the constant spindle speed, in which the angular position increment is proportional to time, in the case of the SVSS this increment follows a sine wave. The instantaneous spindle speed, n , is function of the average spindle speed ω_0 , the speed variation amplitude RVA , speed variation frequency RVF , and previous angular position of the tool θ_{t-1} (eq.6.5-6.6).

$$n = \omega_0(1 + RVA \cdot \sin(RVF \cdot \theta_{t-1})) \quad (6.5)$$

$$\theta_t = \int n \cdot dt \quad (6.6)$$

Figure 58 shows the Simulink block used to obtain θ_t from the average spindle speed as well as amplitude and frequency variations respectively.

CHAPTER 7. TIME DOMAIN MODEL FOR BALL END TOOL AND SINUSOIDAL VARIABLE SPINDLE SPEED (SVSS)

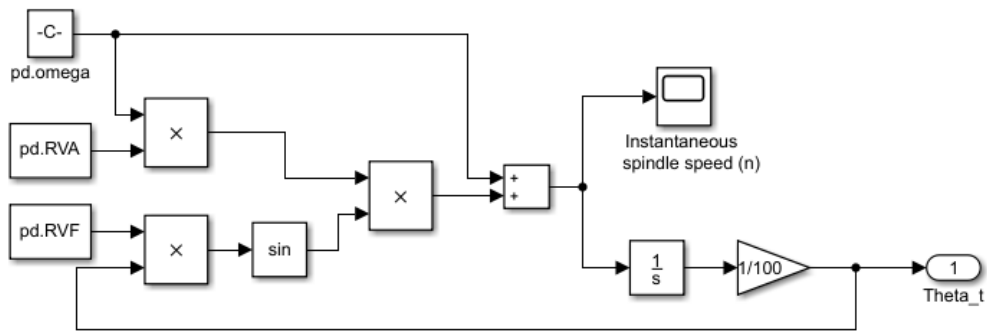


Figure 58. Diagram for the calculation of θ_t

Once the instantaneous tooth angle θ_u is calculated, the instantaneous tooth position coordinates S_{atx}, S_{aty} are calculated (eq. 6.7-6.8).

$$S_{atx} = r_t \cos(\theta_u) \quad (6.7)$$

$$S_{aty} = r_t \sin(\theta_u) \quad (6.8)$$

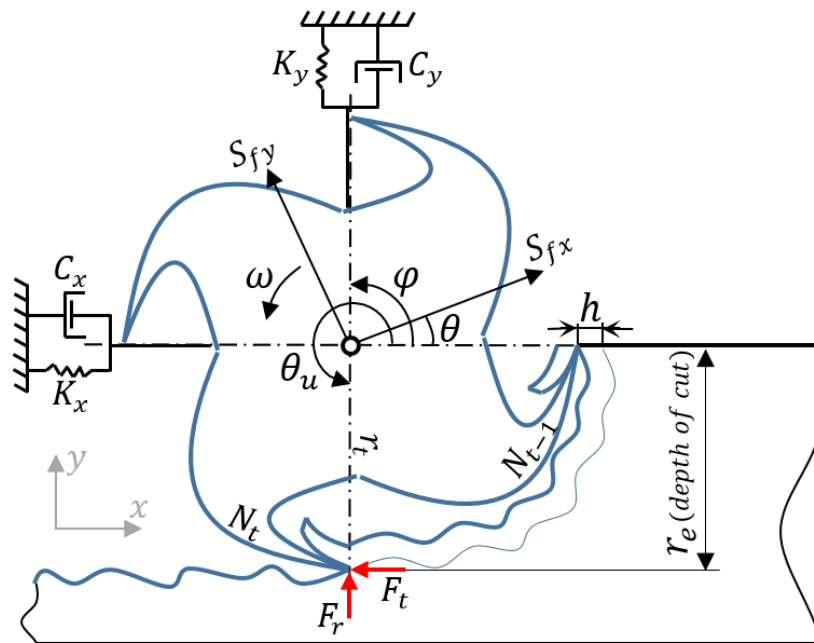


Figure 59. Milling dynamic model for up or conventional milling.

7.3.2 Define the workpiece arc surface points

For every instantaneous revolution, the workpiece arc surface points are defined. The surface of the workpiece, representing the surface generated in the previous pass l_{-1} , is digitised by a number of points which are stored in an array. S_{a0} and S_{a1} are the two closest points in the workpiece surface to the current tooth position, located in A and B points in Figure 60.

S_{a0} and S_{a1} are defined in global coordinates (S_{ax0}, S_{ay0}) and (S_{ax1}, S_{ay1}) respectively with angular positions θ_{a0} and θ_{a1} . These are calculated using the four quadrant inverse tangent function (eq. 6.9-6.10).

$$\theta_{a0} = \text{atan2}(S_{ay0}, S_{ax0}) \quad (6.9)$$

$$\theta_{a1} = \text{atan2}(S_{ay1}, S_{ax1}) \quad (6.10)$$

7.3.3 Calculate dimensions of the intercept segment geometry

For each revolution step, the dimensions of the intercept segment geometry are calculated and updated. First, the distances from the tool centre O to the already defined previous arc points S_{a0} (point A) and S_{a1} (point B) are calculated, as distances r_0 and r_1 respectively (eq. 6.11-6.12).

$$r_0 = \sqrt{(S_{ax0})^2 + (S_{ay0})^2} \quad (6.11)$$

$$r_1 = \sqrt{(S_{ax1})^2 + (S_{ay1})^2} \quad (6.12)$$

The angles θ_0 , defined by r_0 and r_t and θ_1 , defined by r_t and r_1 are obtained from θ_u and the pair θ_{a0}, θ_{a1} (eq. 6.13-6.14).

$$\theta_0 = \theta_u - \theta_{a0} \quad (6.13)$$

$$\theta_1 = \theta_{a1} - \theta_u \quad (6.14)$$

Once the angular positions (θ_0 and θ_1) of the arc surface points (S_{a0}, S_{a1}) relative to the tooth radius point are obtained, the intersection angles ($\theta_{01}, \beta, \alpha$) and dimension L_{01} are defined (eq. 6.15-6.18).

$$\theta_{01} = \theta_0 + \theta_1 \quad (6.15)$$

$$L_{01} = \sqrt{r_0^2 + r_1^2 - 2r_0r_1 \cos(\theta_{01})} \quad (6.16)$$

$$\beta = \sin^{-1} \frac{(r_0 \sin(\theta_{01}))}{L_{01}} \quad (6.17)$$

$$\alpha = \sin^{-1} \frac{(r_1 \sin(\theta_{01}))}{L_{01}} \quad (6.18)$$

The intercept segment radius r_s , which is equal to the distance from the tool centre O to the point O' is calculated next. In order to find this distance, basic geometric calculations are carried out.

When the angle θ_0 is equal to zero, the radius of intercept segment r_s is equal to the dimension r_0 , ($r_s = r_0$) following the geometry of the triangle (AOO') (Figure 60). When the angle θ_1 is equal to zero, the intercept segment radius r_s is equal to the dimension r_1 , ($r_s = r_1$) following the geometry of the triangle (BBO') (eq. 6.19).

$$r_s = \begin{cases} r_0 & \text{when } \theta_0 = 0 \text{ and } \theta_1 > 0 \\ r_1 & \text{when } \theta_1 = 0 \text{ and } \theta_0 > 0 \end{cases} \quad (6.19)$$

For the cases when the angles θ_0 and θ_1 are not equal to zero, the intercept segment radius r_s is calculated in the following way:

When the angle β forming the triangle (OBO') is not found or equals to zero, the intercept segment radius is calculated based on the trigonometric relations of triangle (OAO'). Otherwise, if the angle α forming the triangle (OAO') is equal to zero, r_s is calculated based on the trigonometric relations of triangle (OBO') (eq. 6.20).

$$r_s = \begin{cases} \frac{r_0 \sin \alpha}{\sin(\pi - \alpha - \theta_0)} & \text{when } \beta = 0 \text{ and } \alpha > 0 \\ \frac{r_1 \sin \beta}{\sin(\pi - \beta - \theta_1)} & \text{when } \alpha = 0 \text{ and } \beta > 0 \end{cases} \quad (6.20)$$

There is a last option, which happens when all dimensions are computed and angles θ_0 , θ_1 , α and β are not equal to zero. In this case, the intercept segment radius r_s is calculated separately with the trigonometric relationship of triangle (AOO') to obtain r_{sA} and the

trigonometric relationship of triangle (BOO') to obtain r_{sB} . Finally, r_s is equal to the highest value obtained between r_{sA} and r_{sB} (eq. 6.21-6.22).

$$r_{sA} = \frac{r_0 \sin \alpha}{\sin(\pi - \alpha - \theta_0)} \quad \text{from } \Delta AOO' \quad (6.21)$$

$$r_{sB} = \frac{r_1 \sin \beta}{\sin(\pi - \beta - \theta_1)} \quad \text{from } \Delta BOO' \quad (6.22)$$

$$r_s = r_{sA} \quad \text{if } r_{sA} > r_{sB}$$

$$r_s = r_{sB} \quad \text{if } r_{sB} > r_{sA}$$

The instantaneous uncut chip thickness h , which is an output of the kinematics model is the distance between the current tooth position (S_{atx}, S_{aty}), at point C and the intersection point O' which crosses the intercept segment dimension L_{01} (Figure 60). This is the result of the current tooth radius r_t minus the intercept segment radius r_s (eq. 6.23).

$$h = r_t - r_s \quad (6.23)$$

7.3.4 Update the intercept segment radius

For each revolution step, the intercept segment radius needs to be updated, as the workpiece is fed into the cutting tool at a feedrate f_t ($mm/tooth$). In this model the cutting tooth is assumed to be sharp edged, so the intercept segment radius r_s is updated based in the current tooth radius and position.

At each revolution step, the intercept radius r_s is checked to determine if the tooth is engaged in the cut or not. If the current value is not found, it means that the cutting tool is not cutting. When that happens, the intercept segment radius r_s is updated to the value of the tooth radius r_t ($r_s = r_t$). Then, the intercept segment radius is recalculated for each new surface layer.

The coordinates of the current tool point (S_{atx}, S_{aty}) on the current layer are updated with the current tool radius (eq. 6.24-6.25).

$$S_{atx} = r_t \cos \theta_u \quad (6.24)$$

$$S_{aty} = r_t \sin \theta_u \quad (6.25)$$

and proportional to the tangential cutting force and the axial cutting force F_a . The chip area is determined by the product of the uncut chip thickness h and the depth of cut b .

$$F_t = K_t \cdot b \cdot h \quad (6.26)$$

$$F_r = K_r \cdot F_t = K_r \cdot K_t \cdot b \cdot h \quad (6.27)$$

$$F_a = K_a \cdot F_t = K_r \cdot F_t = K_r \cdot K_t \cdot b \cdot h \quad (6.28)$$

K_t , K_r and K_a are the tangential, radial and axial specific cutting pressure respectively, and $(b \cdot h)$ is the chip area. The milling tools modelled here may have a uniform or variable helical flute, so each flute penetrates into the workpiece depending on the angular position along the helix angle. Also, the tools will have a ball-end geometry which will affect to the chip area.

The tool and workpiece are discretised into a number of layers n_l along the axial depth of cut b (Figure 61). For the ball end-mill, each layer has a disk shape whose thickness is the arc length db . At each axial layer the cutting force of each tooth is calculated by the product of the instantaneous cross-sectional area of uncut chip and the cutting pressure coefficient. At any step time the cutting forces due to the mechanics of chip generation are given by:

$$F_{rc|N_t} = db(K_{rc} \cdot h + K_{re}) \quad (6.29)$$

$$F_{tc|N_t} = db(K_{tc} \cdot h + K_{te}) \quad (6.30)$$

$$F_{ac|N_t} = db(K_{ac} \cdot h + K_{ae}) \quad (6.31)$$

where $F_{rc|N_t}$ is the cutting force acting in the radial direction of the tooth for layer l and tooth N_t . Likewise $F_{tc|N_t}$ is the cutting force due to the chip mechanics acting in the tangential direction of the tooth and layer and $F_{ac|N_t}$ is the cutting force due to the chip mechanics acting in the axial direction. Subscripts (rc , tc and ac) are referring to the radial, tangential and axial cutting respectively. Whereas coefficients K_{rc} , K_{tc} and K_{ac} are widely used cutting force coefficients that must be empirically obtained for a particular workpiece and (often) a particular tool. The edge or rubbing force coefficients K_{re} , K_{te} and K_{ae} can also be included in the model formulation, but in this thesis for simplicity they are initially assumed to be zero.

CHAPTER 7. TIME DOMAIN MODEL FOR BALL END TOOL AND SINUSOIDAL VARIABLE SPINDLE SPEED (SVSS)

The following is the new formulation created to include ball-end geometry and variable spindle speed to the model.

Arc length db has to be calculated for each layer l in order to incorporate the ball-end geometry. It is important to note that any part of the tool engaged in the cut and not corresponding to the spherical geometry, needs to be calculated in a different way.

a) For the spherical part of the tool engaged in the cut:

$$db = r \cdot \vartheta \quad (6.32)$$

$$\vartheta = k' - \vartheta' \quad (6.33)$$

$$k' = \cos^{-1} \left(1 - \frac{l \cdot dz}{r} \right) \quad (6.34)$$

$$dz = \frac{b}{n_l} \quad (6.35)$$

Where r is the radius of the ball geometry, ϑ is the angle formed by the lower and higher points of db with the tool centre, k' is the angle between the tool centre axis and higher point of db , l is the number of layer starting from the end of the ball and dz is the depth of the layer l Figure 61.

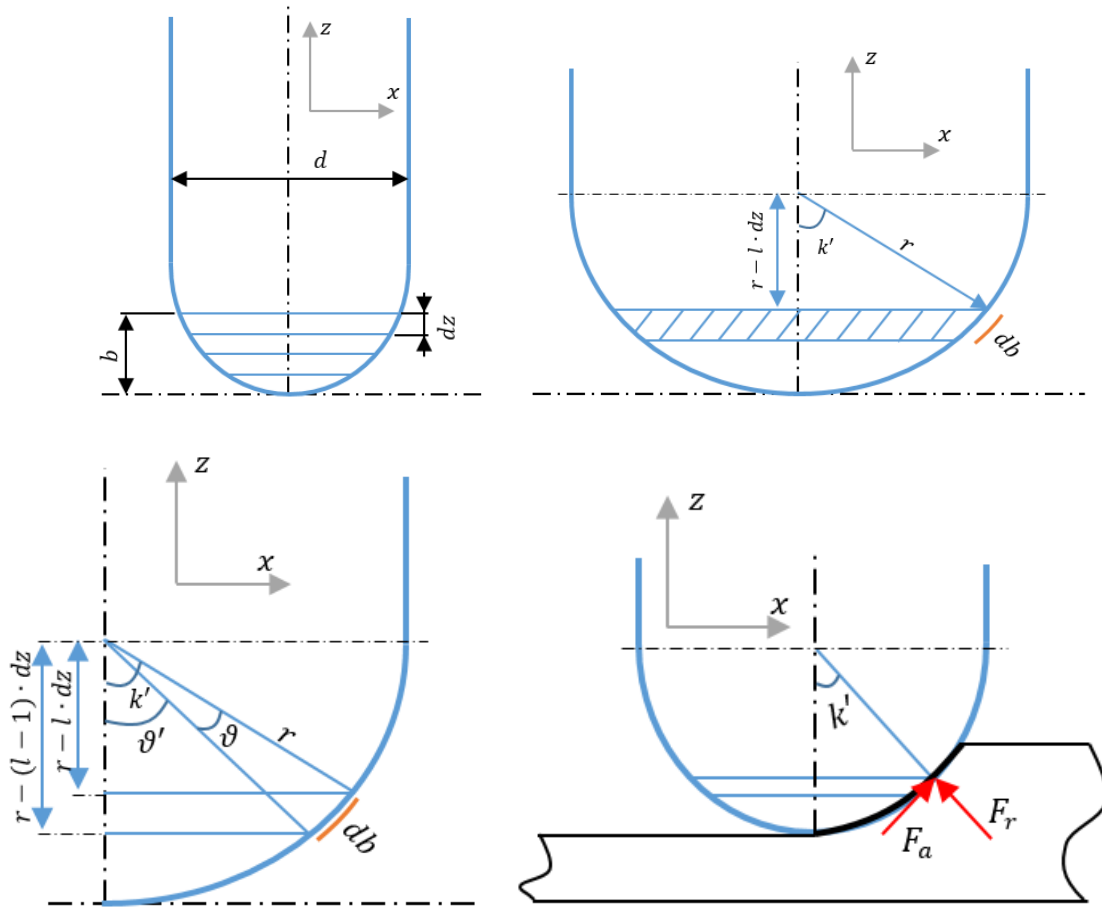


Figure 61. Detail of the ball type tool geometry and sketch for discretized depth, db calculation.

b) For the straight part of the tool engaged in the cut:

$$db = \frac{b}{n_t} \quad (6.36)$$

Then, these forces are transformed to the global coordinates based on the immersion angle θ_u (Figure 61). The cutting forces are resolved into components $F_{x_{lt}}$, $F_{y_{lt}}$ and $F_{z_{lt}}$ and summed up in the x, y and z directions respectively.

$$F_{x_{lnt}} = F_{t_{lnt}} \cos\left(\theta_u - \frac{\pi}{2}\right) + F_{r_{lnt}} \cos(\theta_u + \pi) \sin(k') + F_{a_{lnt}} \cos(\theta_u + \pi) \cos(k') \quad (6.37)$$

$$F_{y_{lnt}} = F_{t_{lnt}} \sin\left(\theta_u - \frac{\pi}{2}\right) + F_{r_{lnt}} \sin(\theta_u + \pi) \sin(k') + F_{a_{lnt}} \sin(\theta_u + \pi) \cos(k') \quad (6.38)$$

$$F_{z1N_t} = F_{r1N_t} \cos(k') + F_{a1N_t} \sin(k') \quad (6.39)$$

The total forces in x, y and z directions are:

$$F_x = \sum_{l=1}^{n_l} \sum_{t=1}^{N_t} F_{xc1N_t} \quad (6.40)$$

$$F_y = \sum_{l=1}^{n_l} \sum_{t=1}^{N_t} F_{yc1N_t} \quad (6.41)$$

$$F_z = \sum_{l=1}^{n_l} \sum_{t=1}^{N_t} F_{zc1N_t} \quad (6.42)$$

Figure 62 shows the cutting force model, built in Simulink as a custom block diagram.

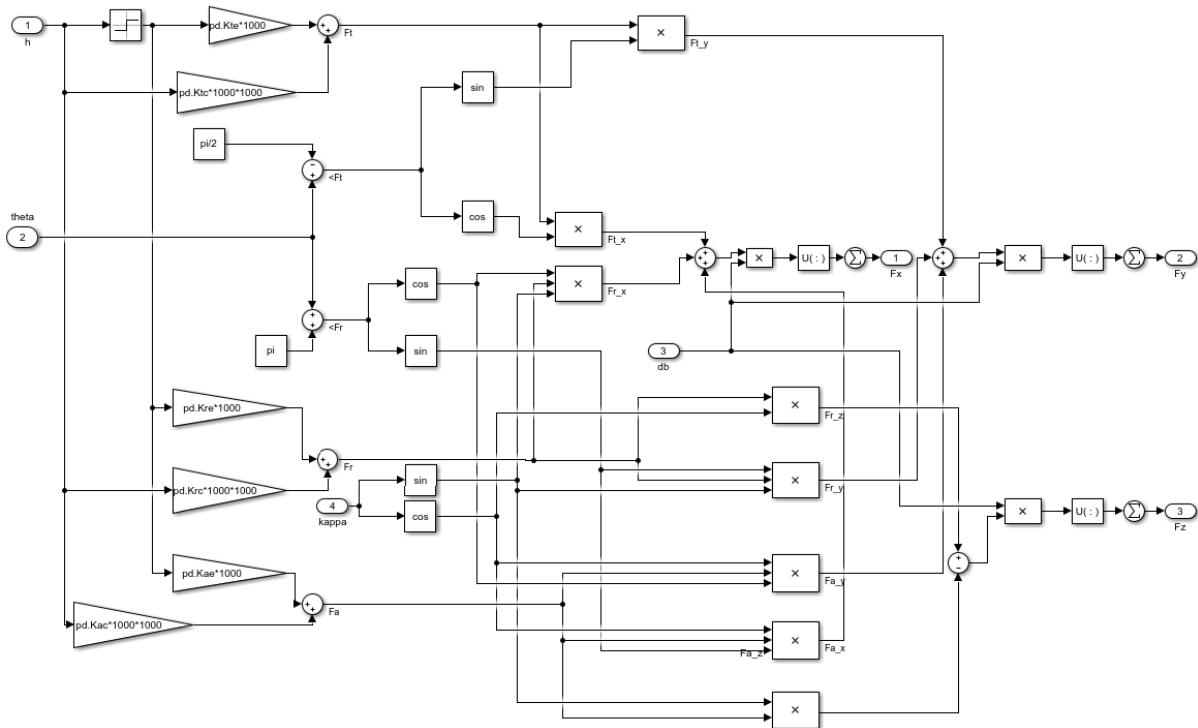


Figure 62. Cutting force diagram built in Simulink

7.5 System dynamics

Finally, in the system dynamics block, for each revolution step, calculated cutting forces are used together with modal parameters to obtain displacements in x and y direction through a

CHAPTER 7. TIME DOMAIN MODEL FOR BALL END TOOL AND SINUSOIDAL VARIABLE
SPINDLE SPEED (SVSS)

transfer function. x and y positions are then used to update the kinematics block for the following time step calculation.

In this model, we will analyse a two degree of freedom system, which is commonly employed for a typical milling scenario flexible in x and y axis, feed and cross-feed directions. The dynamic model is defined by the following equations of motion:

$$m_y \frac{d^2 y}{dt^2} + c_y \frac{dy}{dt} + k_y y = F_y \quad (6.43)$$

$$m_x \frac{d^2 x}{dt^2} + c_x \frac{dx}{dt} + k_x x = F_x \quad (6.44)$$

The force is a function of the current and delayed vibration, together with the instantaneous angle of the tool. Therefore, equations (6.43-6.44) are delayed differential equations with nonlinear and time periodic coefficients. In order to solve these equations, generally time is used as the independent variable and solvers like Ruge Kutta's 4th order method can be used.

However, for the specific case of the Simulink formulation presented above, the milling kinematics model uses a fixed number of time steps for each revolution of the tool. This means that a fixed-step solver (e.g. the Runga Kutta method) must be used, and the spindle speed must be fixed.

This problem was solved by Saleh and Sims [129] using tool revolution as the independent variable in rewriting the systems equations of motion. In this work, the same approach has been followed and Simulink running time has been substituted by number of tool revolutions. With this approach, a fixed step solver will always involve a fixed number of time steps per tool revolution, even if the spindle speed is changed.

Equation (6.44) presents the relationship between the physical time and instantaneous spindle speed, which is necessary to have a revolution dependent system instead of a time dependent system:

$$\frac{d\tau_t}{dt} = n \text{ (rev/sec)} \quad (6.45)$$

Where:

$$\tau_t = \text{number of tool revolutions}$$

CHAPTER 7. TIME DOMAIN MODEL FOR BALL END TOOL AND SINUSOIDAL VARIABLE SPINDLE SPEED (SVSS)

The instantaneous spindle speed, n , which for this application is a sinusoidal type signal, is shown in Figure 63. The signal has a ω_0 average spindle speed with an amplitude of ω_A , given by the ratio of the speed variation amplitude (RVA) and a period T , given by the speed variation frequency (RVF) (eq. 6.46-6.47).

$$RVA = \frac{\omega_0 + \omega_A}{\omega_0} \quad (6.46)$$

$$RVF = \frac{2\pi/T}{\omega_0} = \frac{2\pi \cdot f}{\omega_0} \quad (6.47)$$

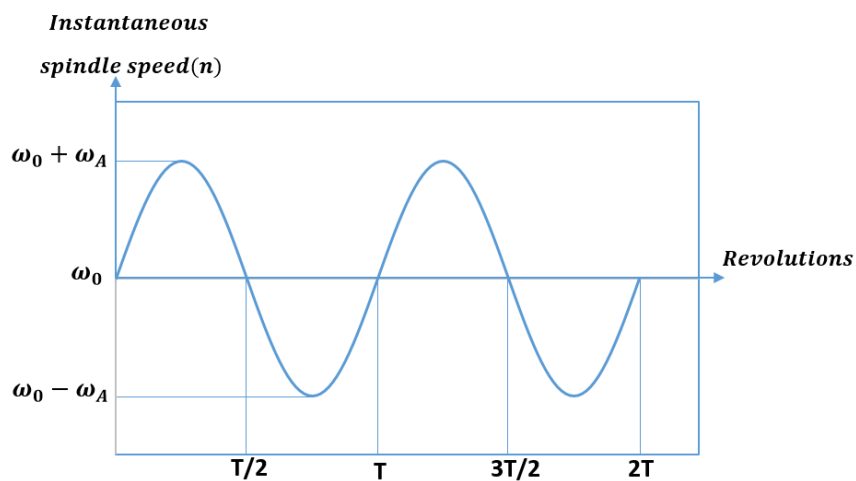


Figure 63. Sinusoidal Variable Spindle Speed (SVSS)

The instantaneous spindle speed has been constructed in Simulink as it is shown in Figure 64.

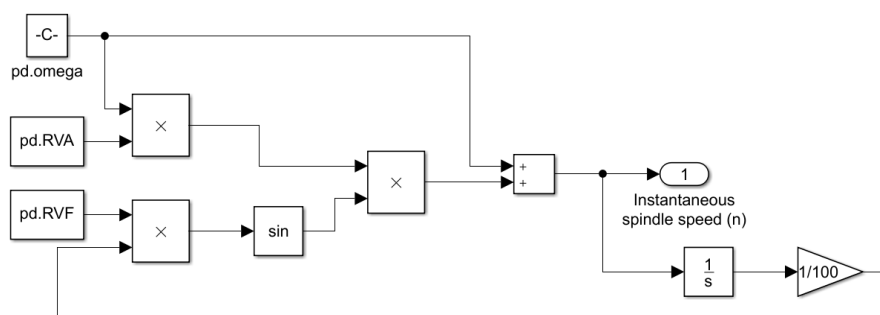


Figure 64. Simulink diagram to generate the instantaneous spindle speed (n) in SVSS.

After defining the relationship between the physical time and instantaneous spindle speed, and once the instantaneous variable spindle speed is obtained, the equation of motion can be rewritten. This is done following the steps below.

CHAPTER 7. TIME DOMAIN MODEL FOR BALL END TOOL AND SINUSOIDAL VARIABLE SPINDLE SPEED (SVSS)

First, velocity is rewritten using the chain rule:

$$\frac{dy}{dt} = \frac{dy}{d\tau_t} \frac{d\tau_t}{dt} = \frac{dy}{d\tau_t} n \quad (6.48)$$

Now, the system acceleration:

$$\frac{d^2y}{dt^2} = \frac{d^2y}{d\tau_t^2} n^2 + \frac{dy}{d\tau_t} \frac{dn}{dt} \quad (6.49)$$

$$\frac{d^2y}{dt^2} = \frac{d^2y}{d\tau_t^2} n^2 + \frac{dy}{d\tau_t} \frac{dn}{d\tau_t} n \quad (6.50)$$

The equation of motion can be written in terms of the derivative expressions above:

$$F_y - k_y y(\tau_t) - c_y \frac{dy}{d\tau_t} n = m_y \left(\frac{d^2y}{d\tau_t^2} n^2 + \frac{dy}{d\tau_t} \frac{dn}{d\tau_t} n \right) \quad (6.51)$$

Rearranging the above expression:

$$\frac{d^2y}{d\tau_t^2} = \frac{F_y}{m_y n^2} - \frac{k_y y(\tau_t)}{m_y n^2} - \frac{c_y}{m_y n} \frac{dy}{d\tau_t} - \frac{1}{n} \frac{dy}{d\tau_t} \frac{dn}{d\tau_t} \quad (6.52)$$

Finally, the equation (6.52) is constructed in Simulink (Figure 65). The given example has the output of displacement in the y direction. The same will apply for the displacement in the x direction.

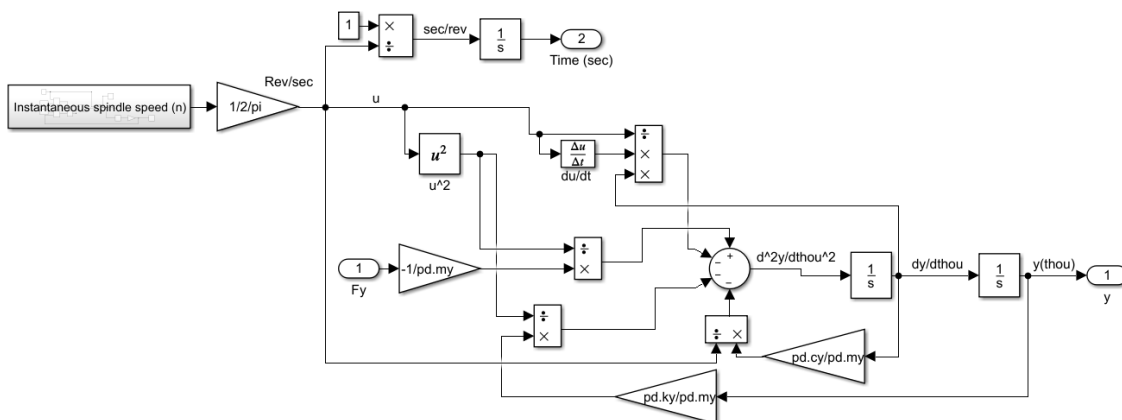


Figure 65. System dynamics block for the equation of motion in y direction.

7.6 Summary

This chapter presents a time domain model to simulate the milling process, in particular the combination of ball-end geometry tool with sinusoidal variable spindle speed (SVSS). It is based on the original concept developed by Campomanes and Altintas [60] for the numerical and discretized surface location and uncut chip thickness calculation. The time domain model is presented in a Matlab/Simulink environment, with the main calculations carried out in a custom block in C language. This model has been created from the reference model built by Sims [130] and further developed by Saleh and Sims [120] with the purpose to include the particularities of the ball-end geometry and sinusoidal variable spindle speed (SVSS).

The model is outlined briefly and the Simulink diagram is shown, with an overview of the steps followed by the simulation program. Three blocks are defined in Simulink; Milling kinematics, milling forces and system dynamics. Milling kinematics block is run by a subprogram in C code language and the main calculations are carried out with x and y position and tool revolution as inputs; The program locates the surface of the tool and workpiece, and finds the uncut chip thickness through the intercept of the tool radius with the previous layer for each revolution step of the simulation. Milling forces are calculated in a Simulink custom block and forces are then fed into the system dynamics block, in which the equation of motion is solved for x and y displacements. Here, instead of using a conventional time independent variable solver (e.g. Runge Kutta 4th order), an approach based on instantaneous tool revolutions as independent variable is used and equation of motion has been re-written to solve, as originally proposed by Saleh and Sims [129]. The output displacements of the system are finally fed into the milling kinematics block to create a closed loop which is run for every step revolution of the simulation.

This model can be used to predict stability at different conditions through the milling of the IBR blades. It is necessary to consider that the dynamic behaviour of the blades constantly change from semi-finishing stock to finished geometry. However, modal parameters of the component at those initial and final conditions are known (Chapter3). In addition, the optimized stock FEA model described in Chapter 4 can easily provide modal parameters for intermediate positions at the new geometry. Once the modal parameters are mapped, the

CHAPTER 7. TIME DOMAIN MODEL FOR BALL END TOOL AND SINUSOIDAL VARIABLE SPINDLE SPEED (SVSS)

time domain model will be capable to find stable, sinusoidal variable cutting parameters across the blade.

Future work on the development process is to validate this model with experimental trials. This will be possible thanks to the new CNC approach to input variable signal into the milling machine that has been developed in Chapter 6. This CNC approach has some limitations, which narrows to a specific working window. Therefore, the model developed in this chapter can be used targeting the mentioned working window to predict which are the most beneficial cutting parameters to mitigate chatter effect.

CHAPTER 8. CONCLUSIONS AND FUTURE WORK

8.1 Summary of thesis

An industrial case study with an Engineering research need is presented and solutions for the presented problem have been developed. An aircraft engine critical part, called Blisk or IBR, which is located in the low pressure compressor stages, is described as the target component to improve its machining process. A preliminary analysis shows that blade finish milling is the most time spending and inefficient machining operation, particularly blade finish milling.

Initial approach is to evaluate a working window based in industrial machining experience and carry out a literature review with the objective of analysing the effects on surface integrity. Results show a lightly damaged subsurface region, independent to the parameters tested and comparable to the rig test approved baseline for the component. However, surface roughness is more affected, specially when higher feed per tooth is employed. A process damping effect is observed, suggesting chatter issues, especially for the blade shape. This concludes that surface integrity is not a limiting factor within the tested working window while chatter mitigation becomes the main challenge of IBR finish milling improvement.

In order to tackle chatter mitigation, a dynamic analysis on the machining system is carried out. Both tool and blade are dynamically analysed and vibration frequencies are experimentally measured for finished and semifinished conditions. A shift in frequency is identified from semi-finishing to finishing stock condition. Moreover, this shift might end up interfering with the dominant frequency of the tool, which needs to be avoided if possible. A method to keep both tool and workpiece natural frequencies apart is proposed by modifying the stock of the finished blade. This approach reveals a potential research line focused on optimizing blade finish milling stock due to its impact on the dominant vibration modes and the stiffness of the blade.

Research work is then directed to blade finish milling stock optimisation. The objective is to design the blade envelope so that the frequency of the main vibration mode is raised, and chatter limits are pushed away to increase productivity of the operation. To do this, an FEA model is developed and stock limits are established, based in industrial experience. Blade

geometry is parametrized in different sections, and a set of analysis is run with highest frequency as target while also monitoring total mass. The analysis tool proposes the right combination of stocks for each parameter locally to optimise global frequency result. These results are then translated to the CAD software and smoothing of the blade geometry is performed in order to achieve a fine transition across the regions of the blade. Resulting optimized blade has a 99.5% higher dominant frequency compared to the baseline blade, achieving the objective of creating a dynamically more stable blade for the last finishing operation and avoiding a natural frequency interference with the tool.

The thesis continues with a broad literature research on chatter mitigation techniques, with the aim of finding a gap in current knowledge and providing a novel contribution while focusing on the initially presented case study. Variable Sinusoidal Spindle Speed is considered a good method for this particular case, providing that other techniques such as high speed machining targeting stability regions or process damping are difficult to apply due to material, geometry and the complexity of the dynamic system respectively. A gap is found both in variable spindle speed modelling for ball-end mill geometry as well as for the industrial application of variable speed.

After the knowledge gaps have been identified, a time domain model initially developed by N.D. Sims has been used as a starting point to further develop by adding ball-end geometry and sinusoidal variable speed features.

Finally, industrial implementation of variable speed on a commercial milling machine is studied to overcome the limitations of using manipulated machines to produce variable speed. A method is proposed which is valid for standard milling machines. However, some limitations have been identified, and a machine characterization is realized to find a valid working window for this method.

Wrapping up, an initial case study is presented and different alternatives have been proposed to respond to the industrial need. A combination of techniques such as the optimization of blade stock for finish milling as well as a new finish milling strategy with variable spindle speed offer a combined and improved strategy to increase machining productivity of this particular component.

8.2 Conclusions

The objective of this thesis was to find key manufacturing improvement areas and develop new solutions for a particular industrial component. As part of an EngD thesis, these solutions need to provide some novelty to the research field. The main conclusions are summarized below:

- A detailed manufacturing process study has been realised for an IBR component and the key operation has been identified for further research. Selected operation, finish milling of IBR blades, is considered the key operation due to the amount of time currently spent machining this feature, 49% of total machining time, and also because finished geometries need to comply with surface integrity criteria as well as the added challenge presented by the particular blade geometry and complex dynamics of the tool/component pair.
- Sub-surface damage is not a limiting factor within the typical working window employed for Ti6-4 alloys in complex geometry machining. However, surface roughness is clearly affected by the selected parameters, especially when high feed per tooth is used, which suggests a process damping effect and therefore the process is affected by chatter.
- Dynamic analysis of the system measures vibration frequencies for both semi-finished stock and finished conditions. A shift in frequency is observed between both stages. At some point during the finish machining an interference between the natural frequencies of the tool and the blade is expected, which is tried to avoid. A good approach to increase stability, separate natural frequencies of tool and workpiece and therefore improve productivity is by optimizing the finish milling stock geometry.
- The method developed to optimize stock geometry by maximizing the dominant vibration mode's frequency provides a result of 99.5% higher vibration frequency in respect to the baseline value. This means a considerably stiffer and dynamically stable blade can be generated in roughing stage for the benefit of the last finishing operation. This comes at a cost of increased material in the lower part of the blade, and tool life repercussions should be considered before implementing this optimized geometry.

However, maximum stock values selected for the analysis come from current knowledge and experience, so tool life is not expected to be a limiting factor.

- After a thorough literature review, Variable Spindle Speed is considered a suitable method to mitigate chatter in IBR blades. This is concluded after reviewing different methods such as high speed machining or process damping. The former targets stability regions but it is not ideal for titanium alloys due to their low machinability and commercial machine capabilities to produce complex geometries at high speeds. The latter, from the other side, benefits from low speeds and high depths of cut. Machining with high depths of cut causes the problem to meet surface roughness and tolerance criteria.
- The time domain model, partly developed in this thesis for ball-end mill geometry and variable spindle speed, produces a sinusoidal signal at the desired frequency and amplitudes. This is useful to characterize a milling machine for its capability to produce accurate spindle speed variation.
- Novelty in the described variable spindle speed method is the capability to produce the desired signal in a commercial milling machine without complex manipulations often carried out in research and/or laboratory environments. However, each machine has its own limits in terms of variable speed working window and this needs to be identified in order to input a signal according to the capability of the machine.

8.3 Contributions

This thesis is created from an EngD project, which in this case it is an industrial case study towards the optimization of the manufacturing process of an IBR or Blisk. Different solutions have been provided which can increase productivity of this component. Besides, these solutions complement each other, so that a new strategy including both optimized stock and variable speed can be applied.

This research work also has some novelty and it does contributions to the current state of the art in machining IBRs. The main contributions are listed below:

- **FEA based optimisation of semi-finished stock geometry.**

The concept of modifying the stock geometry in order to increase the stability of the component is not new. However, this new method has been developed to propose systematically the optimum geometry through the parametrization of the blade envelope. Not only this method proposes optimum parameters for each parametrized point, but also combines FEA tool with CAD smoothing in order to provide a semi-finished stock which is easily manufacturable.

- **Variable speed machining modelling.**

Literature review carried out in this work does refer to many different dynamic models to simulate a milling process under different conditions. These include chatter effect. Ball-end mill geometry has been modelled, and variable spindle speed has been considered through different approaches. However, currently there is not a time domain model particularly developed for ball-end mill geometry which considers variable spindle speed. A novel contribution is made adding ball-end geometry and variable speed to a time domain model originally developed by N.D. Sims.

- **CNC programming for variable speed.**

Literature review on industrial implementation of variable speed is vague. Some work is carried out in modified milling machines or in laboratory conditions, while others just do not refer the machine implementation. This work presents a new method to implement variable speed in a commercial milling machine. It has some limitations which depend on the machine spindle capabilities, and therefore a valid working window needs to be identified prior to producing variable speed signal in the machine. However, the simplicity and easiness to apply this method into a standard machine is considered a novel contribution.

8.4 Future work

This thesis has researched and developed new solutions to improve finish machining process of IBR blades. These solutions have been proven either theoretically or in a local scale and full-scale implementation in an IBR component would be the final step in this implementation and approval process prior to industrialization.

The developed model still needs to be validated with experimental work, using the variable speed implementation method characterised for its use in commercial machines.

Some improvement figures have been presented, but machining time reduction, which is the final objective, remains unquantified. All the evidence supported in this work suggests that a considerable improvement in finish milling process can be achieved but this is yet to be confirmed with further testing in real component.

The above paragraph proposes a future work line to implement the solutions in the industrial context. However, there are broader investigation and development lines which are presented below.

- A working window is initially considered for the surface integrity analysis. The limits of this working window have been selected based on general literature review and engineering experience. Later in the research work, machine characterization for variable spindle speed sets new limitations due to the machine capability to produce a variable signal at certain spindle speed, variation amplitude and frequency conditions. Feed rate is not a limiting factor for variable speed and therefore, surface integrity analysis on higher feed rates is suggested to perform. Therefore, initially tested working window is proposed to re-evaluate for variable speed, considering higher limits for feed rate.
- The dynamic analysis of the system shows a frequency shift from semi-finished to finished condition. However, the stock optimisation process only considers the initial stock, neglecting the frequency shift through the machining operation from tip to root. A new and more detailed iteration is proposed to realize, in which stock is optimized not only for the initial stock condition, but also for intermediate conditions as material is being removed.
- An experimental machine characterization is carried out, measuring output signal and comparing to the nominal. This is valid for a given machine but every machine will have its own limits to produce variable speed. Spindle speed has been identified as the source of the so called "feed failure". A very interesting future research line is to analyse machine spindle dynamics to identify the cause of feed failure in order to extrapolate this limitation to other standard machines.

- Further experimental work is suggested on the validation of the variable speed strategy proposed in this thesis. From one side a time domain model is presented, from the other side machine implementation has been developed. However, the relationship between simulation and machine implementation, as well as the analysis of the effects of variable speed remains a future work.

REFERENCES

- [1] Boeing, "No Title." [Online]. Available: <http://boeing.mediaroom.com/index.php?s=20291&view=category&mode=gallery&cat=27&o=60>.
- [2] Airbus, "No Title." [Online]. Available: <http://www.airbus.com/galleries/photo-gallery/filter/a350-xwb-family/cache/0/?p=14>.
- [3] E. O. Ezugwu and Z. M. Wang, "Titanium alloys and their machinability - a review," *J. Mater. Process. Technol.*, vol. 68, pp. 262–274, 1995.
- [4] B. Rao, C. R. Dandekar, and Y. C. Shin, "An experimental and numerical study on the face milling of Ti–6Al–4V alloy: Tool performance and surface integrity," *J. Mater. Process. Technol.*, vol. 211, no. 2, pp. 294–304, 2011, doi: 10.1016/j.jmatprotec.2010.10.002.
- [5] J. Sun and Y. B. Guo, "A comprehensive experimental study on surface integrity by end milling Ti–6Al–4V," *J. Mater. Process. Technol.*, vol. 209, no. 8, pp. 4036–4042, 2009, doi: 10.1016/j.jmatprotec.2008.09.022.
- [6] C. H. Che-Haron and A. Jawaid, "The effect of machining on surface integrity of titanium alloy Ti–6% Al–4% V," *J. Mater. Process. Technol.*, vol. 166, no. 2, pp. 188–192, 2005, doi: 10.1016/j.jmatprotec.2004.08.012.
- [7] Airbus, "No Title." [Online]. Available: <http://www.a320neo.com/pratt-whitney-pw1000g.php>.
- [8] M. V Ribeiro, M. R. V Moreira, and J. R. Ferreira, "Optimization of titanium alloy (6Al–4V) machining," *J. Mater. Process. Technol.*, vol. 143–144, pp. 458–463, 2003, doi: 10.1016/S0924-0136(03)00457-6.
- [9] M. Bubmann and E. Bayer, "Blisk Production of the Future," MTU Aero Engines, 2009.
- [10] M. B. Mhamdi, M. Boujelbene, E. Bayraktar, and A. Zghal, "Surface Integrity of Titanium Alloy Ti-6Al-4V in Ball end Milling," *Phys. Procedia*, vol. 25, pp. 355–362, 2012, doi:

REFERENCES

- 10.1016/j.phpro.2012.03.096.
- [11] E. O. Ezugwu, J. Bonney, R. B. Da Silva, and O. Çakir, "Surface integrity of finished turned Ti-6Al-4V alloy with PCD tools using conventional and high pressure coolant supplies," *Int. J. Mach. Tools Manuf.*, vol. 47, no. 6, pp. 884-891, 2007, doi: 10.1016/j.ijmachtools.2006.08.005.
- [12] A. K. M. N. Amin, A. F. Ismail, and M. K. Nor Khairusshima, "Effectiveness of uncoated WC-Co and PCD inserts in end milling of titanium alloy—Ti-6Al-4V," *J. Mater. Process. Technol.*, vol. 192-193, pp. 147-158, 2007, doi: 10.1016/j.jmatprotec.2007.04.095.
- [13] J. D. P. Velásquez, A. Tidu, B. Bolle, P. Chevrier, and J. J. Fundenberger, "Sub-surface and surface analysis of high speed machined Ti-6Al-4V alloy," *Mater. Sci. Eng. A*, vol. 527, no. 10-11, pp. 2572-2578, 2010, doi: 10.1016/j.msea.2009.12.018.
- [14] L. N. López de lacalle, J. Pérez, J. I. Llorente, and J. A. Sánchez, "Advanced cutting conditions for the milling of aeronautical alloys," *J. Mater. Process. Technol.*, vol. 100, pp. 1-11, 1998.
- [15] E. Kuljanic, M. Fioretti, L. Beltrame, and F. Miani, "Milling Titanium Compressor Blades with PCD Cutter," *CIRP Ann. - Manuf. Technol.*, vol. 47, no. 1, pp. 61-64, 1998, doi: 10.1016/s0007-8506(07)62785-1.
- [16] I. Arrospide, "EngD mini-project 2," Sheffield, 2015.
- [17] I. Arrospide, "EngD mini-project 1," Sheffield, 2014.
- [18] T. Delio and J. Tlusty, "Manufacturing Laboratories Incorporated (MLI)." [Online]. Available: <https://mfg-labs.weebly.com/>.
- [19] J. Tlusty and F. Ismail, "Special Aspects of Chatter in Milling," *J. Vib. Acoust.*, vol. 105, no. 81, pp. 24-32, 1983.
- [20] Y. Altintas, M. Eynian, and H. Onozuka, "Identification of dynamic cutting force coefficients and chatter stability with process damping," *CIRP Ann. - Manuf. Technol.*, vol. 57, pp. 371-374, 2008, doi: 10.1016/j.cirp.2008.03.048.
- [21] L. T. Tunç and E. Budak, "Effect of cutting conditions and tool geometry on process

REFERENCES

- damping in machining," *Int. J. Mach. Tools Manuf.*, vol. 57, pp. 10–19, 2012, doi: 10.1016/j.ijmachtools.2012.01.009.
- [22] C. M. Taylor, N. D. Sims, and S. Turner, "Process Damping and Cutting Tool Geometry in Machining," *IOP Conf. Ser. Mater. Sci. Eng.*, vol. 26, p. 012009, 2011, doi: 10.1088/1757-899X/26/1/012009.
- [23] N. D. Sims and S. Turner, "The influence of feed rate on process damping in milling: Modelling and experiments," 2011, doi: 10.1243/09544054JEM2141.
- [24] V. Sellmeier and B. Denkena, "High speed process damping in milling," *CIRP J. Manuf. Sci. Technol.*, vol. 5, no. 1, pp. 8–19, 2012, doi: 10.1016/j.cirpj.2011.12.001.
- [25] J. Tlustý and F. Ismail, "Basic Non-Linearity in Machining Chatter," *CIRP Ann. - Manuf. Technol.*, vol. 30, no. 1, pp. 299–304, Jan. 1981, doi: 10.1016/S0007-8506(07)60946-9.
- [26] D. Wu and C. Liu, "An analytical model of cutting dynamics. Part 1: Model building," *J. Manuf. ...*, vol. 107, no. May 1985, pp. 107–111, 1985.
- [27] D. Wu and C. Liu, "An analytical model of cutting dynamics. Part 1: Model building," *J. Manuf. ...*, vol. 107, no. May 1985, pp. 112–118, 1985.
- [28] S. C. Lin, R. E. DeVor, S. G. Kapoor, and J. W. Sutherland, "A New Approach to Estimating the Cutting Process Damping Under Working Conditions," *Transactions of NAMRI/SME*, pp. 154–160, 1990.
- [29] I. Minis, R. Yanushevsky, A. Tembo, and R. Hocken, "Analysis of Linear and Nonlinear Chatter in Milling," *CIRP Ann. - Manuf. Technol.*, vol. 39, no. 1, pp. 459–462, 1990, doi: 10.1016/S0007-8506(07)61096-8.
- [30] M. Tool, "A General Formulation of the Milling Process Equation," pp. 317–324, 2015.
- [31] E. Budak and L. T. Tunc, "Identification and modeling of process damping in turning and milling using a new approach," *CIRP Ann. - Manuf. Technol.*, vol. 59, no. 1, pp. 403–408, 2010, doi: 10.1016/j.cirp.2010.03.078.
- [32] F. W. Taylor, "The Art of Cutting Metals," *Sci. Am.*, vol. 63, no. 1619supp, pp. 25942–25944, 1907, doi: 10.1038/scientificamerican01121907-25942supp.

REFERENCES

- [33] S. A. Tobias and W. Fishwick, "Theory of regenerative machine tool chatter," *Eng.*, vol. 205, no. 7, pp. 199–203, 1958.
- [34] S. Doi and S. Kato, "Chatter vibration of lathe tools," 1955.
- [35] J. D. Smith and S. A. Tobias, "The dynamic cutting of metals," *Int. J. Mach. Tool Des. Res.*, vol. 1, no. 4, pp. 283–292, 1961, doi: 10.1016/0020-7357(61)90008-7.
- [36] J. Tlustý and M. Poláček, "The stability of the machine tool against self-excited vibration in machining," *ASME Prod. Eng. Res. Conf.*, pp. 454–465, 1963.
- [37] S. A. Tobias, "Machine tool vibration research," *Int. J. Mach. Tool Des. Res.*, vol. 1, no. 1–2, 1961, doi: 10.1016/0020-7357(61)90040-3.
- [38] J. P. Gurney and S. A. Tobias, "A graphical analysis of regenerative machine tool instability," *J. Manuf. Sci. Eng. Trans. ASME*, vol. 84, no. 1, pp. 103–111, 1962, doi: 10.1115/1.3667380.
- [39] N. H. Hanna and S. A. Tobias, "A Theory of Nonlinear Regenerative Chatter," *J. Manuf. Sci. Eng.*, vol. 96, no. 1, pp. 247–255, 1974, doi: 10.1115/1.3438305.
- [40] S. Smith and J. Tlustý, "Overview of modeling and simulation of the milling process," *J. Eng. Ind.*, vol. 113, no. 2, pp. 169–175, May 1991, doi: 10.1115/1.2899674.
- [41] J. Tlustý, W. Zaton, and F. Ismail, "Stability Lobes in Milling," *CIRP Ann. - Manuf. Technol.*, vol. 32, no. 1, pp. 309–313, Jan. 1983, doi: 10.1016/S0007-8506(07)63411-8.
- [42] I. Minis and R. Yanushevsky, "A new theoretical approach for the prediction of machine tool chatter in Milling," *J. Manuf. Sci. Eng. Trans. ASME*, vol. 115, no. 1, pp. 1–8, 1993, doi: 10.1115/1.2901633.
- [43] Y. Altıntaş and E. Budak, "Analytical Prediction of Stability Lobes in Milling," *CIRP Ann. - Manuf. Technol.*, vol. 44, no. 2, pp. 357–362, 1995, doi: 10.1016/S0007-8506(07)62342-7.
- [44] T. L. Schmitz and K. S. Smith, *Machining Dynamics*. Springer International Publishing, 2019.
- [45] E. Budak and Y. Altıntaş, "Analytical Prediction of Chatter Stability in Milling—Part I:

REFERENCES

- General Formulation," *J. Dyn. Syst. Meas. Control*, vol. 120, no. 1, pp. 22–30, Mar. 1998, doi: 10.1115/1.2801317.
- [46] E. Budak and Y. Altintas, "Analytical Prediction of Chatter Stability in Milling-Part II: Application of the General Formulation to Common Milling Systems," *J. Dyn. Syst. Meas. Control. Transactions ASME* 120 31–36., 1998.
- [47] M. Wiercigroch and E. Budak, "Sources of nonlinearities, chatter generation and suppression in metal cutting," *Philos. Trans. R. Soc. London. Ser. A Math. Phys. Eng. Sci.*, vol. 359, no. 1781, pp. 663–693, Apr. 2001, doi: 10.1098/rsta.2000.0750.
- [48] Y. Altintas and M. Weck, "Chatter stability of metal cutting and grinding," *CIRP Ann. - Manuf. Technol.*, vol. 53, no. 2, pp. 619–642, 2004, doi: 10.1016/S0007-8506(07)60032-8.
- [49] T. Insperger and G. Stépán, "Semi-discretization method for delayed systems," *Int. J. Numer. Methods Eng.*, vol. 55, no. 5, pp. 503–518, Oct. 2002, doi: 10.1002/nme.505.
- [50] E. A. Butcher, H. Ma, E. Bueler, V. Averina, and Z. Szabo, "Stability of linear time-periodic delay-differential equations via Chebyshev polynomials," *Int. J. Numer. Methods Eng.*, vol. 59, no. 7, pp. 895–922, Feb. 2004, doi: 10.1002/nme.894.
- [51] J.-V. Le Lan, A. Marty, and J.-F. Debongnie, "Providing stability maps for milling operations," *Int. J. Mach. Tools Manuf.*, vol. 47, no. 9, pp. 1493–1496, Jul. 2007, doi: 10.1016/j.ijmachtools.2006.09.026.
- [52] Y. Ding, L. Zhu, X. Zhang, and H. Ding, "Second-order full-discretization method for milling stability prediction," *Int. J. Mach. Tools Manuf.*, vol. 50, no. 10, pp. 926–932, Oct. 2010, doi: 10.1016/j.ijmachtools.2010.05.005.
- [53] Y. Ding, L. M. Zhu, X. J. Zhang, and H. Ding, "A full-discretization method for prediction of milling stability," *Int. J. Mach. Tools Manuf.*, vol. 50, no. 5, pp. 502–509, May 2010, doi: 10.1016/j.ijmachtools.2010.01.003.
- [54] B. P. Mann and B. R. Patel, "Stability of Delay Equations Written as State Space Models," *J. Vib. Control*, vol. 16, no. 7–8, pp. 1067–1085, Jun. 2010, doi: 10.1177/1077546309341111.

REFERENCES

- [55] J. Friedrich, C. Hinze, A. Renner, A. Verl, and A. Lechler, "Estimation of stability lobe diagrams in milling with continuous learning algorithms," *Robot. Comput. Integr. Manuf.*, 2017, doi: 10.1016/j.rcim.2015.10.003.
- [56] J. Tlusty, "Dynamics of high-speed milling," *J. Manuf. Sci. Eng. Trans. ASME*, vol. 108, no. 2, pp. 59–67, 1986, doi: 10.1115/1.3187052.
- [57] S. Smith and J. Tlusty, "Efficient Simulation Programs for Chatter in Milling," *CIRP Ann. - Manuf. Technol.*, vol. 42, no. 1, pp. 463–466, Jan. 1993, doi: 10.1016/S0007-8506(07)62486-X.
- [58] D. Montgomery and Y. Altintas, "Mechanism of cutting force and surface generation in dynamic milling," *J. Manuf. Sci. Eng. Trans. ASME*, vol. 113, no. 2, pp. 160–168, May 1991, doi: 10.1115/1.2899673.
- [59] Y. Altinta and P. Lee, "Mechanics and dynamics of ball end milling," *J. Manuf. Sci. Eng. Trans. ASME*, vol. 120, no. 4, pp. 684–692, Nov. 1998, doi: 10.1115/1.2830207.
- [60] M. L. Campomanes and Y. Altintas, "An improved time domain simulation for dynamic milling at small radial immersions," *J. Manuf. Sci. Eng. Trans. ASME*, vol. 125, no. 3, pp. 416–422, Aug. 2003, doi: 10.1115/1.1580852.
- [61] S. Smith and J. Tlusty, "Update on high-speed milling dynamics," *J. Manuf. Sci. Eng. Trans. ASME*, vol. 112, no. 2, pp. 142–149, May 1990, doi: 10.1115/1.2899557.
- [62] H. Z. Li, X. P. Li, and X. Q. Chen, "A novel chatter stability criterion for the modelling and simulation of the dynamic milling process in the time domain," *Int. J. Adv. Manuf. Technol.*, vol. 22, no. 9–10, pp. 619–625, Jul. 2003, doi: 10.1007/s00170-003-1562-9.
- [63] P. V. Bayly, B. P. Mann, T. L. Schmitz, D. A. Peters, G. Stepan, and T. Insperger, "Effects of radial immersion and cutting direction on chatter instability in end-milling," in *ASME International Mechanical Engineering Congress and Exposition, Proceedings*, 2002, pp. 351–363, doi: 10.1115/IMECE2002-39116.
- [64] N. D. Sims, "The Self-Excitation Damping Ratio: A Chatter Criterion for Time-Domain Milling Simulations," *J. Manuf. Sci. Eng.*, vol. 127, no. 3, p. 433, 2005, doi: 10.1115/1.1948393.

REFERENCES

- [65] W. L. Weingaertner, R. B. Schroeter, M. L. Polli, and J. de Oliveira Gomes, "Evaluation of high-speed end-milling dynamic stability through audio signal measurements," *J. Mater. Process. Technol.*, vol. 179, no. 1–3, pp. 133–138, Oct. 2006, doi: 10.1016/j.jmatprotec.2006.03.075.
- [66] S. Wu, R. Li, X. Liu, L. Yang, and M. Zhu, "Experimental Study of Thin Wall Milling Chatter Stability Nonlinear Criterion," in *Procedia CIRP*, 2016, doi: 10.1016/j.procir.2016.10.075.
- [67] T. C. Ramaraj and E. Eleftheriou, "Analysis of the Mechanics of Machining with Tapered End Milling Cutters," *J. Eng. Ind.*, vol. 116, no. 3, p. 398, 1994, doi: 10.1115/1.2901958.
- [68] Y. Altıntaş and P. Lee, "A General Mechanics and Dynamics Model for Helical End Mills," *CIRP Ann. - Manuf. Technol.*, vol. 45, no. 1, pp. 59–64, 1996, doi: 10.1016/S0007-8506(07)63017-0.
- [69] S. Engin and Y. Altintas, "Generalized modeling of milling mechanics and dynamics: part i - helical end mills," *Am. Soc. Mech. Eng. Manuf. Eng. Div. MED*, vol. 10, no. 1997, pp. 345–352, 1998.
- [70] X. W. Liu, K. Cheng, A. P. Longstaff, M. H. Widiyanto, and D. Ford, "Improved dynamic cutting force model in ball-end milling. Part I: Theoretical modelling and experimental calibration," *Int. J. Adv. Manuf. Technol.*, vol. 26, no. 5–6, pp. 457–465, 2005, doi: 10.1007/s00170-003-2014-2.
- [71] K. Wa and E. Shamoto, "Study on Regenerative Chatter Vibration in Ball End Milling of Flexible Workpieces," pp. 1–6, 2008.
- [72] X. G. Liang and Z. Q. Yao, "An accuracy algorithm for chip thickness modeling in 5-axis ball-end finish milling," *CAD Comput. Aided Des.*, vol. 43, no. 8, pp. 971–978, 2011, doi: 10.1016/j.cad.2011.04.012.
- [73] E. Öztürk, "MECHANICS AND DYNAMICS OF MULTI-AXIS MACHINING OPERATIONS," 2010.
- [74] E. Ozturk and E. Budak, "Dynamics and Stability of Five-Axis Ball-End Milling," *J. Manuf. Sci. Eng.*, vol. 132, no. 2, p. 021003, 2010, doi: 10.1115/1.4001038.

REFERENCES

- [75] W. Ji, X. Liu, L. Wang, Y. Meng, and X. Wu, "A study on geometry modelling of a ball-end mill with chamfered cutting edge," *J. Manuf. Process.*, vol. 19, pp. 205–211, 2015, doi: 10.1016/j.jmapro.2014.10.003.
- [76] L. T. Tunc, "Prediction of tool tip dynamics for generalized milling cutters using the 3D model of the tool body," *Int. J. Adv. Manuf. Technol.*, vol. 95, no. 5–8, pp. 1891–1909, 2018, doi: 10.1007/s00170-017-1286-x.
- [77] Y. Dai, H. Li, Z. Wei, and H. Zhang, "Chatter stability prediction for five-axis ball end milling with precise integration method," *J. Manuf. Process.*, vol. 32, pp. 20–31, 2018, doi: 10.1016/j.jmapro.2018.01.008.
- [78] F. J. Campa, L. N. López de Lacalle, a. Lamikiz, and J. a. Sánchez, "Selection of cutting conditions for a stable milling of flexible parts with bull-nose end mills," *J. Mater. Process. Technol.*, vol. 191, no. 1–3, pp. 279–282, 2007, doi: 10.1016/j.jmatprotec.2007.03.023.
- [79] Y. Altintas, "Analytical Prediction of Three Dimensional Chatter Stability in Milling.," *JSME International Journal Series C*, vol. 44. pp. 717–723, 2001, doi: 10.1299/jsmec.44.717.
- [80] E. Budak, L. T. Tunç, S. Alan, and H. N. Özgüven, "Prediction of workpiece dynamics and its effects on chatter stability in milling," *CIRP Ann. - Manuf. Technol.*, vol. 61, no. 1, pp. 339–342, 2012, doi: 10.1016/j.cirp.2012.03.144.
- [81] T. Delio, J. Tlusty, and S. Smith, "Use of audio signals for chatter detection and control," *J. Manuf. Sci. Eng. Trans. ASME*, vol. 114, no. 2, pp. 146–157, May 1992, doi: 10.1115/1.2899767.
- [82] S. Smith and T. Delio, "Sensor-based chatter detection and avoidance by spindle speed selection," *J. Dyn. Syst. Meas. Control. Trans. ASME*, vol. 114, no. 3, pp. 486–492, 1992, doi: 10.1115/1.2897373.
- [83] S. Smith and J. Tlusty, "Stabilizing Chatter by Automatic Spindle Speed Regulation," *CIRP Ann. - Manuf. Technol.*, vol. 41, no. 1, pp. 433–436, 1992, doi: 10.1016/S0007-8506(07)61238-4.

REFERENCES

- [84] Y. S. Tarng and T. C. Li, "The change of spindle speed for the avoidance of chatter in end milling," *J. Mater. Process. Tech.*, vol. 41, no. 2, pp. 227–236, 1994, doi: 10.1016/0924-0136(94)90063-9.
- [85] Y. S. Liao and Y. C. Young, "A new on-line spindle speed regulation strategy for chatter control," *Int. J. Mach. Tools Manuf.*, vol. 36, no. 5, pp. 651–660, May 1996, doi: 10.1016/0890-6955(95)00076-3.
- [86] E. Soliman and F. Ismail, "A control system for chatter avoidance by ramping the spindle speed," *J. Manuf. Sci. Eng. Trans. ASME*, vol. 120, no. 4, pp. 674–683, Nov. 1998, doi: 10.1115/1.2830206.
- [87] F. Ismail and R. Ziaei, "Chatter suppression in five-axis machining of flexible parts," *Int. J. Mach. Tools Manuf.*, vol. 42, no. 1, pp. 115–122, Jan. 2002, doi: 10.1016/S0890-6955(01)00088-8.
- [88] T. L. Schmitz, "Chatter recognition by a statistical evaluation of the synchronously sampled audio signal," *J. Sound Vib.*, vol. 262, pp. 721–730, 2003, doi: 10.1016/S0022-460X(03)00119-6.
- [89] T. L. Schmitz, M. A. Davies, K. Medicus, and J. Snyder, "Improving high-speed machining material removal rates by rapid dynamic analysis," *CIRP Ann. - Manuf. Technol.*, vol. 50, no. 1, pp. 263–268, Jan. 2001, doi: 10.1016/S0007-8506(07)62119-2.
- [90] T. L. Schmitz, "EXPLORING ONCE-PER-REVOLUTION AUDIO SIGNAL VARIANCE AS A CHATTER INDICATOR," *Mach. Sci. Technol.*, vol. 6, no. 2, pp. 215–233, 2002, doi: 10.1081/MST-120005957.
- [91] N. C. Tsai, D. C. Chen, and R. M. Lee, "Chatter prevention for milling process by acoustic signal feedback," *Int. J. Adv. Manuf. Technol.*, vol. 47, no. 9–12, pp. 1013–1021, Apr. 2010, doi: 10.1007/s00170-009-2245-y.
- [92] N.-C. Tsai, D.-C. Chen, and R.-M. Lee, "Chatter prevention and improved finish of workpiece for a milling process," *Proc. Inst. Mech. Eng. Part B J. Eng. Manuf.*, vol. 224, no. 4, pp. 579–588, Apr. 2010, doi: 10.1243/09544054JEM1601.
- [93] N. J. M. van Dijk, E. J. J. Doppenberg, R. P. H. Faassen, N. van de Wouw, J. A. J.

REFERENCES

- Oosterling, and H. Nijmeijer, "Automatic in-process chatter avoidance in the high-speed milling process," *J. Dyn. Syst. Meas. Control. Trans. ASME*, vol. 132, no. 3, pp. 1–14, May 2010, doi: 10.1115/1.4000821.
- [94] K. J. Kalinski and M. A. Galewski, "Chatter vibration surveillance by the optimal-linear spindle speed control," *Mech. Syst. Signal Process.*, vol. 25, no. 1, pp. 383–399, Jan. 2011, doi: 10.1016/j.ymssp.2010.09.005.
- [95] K. J. Kalinski and M. A. Galewski, "Optimal spindle speed determination for vibration reduction during ball-end milling of flexible details," *Int. J. Mach. Tools Manuf.*, vol. 92, no. 1, pp. 19–30, 2015, doi: 10.1016/j.ijmachtools.2015.02.008.
- [96] F. J. Campa, L. N. Lopez De Lacalle, and A. Celaya, "Chatter avoidance in the milling of thin floors with bull-nose end mills: Model and stability diagrams," *Int. J. Mach. Tools Manuf.*, 2011, doi: 10.1016/j.ijmachtools.2010.09.008.
- [97] J. De Canniere, H. Van Brussel, and J. Van Bogaert, "A contribution to the mathematical analysis variable spindle speed machining."
- [98] M. Rahman and Y. Ito, "Detection of the onset of chatter vibration," *J. Sound Vib.*, vol. 109, no. 2, pp. 193–205, Sep. 1986, doi: 10.1016/S0022-460X(86)80002-5.
- [99] S. C. Lin, R. E. DeVor, and S. G. Kapoor, "The effects of variable speed cutting on vibration control in face milling," *J. Manuf. Sci. Eng. Trans. ASME*, vol. 112, no. 1, pp. 1–11, Feb. 1990, doi: 10.1115/1.2899290.
- [100] T. C. Tsao, M. W. McCarthy, and S. G. Kapoor, "A new approach to stability analysis of variable speed machining systems," *Int. J. Mach. Tools Manuf.*, vol. 33, no. 6, pp. 791–808, Dec. 1993, doi: 10.1016/0890-6955(93)90038-V.
- [101] Y. Altintas and P. K. Chan, "In-process detection and suppression of chatter in milling," *Int. J. Mach. Tools Manuf.*, vol. 32, no. 3, pp. 329–347, Jun. 1992, doi: 10.1016/0890-6955(92)90006-3.
- [102] F. Ismail and E. G. Kubica, "Active suppression of chatter in peripheral milling Part 1. A statistical indicator to evaluate the spindle speed modulation method," *Int. J. Adv. Manuf. Technol.*, vol. 10, no. 5, pp. 299–310, Sep. 1995, doi: 10.1007/BF01178983.

REFERENCES

- [103] E. G. Kubica and F. Ismail, "Active suppression of chatter in peripheral milling. Part II. Application of fuzzy control," *Int. J. Adv. Manuf. Technol.*, vol. 12, no. 4, pp. 236–245, Jul. 1996, doi: 10.1007/BF01239610.
- [104] E. Soliman and F. Ismail, "Chatter detection by monitoring spindle drive current," *Int. J. Adv. Manuf. Technol.*, vol. 13, no. 1, pp. 27–34, 1997, doi: 10.1007/BF01179227.
- [105] M. Pakdemirli and A. G. Ulsoy, "Perturbation Analysis of Spindle Speed Variation in Machine Tool Chatter," *J. Vib. Control*, vol. 3, no. 3, pp. 261–278, Jul. 1997, doi: 10.1177/107754639700300302.
- [106] R. Radulescu, S. G. Kapoor, and R. E. DeVor, "An investigation of variable spindle speed face milling for tool-work structures with complex dynamics, part 1: Simulation results," *J. Manuf. Sci. Eng. Trans. ASME*, vol. 119, no. 3, pp. 266–272, 1997, doi: 10.1115/1.2831103.
- [107] S. Jayaram, S. G. Kapoor, and R. E. DeVor, "Analytical stability analysis of variable spindle speed machining," *J. Manuf. Sci. Eng. Trans. ASME*, vol. 122, no. 3, pp. 391–397, Aug. 2000, doi: 10.1115/1.1285890.
- [108] S. Sastry, S. G. Kapoor, R. E. DeVor, and G. E. Dullerud, "Chatter stability analysis of the variable speed face-milling process," *J. Manuf. Sci. Eng. Trans. ASME*, vol. 123, no. 4, pp. 753–756, Nov. 2001, doi: 10.1115/1.1373649.
- [109] N. Sri Namachchivaya and R. Beddini, "Spindle speed variation for the suppression of regenerative chatter," *J. Nonlinear Sci.*, vol. 13, no. 3, pp. 265–288, May 2003, doi: 10.1007/s00332-003-0518-4.
- [110] E. Al-Regib, J. Ni, and S. H. Lee, "Programming spindle speed variation for machine tool chatter suppression," *Int. J. Mach. Tools Manuf.*, vol. 43, no. 12, pp. 1229–1240, Sep. 2003, doi: 10.1016/S0890-6955(03)00126-3.
- [111] I. Bediaga, I. Egaña, J. Munoa, M. Zatarain, L. Lopez De Lacalle, and L. N. López De Lacalle, "Chatter avoidance method for milling process based on sinusoidal spindle speed variation method: simulation and experimental results," 2007.
- [112] M. Zatarain, I. Bediaga, J. Muñoa, and R. Lizarralde, "Stability of milling processes with

REFERENCES

- continuous spindle speed variation: Analysis in the frequency and time domains, and experimental correlation," *CIRP Ann. - Manuf. Technol.*, vol. 57, no. 1, pp. 379–384, Jan. 2008, doi: 10.1016/j.cirp.2008.03.067.
- [113] I. Bediaga, M. Zatarain, J. Muñoa, and R. Lizarralde, "Application of continuous spindle speed variation for chatter avoidance in roughing milling," *Proc. Inst. Mech. Eng. Part B J. Eng. Manuf.*, vol. 225, no. 5, pp. 631–640, May 2011, doi: 10.1177/2041297510394075.
- [114] H. Zhang and J. Ni, "Internal Energy Based Analysis on Mechanism of Spindle Speed Variation for Regenerative Chatter Control," *J. Vib. Control*, vol. 16, no. 2, pp. 281–301, Feb. 2010, doi: 10.1177/1077546309103562.
- [115] Xinhua Long and B. Balachandran, "Stability of Up-milling and Down-milling Operations with Variable Spindle Speed," *J. Vib. Control*, vol. 16, no. 7–8, pp. 1151–1168, Jun. 2010, doi: 10.1177/1077546309341131.
- [116] S. Seguy, T. Insperger, L. Arnaud, G. Desein, and G. Peigné, "On the stability of high-speed milling with spindle speed variation," *Int. J. Adv. Manuf. Technol.*, vol. 48, no. 9–12, pp. 883–895, Oct. 2010, doi: 10.1007/s00170-009-2336-9.
- [117] S. Seguy, T. Insperger, L. Arnaud, G. Desein, and G. Peigné, "SUPPRESSION OF PERIOD DOUBLING CHATTER IN HIGH-SPEED MILLING BY SPINDLE SPEED VARIATION," *Mach. Sci. Technol.*, vol. 15, no. 2, pp. 153–171, Apr. 2011, doi: 10.1080/10910344.2011.579796.
- [118] Q. Xie and Q. Zhang, "Stability predictions of milling with variable spindle speed using an improved semi-discretization method," *Math. Comput. Simul.*, vol. 85, pp. 78–89, Nov. 2012, doi: 10.1016/j.matcom.2012.09.017.
- [119] Q. Xie, Q. Zhang, W. Wang, G. Jin, and J. Han, "Stability analysis for variable spindle speed milling with helix angle using an improved semi-discretization method," *Sci. China Technol. Sci.*, vol. 56, no. 3, pp. 648–655, Mar. 2013, doi: 10.1007/s11431-012-5090-4.
- [120] K. Saleh and N. Sims, "a New Approach To Time Domain Simulation of Variable."

REFERENCES

- [121] G. Totis, P. Albertelli, M. Sortino, and M. Monno, "Efficient evaluation of process stability in milling with Spindle Speed Variation by using the Chebyshev Collocation Method," *J. Sound Vib.*, vol. 333, no. 3, pp. 646–668, Feb. 2014, doi: 10.1016/j.jsv.2013.09.043.
- [122] Y. Ding, J. Niu, L. M. Zhu, and H. Ding, "Numerical Integration Method for Stability Analysis of Milling With Variable Spindle Speeds," *J. Vib. Acoust. Trans. ASME*, vol. 138, no. 1, Feb. 2016, doi: 10.1115/1.4031617.
- [123] J. Niu, Y. Ding, L. M. Zhu, and H. Ding, "Stability Analysis of Milling Processes with Periodic Spindle Speed Variation Via the Variable-Step Numerical Integration Method," *J. Manuf. Sci. Eng. Trans. ASME*, vol. 138, no. 11, Nov. 2016, doi: 10.1115/1.4033043.
- [124] G. Jin, H. Qi, Z. Li, and J. Han, "Dynamic modeling and stability analysis for the combined milling system with variable pitch cutter and spindle speed variation," *Commun. Nonlinear Sci. Numer. Simul.*, vol. 63, pp. 38–56, 2018, doi: 10.1016/j.cnsns.2018.03.004.
- [125] P. Albertelli, L. Braghieri, M. Torta, and M. Monno, "Development of a generalized chatter detection methodology for variable speed machining," *Mech. Syst. Signal Process.*, vol. 123, pp. 26–42, May 2019, doi: 10.1016/j.ymssp.2019.01.002.
- [126] X. Wang, Q. Bi, T. Chen, L. Zhu, and H. Ding, "Transient Vibration Analysis Method for Predicting the Transient Behavior of Milling with Variable Spindle Speeds," *J. Manuf. Sci. Eng. Trans. ASME*, vol. 141, no. 5, May 2019, doi: 10.1115/1.4043265.
- [127] C. Wang, X. Zhang, R. Yan, X. Chen, and H. Cao, "Multi harmonic spindle speed variation for milling chatter suppression and parameters optimization," *Precis. Eng.*, vol. 55, pp. 268–274, Jan. 2019, doi: 10.1016/j.precisioneng.2018.09.017.
- [128] X. Dong and W. Zhang, "Chatter suppression analysis in milling process with variable spindle speed based on the reconstructed semi-discretization method," *Int. J. Adv. Manuf. Technol.*, vol. 105, no. 5–6, pp. 2021–2037, Dec. 2019, doi: 10.1007/s00170-019-04363-0.
- [129] K. Saleh and N. D. Sims, "The Self-Excitation Damping Ratio in Variable Speed Milling,"

REFERENCES

- Proc. world Congr. Eng.*, vol. 3, 2012.
- [130] N. D. Sims, "The self-excitation damping ratio: A chatter criterion for time-domain milling simulations," *J. Manuf. Sci. Eng. Trans. ASME*, vol. 127, no. 3, pp. 433–445, Aug. 2005, doi: 10.1115/1.1948393.